

Pranjal Chandra
Lalit M. Pandey *Editors*

Biointerface Engineering: Prospects in Medical Diagnostics and Drug Delivery

 Springer

Biointerface Engineering: Prospects in Medical Diagnostics and Drug Delivery

Pranjal Chandra • Lalit M. Pandey
Editors

Biointerface Engineering: Prospects in Medical Diagnostics and Drug Delivery

 Springer

Editors

Pranjal Chandra
Laboratory of Bio-Physio Sensors and
Nano-bioengineering, Department of
Biosciences and Bioengineering
Indian Institute of Technology Guwahati
Guwahati, Assam, India

School of Biochemical Engineering
Indian Institute of Technology (BHU)
Varanasi
Varanasi, Uttar Pradesh, India

Lalit M. Pandey
Bio-interface and Environmental Engineering
Lab, Department of Biosciences and
Bioengineering
Indian Institute of Technology Guwahati
Guwahati, Assam, India

ISBN 978-981-15-4789-8 ISBN 978-981-15-4790-4 (eBook)
<https://doi.org/10.1007/978-981-15-4790-4>

© Springer Nature Singapore Pte Ltd. 2020

This work is subject to copyright. All rights are reserved by the Publisher, whether the whole or part of the material is concerned, specifically the rights of translation, reprinting, reuse of illustrations, recitation, broadcasting, reproduction on microfilms or in any other physical way, and transmission or information storage and retrieval, electronic adaptation, computer software, or by similar or dissimilar methodology now known or hereafter developed.

The use of general descriptive names, registered names, trademarks, service marks, etc. in this publication does not imply, even in the absence of a specific statement, that such names are exempt from the relevant protective laws and regulations and therefore free for general use.

The publisher, the authors, and the editors are safe to assume that the advice and information in this book are believed to be true and accurate at the date of publication. Neither the publisher nor the authors or the editors give a warranty, expressed or implied, with respect to the material contained herein or for any errors or omissions that may have been made. The publisher remains neutral with regard to jurisdictional claims in published maps and institutional affiliations.

This Springer imprint is published by the registered company Springer Nature Singapore Pte Ltd.
The registered company address is: 152 Beach Road, #21-01/04 Gateway East, Singapore 189721, Singapore

Contents

1	Engineered Drug Delivery Systems: Insights of Biointerface	1
	Rushikesh Fopase, Aman Bhardwaj, Vivek Singh Yadav, and Lalit M. Pandey	
2	Tissue Engineering Strategies for Tooth and Dento-alveolar Region with Engineered Biomaterial and Stem Cells	31
	Siddhartha Das, Vivek P. Soni, and Jayesh R. Bellare	
3	Antifouling Peptoid Biointerfaces	55
	Varun Saxena, Martyn G. L. Merrilees, and King Hang Aaron Lau	
4	Structure and Rheology of Hydrogels: Applications in Drug Delivery	75
	Sai Geetha Marapureddy and Prachi Thareja	
5	Surface Engineering in Wearable Sensors for Medical Diagnostic Applications	101
	Devin Schmidt, Anil Mahapatro, and Kim Cluff	
6	Modulation of Physicochemical Properties of Polymers for Effective Insulin Delivery Systems	123
	Prateek Ranjan Yadav and Sudip K. Pattanayek	
7	Organization of Bio-Molecules in Bulk and Over the Nano-Substrate: Perspective to the Molecular Dynamics Simulations	149
	Sunil Kumar and Trilochan Mishra	
8	Medical Diagnostics Based on Electrochemical Biosensor	167
	Nalin H. Maniya and Divesh N. Srivastava	
9	Nanomaterial Functionalization Strategies in Bio-Interface Development for Modern Diagnostic Devices	195
	Kuldeep Mahato, Ashutosh Kumar, Buddhadev Purohit, Supratim Mahapatra, Ananya Srivastava, and Pranjal Chandra	

10	Bio-Nano-Interface Engineering Strategies of AuNPs Passivation for Next-Generation Biomedical Applications	215
	Ashutosh Kumar, Buddhadev Purohit, Kuldeep Mahato, Supratim Mahapatra, Ananya Srivastava, and Pranjal Chandra	
11	Electro-optical Analysis as Sensing System for Detection and Diagnostics of Bacterial Cells	233
	O. I. Guliy and V. D. Bunin	

About the Editors

Pranjal Chandra is currently employed as an Assistant Professor at the School of Biochemical Engineering, Indian Institute of Technology (BHU), Varanasi, India. He earned his Ph.D. from Pusan National University, South Korea, and did post-doctoral training at Technion-Israel Institute of Technology, Israel. His research focus is highly interdisciplinary, spanning a wide range in biotechnology, nanobiosensors, material engineering, nanomedicine, etc. He has designed several commercially viable biosensing prototypes that can be operated for onsite analysis for biomedical diagnostics, environmental monitoring, and other point-of-care testing applications. He has published five books on various aspects of biosensors/medical diagnostics from IET London, Springer Nature, CRC press, USA. He has also published over 85 journal articles in topmost journals of his research area including Biosensors and Bioelectronics, Analytical Chemistry, Biomaterials, Chemical Communications, Electroanalysis, etc. His work has been greatly highlighted in over 300 topmost news agencies globally including Rajya Sabha TV; DD Science; Science Trends, USA; Nature India; Vigyan Prasar; Global Medical Discovery, Canada; APBN Singapore; Business Wire, Dublin; etc. He is a recipient of many prestigious awards and fellowships such as DST Ramanujan fellowship (Government of India); Early Career Research Award (DST, Government of India); Brain Korea-21 and National Research Foundation fellowship, South Korea; Technion post-doctoral fellowship, Israel; NMS Young scientist award, Biotech Research Society India Young Scientist Award, Young Engineers Award 2018, RSC Highly Cited Corresponding Author Award (general chemistry); ACS/Elsevier Outstanding Reviewer Awards; etc. He is a reviewer of over 50 international journals and expert project reviewer of various national/international funding agencies. He is Associate Editor of *Sensors International* and an editorial board member of the *Materials Science for Energy Technologies* by KeAi and Elsevier, *World Journal of Methodology*, USA; *Frontiers of Biosciences*, USA; *Reports in Physical Sciences*, Singapore.

Lalit M. Pandey is an Associate Professor in the Department of Biosciences and Bioengineering, IIT Guwahati. He has completed his Ph.D. in Chemical Engineering from Indian Institute of Technology, Delhi. He was awarded Erasmus Mundus India4EU fellowship to pursue his research at Laboratoire des Matériaux et du

Génie Physique (LMGP), Grenoble-INP, France, for 18 months during 2010–2012. Prior to joining IIT Guwahati, he was working as a Scientist with the Central Pollution Control Board, Ministry of Environment & Forests, Govt. of India, from 2009 to 2014 and was involved in research/study relating to water and air pollution in agro-based industries. He has received DST-UKIERI award 2018, IEI (The Institution of Engineers [India]) Young Engineers Award 2017, Innovation in Science Pursuit for Inspired Research (INSPIRE) Faculty Award 2014, and Early Career Research Award from Science and Engineering Research Board (SERB) by Department of Science & Technology, Govt. of India. His research area includes Biointerfaces and Biomaterials, Biochemical engineering and Environmental Biotechnology. He has published about 50 scientific articles in international journals, including *J. Phys. Chem. C, Colloids and Surface: B, Langmuir, ACS Biomater. Sci. Eng., Materials Science and Engineering: C, Applied Surface Science, J. Chem. Eng. Data, Bioresource Technology, Journal of Environmental Chemical Engineering*, etc. He is on the Editorial Board of four international journals and Guest Associate Editor in Biomaterials (Frontiers). He is a life member of the International Association of Engineers (IAENG), the Indian Institute of Chemical Engineers (IChE), Nano and Molecular Society (India), and reviewer of several peer-reviewed journals.



Engineered Drug Delivery Systems: Insights of Biointerface

1

Rushikesh Fopase, Aman Bhardwaj, Vivek Singh Yadav,
and Lalit M. Pandey

Abstract

Drug delivery systems are now well developed and in use for various therapies. These systems surpass conventional mode of drug administration by efficiently delivering the desired concentrations of bioactive drug. Typically, drug delivery in the body is an interfacial phenomenon. Interaction of the administered carrier molecules with the body fluid depends on the physiochemical properties of the carrier molecules and hence controls its pharmacokinetics. However, nonspecific interactions and physiological stability of these molecules within biological systems may result in complications during the therapy and stimulate the immune responses. Also, the insolubility of hydrophobic drugs is a major problem in their therapeutic applications. Target-specific drug delivery with controlled interfacial interactions is a possible alternative to overcome these challenges. The regulation of interactions at biointerface allows modulating the in vivo administration of a carrier system. Various engineered nanomaterials, emulsion and polymer-based drug delivery systems, have been explored in the literature. Further, surface modifications and functionalization of these delivery systems are found to regulate interfacial interactions. The modification not only controls the reaction potency of drug with the biological systems but also enhances the stability and compatibility. This chapter describes the designing of engineered drug delivery systems using polymers, self-assembled monolayers, and emulsions. Application of these strategies to alter the surface chemistry of drug molecules and delivery systems is elaborated through recent studies. Bio-interfacial aspects of the above-designed systems are highlighted to confirm their fidelity to be used as effective drug delivery systems.

R. Fopase · A. Bhardwaj · V. S. Yadav · L. M. Pandey (✉)

Bio-interface and Environmental Engineering Lab, Department of Biosciences and Bioengineering,
Indian Institute of Technology Guwahati, Guwahati, Assam, India

e-mail: lalitpandey@iitg.ac.in

© Springer Nature Singapore Pte Ltd. 2020

P. Chandra, L.M. Pandey (eds.), *Biointerface Engineering: Prospects in Medical
Diagnostics and Drug Delivery*, https://doi.org/10.1007/978-981-15-4790-4_1

1

KeywordsDrug delivery · Biointerface · Emulsions · Polymers · Self-assembled monolayers

1.1 Introduction

Drug delivery plays a vital role in the success of therapeutics. Drug delivery systems are intended to deliver desired concentrations of a drug molecule to a specific site to achieve efficient treatment without exhibiting side effects. Concept of drug delivery was first coined in the 1950s, and since then the advancements in the technology resulted in the arising of drug delivery systems with long-term stability and sustainable release (Park 2014). These systems offer advantages like improved stability and activity of the drug molecules, better pharmacokinetics, and reduced side effects (Li et al. 2019).

Interaction of the drug delivery systems with biological system determines the fate of drug molecules and hence the success of the treatment (Mahon et al. 2012). Drug delivery is an interfacial phenomenon and governed by the surface properties of the carrier (Buckton 2000). When the carrier system enters the body, it initially interacts with the different biological fluids depending on the mode of administration. The interaction of drug molecules with body fluid is referred to as medium effect and depends on the interfacial potential, for example, self-energy of surface moieties. Medium effect involves the simultaneous short-range interactions of solvent and solute molecules such as adhesion and bonding forces (Israelachvili 2015). Proteins present in biological fluid get adsorbed on the carrier surface forming protein corona and decides the cell interaction and biocompatibility with the carrier molecules, ultimately the progression of the carrier system (Gan et al. 2019; Hasan et al. 2018a). The surface energy of the system which controls the protein adhesion is the function of hydrophobicity or hydrophilicity (Lima et al. 2011; Dallin and Van Lehn 2019; Pandey et al. 2013; Hasan et al. 2018a). Solid–liquid interface regulates the process in case of in vivo solid-state drug delivery systems such as nanomaterials, while liquid–liquid interface controls the process in case of liquid state drug delivery systems such as nanoemulsions (Packham 2003). Interfacial energy between these two types of carrier systems determines the adhesion of the protein and other biological macromolecules on the carrier molecules. Lower surface energy favors the optimum compatibility with blood, while better protein adsorption is favored by high interfacial energy (Andrade et al. 1987; Leininger 1972).

In conventional drug delivery, drug molecules were administrated in the form of pills, ointments, gels, suspensions, and oral solutions to treat various health conditions. However, such approaches result in the reduced efficiency due to inactivation of the native structure of drug molecules by biological fluid and other factors leading to the requirement of a higher dose. Moreover, nonspecific interactions of drug molecules with healthy tissues and different biological processes result in some side effects (Sharma et al. 2011; Lang 1995; Langer 1990). Focusing the therapy to a specific diseased site is the best possible approach to avoid such side effects and to

achieve efficient performance (Agnihotri et al. 2011; Mehta et al. 2011). In this regard, the targeted delivery of drug molecules offers various advantages and confirms the fidelity of the activity of a drug. Delivery of desired drug concentrations to the target site and sustained release of the drug molecules enhances the treatment efficacy with the time (Bae and Park 2011). Drug carriers also offer the advantages of delivery through biological barriers such as blood–brain barrier, blood–labyrinth, and blood–retina barriers (Urtti 2006; Song et al. 2018; Nyberg et al. 2019). Various alternatives are available for the site-specific drug delivery such as protein or peptide conjugated carriers, nanomaterials-based carriers, polymeric drug carriers, drug-loaded emulsions, self-assembled monolayer-based carriers (Sun et al. 2010; Couvreur et al. 2018; Jaiswal et al. 2015; Habibi et al. 2016). These carriers enter the body via various routes and approaches targeted site by means of specific domain or affinity. After reaching the site, respective stimuli such as pH and ionic strength lead to the release of the drug molecules for the desired purpose (Choi and Han 2018; Mahon et al. 2012).

Additionally, poor solubility and stability of such drugs and biomolecules are the significant challenges for researchers working in the domain of therapeutics (Bohley et al. 2019; Pangeni et al. 2017). Such obstacles in the formation of these drugs into viable medicines limit the bioavailability, delivery of required concentrations, and reduced efficiency of the process. Additionally, when administered orally, variation in pH at the levels of gastrointestinal tract leads to loss of drug activity (Gavhane and Yadav 2012). One possible solution over the solubility issue is the incorporation of such hydrophobic drugs or biomolecules into some carrier molecules. The carrier molecules ensure the delivery of a natural and active form of drug molecules to the target site *in vivo* to achieve its desired activity (Lu et al. 2018). Surface modification of carriers is one of the ways to control the undesired interactions occurring at the biointerface under *in vivo* conditions. Surface modification is a potential strategy to manipulate the properties of the drug delivery carrier by using different polymers and functionalization (Hasan and Pandey 2015). Natural polymers like cellulose, pectin, starch, dextran, glycan, chitosan, and synthetic polymers like polyether, polyethylene imines, and polyesters are extensively used in the various biomedical applications to alter the surface properties (Xiao et al. 2018). Polymers alter the surface charges, topography, and hydrophobicity to modulate protein and surface interactions (Prajapati et al. 2019). Self-assembled monolayers (SAMs) control the functionalities of the surface and prevent the elimination of hydrophobic drugs. In the aqueous medium, SAMs arrangement occurs by hydrophilic portion interacting with the physiological medium, and the hydrophobic drug gets sequestered inside the relatively hydrophobic portion of the SAMs. In the different approach like encapsulation and emulsion, separation of drug molecules from the external environment improves the stability and solve the issue related to the solubility of drug molecules.

This chapter describes the three-drug delivery systems: polymers, SAMs, and emulsions. Characteristics of these carrier systems have been discussed with some applications in drug delivery. Polymers are used to modify the surface charges and energy, which decides the interactions between the proteins and other biomolecules

with carrier molecules. While SAMs form an assembly which controls the surface functionality and help in the site targeting and anchoring of signal molecules. Emulsions enclose the drug molecules within and separate from the external environment. The solubility of the drug molecules is dealt with based on the hydrophilic and hydrophobic properties and accordingly use of continuous and dispersed phase. Delivery of drug to the specific sites and its sustained release is the perspectives of attempts made for delivery systems. The chapter discusses a few case studies of drug delivery systems with their proven potentiality for the in vivo applications in the therapeutics.

1.2 Emulsions-based Drug Delivery Systems

Emulsions are metastable colloids of two immiscible liquids, one dispersed into others with the help of emulsifier (surfactant). The biphasic structure possessed by emulsions is a distinct dispersed phase surrounded by the continuous phase along with the interface covered with surfactant (Jaiswal et al. 2015). Oil, water, and surfactants are the constituents of emulsions, and based on dispersion of one component into another determines the type of emulsion as oil in water or water in oil as shown in Fig. 1.1 (Langevin 1992). There is another type of emulsion called as a double emulsion in which droplets of dispersed phase contain smaller droplets of continuous phase dispersed within (van der Graaf et al. 2005). Table 1.1 has listed out some examples of oil and surfactants used in the preparation of emulsion.

Delivery of drugs or biomolecules by emulsions to desired site offers many more advantages over the typical suspension-based delivery. In the typical suspension-based delivery, drug molecules are mixed/dissolved in the aqueous solution such as saline or PBS and administered in the body via oral or injection routes. However, these types of delivery systems are not suitable for drug molecules having low

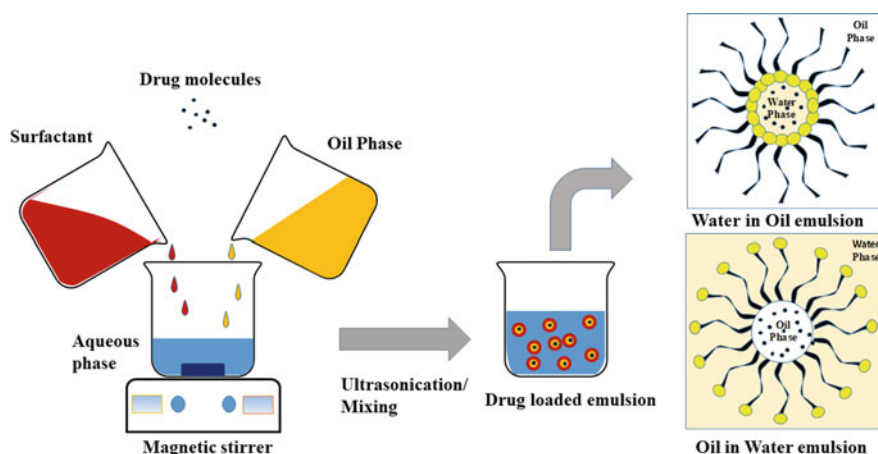


Fig. 1.1 Synthesis of nanoemulsions and drug loading

Table 1.1 Various emulsions used for the drug delivery applications

Applications	Types of emulsion	Oil phase	Aqueous phase	Surfactant	Drug	Loaded drug amount	Release time	References
Across Blood-brain barrier	O/W	Ethyl acetate 20/80 with PLGA	PBS	Polysorbate 80	Loperamide	25.23 ± 1.84 mg per g of PLGA NPs	75% in 120 h	Fornaguera et al. (2015a)
Neurodegenerative drug delivery	O/W	Ethyl acetate	PBS	Polysorbate 80	Galantamine	56.87 ± 3.48 mg per 100 ml	80% in 120 h	Fornaguera et al. (2015b)
Probiotic-drug delivery	O/W	Sunflower oil	Water	Xanthan gum	Metronidazole	50 µg/g emulsion	55% in 7 h	Pandey et al. (2016)
Drug-loaded nanoparticle dispersion	O/W	Ethyl acetate and polymer	Water	Polyoxyethylene 10 oleyl ether	Dexamethasone	2.66 × 1012 per ml	6% in 15 min	Calderó et al. (2016)
Eye drop formulation	O/W	Castor oil	Glycerol in water	Egg phosphatidylcholine	Coumairm-6	98%	0.03% in 4 h	Ying et al. (2013)
Hybrid drug delivery systems	O/W	Gelucire 43/01™	PEG 4000 in water	IMWITOR® 600	Ketoprofen	99%	86% in 2 h	Gonçalves et al. (2015)
Controlled-release drug carriers	W/O	Ethyl acetate	Alginate water solution	–	Blue dextran	82%	5% in 2 h	Baimark and Srisuwan (2014)
Long-term drug delivery	W1/O/W2	Pullan acetate in methylene chloride	PVA in water	–	Exenatide	90.3%	100% in 20 days	Yang et al. (2009)
Topical drug application	W/O	Isopropyl myristate, liquid paraffin	Water	Dow Corning™	Fluorescein sodium	47 ± 3%	–	Binder et al. (2019)
Drug delivery	W/O	Medium-chain triglyceride oil	Water	Cremophor® EL/2-HDG	Ketoprofen	–	98.6% in 24 h	Ahmad et al. (2014)

PLGA poly(lactide-co-glycolide); PEG polyethylene glycol; HDG 2-hexyldecyl-β(α)-d-glucoside; PBS phosphate buffered saline

stability and hydrophobic nature and require higher dosage due to the loss of drug during the transport. Thus, the use of emulsions based on the delivery of a hydrophobic drug overcomes the solubility problem. The solubility of drug molecules plays a crucial role in determining their effects based on physiochemical properties. Based on the solubility in the water and oil, and the surface charges of drug molecules, the selection of the emulsion system is carried out (Washington 1996). The stability of emulsions depends on the nature of forces acting on them. Repulsive forces repel the incoming droplets and maintain the stability of the system (Lu et al. 2018). However, attractive forces result in the formation of droplet clumps and disorders of the system. The emulsion system is stabilized by the equilibrium of the various forces involving Van der Waals, electrostatic, solvent, and steric forces (Helgeson 2016; Sari et al. 2015). Typically, the small size of emulsions offers long-term stability by overcoming the coalescence and sedimentation via significant Brownian motion of the nanosize droplets (Lovelyn and Attama 2011).

The size of emulsions categorizes them as nanoemulsion and microemulsion. Nanosize droplets formation takes a higher amount of energy due to the requirement of higher shear rates (El-Aasser et al. 1997; Tadros et al. 2004). The energy required to produce particular droplet size is expressed as follows:

$$\varepsilon_{min} = 3\gamma\varnothing_d^3/a$$

where γ is interfacial tension between two immiscible phases, \varnothing_d is the volume fraction of the dispersed phase, and a is the size of the particle (Helgeson 2016). Surfactants play a crucial role in lowering the γ values and stabilizing the interfacial area (Leal-Calderon et al. 2007; Mason et al. 2006).

Nanoemulsions range below 100 nm in size with narrow size distribution and are widely used as a carrier for drug delivery systems (Sonneville-Aubrun et al. 2004). Nanoemulsions have been popularly used in therapeutics like the treatment of liver enzyme replacement therapy, neurodegenerative diseases, oral therapy, and cancer treatment (Qi et al. 2011; Nandivada et al. 2016; Fornaguera et al. 2015a). Various studies have been performed to analyze the effect of emulsions-based drugs and biomolecules and the release profile to understand the pharmacokinetics emulsion-based delivery. Surrounding pH, temperature, temperature, ionic concentration, and enzymes triggers the release of drugs from the emulsions and mostly due to diffusion or sometimes coalescence or both (Herzi and Essafi 2019; Llinàs et al. 2013).

In a study by Saxena et al., edible oil-based nanoemulsion was tested for its potentiality as a delivery vehicle for a hydrophobic molecule, α -tocopherol (Saxena et al. 2018). Coconut oil was used to prepare the nanoemulsion of size 386 (± 20) nm using Triton X100 and water. Loading capacity of nanoemulsion for α -tocopherol was observed as 9.5 mg/ml and was stable up to 30 days of storage without any phase separation. The formulation showed temperature stability up to 275 °C along with pH stability for 8 h in basic and 6 h in acidic mediums. The noted stability of the prepared nanoemulsion proved its potential for drug delivery. Cytotoxicity studies performed on L929 (mouse fibroblast) confirmed the biocompatibility of α -tocopherol-loaded nanoemulsion for the concentration up to 20 μ g/ml.

Antibacterial activity studies on *E. coli* and *E. hirae* showed zones of inhibition of 21.1 (± 0.8) mm and 24.8 (± 1.0) mm for unloaded and drug-loaded nanoemulsions, respectively. Release of drug from the nanoemulsion was found to follow a combined of a diffusion-controlled (Higuchi model) and kinetic-controlled (first-order kinetics) models (Costa and Lobo 2001). Kinetic model contributed 70% release, and Higuchi model contributed to 30% of release. The rate constant for the release profile was observed as 0.133 (± 0.010) h^{-1} and 100% release observed within 24 h. These features confirmed the suitability of delivery vehicle (nanoemulsion) for the delivery of α -tocopherol. Figure 1.2 summarizes the preparation and characteristics features of the abovementioned α -tocopherol-loaded coconut oil-based nanoemulsion.

Emulsion offers the delivery of hydrophobic drugs to the desired site by the means of oil in water emulsion. Hydrophobic drug molecules such as curcumin is used for the treatment of cancer, Alzheimer disease, and as antioxidant and anti-inflammatory drugs (Fan et al. 2013). A study by Wang et al. showed the capability of oil in water emulsion for the delivery of curcumin synthesized using bovine serum albumin (BSA)–dextran conjugate as emulsifier and stabilizer (Wang et al. 2016). BSA–dextran conjugate was prepared by Maillard reaction and used with oil phase of medium chain triglyceride. Size of the prepared nanoemulsion was around 350 nm with the different tested ratios of constituents. Nanoemulsions with the highest curcumin loading capacity of 15 mg/ml showed the stability up to 60 days at 4 °C and 10 days at 37 °C. For oral mode of administration, the digestive tract pH range of 2–8 showed no significant effects on the emulsions loaded with curcumin. The ex vivo fluorescence studies performed on the mice models showed gradual release of curcumin mainly in the gastrointestinal tract and enhanced bioavailability to 4.8-fold compared to suspension-based delivery system. Protection of curcumin against denaturation and increased bioavailability in the gastrointestinal tract proved the potentiality of the prepared nanoemulsion for oral drug delivery.

Double water in oil emulsions systems are more complex and used in the delivery of both hydrophilic and hydrophobic drugs (Aditya et al. 2015). These systems comprise water droplets within larger oil droplets and are dispersed in the aqueous phase with surfactants (Zhao et al. 2011). In a study by Shakeel et al., an oral drug delivery system for 5-fluorouracil was developed using double water in oil self-emulsifying emulsions system (Shakeel et al. 2014). Primary water in oil nanoemulsions was prepared using Transcutol-HP and isopropyl alcohol as surfactant and co-surfactant with deionized water, respectively. The mixture was titrated with slow addition of different ratios of lauroglycol-90 as oil phase and 5-fluorouracil to prepare primary nanoemulsions. The prepared primary water in oil nanoemulsion was characterized and selected based on the smallest droplet size, lowest polydispersity index, and the optimal zeta potential to prepare double water in oil nanoemulsions using primary nanoemulsion as oil phase and deionized water as aqueous phase. In vitro drug release studies for 1 g self-emulsifying nanoemulsions containing 25 mg 5-fluorouracil were performed at 37 °C at 50 rpm in deionized water and analyzed through reverse-phase high-performance liquid chromatography method. Highest drug release was observed for the sample SN6 (mix ratio of

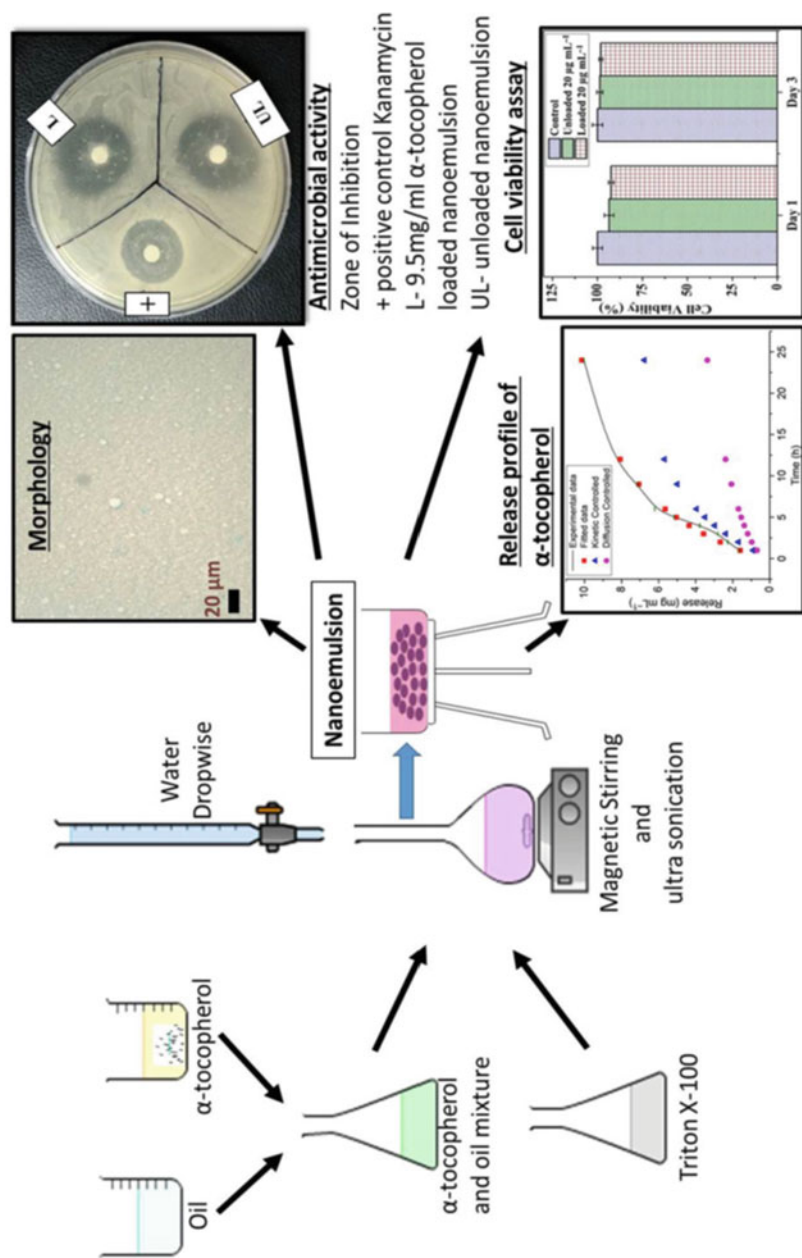


Fig. 1.2 Synthesis and properties of coconut oil-based nanoemulsion for the delivery of α -tocopherol along with its biocompatibility and antibacterial activity. Adapted and reprinted from Saxena et al. (2018) with permission from Taylor & Francis, Copyright (2018)

10:45:45 (w/w/w)) and showed 98% release of 5-fluorouracil in 60 min. The rapid release of 5-fluorouracil was due to the smallest droplet size of 16.1 nm, lowest polydispersity index value of 0.086, and the lowest viscosity value of 6.15 centipoise compared to other combinations. Cytotoxicity studies performed on the HT-29 colon cancer cell lines showed up to 95% cell deaths with 1200 μM of 5-fluorouracil and confirmed the capability of complex double water in oil nanoemulsions for the drug delivery against cancer cells.

Many studies have elaborated the mechanisms and reactions occurring when emulsion-loaded drug is administered via the oral route (Gumus et al. 2016; Liu et al. 2017). In a particular study, the fate of β -carotene-loaded emulsion in the gastrointestinal tract and antioxidant properties were analyzed by Zhong et al. (2019). A hydrophobic molecule, β -carotene, was encapsulated into three types of oil in water emulsions using oat protein isolate (OPI) and β -glucan from *P. ostreatus* (POG) ($\sim 60 \mu\text{m}$), OPI–POG mixture ($\sim 30 \mu\text{m}$), and OPI–POG conjugate ($\sim 3.1 \mu\text{m}$). OPI–POG conjugate emulsion synthesized by Maillard reaction showed the stability in pH range of 3.0–7.0, temperature stability for 30–90 $^{\circ}\text{C}$, and high salt concentration tolerance up to 350 mM concentration of NaCl. The gastrointestinal fate of β -carotene emulsions was studied using a reported stomach model (Chen et al. 2016; Minekus et al. 2014). For the mouth stage, emulsions were preheated at 37 $^{\circ}\text{C}$ and mixed with simulated saliva containing mucin with pH 6.8. No change on the particle size was observed for the OPI–POG conjugate emulsion as compared to the other two. Anionic mucin was repelled by covalent bonding of POG, and hence the stability was observed for conjugate emulsion. For the stomach stage, samples from the mouth stage were mixed with simulated gastric juice having NaCl and HCl along with pepsin. The pH for the stomach stage was adjusted to 2.5 and agitated at 100 rpm for 2 h at 37 $^{\circ}\text{C}$. At this level, OPI and OPI–POG mixture micelles were broken and formed droplet flocculation. However, conjugate-based emulsion was found to be distributed uniformly with steric hindrances with pepsin avoiding proteolysis of OPI. The zeta potentials of the emulsions were reduced to near zero in the presence of anionic mineral ions. In the small intestine level, intestinal juice having saline solution, lipase, pancreatin, and bile salts was maintained at pH 7 and analyzed for the generation of free fatty acids. Increase in the sizes of OPI and OPI–POG mixture emulsions were observed due to replacement of OPI and OPI–POG mixture by bile salts and free fatty acids generated. However, no change in size was observed for conjugate-based emulsion with 93% release of free fatty acids and conversion to mixed micelles for solubilizing β -carotene. The prepared emulsions showed initial rapid release of free fatty acids for around 25 min followed by a slower release rate for more prolonged time up to 100 min. Based on the bioaccessibility, stability, and adsorptions results, bioavailability of the OPI–POG conjugate emulsion showed the highest value of 11.06% as compared to 2.24% of OPI and 4.06% OPI–POG mixture. Enhanced bioavailability resulted in the enhanced cellular antioxidant activity through the elimination of peroxy radicals by β -carotene in the Caco-2 cells, a type of human colon carcinoma cell line. This proved the potentiality of conjugate-based emulsion for the delivery of

biomolecules. Figure 1.3 shows the synthesis of OPI–POG-stabilized β -carotene emulsion and antioxidant effect of β -carotene to Caco-2 cells.

In conclusions, emulsions offer various advantages over the conventional mode of drug delivery. Especially in the case of hydrophobic drugs, oil in water emulsions are very useful to deliver a drug molecule in its active form. Emulsions possess better stability in a wide range of pH and thus pass through various levels of gastrointestinal tract. Moreover, improvement in the bioavailability of the administered drug was observed during various studies. Although there are certain drawbacks of the emulsion-based drug delivery systems such as a short shelf life, flocculation, and creaming during storage (Kale and Deore 2017). These drawbacks of the emulsions can be overcome by controlling the factors like surfactant concentration, use of co-surfactant, and ratio of oil phase and aqueous phase. Therefore, emulsion-based drug delivery systems are successfully being used for various therapeutical applications.

1.3 Surface Modifications in Drug Delivery

Surface modification is a powerful tool to alter the surface energy of a system which has been potentially explored for various applications in biomedical, pharmaceutical, and biological fields (Song et al. 2019a; Mardilovich et al. 2006; Hasan et al. 2017, 2018b). For drug delivery, surface modifications have tuned hydrophobicity, enhanced stability, and imparted targeted delivery.

Hydrophobic drugs are nearly insoluble in an aqueous medium in the physiological environment. These physiochemical and pharmacokinetic issues hinder the bioavailability and usage in biomedical applications. In this regard, surface modification offers a promising solution for manipulating surface properties for various applications such as tissue engineering, implants, and drug delivery (Hasan et al. 2018a, b, c; Hasan and Pandey 2016; Pandey et al. 2013; Pandey and Pattanayek 2013). Szegedi et al. have used modified mesoporous silica nanoparticles (NPs) for entrapment of curcumin. NPs were modified with amino groups using 3-aminopropyltriethoxysilane (APTES) to enhance the drug-loading capacity. APTES modification strategy employed for surface modification is shown in Fig. 1.4. Typically, a surface to be modified is firstly activated by piranha treatment to convert SiO_2 surface groups to Si-OH groups followed by silanization to provide amine terminal group on the surface. After drug loading, the modification was also carried out using four alternating layers of polyelectrolytes k-carrageenan and chitosan to improve drug release profile and biocompatibility. Therapeutic potential of the curcumin remained intact after the above entrapments (Szegedi et al. 2019).

Amphiphilic self-assembled NPs of polyvinyl alcohol (PVA) decorated with hydrophobic side-arms were used by Delbecq et al. for the encapsulation of hydrophobic drugs such as prednisolone or cholesterol (Delbecq and Kawakami 2014). PVA was chosen due to modification flexibility, non-immunogenicity, and biocompatibility. PVA self-assembled NPs were formed via hydrophobic–hydrophobic interactions resulting due to the presence of two entirely different pendant

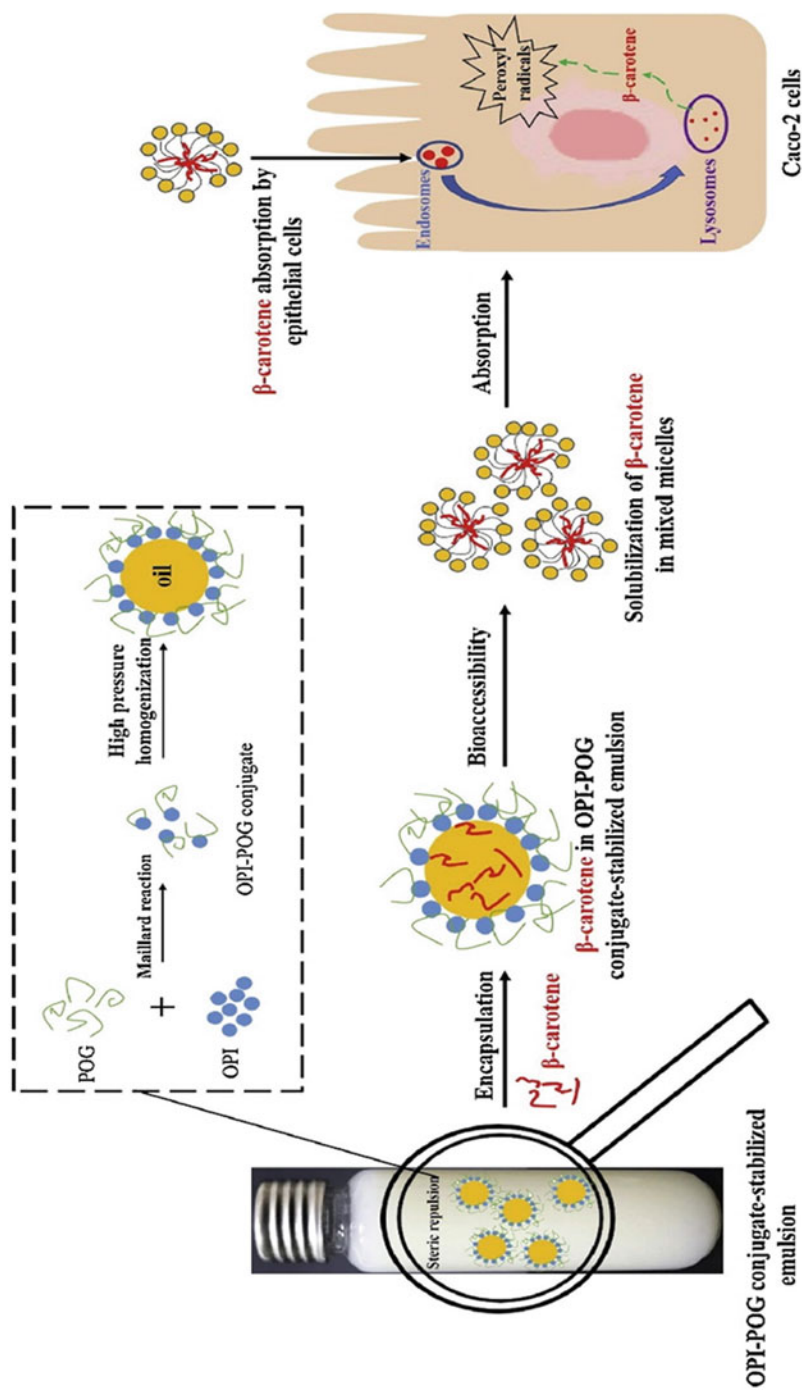


Fig. 1.3 OPI-POG conjugate-based emulsion and delivery of β -carotene to Caco-2 cells. Adapted and reprinted from Zhong et al. (2019) with permission from Elsevier, Copyright (2019)

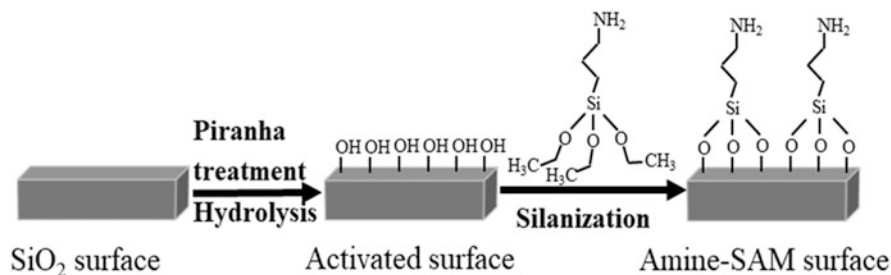


Fig. 1.4 Schematic showing silica surface modification with APTES to form amine self-assembled monolayers (SAMs)

hydrophobic moieties. PVA was utilized due to its biocompatibility and non-immunogenic nature, which is also modified according to the desired application. In this case, random acetylation with oleyl chloride was done to provide hydrophobicity to the PVA. These amphiphilic PVA NPs were successful in enhancing the water solubility and bioavailability of hydrophobic drugs (Delbecq and Kawakami 2014).

Surface modifications have been explored for the enhanced stability of the drug delivery system. In a recent study, 9-O-octadecyl-substituted berberine derivative was used for the construction of the self-assembled nano-drug, which was coated with 1,2-distearoyl-sn-glycero-3-phosphoethanolamine-N-[amino(polyethylene glycol)-2000] (DSPE-PEG 2000) for its stability enhancement. To avoid instability of this positively charged nano-drug (34.1 mV) and clearance from blood plasma, hyaluronic acid (HA) coating was done onto PEGylated surfaces as shown in Fig. 1.5. HA/PEGylated berberine nano-drug (HA/PEG/berberine-ND) showed -25.8 mV surface charge, and drug loading efficiency was $>70\%$. Tumor site is enriched in hyaluronidase (HAase), which degraded HA and re-exposed PEGylated nano-drug. This positively charged nano-drug (PEGylated) interacted with the negatively charged cell membrane, bypassed lysosome, and targeted mitochondria. Thus, the surface-modified nano-drug was found to be efficient in mitochondrial targeting (cell apoptosis) for the cancer treatment (Song et al. 2019a).

1.3.1 Role of Surface Modifications in Targeted Drug Delivery

Various macromolecules like peptides, proteins, aptamers, and protein amphiphiles (PAs) have been explored for the targeted delivery of a drug molecule (Xu et al. 2018; Mardilovich et al. 2006). Aptamers are single-stranded oligonucleotides or proteins that have high stability, specificity, and ease of manufacture compared to the conventional antibodies. Aptamers can be conjugated onto the surface of various NPs for the targeted drug delivery. Proteins show great potential as nano-carriers due to versatility, non-immunogenicity, ease of surface modification, and biocompatibility. Among proteins, albumin is the most abundant plasma protein, which is involved

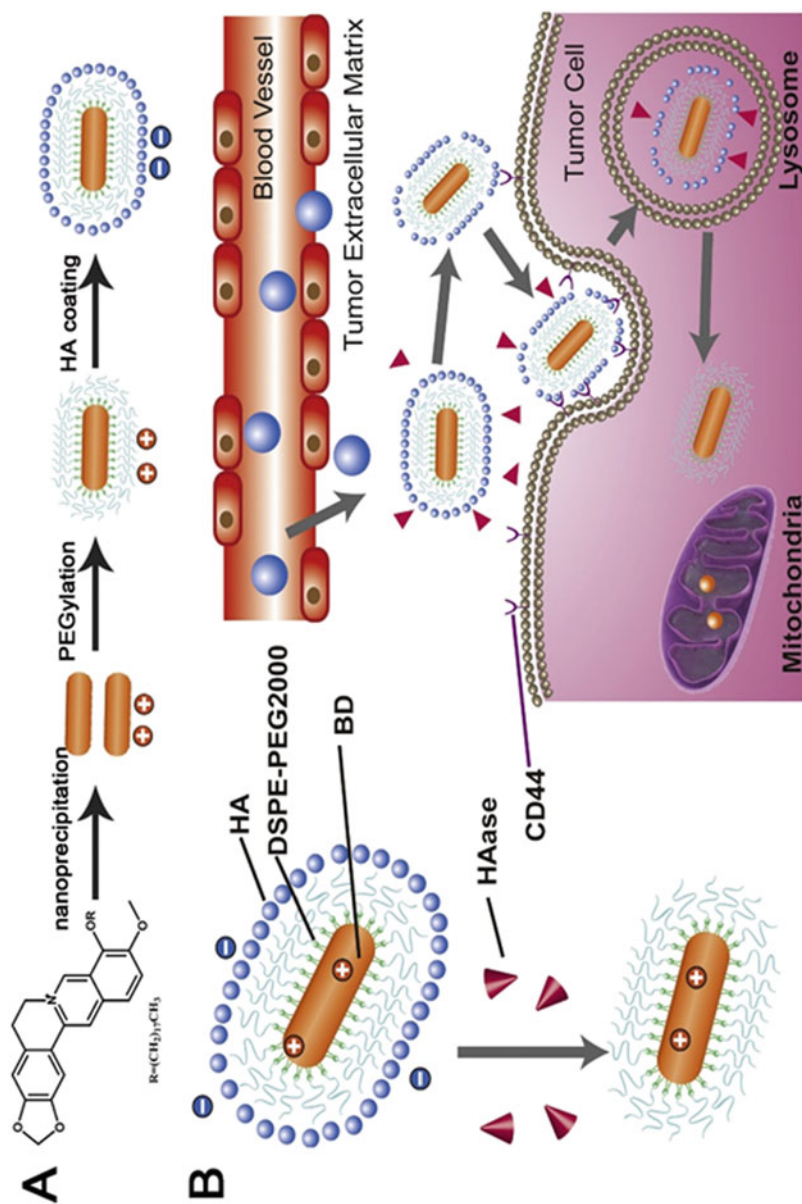


Fig. 1.5 Schematic showing the interaction of self-assembled nano-drug with mitochondria. (a) Formation of HA/PEG/berberine nano-drug, and (b) at the tumor site, HA coating was degraded by HAase followed by interaction of PEGylated nano-drug with the cell membrane. Adapted and reprinted from Song et al. (2019a) with permission from Elsevier, Copyright (2019)

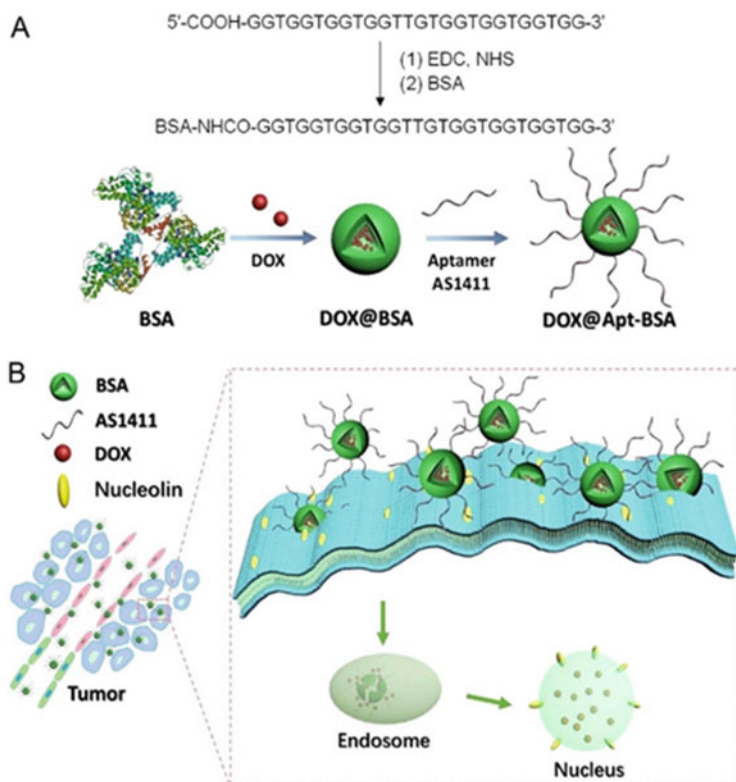


Fig. 1.6 Schematic representation of DOX@Apt-BSA NPs formation. (a) DOX triggered BSA NPs formation followed by Aptamer conjugation on the NPs surface, and (b) Aptamer AS1411 targeted over-expressed nucleolin on cancer cells resulting in the targeted DOX delivery. Adapted and reprinted from Xu et al. (2018) with permission from Elsevier, Copyright (2018)

in the maintenance of osmotic pressure and has the long-circulating ability. Albumin shows co-existence of hydrophobic and hydrophilic domains, which makes it an ideal carrier for the loading of both hydrophilic and hydrophobic drugs. Xu et al. fabricated self-assembled bovine serum albumin (BSA) NPs triggered by doxorubicin (DOX) and coupled with Aptamer AS1411 (Apt) as shown in Fig. 1.6. Aptamer AS1411 is specific against nucleolin, which is over-expressed in cancer cells. The average molar ratio of BSA and Aptamer in the above assembly was 10:1. The hydrodynamic diameters of DOX@BSA and DOX@Apt-BSA were 145 ± 2.5 nm and 163 ± 2.5 nm, respectively, which indicated successful modification with aptamer. The cell inhibition efficiency was performed against MCF-7 and showed upregulation of pBR, Bax, PARP, p21, p16, and E-cadherin. It also exhibited downregulation of Bcl-2, PCNA, EpCAM, Vimentin, MMP-9, Snail, CD133, and CD44. These observations indicated modified BSA NPs-suppressed tumor progression and metastasis (Xu et al. 2018).

Targeting the activity of common recognition motifs can be enhanced by designed PAs. In a study, stealth liposomes (PEGylated liposomes) were coupled with PR_b peptide (PAs) that resembles fibronectin (cell-binding domain) and targets integrin $\alpha_5\beta_1$. Thus, PR_b coupled with stealth liposomes was efficiently internalized into colon carcinoma cells and targeted integrin $\alpha_5\beta_1$. Another research group utilized antimicrobial peptide based on D,L-amphipathic helix motif against various cancer lines. Cancer cells express a higher level of phosphatidylserine (PS), thus imparting a higher negative charge compared to normal cells. The designed diastereomeric peptides were found to be active against both zwitterionic and negatively charged membranes, which imparted selectivity against cancer cells than normal cells. Binding of these cationic antimicrobial peptides enhanced permeability of the cancer cell membrane leading to the membrane disruption (Papo and Shai 2003).

Researchers have fabricated protease responsive peptide for drug delivery. The KLD-12 peptide contains alternating hydrophobic and hydrophilic amino acids resulting in the formation of β -sheet hydrogels in aqueous solutions (Kisiday et al. 2002). This fabricated peptide consists of protease cleavable region flanked by β -sheet motifs at both sides, which make them sensitive to proteases. The drug was loaded inside the gel matrix, which was released on enzymatic treatment (Law et al. 2006). The above system can be manipulated to release a drug on interaction with protease-associated disease. Furthermore, SAMs can be designed for pH-responsive drug delivery because of its surface chemistry. In a study, SAMs with aldehyde terminal was prepared by the Kazemi et al. on a gold substrate. Amine-based drugs such as dopamine were attached to the aldehyde functional group by imine bond formation (Fig. 1.7). This self-assembly was found to regulate the reversible release and loading of dopamine as a function of pH (3–7), which can

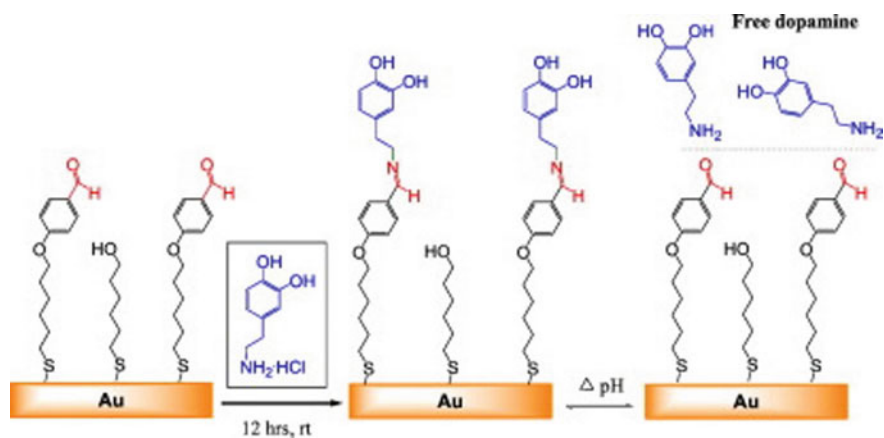


Fig. 1.7 Schematic representation of reversible loading and release of dopamine to aldehyde terminated thiol attached on a gold surface. Adapted and reprinted from Kazemi et al. (2013) with permission from Elsevier, Copyright (2013)

be explored for drug delivery and biological application. Dopamine release was found to be the highest at pH 3 (Kazemi et al. 2013).

Surface modification successfully addresses the critical issues of drug delivery like delivery of the hydrophobic drugs, the stability of drug carrier, and targeted delivery at the diseased site. Table 1.2 summarizes various surface modification strategies used for the drug delivery systems. These alternate modern-day drug delivery vehicles enhance the bioavailability of the drug by resolving the pharmacokinetics issues. Drug loading enhancement is carried out via surface modifications (silanization). Drug release is improved using a suitable coating like chitosan to the delivery vehicle. For the stability enhancement, polymers such as PEG and hyaluronic acid are of potential use. Targeted delivery is achieved by coupling the delivery vehicle with the site-specific aptamers/peptides/PAs/proteins. For such cases, the drug release is triggered via pH or enzymatic responses. Summarily, a drug delivery vehicle is fabricated depending on the type of drug molecule to be encapsulated inside or conjugated onto the surface as well as the physiological conditions and biomarkers present at the target site.

1.4 Modified Polymers-Based Drug Delivery Systems

Now a days, synthetic polymers are of increasing interest in drug delivery as a therapeutic vehicle. A polymer consists of four major mechanisms through which it gets activated to perform biointerface activities as shown in Fig. 1.8 (Wang and Dong 2015). In first simple mechanism (A), it directly attaches to the biomolecule and thereby triggering downstream cellular signals. In the second type of mechanism (B), instead of applying directly to the receptor, it binds to a growth factor and forms complexes, thus blocking or enhancing the function of the growth factor. For its enhanced third mechanism (C), polymer is engineered to conjugate ligands and form into a multivalent conjugate with high efficiency and specificity to control cell behavior and activate cellular receptors. A polymer is also encapsulated by biomolecular coronas, which redefines its function as revealed in the last mechanism (D).

The polymeric NPs have been applied to deal for various therapies like to treat or in hepatitis infection and as efficient drug delivery system (Sun et al. 2019; Verma et al. 2019). These polymeric NPs protected or encapsulated inside a core have more advantageous than direct application. Further, surface of the encapsulated NP can be functionalized by various methods, which can further be utilized to reduce nonspecific distribution, increase residence time in the blood and in some cases for targeting specific cells surface antigens with targeted ligand (aptamers, peptide, fragment, small molecule, antibody) (Bazak et al. 2015; Accardo et al. 2014).

Enhanced bioactivity of VEGF₁₆₅, being used for the treatment of peripheral arterial diseases or cardiovascular diseases, was observed by binding with isolated heparan sulfate glycotherapeutic (HS7^{+ve}) as shown in figure 2(B) (Wang et al. 2014). In another study, activation of dectin-1 was demonstrated through its binding to β -glucan polymers as shown in figure 2 (C). Dectin-1 detects β -glucans in fungal cell walls and triggers cellular antimicrobial function. It was observed that the

Table 1.2 Various surface modification strategies used for the drug delivery applications

Delivery vehicles	Modifications		Drugs	Remarks	References
	Types	Materials			
Gelatin microsphere	Crosslinker; Silane	Glutaraldehyde; GPTMS	Vancomycin	Controlled and sustained release of vancomycin	Nouri-Felekori et al. (2019)
Halloysite nanotube	Silane	APTES	Gentamicin	Used as a coupling agent to incorporate gentamicin inside halloysite nanotube	Rapacz-Kmita et al. (2019)
Fe ₃ O ₄ NPs	Silane	APTES	Methotrexate	Adsorption of drug carried out with 91% efficiency; Drug loading capacity was 55.55 mg/L, and monolayer drug adsorption occurred	Langeroudi and Binaeian (2018)
MNPs	Silane	APTES	Telmisartan (TEL)	Direct surface coupling of TEL; Retained magnetic properties; Dose-dependent effect against PC-3 cell line; Reversible conjugation; Drug release at acidic site	Dhivale et al. (2018)
Chitosan microsphere	Silane	GPTMS	Pelargonidin	Chitosan-3-glycidoxypropyltrimethoxysilane- β -glycerophosphate hybrid microspheres fabricated; Microsphere weight lose least (27–32%) at pH 7.4 and highest at pH (1.7 & 5.4)	Cruz-Neves et al. (2017)
Mesoporous silica NPs (MSN)	Silane	3-MPTMS	Epirubicin	MUC1 aptamer conjugation via disulfide bond formation; MUC1 specific against breast cancer cells (MCF7); Predrug loading MSN size 163 nm & postdrug loading size 258 nm; pH- and time-dependent delivery system	Hanafi-Bojdi et al. (2018)
MSN	Silane	Tetraethoxy silane	Insulin	Poly-(methacrylic acid-co vinyl triethoxysilane) coated MSN; Surface area was 304.4 m ² /g; Loading efficiency 39.39%; Relative bioavailability 73.10%;	Guha et al. (2016)

(continued)

Table 1.2 (continued)

Delivery vehicles	Modifications		Drugs	Remarks	References
	Types	Materials			
Fe ₃ O ₄ MSN	Silane	Alkoxy silane	Doxorubicin	Mitochondria drug targeting; Guanidinium derivative (GA) as mitochondria targeting ligand; GA coupling via alkoxy silane	Ahn et al. (2018)
Poly (ethylene glycol)-block poly (ε-caprolactone)	Vitamin	Folic acid	Methotrexate	Selective cancer cells targeting; increased higher critical micellar concentration	Brandt et al. (2019)
Polyamidoamine dendrimers	Polymer	mPEG	Carboplatin (CAR)	High entrapment efficiency; Sustained bioactive CAR release	Nguyen et al. (2019)

GPTMS Glycidyoxypropyltrimethoxysilane; APTES 3-Aminopropyltriethoxysilane; MPTMS 3-mercaptopropyltrimthoxysilane; GPTMS (3-Glycidyoxypropyl)trimethoxysilane; mPEG Methoxypolyethylene glycol

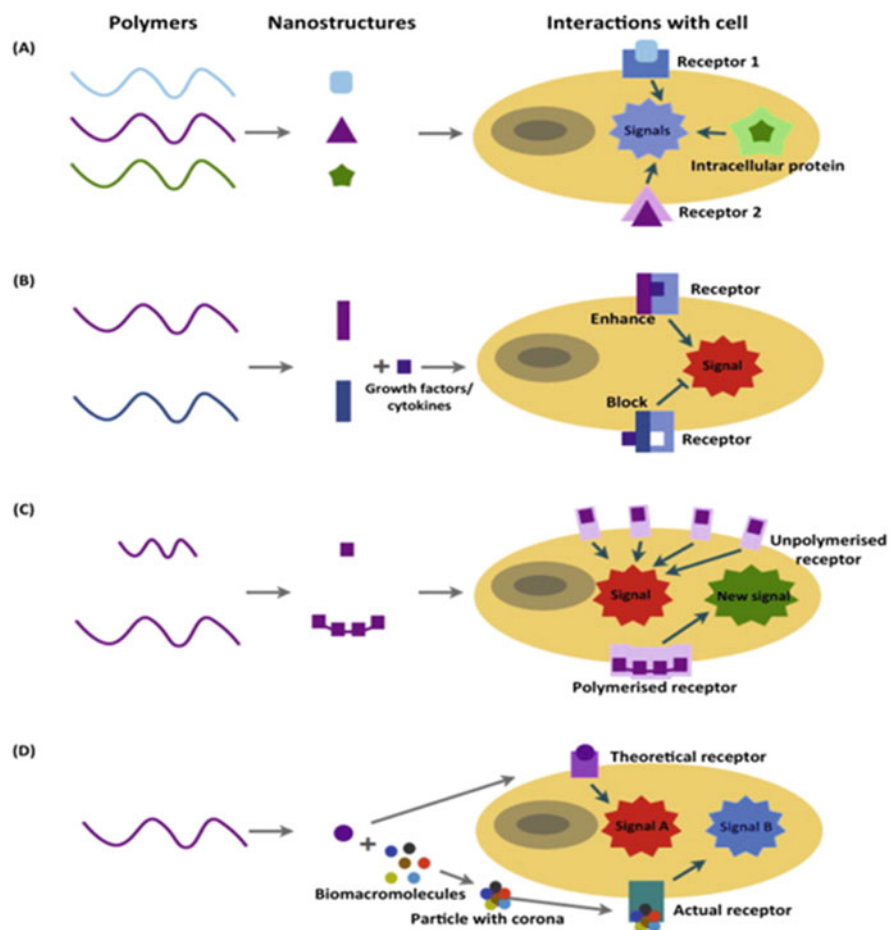


Fig. 1.8 Four mechanisms of polymer to get activated for biointerface activities. Adapted and reprinted from Wang and Dong (2015) with permission from Elsevier, Copyright (2015)

signaling of dectin-1 was activated only after binding to particulate β -glucan polymer and not to soluble polymer (Goodridge et al. 2011). Additionally, when nano-sized polymer particle gets into human body, number of biomolecules gets attached on its surface to form coronas. After which it redefines the property of the polymer and improvises targeted efficiency as shown in figure (1D) (Monopoli et al. 2012). Recently, zwitterionic polymers (sulfobetaine (SB), carboxybetaine (CB), and phosphorylcholine (PC)) have been studied as ligands to modulate protein-NPs corona formation. SB-coated NPs resulted the complete absence of protein corona, while the other two polymers-coated NPs exhibited protein adsorption (Debayle et al. 2019; Papi and Caracciolo 2018).

Natural polymers and their modifications are extensively studied materials for enhancing the therapeutic effects. These polymers are easily available and

biocompatible. Various sources for natural polymers include plants (cellulose, guar gum, karaya gum, pectin, and starch), animals (alginate, psyllium, chitin, and carrageenans), marine (agar, alginates, and carrageenans), and microbial origins (pullulan, gellan, xanthum gum, dextran, glycan, and biosurfactants) (George et al. 2019; Wali et al. 2019). Cellulose and chitosan have been extensively explored for the drug delivery applications (Edgar 2007). Cellulose esters possess desired feature for pharmaceutical requirements like stability, high water permeability, film strength, low toxicity, compatibility with wide range of activities, and ability to form micro and NPs. In addition, modifications of cellulose have been tested in literature. For example, electrospun cellulose acetate phthalate fibers for semen induced anti-HIV vaginal drug (Huang et al. 2012), hydroxypropylmethyl cellulose for cartilage tissue engineering (Talukdar et al. 1996), and cellulose nanocrystal with chitosan oligosaccharide for health care (Akhlaghi et al. 2013). Chitosan possesses similar appealing properties such as low toxicity, biodegradability, biocompatibility, and low cost of production due to its easy availability in nature. A number of researches have been explored chitosan and modified chitosan for various applications. In a study, N-[(2-hydroxy-3-trimethylammonium) propyl] chloride chitosan was synthesized to inhibit the growth of microorganisms for pharmaceutical and food industries (Shagdarova et al. 2019). In a separate study, PEG-trimethyl chitosan was used for improving the colloidal stability of polyplexes and enhanced transfection efficiency in gene delivery (Germershaus et al. 2008).

Apart from natural polymers, synthetic polymers, also referred as “Pharmapolymers” or smart polymers, have been explored for application in medicine. A significant focus has been drawn on the elegant chemistry for developing the improved macromolecules with desired physicochemical characteristics. However, complete understanding of the interplay of these synthesized materials at the interface of chemistry, biology, and medicine must be described. For example, synthetic polymers have biological action in a particular range, from food to pharmaceuticals (Hunter and Moghimi 2002). Various synthetic polymers, their characteristics, and their applications are summarized in Table 1.3. Initially PEG and its derivatives were used for the drug delivery applications due to their biocompatibility and anti-fouling properties. Each ethylene glycol in the PEG backbone strongly binds to water molecule, which bridges the ether oxygen and imparts anti-fouling character (Lüsse and Arnold 1996; Oesterhelt et al. 1999; Aray et al. 2004). However poor stability of PEG in physiological environments limited its applications. Hence, surface modification of PEG helped in improving its stability in body fluids along with facilitated targeted drug delivery (Song et al. 2019b; Gupta et al. 2019; Herranz-Diez et al. 2016; Shahabi et al. 2014). For example, PEG-PCL (polycaprolactone) copolymers have been developed and explored for various targeted drug delivery applications (Grossen et al. 2017).

Both the natural and synthetic polymers have also been integrated and tested for drug delivery applications. Recently, Hasan et al. have synthesized a nanocomposite of chitosan, polyvinylpyrrolidone (PVP), and cellulose nanowhiskers (CWC) and tested for the controlled/sustained release of a model drug (curcumin) for potential application in wound healing. Chitosan is termed as bioactive dressing and

Table 1.3 Various synthetic polymers, their characteristics, and applications for the drug delivery

Synthetic polymers	Sub classes	Identifications	Applications	References
Polyethers	PEG Poly(propylene glycol) Poly(glycerol)	<ul style="list-style-type: none"> • Ether functional group in their main chain • Lack of biodegradability 	<ul style="list-style-type: none"> • Food additive, skin healing creams and skin substitutes and pharmaceuticals • Emulsifier in food 	Herzberger et al. (2015)
Poly(ethylene imine)s	Branched poly(ethylene imine) linear poly(ethylene imine)	<ul style="list-style-type: none"> • High cationic charge densities. • Highly efficient vector for delivering oligonucleotides in vitro and in vivo 	<ul style="list-style-type: none"> • In tissue culture • Promoter attachment • Transfection reagent 	Boussif et al. (1995)
Polyesters	Poly(caprolactone) Poly(lactic acid) and poly(glycolic acid) Poly(oxalate)s Poly(butylene terephthalate)	<ul style="list-style-type: none"> • Semi-crystalline aliphatic polyester • Soluble in several solvents • Tunable degradation properties 	<ul style="list-style-type: none"> • Drug delivery systems, sutures • Long-term implants • Adhesion barriers as well as new tissue scaffold host systems 	Englert et al. (2018)
Polycarbonates	Poly(oxalate) Poly(butylene terephthalate) Poly(γ -glutamic acid)	<ul style="list-style-type: none"> • Nontoxic degradation products • Biocompatibility • Absence of autocatalytic degradation processes 	<ul style="list-style-type: none"> • Intracellular delivery of anticancer drugs 	Zhang et al. (2013), Seyednejad et al. (2011), Guo et al. (2019)
Polyamino acid	Different functionalities such as ionic or stimuli-responsive side group can be easily formed	<ul style="list-style-type: none"> • Exhibit a good biodegradability and excellent biocompatibility 	<ul style="list-style-type: none"> • Cancer treatment 	Mauro et al. (2019)
Poly(peptoids)s	Poly- β -peptoids Poly- γ -peptoids	<ul style="list-style-type: none"> • Side chain with amid nitrogen. 	<ul style="list-style-type: none"> • Excitation antibodies production 	
Poly(N-acrylamide)s	Poly-N-2-hydroxypropyl-methacrylamide Poly-N-isopropyl-acrylamide	<ul style="list-style-type: none"> • Amide at side chain • Severe toxic 	<ul style="list-style-type: none"> • Lung cancer 	Havanur et al. (2019)

(continued)

Table 1.3 (continued)

Synthetic polymers	Sub classes	Identifications	Applications	References
Polysiloxanes	Poly-dimethylsiloxane	<ul style="list-style-type: none"> • Silicon and oxygen atoms having two alkyl or aryl moieties • Permeable, flexible, low gas transition temperature 	<ul style="list-style-type: none"> • In coating technology as target. • Vascular surgery 	Xu et al. (2019)
Poly-methacrylates	Polyacrylic acid Polymethacrylic acid Poly-methyl methacrylate	<ul style="list-style-type: none"> • Methacrylic acid and acrylic acid or their esters 	<ul style="list-style-type: none"> • Stimuli-sensitive drug • Tissue engineering • Gene therapy 	Arya et al. (2018), Havanur et al. (2019)
Polyolefins	Polypropylene Polybutene polyethylene	<ul style="list-style-type: none"> • Alkene or olefin as monomer • With minimum one C-C double bond 	<ul style="list-style-type: none"> • Packaging Industries to preserve food. • Antifouling coating 	Zaikov et al. (1999), Francolini et al. (2017)

accelerates wound healing by macrophage activation, granulation, and promotion of inflammatory cells infiltration. PVP holds potential for a sustained drug release from drug-conjugated matrices. CWC acts as nanofillers and regulates controlled drug release via modulating the swelling behavior of composite. The synthesized composite exhibited controlled drug release (biphasic release profile) along with excellent antibacterial activities and biocompatibility (Hasan et al. 2017).

1.5 Conclusion and Future Perspectives

In recent decades, drug delivery has proven its effectiveness in the field of therapeutics with the advancement in the technologies. Various drug delivery systems showed development in the preparation techniques, strategies of delivery, tuning of materials, and thus resulted in improved pharmacokinetics, biocompatibility, and bioavailability. Limiting drug molecules to the specific diseased site has resulted in reduced side effects and high efficiency. Controlling interaction of carrier systems with the biological fluid determines the fate of drug molecules as drug delivery is an interfacial phenomenon. Surface properties like surface energy, hydrophobicity, and surface charges regulate the bio-interfacial interactions. Modifying surface properties helps to achieve optimum interaction with biological systems to avoid adverse effects. Incorporation of target-specific ligands to these carrier systems enables the transport of the loaded drug molecules to the desired site and their

release in the vicinity of diseased tissues. Ligand attachment to carrier molecules is carried through some functional groups or some other modifications. Such modifications are possible to achieve by applying polymers, SAMs, and other approaches such as enclosed carriers like nanoemulsion and encapsulations. Polymeric surface modifications offer anchoring of drug molecules over the surface for the optimum loading with controlled delivery. While SAMs provide protections to drug molecules in according to the hydrophobic conditions of the local environment and offer different functionalities over the surfaces, which facilitate the delivery of the hydrophobic drugs, stability of drug carrier, and targeted delivery. Emulsion-based drug delivery systems deliver hydrophobic drugs by encapsulation and hence resolving solubility issues for such drugs.

However, there are yet some bottlenecks in the practical applications of drug delivery systems which need to be resolved to achieve the optimum and safe delivery. Retention of carrier systems in the body, undesired interactions, and stability of the drug molecules after the release are the major issues in the success of drug delivery systems. Emulsion systems have problems with short shelf life and unstable structure. The range of pH and temperature may cause disturbance of the emulsion structure. SAMs and polymeric modifications over the surface may vary with time and thus require high stability. Targeting of carrier systems to the desired site requires highly specific ligand with high affinity. Designing and attachment of such ligands to delivery systems is a challenge for successful delivery of drug molecules. Researches on such aspects are expected to improve the potential of drug delivery systems for the assured treatments and therapies.

References

- Accardo A, Aloj L, Aurilio M, Morelli G, Tesaro D (2014) Receptor binding peptides for target-selective delivery of nanoparticles encapsulated drugs. *Int J Nanomedicine* 9:1537–1557
- Aditya N, Aditya S, Yang H, Kim HW, Park SO, Ko S (2015) Co-delivery of hydrophobic curcumin and hydrophilic catechin by a water-in-oil-in-water double emulsion. *Food Chem* 173:7–13
- Agnihotri J, Saraf S, Khale A (2011) Targeting: new potential carriers for targeted drug delivery system. *Int J Pharm Sci Rev Res* 8(2):117–123
- Ahmad N, Ramsch R, Llinàs M, Solans C, Hashim R, Tajuddin HA (2014) Influence of nonionic branched-chain alkyl glycosides on a model nano-emulsion for drug delivery systems. *Colloids Surf B Biointerfaces* 115:267–274
- Ahn J, Lee B, Choi Y, Jin H, Lim NY, Park J, Kim JH, Bae J, Jung JH (2018) Non-peptidic guanidinium-functionalized silica nanoparticles as selective mitochondria-targeting drug nanocarriers. *J Mater Chem* 6(36):5698–5707
- Akhlaghi SP, Berry RC, Tam KC (2013) Surface modification of cellulose nanocrystal with chitosan oligosaccharide for drug delivery applications. *Cellulose* 20(4):1747–1764
- Andrade J, Nagaoka S, Cooper S, Okano T, Kim S (1987) Surfaces and blood compatibility current hypotheses. *ASAIO Journal* 33(2):75
- Aray Y, Marquez M, Rodríguez J, Vega D, Simon-Manso Y, Coll S, Gonzalez C, Weitz DA (2004) Electrostatics for exploring the nature of the hydrogen bonding in polyethylene oxide hydration. *J Phys Chem B* 108(7):2418–2424

- Arya G, Kumari RM, Sharma N, Gupta N, Chandra R, Nimesh S (2018) Polymeric nanocarriers for site-specific gene therapy. In: Drug targeting and stimuli sensitive drug delivery systems. Elsevier, Oxford, pp 689–714
- Bae YH, Park K (2011) Targeted drug delivery to tumors: myths, reality and possibility. *J Control Release* 153(3):198
- Baimark Y, Srisuwan Y (2014) Preparation of alginate microspheres by water-in-oil emulsion method for drug delivery: effect of Ca²⁺ post-cross-linking. *Adv Powder Technol* 25 (5):1541–1546
- Bazak R, Hourri M, El Achy S, Kamel S, Refaat T (2015) Cancer active targeting by nanoparticles: a comprehensive review of literature. *J Cancer Res Clin Oncol* 141(5):769–784. <https://doi.org/10.1007/s00432-014-1767-3>
- Binder L, Klang V, Rezaei SS, Neuer O, Zhang Z, Lunter DJ, Wolzt M, Valenta C (2019) Topical application of highly concentrated water-in-oil emulsions: physiological skin parameters and skin penetration in vivo-A pilot study. *Int J Pharm* 571:118694
- Bohley M, Haunberger A, Goepferich AM (2019) Intracellular availability of poorly soluble drugs from lipid nanocapsules. *Eur J Pharm Biopharm* 139:23–32
- Boussif O, LezoualC'H F, Zanta MA, Mergny MD, Scherman D, Demeneix B, Behr JP (1995) A versatile vector for gene and oligonucleotide transfer into cells in culture and in vivo: polyethylenimine. *P Natl Acad Sci USA* 92(16):7297–7301
- Brandt JV, Piazza RD, dos Santos CC, Vega-Chacón J, Amantéa BE, Pinto GC, Magnani M, Piva HL, Tedesco AC, Primo FL (2019) Synthesis and colloidal characterization of folic acid-modified PEG-b-PCL micelles for methotrexate delivery. *Colloids Surf B Biointerfaces* 177:228–234
- Buckton G (2000) *Interfacial phenomena in drug delivery and targeting*. CRC Press, Boca Raton
- Calderó G, Montes R, Llinàs M, García-Celma M, Porrás M, Solans C (2016) Studies on the formation of polymeric nano-emulsions obtained via low-energy emulsification and their use as templates for drug delivery nanoparticle dispersions. *Colloids Surf B Biointerfaces* 145:922–931
- Chen X, Zou L, Liu W, McClements DJ (2016) Potential of excipient emulsions for improving quercetin bioaccessibility and antioxidant activity: an in vitro study. *J Agric Food Chem* 64 (18):3653–3660
- Choi YH, Han H-K (2018) Nanomedicines: current status and future perspectives in aspect of drug delivery and pharmacokinetics. *Int J Pharm Investig* 48(1):43–60
- Costa P, Lobo JMS (2001) Modeling and comparison of dissolution profiles. *Eur J Pharm Sci* 13 (2):123–133
- Couvreur P, Grislain L, Lenaerts V, Brasseur F, Guiot P, Biernacki A (2018) Biodegradable polymeric nanoparticles as drug carrier for antitumor agents. In: *Polymeric nanoparticles and microspheres*. CRC Press, Boca Raton, pp 27–94
- Cruz-Neves S, Shirotsaki Y, Miyazaki T, Hayakawa S (2017) Characterization and degradation study of chitosan-siloxane hybrid microspheres synthesized using a microfluidic approach. *Mater Sci Eng C* 81:571–579
- Dallin BC, Van Lehn RC (2019) Spatially heterogeneous water properties at disordered surfaces decrease the hydrophobicity of nonpolar self-assembled monolayers. *J Phys Chem Lett* 10 (14):3991–3997
- Debayle M, Balloul E, Dembele F, Xu X, Hanafi M, Ribot F, Monzel C, Coppey M, Fragola A, Dahan M, Pons T, Lequeux N (2019) Zwitterionic polymer ligands: an ideal surface coating to totally suppress protein-nanoparticle corona formation? *Biomaterials* 219:119357
- Delbecq F, Kawakami K (2014) Self-assembly study and formation of hydrophobized PVA dense and stable nanoparticles loaded with cholesterol or a steroid-type drug. *J Colloid Interface Sci* 428:57–62
- Dhavale R, Waifalkar P, Sharma A, Sahoo SC, Kollu P, Chougale A, Zahn D, Salvan G, Patil P, Patil P (2018) Monolayer grafting of aminosilane on magnetic nanoparticles: an efficient approach for targeted drug delivery system. *J Colloid Interface Sci* 529:415–425

- Edgar KJ (2007) Cellulose esters in drug delivery. *Cellulose* 14(1):49–64
- El-Aasser M, Miller C, Asua J (1997) *Polymeric dispersions: principles and applications*. Kluwer Academic Publishers, Dordrecht
- Englert C, Brendel JC, Majdanski TC, Yildirim T, Schubert S, Gottschaldt M, Windhab N, Schubert US (2018) *Pharmapolymers in the 21st century: synthetic polymers in drug delivery applications*. *Prog Polym Sci* 87:107–164
- Fan X, Zhang C, D-b L, Yan J, Liang H-p (2013) The clinical applications of curcumin: current state and the future. *Curr Pharm Des* 19(11):2011–2031
- Fornaguera C, Dols-Perez A, Caldero G, Garcia-Celma M, Camarasa J, Solans C (2015a) PLGA nanoparticles prepared by nano-emulsion templating using low-energy methods as efficient nanocarriers for drug delivery across the blood–brain barrier. *J Control Release* 211:134–143
- Fornaguera C, Feiner-Gracia N, Calderó G, García-Celma M, Solans C (2015b) Galantamine-loaded PLGA nanoparticles, from nano-emulsion templating, as novel advanced drug delivery systems to treat neurodegenerative diseases. *Nanoscale* 7(28):12076–12084
- Francolini I, Vuotto C, Piozzi A, Donelli G (2017) Antifouling and antimicrobial biomaterials: an overview. *APMIS* 125(4):392–417
- Gan N, Sun Q, Zhao L, Tang P, Suo Z, Zhang S, Zhang Y, Zhang M, Wang W, Li H (2019) Protein corona of metal-organic framework nanoparticles: study on the adsorption behavior of protein and cell interaction. *Int J Biol Macromol* 140:709–718
- Gavhane YN, Yadav AV (2012) Loss of orally administered drugs in GI tract. *Saudi Pharm J* 20(4):331–344
- George A, Shah PA, Shrivastav PS (2019) Natural biodegradable polymers based nano-formulations for drug delivery: a review. *Int J Pharm* 561:244–264
- Germershaus O, Mao S, Sitterberg J, Bakowsky U, Kissel T (2008) Gene delivery using chitosan, trimethyl chitosan or polyethyleneglycol-graft-trimethyl chitosan block copolymers: establishment of structure–activity relationships in vitro. *J Control Release* 125(2):145–154
- Gonçalves V, Rodríguez-Rojo S, Matias A, Nunes A, Nogueira I, Nunes D, Fortunato E, de Matos AA, Cocero M, Duarte C (2015) Development of multicore hybrid particles for drug delivery through the precipitation of CO₂ saturated emulsions. *Int J Pharm* 478(1):9–18
- Goodridge HS, Reyes CN, Becker CA, Katsumoto TR, Ma J, Wolf AJ, Bose N, Chan ASH, Magee AS, Danielson ME, Weiss A, Vasilakos JP, Underhill DM (2011) Activation of the innate immune receptor Dectin-1 upon formation of a ‘phagocytic synapse’. *Nature* 472:471
- Grossen P, Witzigmann D, Sieber S, Huwyler J (2017) PEG-PCL-based nanomedicines: a biodegradable drug delivery system and its application. *J Control Release* 260:46–60
- Guha A, Biswas N, Bhattacharjee K, Sahoo N, Kuotsu K (2016) pH responsive cylindrical MSN for oral delivery of insulin-design, fabrication and evaluation. *Drug Deliv* 23(9):3552–3561
- Gumus CE, Davidov-Pardo G, McClements DJ (2016) Lutein-enriched emulsion-based delivery systems: impact of Maillard conjugation on physicochemical stability and gastrointestinal fate. *Food Hydrocoll* 60:38–49
- Guo Z, Liu X, Chen Z, Hu J, Yang L (2019) New liquid crystal polycarbonate micelles for intracellular delivery of anticancer drugs. *Colloids Surf B Biointerfaces* 178:395–403
- Gupta V, Mohiyuddin S, Sachdev A, Soni PK, Gopinath P, Tyagi S (2019) PEG functionalized zirconium dicarboxylate MOFs for docetaxel drug delivery in vitro. *J Drug Deliv Sci Technol* 52:846–855
- Habibi N, Kamaly N, Memic A, Shafiee H (2016) Self-assembled peptide-based nanostructures: smart nanomaterials toward targeted drug delivery. *Nano Today* 11(1):41–60
- Hanafi-Bojd MY, Moosavian Kalat SA, Taghdisi SM, Ansari L, Abnous K, Malaekheh-Nikouei B (2018) MUC1 aptamer-conjugated mesoporous silica nanoparticles effectively target breast cancer cells. *Drug Dev Ind Pharm* 44(1):13–18
- Hasan A, Pandey LM (2015) Polymers, surface-modified polymers, and self assembled monolayers as surface-modifying agents for biomaterials. *Polymer Plast Tech Eng* 54(13):1358–1378

- Hasan A, Pandey LM (2016) Kinetic studies of attachment and re-orientation of octyltriethoxysilane for formation of self-assembled monolayer on a silica substrate. *Mater Sci Eng C* 68:423–429
- Hasan A, Waibhaw G, Tiwari S, Dharmalingam K, Shukla I, Pandey LM (2017) Fabrication and characterization of chitosan, polyvinylpyrrolidone, and cellulose nanowiskers nanocomposite films for wound healing drug delivery application. *J Biomed Mater Res A* 105(9):2391–2404
- Hasan A, Pattanayek SK, Pandey LM (2018a) Effect of functional groups of self-assembled monolayers on protein adsorption and initial cell adhesion. *ACS Biomater Sci Eng* 4(9):3224–3233
- Hasan A, Saxena V, Pandey LM (2018b) Surface functionalization of Ti6Al4V via self-assembled monolayers for improved protein adsorption and fibroblast adhesion. *Langmuir* 34(11):3494–3506
- Hasan A, Waibhaw G, Pandey LM (2018c) Conformational and organizational insights into serum proteins during competitive adsorption on self-assembled monolayers. *Langmuir* 34(28):8178–8194
- Havanur S, Batish I, Cheruku SP, Gourishetti K, PE JB, Kumar N (2019) Poly(N,N-diethyl acrylamide)/functionalized graphene quantum dots hydrogels loaded with doxorubicin as a nano-drug carrier for metastatic lung cancer in mice. *Mater Sci Eng C* 105:110094
- Helgeson ME (2016) Colloidal behavior of nanoemulsions: interactions, structure, and rheology. *Curr Opin Colloid Interface Sci* 25:39–50
- Herranz-Diez C, Mas-Moruno C, Neubauer S, Kessler H, Gil FJ, Pegueroles M, Manero JM, Guillem-Marti J (2016) Tuning mesenchymal stem cell response onto titanium–niobium–hafnium alloy by recombinant fibronectin fragments. *ACS Appl Mater Interfaces* 8(4):2517–2525
- Herzberger J, Niederer K, Pohlit H, Seiwert J, Worm M, Wurm FR, Frey H (2015) Polymerization of ethylene oxide, propylene oxide, and other alkylene oxides: synthesis, novel polymer architectures, and bioconjugation. *Chem Rev* 116(4):2170–2243
- Herzi S, Essafi W (2019) Crystallizable W/O/W double emulsions made with milk fat: formulation, stability and release properties. *Food Res Int* 116:145–156
- Huang C, Soenen SJ, van Gulck E, Vanham G, Rejman J, Van Calenbergh S, Vervaeet C, Coenye T, Verstraelen H, Temmerman M (2012) Electrospun cellulose acetate phthalate fibers for semen induced anti-HIV vaginal drug delivery. *Biomaterials* 33(3):962–969
- Hunter AC, Moghimi SM (2002) Therapeutic synthetic polymers: a game of Russian roulette? *Drug Discov Today* 7(19):998–1001
- Israelachvili JN (2015) Intermolecular and surface forces. Academic Press, Amsterdam
- Jaiswal M, Dudhe R, Sharma P (2015) Nanoemulsion: an advanced mode of drug delivery system. *3 Biotech* 5(2):123–127
- Kale SN, Deore SL (2017) Emulsion micro emulsion and nano emulsion: a review. *Sys Rev Pharm* 8(1):39
- Kazemi SH, Alizadeh A, Mohamadi R, Khodaei MM, Kordestani D (2013) pH-regulated release of dopamine from well-ordered self-assembled monolayers: electrochemical studies. *Mater Sci Eng C* 33(8):5095–5099
- Kisiday J, Jin M, Kurz B, Hung H, Semino C, Zhang S, Grodzinsky A (2002) Self-assembling peptide hydrogel fosters chondrocyte extracellular matrix production and cell division: implications for cartilage tissue repair. *Proceed Nat Acad Sci* 99(15):9996–10001
- Lang JC (1995) Ocular drug delivery conventional ocular formulations. *Adv Drug Deliv Rev* 16(1):39–43
- Langer R (1990) New methods of drug delivery. *Science* 249(4976):1527–1533
- Langeroudi MP, Binaeian E (2018) Tannin-APTES modified Fe₃O₄ nanoparticles as a carrier of Methotrexate drug: kinetic, isotherm and thermodynamic studies. *Mater Chem Phys* 218:210–217
- Langevin D (1992) Micelles and microemulsions. *Annu Rev Phys Chem* 43(1):341–369

- Law B, Weissleder R, Tung C-H (2006) Peptide-based biomaterials for protease-enhanced drug delivery. *Biomacromolecules* 7(4):1261–1265
- Leal-Calderon F, Schmitt V, Bibette J (2007) *Emulsion science: basic principles*. Springer Science & Business Media, New York
- Leininger R (1972) Polymers as surgical implants. *CRC Crit Rev Bioeng* 1(3):333–381
- Li C WJ, Wang Y, Gao H, Wei G, Huang Y, Yu H, Gan Y, Wang Y, Mei L, Chen H, Hu H, Zhang Z, Jin Y (2019) Recent progress in drug delivery. *Acta Pharm Sin B*.
- Lima AC, Song W, Blanco-Fernandez B, Alvarez-Lorenzo C, Mano JF (2011) Synthesis of temperature-responsive dextran-MA/PNIPAAm particles for controlled drug delivery using superhydrophobic surfaces. *Pharm Res* 28(6):1294–1305
- Liu F, Ma C, Zhang R, Gao Y, McClements DJ (2017) Controlling the potential gastrointestinal fate of β -carotene emulsions using interfacial engineering: impact of coating lipid droplets with polyphenol-protein-carbohydrate conjugate. *Food Chem* 221:395–403
- Llinàs M, Calderó G, García-Celma MJ, Patti A, Solans C (2013) New insights on the mechanisms of drug release from highly concentrated emulsions. *J Colloid Interface Sci* 394:337–345
- Lovelyn C, Attama AA (2011) Current state of nanoemulsions in drug delivery. *J Biomater Nanobiotechnol* 2(05):626
- Lu W-C, Huang D-W, Wang C-C, Yeh C-H, Tsai J-C, Huang Y-T, Li P-H (2018) Preparation, characterization, and antimicrobial activity of nanoemulsions incorporating citral essential oil. *J Food Drug Anal* 26(1):82–89
- Lüsse S, Arnold K (1996) The interaction of poly (ethylene glycol) with water studied by ¹H and ²H NMR relaxation time measurements. *Macromolecules* 29(12):4251–4257
- Mahon E, Salvati A, Bombelli FB, Lynch I, Dawson KA (2012) Designing the nanoparticle–biomolecule interface for “targeting and therapeutic delivery”. *J Control Release* 161 (2):164–174
- Mardilovich A, Craig JA, McCammon MQ, Garg A, Kokkoli E (2006) Design of a novel fibronectin-mimetic peptide–amphiphile for functionalized biomaterials. *Langmuir* 22 (7):3259–3264
- Mason TG, Wilking JN, Meleson K, Chang CB, Graves SM (2006) Nanoemulsions: formation, structure, and physical properties. *J Phys Condens Matter* 18(41):R635
- Mauro N, Scialabba C, Puleio R, Varvarà P, Licciardi M, Cavallaro G, Giammona G (2019) SPIONs embedded in polyamino acid nanogels to synergistically treat tumor microenvironment and breast cancer cells. *Int J Pharm* 555:207–219
- Mehta TJ, Patel A, Patel MR, Patel N (2011) Need of colon specific drug delivery system: review on primary and novel approaches. *IJPRD* 3(1):134–153
- Minekus M, Alminger M, Alvito P, Ballance S, Bohn T, Bourlieu C, Carriere F, Boutrou R, Corredig M, Dupont D (2014) A standardised static in vitro digestion method suitable for food: an international consensus. *Food Funct* 5(6):1113–1124
- Monopoli MP, Åberg C, Salvati A, Dawson KA (2012) Biomolecular coronas provide the biological identity of nanosized materials. *Nat Nanotechnol* 7:779. <https://doi.org/10.1038/nnano.2012.207>
- Nandivada P, Fell GL, Gura KM, Puder M (2016) Lipid emulsions in the treatment and prevention of parenteral nutrition–associated liver disease in infants and children. *Am J Clin Nutr* 103 (2):629S–634S
- Nguyen DH, Bach LG, Nguyen Tran D-H, Cao VD, Nguyen TNQ, Le TTH, Tran TT, Thi TTH (2019) Partial surface modification of low generation polyamidoamine dendrimers: gaining insight into their potential for improved carboplatin delivery. *Biomolecules* 9(6):214
- Nouri-Felekori M, Khakbiz M, Nezafati N, Mohammadi J, Eslaminejad MB (2019) Comparative analysis and properties evaluation of gelatin microspheres crosslinked with glutaraldehyde and 3-glycidoxypropyltrimethoxysilane as drug delivery systems for the antibiotic vancomycin. *Int J Pharm* 557:208–220
- Nyberg S, Abbott NJ, Shi X, Steyger PS, Dabdoub A (2019) Delivery of therapeutics to the inner ear: the challenge of the blood-labyrinth barrier. *Sci Transl Med* 11(482):eaao0935

- Oosterhelt F, Rief M, Gaub H (1999) Single molecule force spectroscopy by AFM indicates helical structure of poly (ethylene-glycol) in water. *New J Phys* 1(1):6
- Packham DE (2003) Surface energy, surface topography and adhesion. *Int J Adhes Adhes* 23 (6):437–448
- Pandey LM, Pattanayek SK (2013) Properties of competitively adsorbed BSA and fibrinogen from their mixture on mixed and hybrid surfaces. *Appl Surf Sci* 264:832–837
- Pandey LM, Pattanayek SK, Delabouglise D (2013) Properties of adsorbed bovine serum albumin and fibrinogen on self-assembled monolayers. *J Phys Chem C* 117(12):6151–6160
- Pandey S, Senthilguru K, Uvanesh K, Sagiri S, Behera B, Babu N, Bhattacharyya M, Pal K, Banerjee I (2016) Natural gum modified emulsion gel as single carrier for the oral delivery of probiotic-drug combination. *Int J Biol Macromol* 92:504–514
- Pangeni R, Kang S-W, Oak M, Park EY, Park JW (2017) Oral delivery of quercetin in oil-in-water nanoemulsion: in vitro characterization and in vivo anti-obesity efficacy in mice. *J Funct Foods* 38:571–581
- Papi M, Caracciolo G (2018) Principal component analysis of personalized biomolecular corona data for early disease detection. *Nano Today* 21:14–17
- Papo N, Shai Y (2003) New lytic peptides based on the D, L-amphipathic helix motif preferentially kill tumor cells compared to normal cells. *Biochemistry* 42(31):9346–9354
- Park K (2014) Controlled drug delivery systems: past forward and future back. *J Control Release* 190:3–8
- Prajapati SK, Jain A, Jain A, Jain S (2019) Biodegradable polymers and constructs: a novel approach in drug delivery. *Eur Polymer J* 120:109191
- Qi X, Wang L, Zhu J, Hu Z, Zhang J (2011) Self-double-emulsifying drug delivery system (SDEDDS): a new way for oral delivery of drugs with high solubility and low permeability. *Int J Pharm* 409(1–2):245–251
- Rapacz-Kmita A, Foster K, Mikołajczyk M, Gajek M, Stodolak-Zych E, Dudek M (2019) Functionalized halloysite nanotubes as a novel efficient carrier for gentamicin. *Mater Lett* 243:13–16
- Sari T, Mann B, Kumar R, Singh R, Sharma R, Bhardwaj M, Athira S (2015) Preparation and characterization of nanoemulsion encapsulating curcumin. *Food Hydrocoll* 43:540–546
- Saxena V, Hasan A, Sharma S, Pandey LM (2018) Edible oil nanoemulsion: an organic nanoantibiotic as a potential biomolecule delivery vehicle. *Int J Polym Mater Polym Biomater* 67(7):410–419
- Seyednejad H, Ghassemi AH, van Nostrum CF, Vermonden T, Hennink WE (2011) Functional aliphatic polyesters for biomedical and pharmaceutical applications. *J Control Release* 152 (1):168–176
- Shagdarova B, Lunkov A, Il'ina A, Varlamov V (2019) Investigation of the properties of N-[(2-hydroxy-3-trimethylammonium) propyl] chloride chitosan derivatives. *Int J Biol Macromol* 124:994–1001
- Shahabi S, Najafi F, Majdabadi A, Hooshmand T, Haghbin Nazarpak M, Karimi B, Fatemi SM (2014) Effect of gamma irradiation on structural and biological properties of a PLGA-PEG-hydroxyapatite composite. *Sci World J* 2014:420616
- Shakeel F, Haq N, Al-Dhfyani A, Alanazi FK, Alsarra IA (2014) Double w/o/w nanoemulsion of 5-fluorouracil for self-nanoemulsifying drug delivery system. *J Mol Liq* 200:183–190
- Sharma N, Agarwal D, Gupta M, Khinchi M (2011) A comprehensive review on floating drug delivery system. *Int J Pharm Biomed Res* 2(2):428–441
- Song Z, Liu T, Chen T (2018) Overcoming blood–brain barrier by HER2-targeted nanosystem to suppress glioblastoma cell migration, invasion and tumor growth. *J Mater Chem B* 6 (4):568–579
- Song J, Lin C, Yang X, Xie Y, Hu P, Li H, Zhu W, Hu H (2019a) Mitochondrial targeting nanodrugs self-assembled from 9-O-octadecyl substituted berberine derivative for cancer treatment by inducing mitochondrial apoptosis pathways. *J Control Release* 294:27–42

- Song X, Wang J, Xu Y, Shao H, Gu J (2019b) Surface-modified PLGA nanoparticles with PEG/LA-chitosan for targeted delivery of arsenic trioxide for liver cancer treatment: inhibition effects enhanced and side effects reduced. *Colloids Surf B Biointerfaces* 180:110–117
- Sonneville-Aubrun O, Simonnet J-T, L'allouret F (2004) Nanoemulsions: a new vehicle for skincare products. *Adv Colloid Interface Sci* 108:145–149
- Sun D, Zhuang X, Xiang X, Liu Y, Zhang S, Liu C, Barnes S, Grizzle W, Miller D, Zhang H-G (2010) A novel nanoparticle drug delivery system: the anti-inflammatory activity of curcumin is enhanced when encapsulated in exosomes. *Mol Ther* 18(9):1606–1614
- Sun X, Dong S, Li X, Yu K, Sun F, Lee RJ, Li Y, Teng L (2019) Delivery of siRNA using folate receptor-targeted pH-sensitive polymeric nanoparticles for rheumatoid arthritis therapy. *Nanomedicine* 20:102017
- Szegedi Á, Shestakova P, Trendafilova I, Mihayi J, Tsacheva I, Mitova V, Kyulavska M, Koseva N, Momekova D, Konstantinov S (2019) Modified mesoporous silica nanoparticles coated by polymer complex as novel curcumin delivery carriers. *J Drug Deliv Sci Technol* 49:700–712
- Tadros T, Izquierdo P, Esquena J, Solans C (2004) Formation and stability of nano-emulsions. *Adv Colloid Interface Sci* 108:303–318
- Talukdar MM, Michael A, Rombaut P, Kinget R (1996) Comparative study on xanthan gum and hydroxypropylmethyl cellulose as matrices for controlled-release drug delivery I. Compaction and in vitro drug release behaviour. *Int J Pharm* 129(1–2):233–241
- Urtti A (2006) Challenges and obstacles of ocular pharmacokinetics and drug delivery. *Adv Drug Deliv Rev* 58(11):1131–1135
- van der Graaf S, Schroën C, Boom R (2005) Preparation of double emulsions by membrane emulsification—a review. *J Membr Sci* 251(1–2):7–15
- Verma R, Sahu R, Singh DD, Egbo TE (2019) A CRISPR/Cas9 based polymeric nanoparticles to treat/inhibit microbial infections. *Semin Cell Dev Biol* 96:44–52
- Wali AF, Majid S, Rasool S, Shehada SB, Abdulkareem SK, Firdous A, Beigh S, Shakeel S, Mushtaq S, Akbar I, Madhkali H, Rehman MU (2019) Natural products against cancer: review on phytochemicals from marine sources in preventing cancer. *Saudi Pharm J* 27(6):767–777
- Wang C, Dong L (2015) Exploring 'new' bioactivities of polymers at the nano-bio interface. *Trends Biotechnol* 33(1):10–14
- Wang C, Poon S, Murali S, Koo C-Y, Bell TJ, Hinkley SF, Yeong H, Bhakoo K, Nurcombe V, Cool SM (2014) Engineering a vascular endothelial growth factor 165-binding heparan sulfate for vascular therapy. *Biomaterials* 35(25):6776–6786
- Wang C, Liu Z, Xu G, Yin B, Yao P (2016) BSA-dextran emulsion for protection and oral delivery of curcumin. *Food Hydrocoll* 61:11–19
- Washington C (1996) Stability of lipid emulsions for drug delivery. *Adv Drug Deliv Rev* 20(2–3):131–145
- Xiao H, Yan L, Dempsey EM, Song W, Qi R, Li W, Huang Y, Jing X, Zhou D, Ding J (2018) Recent progress in polymer-based platinum drug delivery systems. *Prog Polym Sci* 87:70–106
- Xu L, He X-Y, Liu B-Y, Xu C, Ai S-L, Zhuo R-X, Cheng S-X (2018) Aptamer-functionalized albumin-based nanoparticles for targeted drug delivery. *Colloids Surf B Biointerfaces* 171:24–30
- Xu Y, Li M, Liu M (2019) Corrosion and fouling behaviors of phosphatized Q235 carbon steel coated with fluorinated polysiloxane coating. *Prog Org Coat* 134:177–188
- Yang HJ, Park IS, Na K (2009) Biocompatible microspheres based on acetylated polysaccharide prepared from water-in-oil-in-water (W1/O/W2) double-emulsion method for delivery of type II diabetic drug (exenatide). *Colloids Surf Physicochem Eng Aspects* 340(1–3):115–120
- Ying L, Tahara K, Takeuchi H (2013) Drug delivery to the ocular posterior segment using lipid emulsion via eye drop administration: effect of emulsion formulations and surface modification. *Int J Pharm* 453(2):329–335
- Zaikov G, Gumargalieva K, Polishchuk AY, Adamyan A, Vinokurova T (1999) Biodegradation of polyolefins biomedical applications. *Polymer Plast Tech Eng* 38(4):621–646

- Zhang Y, Chan HF, Leong KW (2013) Advanced materials and processing for drug delivery: the past and the future. *Adv Drug Deliv Rev* 65(1):104–120
- Zhao Y, Zhang J, Wang Q, Li J, Han B (2011) Water-in-oil-in-water double nanoemulsion induced by CO₂. *Phys Chem Chem Phys* 13(2):684–689
- Zhong L, Ma N, Wu Y, Zhao L, Ma G, Pei F, Hu Q (2019) Gastrointestinal fate and antioxidation of β -carotene emulsion prepared by oat protein isolate-*Pleurotus ostreatus* β -glucan conjugate. *Carbohydr Polym* 221:10–20



Tissue Engineering Strategies for Tooth and Dento-alveolar Region with Engineered Biomaterial and Stem Cells

2

Siddhartha Das, Vivek P. Soni, and Jayesh R. Bellare

Abstract

This chapter summarizes the progress made in the therapeutic application of adult multipotent stem cells, in conjunction with biomaterials for regeneration of whole tooth and associated structures. The management of edentulous space and alveolar bone resorption, following extraction of tooth or periodontal pathology, represents a major challenge in clinical dentistry. Additionally, the precise role of surface topography and its chemical constituents for dental implants in the dynamics of osseointegration and alveolar bone regeneration (used for replacing those missing teeth) remains poorly understood. Hence, a broader therapeutic strategy, involving interdisciplinary knowledge-based approach from scientist to clinicians, is essential for the development of engineered nanostructure biomaterials with exogenous or endogenous mesenchymal stem cells for translating the evolved cross-disciplinary concepts into clinical application and products.

S. Das

Department of Biosciences and Bioengineering, Indian Institute of Technology Bombay, Mumbai, India

Department of Chemical Engineering, Indian Institute of Technology Bombay, Mumbai, India

V. P. Soni

Department of Biosciences and Bioengineering, Indian Institute of Technology Bombay, Mumbai, India

J. R. Bellare (✉)

Department of Chemical Engineering, Indian Institute of Technology Bombay, Mumbai, India

Wadhvani Research Centre for Bioengineering (WRCB), Indian Institute of Technology Bombay, Mumbai, India

e-mail: jb@iitb.ac.in

Keywords

Tissue engineering · Scaffolds · Mesenchymal stem cells · Periodontium · Alveolar bone · Dental implant

2.1 Introduction

Edentulism (partial/complete) may arise from incidence related to dental caries (Dye et al. 2015), periodontitis (Pihlstrom et al. 2005), maxillo-facial trauma (Wiens 1990), malignancies (Zeng et al. 2013), etc., resulting in undesirable consequences such as irreversible alveolar bone resorption (Atwood 1971) leading to a decrease in height and width of alveolar bone (Allen and McMillan 2003), impaired masticatory function (Helkimo et al. 1977), objectionable aesthetics and phonetics (Roumanas 2009), decreased postural control (Yoshida et al. 2009) and impaired proprioception (Ghi and McGivney 1979), to name a few. In physiological environment, the healthy functioning tooth provides crucial stimulus to alveolar bone necessary for its development and maintenance (Misch 2004). In events related to tooth loss, gradual resorption and remodelling of the alveolar bone occurs leading to atrophic edentulous ridges (Misch 2004) which further results in changes in natural jaw relationship, facial musculature and facial morphology (Cawood and Howell 1991; Sutton et al. 2004), thus affecting the oral function and facial form (Sutton et al. 2004) (Fig. 2.1). As mentioned earlier, alveolar bone loss is also a common occurrence in case of

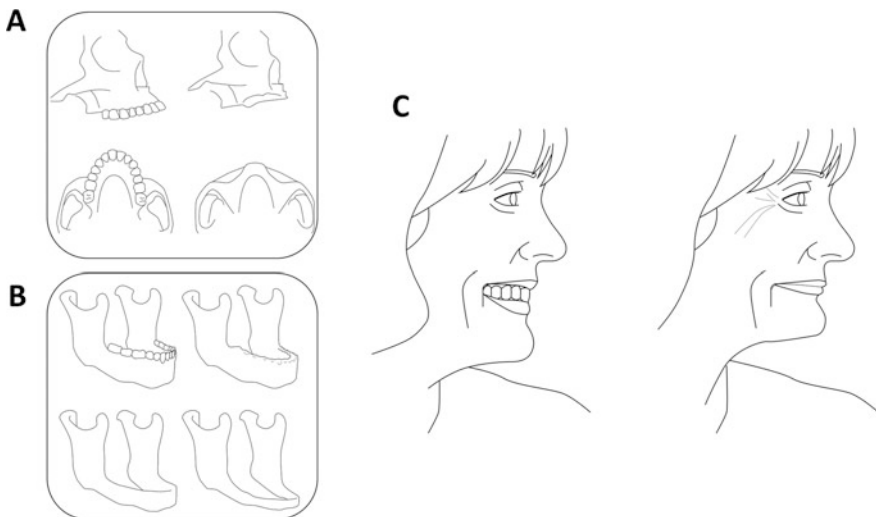


Fig. 2.1 Alveolar bone resorption. (a) In maxilla, the crest of the edentulous ridge had shifted palatally with an overall decrease in the vertical height of the ridge. (b) The most pronounced resorption in the mandible are noted on superior surface and in the posterior lingual surface of the ridge. (c) Changes in facial profile in relation to alveolar ridge resorption. (Adapted and redrawn from Nobel Biocare AG)

periodontitis (Cochran 2008). Of note, statistics from epidemiological studies have further confirmed the higher incidence of periodontitis associated with tooth mortality (Ong 1998) and alveolar bone loss (Edman et al. 2015) in adult population. Hence, in the past, several strategies have been outlined in the literature for alveolar ridge preservation (ARP) like root retention (Osburn 1974), socket grafting with deproteinized bovine bone mineral (Artzi and Nemcovsky 1998), socket filling with autologous bone, bone substitutes and bioactive materials (Darby et al. 2009). Advantageously, it was also noted that the prosthesis on osseointegrated implants provide a different stimulus on alveolar bone when compared to conventional denture resulting in a maximum of 0.1 mm marginal bone loss, annually (Lindquist et al. 1988). However, as stated by many authors, majority of these literature based on ARP have limitations and do not substantially translate into clinically relevant conclusions (Hämmerle et al. 2012, Ten Hegeler et al. 2011; Horváth et al. 2013; Vittorini Orgeas et al. 2013).

The recent advances in stem cell technology, biomaterials and scaffold fabrication-based research has led to the emergence of advanced tissue engineering options used for preservation/regeneration of maxillo-mandibular complex circumventing the traditional drawbacks of conventional replacement therapies such as autografts, allografts or xenografts (Oryan et al. 2014; Chai and Leong 2007). Further, the ethical concern free with significantly less risk of malignant disease development; adult mesenchymal stem cells (MSCs) (Wei et al. 2013b) with biomaterials (Sekula and Zuba-Surma 2018) have emerged as a remarkable prospect for tissue engineering-based applications (Egusa et al. 2012). These emerging stem cell-based technologies that facilitates regeneration of complete/partial tooth structure (Ikeda et al. 2009; Sonoyama et al. 2006), periodontium (Pagni 2016) and alveolar bone (Kim et al. 2009b) with various studies focused on surface kinetics of dental implants for optimal alveolar bone integration (Le Guéhennec et al. 2007; Das et al. 2018) are receiving considerable attention owing to their multifaceted prospect in management of maxillo-mandibular pathologies. As a result, there is a gradual and progressive transition towards the application-oriented mindset, leading to various pioneered works related to the manufacturing process as per good manufacturing practices (GMPs) further assessing the safety, efficacy and quality control of products used for regenerative therapies for dental tissues (Nakashima and Iohara 2017; Nakashima et al. 2017).

Hence, this chapter reviews the current strategies and explores the therapeutic potentials of different biomaterials and dental stem cells in relation to their implication towards potential clinical applications. Therefore, we have attempted to selectively choose relevant concepts and methodological approaches rather than a comprehensive review from the rapidly evolving and vast domain of regenerative medicine, biomaterials and tissue engineering. Further, we hope that the cluster of information could be used as an effective approach, specifically directed towards development of regenerative therapeutics in dento-alveolar region.

2.2 Tooth Regeneration

Apart from speech (Johnson and Sandy 1999) and aesthetics (Dong et al. 1999), teeth along with their investing structures are among the most vital components of masticatory system (Orchardson and Cadden 1998). The adverse consequences related to tooth loss and edentulism have been well-documented elsewhere (Emami et al. 2013). Hence, prosthetic considerations for replacing missing teeth are of significant importance (Carr and Brown 2010) (Shillingburg et al. 2012) (Misch 2004). Yet, varying degrees of limitations and disadvantages are often associated with the current prosthetic treatment options involving removable partial dentures (Hall 2013), fixed partial dentures (Misch 2004) and dental implants (Taylor 1998). Thus, deriving the benefits from immense advances in stem cell biology and biomaterials, exploration of numerous achievable regenerative approaches like induction of odontogenesis (Modino and Sharpe 2005) and bioengineering tooth and dental tissues have been attempted (Ohazama et al. 2004; Yen and Sharpe 2008). Based on our understandings, there are multiple approaches documented in the literature employed for complete/partial tooth regeneration and could be broadly summarized into—(1) complete tooth regeneration with specialized cells obtained from in vitro embryonic tooth development process and implanted in vivo; (2) cultured cells with polymers for in vivo implantation for complete tooth regeneration and (3) partial regeneration of tooth with bioactive materials, stem cells and polymers.

2.2.1 Whole Tooth Regeneration

Based on the principle that development of tooth involves complex epithelial–mesenchymal interaction as a prerequisite (Thesleff and Hurmerinta 1981), Ohazama, A. et al. showed that odontogenesis could be initiated through recombination of non-dental-cells-derived mesenchyme and embryonic oral epithelium; further, in vivo transplantation of such explants gave rise to teeth (crowns) and associated structures (Ohazama et al. 2004). In another study, recombinant explants (i.e. stem cells from embryo and adult mice were covered by embryonic epithelium obtained from mouse embryos) provided evidence of odontogenic events in vitro and also when transplanted in the maxilla of adult mice (Modino and Sharpe 2005). Mina M et al. reported that non-odontogenic epithelium may induce odontogenesis in instances related to the interaction of mandibular mesenchyme and mandibular epithelium (Mina and Kollar 1987). Findings also suggests that mature tooth structures could be bioengineered from cultured tooth bud cells of rat (Duailibi et al. 2004). Komine, Akihiko et al. bioengineered tooth germs with dental epithelial and mesenchymal cells, which later formed structures similar to teeth in vivo (Komine et al. 2007). In the past, literature describes the method for formation of structurally correct tooth from bioengineered tooth germ (Nakao et al. 2007). Recent studies also show that dissociated odontogenic cells were involved in the formation of dentine and bone in canine jaw (Honda et al. 2006). Scaffold composed of gelatin-

chondroitin-hyaluronan-tri-copolymer with swine dental bud cells also gave rise to dental tissue complex when autografted in alveolar socket (Kuo et al. 2008). Young et al. reported positive findings when he tested the feasibility of tooth regeneration by using cells isolated from porcine third molar tooth bud onto biodegradable polymeric scaffolds such as those fabricated from polyglycolate/poly-L-lactate (PGA/PLLA) and implanted in vivo (Young et al. 2002). He also emphasized the concept of tooth-bone hybrid tissues engineering, where tooth bud cells and osteoblast induced from bone marrow progenitor cells were seeded in polyglycolide (PGA) and polyglycolide-colactide (PLGA) scaffolds and PLGA-fused wafer scaffold, respectively, later harvested, sutured together, reimplanted and grown in the omenta of adult rat host to regenerate respective tissues (Young et al. 2005). Interestingly, a recently published report discusses about an erupted and occluded bioengineered tooth into the alveolus of an adult mouse accomplished by transplantation of bioengineered tooth germ (Ikeda et al. 2009). Masamitsu Oshima et al. reported that engrafted bioengineered tooth unit in a murine model exhibited tooth and periodontal ligament (PDL)-related functions (Oshima et al. 2011).

2.2.2 Partial Tooth Regeneration

Although, the concept of whole tooth regeneration appears to be relatively simple in proposition, the dynamics and highly complex biology of the dental cells and tissues together as a unit makes the feasibility potential far from straight forward (Sonoyama et al. 2006). Hence, as suggested by many authors, the focus has to be rather on clinical significance in devising a strategy appropriate for a relevant and high treatment outcome. Clinically, an artificial/prosthetic or natural crown is supported by the root of tooth, indicating that regeneration of a physiologically functional tooth root could be a more viable option (Yuan et al. 2011). Taking note of the above-perceived notion, Wataru Sonoyama et al. transplanted stem cells isolated from periodontium and apical papilla of human teeth to regenerate root, which was later found to be competent enough for supporting a porcelain crown in minipig model (Sonoyama et al. 2006). Likewise, in another study, BoYang et al. used dental follicle cells in treated dentine matrix (TDM) from human, for regeneration of tooth root, when implanted subcutaneously into the dorsum of mice (Yang et al. 2012). Baohui Ji et al. in their study showed that combined use of platelet-rich fibrin (PRF) and TDM leads to regeneration of tooth root by cell homing when transplanted orthotopically in beagle dogs (Ji et al. 2014). Interestingly, a bio-root was formed by using allogenic dental stem cells and Vit C-induced PDL cell sheet with root shape hydroxyapatite tricalcium phosphate scaffold in swine for artificial crown restoration (Wei et al. 2013a). Recent findings also suggests that, aligned PLGA/Gelatin electrospun sheet (APES), TDM and native dental pulp extracellular matrix (DPEM) seeded with stem cells regenerate tooth-root-like tissues in porcine jaws (Chen et al. 2015). Weihua Guo et al. claimed that an inductive alveolar fossa microenvironment with dental follicle stem cells (DFCs) and TDM scaffolds could be utilized for regeneration of tooth root (Guo et al. 2012). In spite of all the exciting

advances, strategies to successfully regenerate fully functional tooth roots have *achieved no* concrete results.

Furthermore, much effort has been made lately to regenerate dentine or dentine/pulp complex as the approach is viewed as crucial for successful engineering of bio-root (Na et al. 2016). Study indicates that when implanted intramuscularly, hydroxyapatite ceramic (HAC) granules and dental papilla cells gave rise to structures comparable to tooth root and pulp tissues (Holtgrave and Donath 1995). Likewise, cells isolated from pulp tissues in the presence of β -glycerophosphate gave rise to structures comparable to human dentine matrix (About et al. 2000). Experimental studies also confirm about the formation of dentine and pulp-like tissues upon transplantation of dental pulp stem cells (DPSCs) in immunocompromised mice (Gronthos et al. 2000). Sakai VT et al. suggested that tubular dentine could be formed when MSCs from deciduous teeth were seeded in tooth slice/scaffolds and implanted subcutaneously into immunodeficient mice (Sakai et al. 2010). Similarly, formation of ectopic dentine and associated pulp tissues upon transplantation of DPSCs in mice was also reported (Gronthos et al. 2002). Findings further suggest that cultured rat tooth bud cells in PGA/PLLA and PLGA scaffolds implanted into the jaws of adult rat hosts can form organized bioengineered dental tissues containing dentine, enamel, pulp and PDL (Duailibi et al. 2008). Huang, George T-J et al. reported the formation of pulp and dentine-like tissue when stem cells/progenitor cells from apical papilla and dental pulp stem cells were seeded onto synthetic scaffolds consisting of poly-D,L-lactide/glycolide and subsequently were inserted into the tooth fragments placed in mouse model (Huang et al. 2009). Y. Zheng et al. documented the benefits of using porcine deciduous pulp stem cells/progenitor cells in beta-tricalcium phosphate (β -TCP) scaffold for dentine regeneration (Zheng et al. 2012). In another study, autologous pulp stem cells and stromal cell-derived factor-1 were transplanted into a root canal displayed pulp and dentine regeneration (Iohara et al. 2011). Some studies relate the use of triacrylate polymers (Vining et al. 2018), propolis (Ahangari et al. 2012), magnesium-containing nanostructured hybrid scaffolds (Qu et al. 2014), PLLA nanofibrous microspheres (NF-MS) with bone morphogenetic protein-2 (BMP-2) (Wang et al. 2016), biphasic calcium phosphate scaffold (AbdulQader et al. 2013), gelatin hydrogels with fibroblast growth factor-2 (Ishimatsu et al. 2009), lithium chloride (Ishimoto et al. 2015), etc., in the promotion of dentine regeneration.

Recent therapeutic strategies under investigation for dentine regeneration also includes the use of acellular matrix, largely due to its biological recognition and comparable features to native tissues (Dhandayuthapani et al. 2011; Kim 2018). Level of evidence shows that human dental follicle cells in human-treated dentine matrix is suitable for dentine regeneration (Li et al. 2011). Moreover, Liang Jiao et al. stated that cryopreserved dentine matrix will safeguard the effectiveness of dentinogenesis-related proteins in the bio-scaffold (Jiao et al. 2014). Related studies further shows that bioactive molecules such as bone morphogenetic protein (BMP), transforming growth factor β 1 (TGF- β 1) and extracted soluble dentine matrix protein result in enhanced dentine formation (Luiz de Oliveira da Rosa et al. 2017; Nakashima 2005). In another case, BMP2-treated 3D pellet culture of pulp cells on

amputated pulp induced formation of reparative dentine (Iohara et al. 2004). Of late, it was also noted that the scaffold geometry and shape determine the type of dental tissue regeneration when seeded with dental pulp-derived cells (Tonomura et al. 2010). However, as stated by Weihua Guo et al., majority of these experimental studies have issues on regenerating prefabricated-shaped dentine (Guo et al. 2009). Limitations like exogenous cell transplantation (Sakai et al. 2010) and possible risk of mutation, contamination or infection associated with cell-based therapies for pulp–dentine regeneration could additionally pose technical challenges (Huang et al. 2013).

2.3 Periodontal Regeneration

The priority of regenerative periodontal therapy is to reconstruct tooth's functional periodontium, alveolar bone and related connective tissue attachments (Sculean et al. 2008). Apart from serving as a supporting and anchoring tissue between the tooth and alveolar bone, periodontium is also known for its proprioceptive mechanism (Willis and DiCosimo 1979). As discussed in earlier sections, the higher prevalence of periodontitis with corresponding tooth loss has prompted clinicians to solicit novel regenerative strategies.

Approaches under periodontal therapy includes periodontal surgery (Caton et al. 1980), bone graft/substitutes (Reynolds et al. 2010), growth factors (Darby and Morris 2013) and barrier membranes (Bottino et al. 2012). Studies show that periodontal surgical techniques like modified Widman flap procedure had no significant effect on restoring connective tissue attachments (Caton et al. 1980) (Caton and Nyman 1980). Conversely, the abilities of various growth factors for enhancing the regenerative potentials of stem cells in the periodontium are studied extensively. Earlier studies have documented the combine use of recombinant human (rh) platelet-derived growth factor (PDGF) and (rh) insulin-like growth factor-I (IGF-I) in the management of periodontal osseous defects in humans (Howell et al. 1997). The beneficial effect of recombinant human bone morphogenetic protein-2 (rhBMP-2) in an absorbable sponge (ACS) for periodontal regeneration was also documented (Selvig et al. 2002). However, there are still important issues to be addressed for utilizing various growth factors such as negating the incidence of tooth ankylosis and excessive bone formation in relation to the use of BMPs, etc., to name a few. Literature also indicates the extensive use of other alternatives like bone grafts to enhance treatment effects and outcome (clinical attachment, regeneration of new bone, cementum and periodontium, etc.) (Schallhorn 1977; Brunsvold and Mellonig 1993). Various bone grafting materials like freeze-dried bone allografts (FDBA) (Quattlebaunr et al. 1988), demineralized freeze-dried bone allografts (DFDBA) (Russell et al. 1997), Deproteinized bovine bone matrix (DBBM) (Sartori et al. 2003), bioactive glass (Schepers et al. 1991), tricalcium phosphate (TCP) (Shetty and Han 1991), enamel matrix derivatives (EMD) (Miron et al. 2016) and platelet-rich plasma (PRP) (Plachokova et al. 2008) are either used alone or in combination with various growth factors for regenerative therapies (Orsini et al.

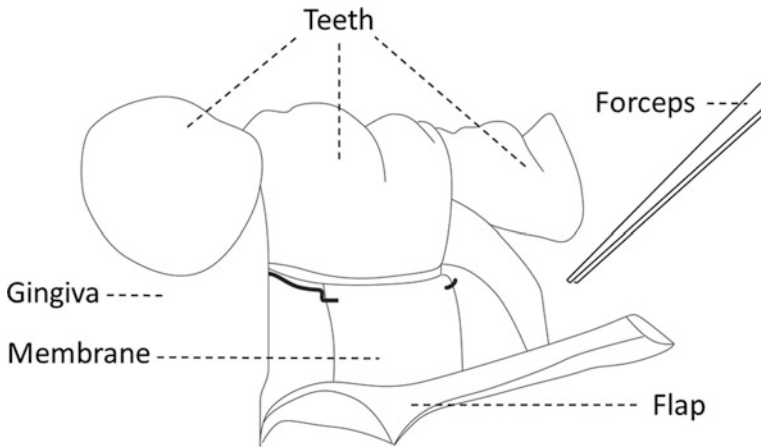


Fig. 2.2 Guided tissue regeneration with barrier membranes. Placement of a physical barrier between the gingival flap (reflected) and the defect before flap repositioning and suturing allows desired cell population to regenerate targeted tissue while preventing gingival epithelium and connective tissue (undesirable cells) from contacting the space created by the barrier

2018). However, as stated by Dieter d. Bosshardt et al., the limitations for majority of these bone filler materials is the absence of “biologic rationale” in relation to the regeneration of lost connective tissue attachment or periodontium (Bosshardt and Sculean 2009). In addition, methods such as barrier techniques for guided tissue regeneration of periodontal tissues have been reported (Tatakis et al. 1999). These barriers like Gore-tex[®] membrane and Millipore[®] filter are placed on the denuded root surface for the preferential proliferation of PDL cells which later amounts to favourable connective tissue attachments (Gottlow et al. 1986) (Karring et al. 1993) (Fig. 2.2). Nevertheless, there are numerous published studies suggesting potential limitations associated with these conventional membranes (Bottino et al. 2012; Villar and Cochran 2010). Other tissue engineering approaches like cell sheets (Hasegawa et al. 2005; Akizuki et al. 2005; Flores et al. 2008; Iwata et al. 2009) and implanting 3D scaffold seeded with stem cells/progenitor cells in the defect site has also been explored (Bartold et al. 2000) (Nakahara et al. 2004; Liu et al. 2008). However, the favourable/anticipated outcome of these approaches are not always ensured (Orsini et al. 2018) and satisfied regeneration are hardly observed (Iwata et al. 2009). In a recent in vivo study, 3D printed, micropatterned polycaprolactone (PCL) scaffolds with mesoscale and microscale architectural cues were investigated for regeneration of bone–ligament–cementum complex (Pilipchuk et al. 2016).

2.4 Alveolar Bone Regeneration

Earlier studies have established the correlation between the patterns of root and alveolar bone growth associated with development and eruption of teeth (Kenney and Ramfjord 1969). This complex connection between the teeth and jaw is interfaced by periodontium (Nanci 2017). As discussed earlier, alveolar bone resorption as a consequence of periodontal diseases (Schei et al. 1959) and tooth loss (Pietrokovski and Massler 1967) represents a significant clinical problem. Hence, treatment strategies for regenerating/restoring alveolar bone mass is of vital importance (Hämmerle and Jung 2003). Several treatment modalities such as autogenous bone grafts (Peleg et al. 2010), grafts with titanium mesh (Rocuzzo et al. 2004), β -phase tricalcium phosphate (Zerbo et al. 2001), bioabsorbable membranes (Lekovic et al. 1998), collagen type I matrices seeded with cells (Xiao et al. 2003), rhBMP-2 (Wikesjö et al. 1999) and adenoviral vector-loaded chitosan/collagen scaffolds encoding human BMPs (Zhang et al. 2007) for regeneration of alveolar bone has been reported. Further, recent reports highlight newer avenues such as understanding the importance of hierarchical organization of a material or tissue in relation to its corresponding functionality, leading to the development of novel functional materials (Elsharkawy and Mata 2018) such as those in protein-mediated mineralization process and could be utilized towards hard tissue repair (Elsharkawy et al. 2018).

In the past, Bruder et al. used human BMSCs loaded onto a ceramic carrier for bone regeneration in critical size bone defects in adult athymic rats (Bruder et al. 1998b). Bruder et al. also demonstrated the usefulness of autologous MSCs loaded onto porous ceramic cylinders composed of hydroxyapatite and β -tricalcium phosphate ceramic in the healing of critical-sized segmental defects in the femora of adult female dogs (Bruder et al. 1998a). In another study, nano-hydroxyapatite/gelatin and carboxymethylated chitin (n-HA/gel/CMC) scaffold construct was used in critical size defects of rabbits (Sagar et al. 2013). PLLA/Gelatin/hydroxyapatite (HA) scaffolds (Jaiswal et al. 2013a, b) and 3D printed gelatin/carboxymethylchitin/hydroxyapatite (HA) composite gel constructs were also reported to be beneficial in bone regenerative approaches (Gupta et al. 2019). Apart from these, incorporation of silver nanoparticles (AgNPs) on cellulose nanowhiskers (Hasan et al. 2018c) and similar studies (Hasan et al. 2017) indicates a beneficial antimicrobial role of such scaffolds towards bone tissue engineering.

Further, Yamada et al. documented the use of platelet-rich plasma (PRP) as an autologous scaffold with in vitro-expanded MSCs as an osteogenic bone substitute (Yamada et al. 2004). It has also been demonstrated that dental pulp cells (DPCs) seeded onto collagen scaffold repair alveolar defects (d'Aquino et al. 2009). In another study, a combination of β -tricalcium phosphate and PRP was used to enhance alveolar bone regeneration in beagle dogs (Suba et al. 2004). Recently, in a very interesting finding, conditioned medium from bone marrow-derived mesenchymal stem cells (MSC-CM) was found to have osteogenic features promoting alveolar bone regeneration (Katagiri et al. 2016). Yet, numerous published articles express several noted potential limitations that warrant consideration. Study

performed by Arrington ED et al. discussed the associated major and minor complications with autologous bone grafts (Arrington et al. 1996). A recent review article also discussed the morbidity and a number of complications associated with autologous bone grafts (Dimitriou et al. 2011). Additionally, biomaterials like collagen grafts used for bone regeneration are known for their potential immunogenicity and poor structural support (Giannoudis et al. 2005). Synthetic bone substitutes like coral-derived hydroxyapatite also showed unsatisfactory clinical results with incidental inflammatory foreign body reactions (Giannoudis et al. 2005). Furthermore, studies have demonstrated the incidence of severe inflammatory response and cyst-like bone formation in relation to the use of growth factors such as BMPs (Zara et al. 2011).

2.5 Dental Implants

The clinical success of dental implants in edentulous and partially edentulous patients has been studied extensively (Adell et al. 1990; Lekholm et al. 1994). Given the fact that numerous studies on dental implant suggests predictable and frequent success with osseointegration (Smith and Zarb 1989), they are used substantially as a reliable treatment option for edentulism and to replace the lost anatomical structures of orofacial region. *“Osseointegration implies a firm, direct and lasting connection between vital bone and screw-shaped titanium implants of defined finish and geometry-fixtures. Thus, there is no interposed tissue between fixture and bone. Osseointegration can only be achieved and maintained by a gentle surgical installation technique, a long healing time and a proper stress distribution when in function”* (Adell et al. 1981). Further, over the years, the number of dental implants has increased manifold (Le Guéhennec et al. 2007), suggesting the numerous advantages of dental implant have been acknowledged and established (Jivraj and Chee 2006).

The quality of osseointegration depends on the surface properties of titanium implants (Le Guéhennec et al. 2007). Implant surface properties such as surface chemistry, nanoscale features, wettability and porosity have been proposed to influence clinical performances (Das et al. 2018). Thus, there have been many attempts to modify surface topography of dental implants to evoke a favourable bone bio-response for enhanced osseointegration (Marco et al. 2005; Anil et al. 2011). G Zhao et al. reported that submicron-scale structure on titanium (Ti) surfaces affects osteoblast response (Zhao et al. 2006). In another study, sandblasted and acid etched implant surface demonstrated good clinical performance (Kim et al. 2008). Additionally, plasma sprayed coatings of hydroxylapatite (De Groot et al. 1987), anodization (Park et al. 2007), fluoride treatment (Ellingsen et al. 2004), bisphosphonates (Kurth et al. 2005), statins (Yang et al. 2011a), growth factors (Liu et al. 2007), proteins (Raphel et al. 2016), self-assembled layers (Hasan et al. 2018a, b; Pandey and Pattanayek 2011), etc., are evaluated to establish ideal surface nanotopography towards enhanced osseointegration. Interestingly, in a recent proof of concept trial, biodegradable osteogenic nanofibres coated titanium implant

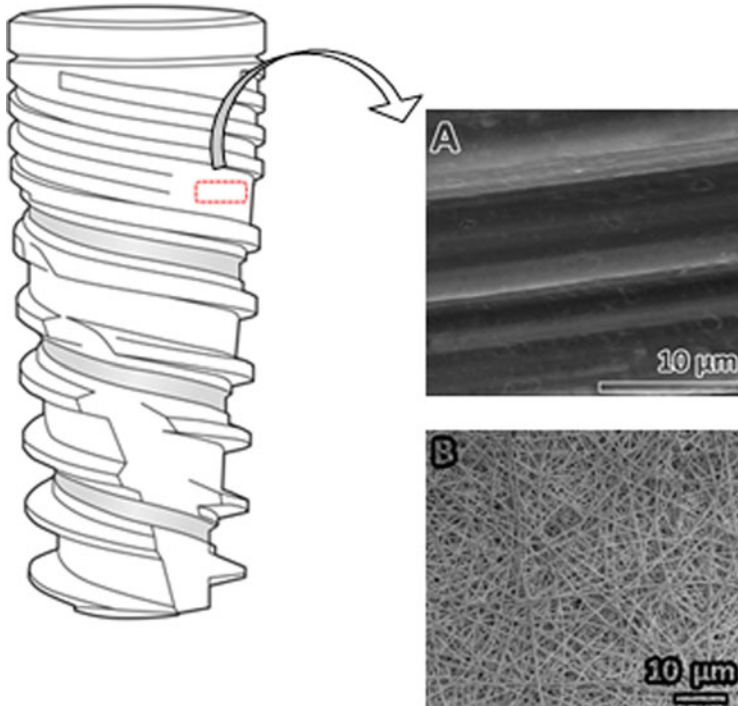


Fig. 2.3 Surface modification of dental implants such as uncoated pure titanium implant (a) is coated with osteogenic nanofibres (b) for improved osseointegration. (Adapted and redrawn from Ditrion dental implant systems)

showed enhanced osseointegration suggesting nanofibrous coated implants may serve as an ideal anchorage modules (Das et al. 2018) (Fig. 2.3).

However, in dental implant osseointegration, PDL; a specialized connective (Seo et al. 2004) and proprioceptive attachment (Jacobs and van Steenberghe 1994) that links tooth cementum and alveolar bone is missing (Lee et al. 2017). Thus, attempts have been made to compensate the current sequence of events for conventional “bone—integrated implants” by incorporating functional PDL connection onto titanium implants. Fortunately, numerous experimental studies have provided the basis for regeneration of periodontium around titanium implants (Buser et al. 1990). Studies in monkeys show that hollow titanium plasma sprayed implants close to retained root tips were surrounded by regenerated cementum and PDL with perpendicularly oriented collagen fibres (Buser et al. 1990). In a similar study, PDL formation was noted in self-tapping, screw-type titanium dental implants (Warrer et al. 1993). A case report further discusses the formation of continuous layer of cementum on the implant surface in contact with retained root residue (Guarnieri et al. 2002). Other approaches such as approximating a tooth-to-implant contact (Jahangiri et al. 2005; Urabe et al. 2000) and cells with/without scaffold-based tissue engineering strategies have been explored with limited success (Choi 2000; Lang

et al. 1998; Kawaguchi et al. 2004; Marei et al. 2009; Lin et al. 2011; Gault et al. 2010).

2.6 Scaffolds for Dental Tissue Engineering

The recent progress in bio-fabrication technologies and bioengineering involves mainly the combination of scaffolds and bioactive molecules for enhanced recovery or regeneration of intended tissues (Tables 2.1 and 2.2). Further, combinations of stem cells from different sources with scaffold fabricated from a wide variety of biomaterials have been proposed to regenerate native functional tissue (Weigel et al. 2006). Based on their origin, biodegradable polymeric biomaterials are broadly classified into biologically derived/natural and synthetic polymers (Marin et al. 2013). Additionally, biodegradable natural polymers are known to evoke minimal incidences of foreign body reactions (Hutmacher et al. 2001). Initially, for clinical use, natural polymers were considered among others (Nair and Laurencin 2007). Hence, to support the presumption, experimental studies demonstrated that natural polymer such as collagen promotes differentiation of human dental pulp cells (HDPC) and their subsequent mineralization by probably retaining non-collagenous proteins (Kim et al. 2009a). Literature suggests that collagen sponge scaffold (Sumita et al. 2006) and chitosan/collagen scaffold containing BMP-7 DNA (Yang et al. 2011b) were suitable for dental tissue engineering. However, some reports also suggest that maturation of tooth buds could be difficult in collagen and fibrin gels (Ohara et al. 2010). Other natural polymers, like alginate hydrogel were shown to support dental pulp regeneration by delivering growth factors such as TGF- β 1 (Dobie et al. 2002). On the other hand, synthetic biodegradable polymer offers greater potential advantages compared to their respective counterpart (Vroman and Tighzert 2009). Barrier membranes made from synthetic polymers such as polylactic acid (PLA) and polyglactin-910 (PG-910) demonstrated appreciative results in the management of intrabony periodontal defects (Christgau et al. 1998). It was also claimed that pulp-derived fibroblasts proliferate in PGA fibres forming tissue constructs comparable to native pulp (Mooney et al. 1996). Similar studies further suggest that fibroblasts isolated from pulp and gingival tissue proliferates in PGA scaffolds and secretes type 1 collagen, cellular fibronectin and probably transduce BMP signals, in vivo (Buurma et al. 1999). In another study, enhanced DPSCs differentiation towards an odontoblast-like phenotype was reported in nano-hydroxyapatite incorporated poly(epsilon-caprolactone) (PCL)/gelatin scaffolds (Yang et al. 2010). Interestingly, histological samples of transplanted DPSC seeded PLGA scaffold in rabbits exhibited osteodentine and tubular-like dentine structures (El-Backly et al. 2008). In a recent study, composite nanofibrous scaffold incorporating PCL and gelatin were optimized in various 3D geometries and were found to support DPSCs, proliferation and their subsequent neural differentiation (Das and Bellare 2018). However, despite the recent advancement in physico-chemical properties and processing parameters of biodegradable

Table 2.1 Common polymers used in oro-dental regenerative approaches

Sl. no.	Polymer	Origin	Biocompatibility	Biodegradability	Reported uses
1	Matrigel	Naturally derived polymer	+	+	PDL regeneration on titanium implants (Lin et al. 2011) etc.
2	Collagen	Naturally derived polymer	+	+	Useful for guided bone regeneration (GBR) (Song et al. 2007)
3	Chitosan	Naturally derived polymer	+	+	Useful towards periodontal regenerative approaches (Yar et al. 2016)
4	Poly-glycolic acid (PGA)	Synthetic biomaterial	+	+	Promotes new bone formation in the alveolar socket (Chang et al. 2014), PDL regeneration (Wu et al. 2018) etc.
5	Polylactic acid (PLA)	Synthetic biomaterial	+	+	Physiological bone filler (Tomlin et al. 2014), etc.
6	Poly(lactide-co-glycolide) (PLGA)	Synthetic biomaterial	+	+	Useful for PDL regeneration (Marei et al. 2009), etc.
7	Poly-ε-caprolactone (PCL)	Synthetic biomaterial	+	+	Enhanced implant osseointegration (Das et al. 2018), dental wound dressing with antibacterial activity (Baranowska-Korczync et al. 2016), etc.
8	Polyanhydrides (PAN)	Synthetic biomaterial	+	+	Useful in crestal augmentation during immediate implant placement (Hasturk et al. 2014)
9	Polyamide (PA)	Synthetic polymeric collagen analogue	+	+	Repair of mandibular defects in rabbits (Li et al. 2010), etc.
10	Polyethylene glycol (PEG)	Synthetic biomaterial	+	+	Treatment of bone defects (Lops et al. 2014)

Table 2.2 Some of the commercially available scaffold materials

Product	Manufacturer	Composition	Usage/Clinical indication
Bio-Oss®	Geistlich	Geistlich Bio-Oss® granules and porcine collagen	Ridge preservation, minor bone augmentation, periodontal regeneration
Puros®	Zimmer Biomet	Puros cancellous particulate allograft	Regeneration in periodontium, furcation defects, osseous defects, sinus augmentation, horizontal alveolar crest augmentation
Grafton® (DBM)	BioHorizons	Deminerlized bone matrix allograft	Extraction socket grafting, ridge and sinus augmentation, bone augmentation around implants, bony defects, periodontal regeneration
Vitoss®	Stryker	β-tricalcium phosphate	Bone augmentation
Guidor easy-graft®	Sunstar	β-tricalcium phosphate granules coated with poly lactide-co-glycolide	Ideally suited for ridge preservation after tooth extraction and filling voids around immediate implant placements
Raptos®	Citagenix	Mineralized/ deminerlized bone allograft	Osseous defects
Gen-os®	OsteoBiol by Tecnos	Cortico-cancellous heterologous bone mix	Alveolar ridge preservation, lateral access maxillary sinus lift, dehiscence regeneration
Interpore 200®	Interpore International	Porous Hydroxyapatite	Periodontal osseous defect
OsteoGraf/ N-300	Dentsply Sirona	Sintered bovine-derived hydroxylapatite	Provides a scaffold for new bone growth
Cytoflex Tefguard®	Unicare Biomedical	Micro-porous polytetrafluoroethylene thin film	Use as a barrier membrane for guided tissue regeneration procedures
Epi-Guide®	Curasan Inc.	Poly-DL-Lactic Acid	Use as an adjunct to periodontal restorative surgeries and assists in the regeneration of bone and periodontal support tissues

Source: Product Catalogues

scaffolds, concern remains regarding the numerous associated limitations such as reaction and tissue necrosis (O'Brien 2011).

2.7 Conclusion

Even though tissue engineering is in the early period of existence, it offers significant promise due to the combinatorial effect of MSCs and biodegradable polymers. However, the ethical issues tied to the source of cells and stringent regulatory approval process pose challenges in the translation of stem cell-based tissue

engineering concepts to the clinics. Fortunately, the advancement of materials science led to the development of a wide range of biodegradable polymers exhibiting ease of manufacturability including fabrication of scaffolds with complex geometries and processability demonstrating favourable mechanical and physical properties. The feasibility of therapeutic application of stem cell/scaffold-based tissue engineering approaches lies on our ability to identify and optimize the existing or novel biomaterials and its corresponding interaction with MSCs to elicit synergistic bio-response. Hence, further exploration of various modalities for polymeric biodegradable biomaterials and stem cells in tissue engineering especially on the perspective of teeth and dento-alveolar region is warranted.

References

- Abdulqader ST, Ab Rahman I, Ismail H, Kannan TP, Mahmood Z (2013) A simple pathway in preparation of controlled porosity of biphasic calcium phosphate scaffold for dentin regeneration. *Ceram Int* 39:2375–2381
- About I, Bottero M-J, De Denato P, Camps J, Franquin J-C, Mitsiadis TA (2000) Human dentin production in vitro. *Exp Cell Res* 258:33–41
- Adell R, Lekholm U, Rockler B, Brånemark P-I (1981) A 15-year study of Osseointegrated implants in the treatment of the edentulous jaw. *Int J Oral Surg* 10:387–416
- Adell R, Eriksson B, Lekholm U, Brånemark P-I, Jemt T (1990) A Long-term follow-up study of Osseointegrated implants in the treatment of totally edentulous jaws. *Int J Oral Max Impl* 5:347–359
- Ahangari Z, Naseri M, Jalili M, Mansouri Y, Mashhadiabbas F, Torkaman A (2012) Effect of Propolis on dentin regeneration and the potential role of dental pulp stem cell in Guinea pigs. *Cell J (Yakhteh)* 13:223
- Akizuki T, Oda S, Komaki M, Tsuchioka H, Kawakatsu N, Kikuchi A, Yamato M, Okano T, Ishikawa I (2005) Application of periodontal ligament cell sheet for periodontal regeneration: A pilot study in beagle dogs. *J Periodontol* 40:245–251
- Anil S, Anand P, Alghamdi H, Jansen J (2011) Dental implant surface enhancement and Osseointegration. *Implant Dentistry-A Rapidly Evolving Practice*, Intech
- Arrington ED, Smith WJ, Chambers HG, Bucknell AL, Davino NA (1996) Complications of iliac crest bone graft harvesting. *Clin Orthop Relat Res* 329:300–309
- Artzi Z, Nemcovsky CE (1998) The application of Deproteinized bovine bone mineral for ridge preservation prior to implantation. Clinical and histological observations in a case report. *J Periodontol* 69:1062–1067
- Atwood DA (1971) Reduction of residual ridges: A Major Oral disease entity. *J Prosthet Dent* 26:266–279
- Baranowska-Korczyn A, Warowicka A, Jasiurkowska-Delaporte M, Grześkowiak B, Jarek M, Maciejewska BM, Jurga-Stopa J, Jurga S (2016) Antimicrobial electrospun poly (-E-Caprolactone) scaffolds for gingival fibroblast growth. *RSC Adv* 6:19647–19656
- Bartold PM, McCulloch CA, Narayanan AS, Pitaru S (2000) Tissue engineering: A new paradigm for periodontal regeneration based on molecular and cell biology. *Periodontology* 2000 (24):253–269
- Bosshardt DD, Sculean A (2009) Does periodontal tissue regeneration really work? *Periodontology* 2000(51):208–219
- Bottino MC, Thomas V, Schmidt G, Vohra YK, Chu T-MG, Kowolik MJ, Janowski GM (2012) Recent advances in the development of Gtr/Gbr membranes for periodontal regeneration – a materials perspective. *Dent Mater* 28:703–721

- Bruder SP, Kraus KH, Goldberg VM, Kadiyala S (1998a) The effect of implants loaded with autologous Mesenchymal stem cells on the healing of canine segmental bone defects. *JBJS* 80:985–996
- Bruder SP, Kurth AA, Shea M, Hayes WC, Jaiswal N, Kadiyala S (1998b) Bone regeneration by implantation of purified, culture-expanded human Mesenchymal stem cells. *J Orthop Res* 16:155–162
- Brunsvold MA, Mellonig JT (1993) Bone grafts and periodontal regeneration. *Periodontology* 2000 (1):80–91
- Buser D, Warrer K, Karring T (1990) Formation of a periodontal ligament around titanium implants. *J Periodontol* 61:597–601
- Buurma B, Gu K, Rutherford RB (1999) Transplantation of human pulpal and gingival fibroblasts attached to synthetic scaffolds. *Eur J Oral Sci* 107:282–289
- Carr AB, Brown DT (2010) Mccracken's removable partial prosthodontics-E-book. Elsevier Health Sciences, London
- Caton J, Nyman S (1980) Histometric evaluation of periodontal surgery I. the modified Widman flap procedure. *J Clin Periodontol* 7:212–223
- Caton J, Nyman S, Zander H (1980) Histometric evaluation of periodontal surgery ii. Connective tissue attachment levels after four regenerative procedures. *J Clin Periodontol* 7:224–231
- Cawood J, Howell R (1991) Reconstructive Preprosthetic surgery: I. anatomical considerations. *Int J Oral Max Surg* 20:75–82
- Chai C, Leong KW (2007) Biomaterials approach to expand and direct differentiation of stem cells. *Mol Ther* 15:467–480
- Chang H-H, Wang Y-L, Chiang Y-C, Chen Y-L, Chuang Y-H, Tsai S-J, Heish K-H, Lin F-H, Lin C-P (2014) A novel chitosan- Γ pga polyelectrolyte complex hydrogel promotes early new bone formation in the alveolar socket following tooth extraction. *PLoS One* 9:E92362
- Chen G, Chen J, Yang B, Li L, Luo X, Zhang X, Feng L, Jiang Z, Yu M, Guo W (2015) Combination of aligned Plga/gelatin electrospun sheets, native dental pulp extracellular matrix and treated dentin matrix as substrates for tooth root regeneration. *Biomaterials* 52:56–70
- Choi B-H (2000) Periodontal ligament formation around titanium implants using cultured periodontal ligament cells: A pilot study. *Int J Oral Max Impl* 15:193–196
- Christgau NM, Bader N, Schmalz G, Hiller KA, Wenzel A (1998) Gtr therapy of Intrabony defects using 2 different Bioresorbable membranes: 12-month results. *J Clin Periodontol* 25:499–509
- Cochran DL (2008) Inflammation and bone loss in periodontal disease. *J Periodontol* 79:1569–1576
- D'acquino R, De Rosa A, Lanza V, Tirino V, Laino L, Graziano A, Desiderio V, Laino G, Papaccio G (2009) Human mandible bone defect repair by the grafting of dental pulp stem/progenitor cells and collagen sponge biocomplexes. *Eur Cell Mater* 18:75–83
- Darby IB, Morris KH (2013) A systematic review of the use of growth factors in human periodontal regeneration. *J Periodontol* 84:465–476
- Darby I, Chen ST, Buser D (2009) Ridge preservation techniques for implant therapy. *Int J Oral Max Impl* 24:260–271
- Das, S. & Bellare, J. R. 2018. Dental pulp stem cells in customized 3d Nanofibrous scaffolds for regeneration of peripheral nervous system
- Das S, Gurav S, Soni V, Ingle A, Mohanty BS, Chaudhari P, Bendale K, Dholam K, Bellare JR (2018) Osteogenic Nanofibrous coated titanium implant results in enhanced Osseointegration: In vivo preliminary study in a rabbit model. *Tissue Eng Regen Med* 15:231–247
- De Groot K, Geesink R, Klein C, Serekian P (1987) Plasma sprayed coatings of Hydroxylapatite. *J Biomed Mater Res* 21:1375–1381
- Dhandayuthapani B, Yoshida Y, Maekawa T, Kumar DS (2011) Polymeric scaffolds in tissue engineering application: A review. *Int J Polym Sci* 2011:1–19
- Dimitriou R, Mataliotakis GI, Angoules AG, Kanakaris NK, Giannoudis PV (2011) Complications following autologous bone graft harvesting from the iliac crest and using the Ria: A systematic review. *Injury* 42:S3–S15

- Dobie K, Smith G, Sloan A, Smith A (2002) Effects of alginate hydrogels and Tgf- β 1 on human dental pulp repair in vitro. *Connect Tissue Res* 43:387–390
- Dong J-K, Jin T-H, Cho H-W, Oh S-C (1999) The esthetics of the smile: A review of some recent studies. *Int J Prosthodont* 12:9–19
- Duailibi MT, Duailibi SE, Young CS, Bartlett JD, Vacanti JP, Yelick PC (2004) Bioengineered teeth from cultured rat tooth bud cells. *J Dent Res* 83:523–528
- Duailibi S, Duailibi M, Zhang W, Asrican R, Vacanti J, Yelick P (2008) Bioengineered dental tissues grown in the rat jaw. *J Dent Res* 87:745–750
- Dye BA, Thornton-Evans G, Li X, Iafolla T (2015) Dental caries and tooth loss in adults in the United States, 2011–2012. Us Department of Health and Human Services, Centers for Disease Control and Prevention, National Center for Health Statistics, Hyattsville, MD
- Edman K, Öhrn K, Nordström B, Holmlund A, Hellberg D (2015) Trends over 30 years in the prevalence and severity of alveolar bone loss and the influence of smoking and socio-economic factors—based on epidemiological surveys in Sweden 1983–2013. *Int J Dent Hyg* 13:283–291
- Egusa H, Sonoyama W, Nishimura M, Atsuta I, Akiyama K (2012) Stem cells in dentistry—part II: Clinical applications. *J Prosthodont Res* 56:229–248
- El-Backly RM, Massoud AG, El-Badry AM, Sherif RA, Marei MK (2008) Regeneration of dentine/pulp-like tissue using a dental pulp stem cell/poly (lactic-co-glycolic) acid scaffold construct in New Zealand white rabbits. *Aust Endod J* 34:52–67
- Ellingsen JE, Johansson CB, Wennerberg A, Holmén A (2004) Improved retention and bone-to-implant contact with fluoride-modified titanium implants. *Int J Oral Max Impl* 19:659–666
- Elsharkawy S, Mata A (2018) Hierarchical biomineralization: From Nature’s designs to synthetic materials for regenerative medicine and dentistry. *Adv Healthc Mater* 7:1800178
- Elsharkawy S, Al-Jawad M, Pantano MF, Tejada-Montes E, Mehta K, Jamal H, Agarwal S, Shaturminska K, Rice A, Tarakina NV (2018) Protein disorder—order interplay to guide the growth of hierarchical mineralized structures. *Nat Commun* 9:2145
- Emami E, De Souza RF, Kabawat M, Feine JS (2013) The impact of Edentulism on Oral and general health. *Int J Dent* 2013:1–7
- Flores MG, Hasegawa M, Yamato M, Takagi R, Okano T, Ishikawa I (2008) Cementum—periodontal ligament complex regeneration using the cell sheet technique. *J Periodontol Res* 43:364–371
- Gault P, Black A, Romette JL, Fuente F, Schroeder K, Thillou F, Brune T, Berdal A, Wurtz T (2010) Tissue-engineered ligament: Implant constructs for tooth replacement. *J Clin Periodontol* 37:750–758
- Ghi H, McGivney GP (1979) Influence of tooth proprioception on speech articulation. *J Prosthet Dent* 42:609–613
- Giannoudis PV, Dinopoulos H, Tsiridis E (2005) Bone substitutes: An update. *Injury* 36:S20–S27
- Gottlow J, Nyman S, Lindhe J, Karring T, Wennström J (1986) New attachment formation in the human Periodontium by guided tissue regeneration case reports. *J Clin Periodontol* 13:604–616
- Gronthos S, Mankani M, Brahimi J, Robey PG, Shi S (2000) Postnatal human dental pulp stem cells (DpSCs) in vitro and in vivo. *Proc Natl Acad Sci* 97:13625–13630
- Gronthos S, Brahimi J, Li W, Fisher L, Cherman N, Boyde A, Denbesten P, Robey PG, Shi S (2002) Stem cell properties of human dental pulp stem cells. *J Dent Res* 81:531–535
- Guarnieri R, Giardino L, Crespi R, Romagnoli R (2002) Cementum formation around a titanium implant: A case report. *Int J Oral Max Impl* 17:729–732
- Guo W, He Y, Zhang X, Lu W, Wang C, Yu H, Liu Y, Li Y, Zhou Y, Zhou J (2009) The use of dentin matrix scaffold and dental follicle cells for dentin regeneration. *Biomaterials* 30:6708–6723
- Guo W, Gong K, Shi H, Zhu G, He Y, Ding B, Wen L, Jin Y (2012) Dental follicle cells and treated dentin matrix scaffold for tissue engineering the tooth root. *Biomaterials* 33:1291–1302
- Gupta D, Singh AK, Dravid A, Bellare JR (2019) Multiscale porosity in compressible cryogenically 3d printed gel for bone tissue engineering. *ACS Appl Mater Interfaces* 11:20437–20452
- Hall WB (2013) Hall’s critical decisions in periodontology and dental Implantology. Pmph-USA, Shelton, CT

- Hämmerle CH, Jung RE (2003) Bone augmentation by means of barrier membranes. *Periodontology* 2000(33):36–53
- Hämmerle CH, Araújo MG, Simion M, Group OC (2012) Evidence-based knowledge on the biology and treatment of extraction sockets. *Clin Oral Impl Res* 23:80–82
- Hasan A, Waibhaw G, Tiwari S, Dharmalingam K, Shukla I, Pandey LM (2017) Fabrication and characterization of chitosan, Polyvinylpyrrolidone, and cellulose Nanowhiskers Nanocomposite films for wound healing drug delivery application. *J Biomed Mater Res A* 105:2391–2404
- Hasan A, Pattanayek SK, Pandey LM (2018a) Effect of functional groups of self-assembled monolayers on protein adsorption and initial cell adhesion. *ACS Biomater Sci Eng* 4:3224–3233
- Hasan A, Saxena V, Pandey LM (2018b) Surface functionalization of Ti6Al4v via self-assembled monolayers for improved protein adsorption and fibroblast adhesion. *Langmuir* 34:3494–3506
- Hasan A, Waibhaw G, Saxena V, Pandey LM (2018c) Nano-biocomposite scaffolds of chitosan, Carboxymethyl cellulose and silver nanoparticle modified cellulose Nanowhiskers for bone tissue engineering applications. *Int J Biol Macromol* 111:923–934
- Hasegawa M, Yamato M, Kikuchi A, Okano T, Ishikawa I (2005) Human periodontal ligament cell sheets can regenerate periodontal ligament tissue in an Athymic rat model. *Tissue Eng* 11:469–478
- Hasturk H, Kantarci A, Ghattas M, Dangaria SJ, Abdallah R, Morgan EF, Diekwisch TG, Ashman A, Van Dyke T (2014) The use of light/chemically hardened Polymethylmethacrylate, Polyhydroxyethylmethacrylate, and calcium hydroxide graft material in combination with Polyamide around implants and extraction sockets in Minipigs: Part II: Histologic and micro-Ct evaluations. *J Periodontol* 85:1230–1239
- Helkimo E, Carlsson GE, Helkimo M (1977) Bite force and state of dentition. *Acta Odontol Scand* 35:297–303
- Holtgrave E, Donath K (1995) Response of Odontoblast-like cells to hydroxyapatite ceramic granules. *Biomaterials* 16:155–159
- Honda MJ, Ohara T, Sumita Y, Ogaeri T, Kagami H, Ueda M (2006) Preliminary study of tissue-engineered Odontogenesis in the canine jaw. *J Oral Max Surg* 64:283–289
- Horváth A, Mardas N, Mezzomo LA, Needleman IG, Donos N (2013) Alveolar ridge preservation. A systematic review. *Clin Oral Investig* 17:341–363
- Howell TH, Fiorellini JP, Paquette DW, Offenbacher S, Giannobile WV, Lynch SE (1997) A phase I/II clinical trial to evaluate a combination of recombinant human platelet-derived growth factor-bb and recombinant human insulin-like growth factor-I in patients with periodontal disease. *J Periodontol* 68:1186–1193
- Huang GT-J, Yamaza T, Shea LD, Djouad F, Kuhn NZ, Tuan RS, Shi S (2009) Stem/progenitor cell-mediated De novo regeneration of dental pulp with newly deposited continuous layer of dentin in an in vivo model. *Tissue Eng Part A* 16:605–615
- Huang GTJ, Al-Habib M, Gauthier P (2013) Challenges of stem cell-based pulp and dentin regeneration: A clinical perspective. *Endod Top* 28:51–60
- Hutmacher D, Goh J, Teoh S (2001) An introduction to biodegradable materials for tissue engineering applications. *Ann Acad Med Singap* 30:183–191
- Ikeda E, Morita R, Nakao K, Ishida K, Nakamura T, Takano-Yamamoto T, Ogawa M, Mizuno M, Kasugai S, Tsuji T (2009) Fully functional bioengineered tooth replacement as an organ replacement therapy. *Proc Natl Acad Sci* 106:13475–13480
- Iohara K, Nakashima M, Ito M, Ishikawa M, Nakasima A, Akamine A (2004) Dentin regeneration by dental pulp stem cell therapy with recombinant human bone morphogenetic protein 2. *J Dent Res* 83:590–595
- Iohara K, Imabayashi K, Ishizaka R, Watanabe A, Nabekura J, Ito M, Matsushita K, Nakamura H, Nakashima M (2011) Complete pulp regeneration after Pulpectomy by transplantation of Cd105 + stem cells with stromal cell-derived Factor-1. *Tissue Eng Part A* 17:1911–1920
- Ishimatsu H, Kitamura C, Morotomi T, Tabata Y, Nishihara T, Chen K-K, Terashita M (2009) Formation of dentinal bridge on surface of regenerated dental pulp in dentin defects by controlled release of fibroblast growth factor-2 from gelatin hydrogels. *J Endod* 35:858–865

- Ishimoto K, Hayano S, Yanagita T, Kurosaka H, Kawanabe N, Itoh S, Ono M, Kuboki T, Kamioka H, Yamashiro T (2015) Topical application of lithium chloride on the pulp induces dentin regeneration. *PLoS One* 10:E0121938
- Iwata T, Yamato M, Tsuchioka H, Takagi R, Mukobata S, Washio K, Okano T, Ishikawa I (2009) Periodontal regeneration with multi-layered periodontal ligament-derived cell sheets in a canine model. *Biomaterials* 30:2716–2723
- Jacobs R, Van Steenberghe D (1994) Role of periodontal ligament receptors in the tactile function of teeth: A review. *J Periodontal Res* 29:153–167
- Jahangiri L, Hessamfar R, Ricci JL (2005) Partial generation of periodontal ligament on Endosseous dental implants in dogs. *Clin Oral Impl Res* 16:396–401
- Jaiswal AK, Dhumal RV, Ghosh S, Chaudhari P, Nemani H, Soni VP, Vanage GR, Bellare JR (2013a) Bone healing evaluation of Nanofibrous composite scaffolds in rat Calvarial defects: A comparative study. *J Biomed Nanotechnol* 9:2073–2085
- Jaiswal AK, Kadam SS, Soni VP, Bellare JR (2013b) Improved functionalization of electrospun PIIa/gelatin scaffold by alternate soaking method for bone tissue engineering. *Appl Surf Sci* 268:477–488
- Ji B, Sheng L, Chen G, Guo S, Xie L, Yang B, Guo W, Tian W (2014) The combination use of platelet-rich fibrin and treated dentin matrix for tooth root regeneration by cell homing. *Tissue Eng Part A* 21:26–34
- Jiao L, Xie L, Yang B, Yu M, Jiang Z, Feng L, Guo W, Tian W (2014) Cryopreserved dentin matrix as a scaffold material for dentin-pulp tissue regeneration. *Biomaterials* 35:4929–4939
- Jivraj S, Chee W (2006) Rationale for dental implants. *Br Dent J* 200:661
- Johnson NC, Sandy JR (1999) Tooth position and speech – is there a relationship? *Angle Orthod* 69:306–310
- Karring T, Nyman S, Gottlow J, Laurell L (1993) Development of the biological concept of guided tissue regeneration – animal and human studies. *Periodontology* 2000(1):26–35
- Katagiri W, Osugi M, Kawai T, Hibi H (2016) First-in-human study and clinical case reports of the alveolar bone regeneration with the Secretome from human Mesenchymal stem cells. *Head Face Med* 12:5
- Kawaguchi H, Hirachi A, Hasegawa N, Iwata T, Hamaguchi H, Shiba H, Takata T, Kato Y, Kurihara H (2004) Enhancement of periodontal tissue regeneration by transplantation of bone marrow Mesenchymal stem cells. *J Periodontol* 75:1281–1287
- Kenney EB, Ramfjord SP (1969) Patterns of root and alveolar-bone growth associated with development and eruption of teeth in rhesus monkeys. *J Dent Res* 48:251–256
- Kim BW (2018) *Clinical regenerative medicine in urology*. Springer, Singapore
- Kim H, Choi S-H, Ryu J-J, Koh S-Y, Park J-H, Lee I-S (2008) The biocompatibility of Sla-treated titanium implants. *Biomed Mater* 3:025011
- Kim NR, Lee DH, Chung P-H, Yang H-C (2009a) Distinct differentiation properties of human dental pulp cells on collagen, gelatin, and chitosan scaffolds. *Oral Surg Oral Med Oral Pathol Oral Radiol Endod* 108:E94–E100
- Kim SH, Kim KH, Seo BM, Koo KT, Kim TI, Seol YJ, Ku Y, Rhyu IC, Chung CP, Lee YM (2009b) Alveolar bone regeneration by transplantation of periodontal ligament stem cells and bone marrow stem cells in a canine Peri-implant defect model: A pilot study. *J Periodontol* 80:1815–1823
- Komine A, Suenaga M, Nakao K, Tsuji T, Tomooka Y (2007) Tooth regeneration from newly established cell lines from a molar tooth germ epithelium. *Biochem Biophys Res Commun* 355:758–763
- Kuo TF, Huang AT, Chang HH, Lin FH, Chen ST, Chen RS, Chou CH, Lin HC, Chiang H, Chen MH (2008) Regeneration of dentin-pulp complex with Cementum and periodontal ligament formation using dental bud cells in gelatin-chondroitin-Hyaluronan tri-copolymer scaffold in swine. *J Biomed Mater Res A: An Official Journal of the Society for Biomaterials, the Japanese Society for Biomaterials, and the Australian Society for Biomaterials and the Korean Society for Biomaterials* 86:1062–1068

- Kurth A, Eberhardt C, Müller S, Steinacker M, Schwarz M, Bauss F (2005) The bisphosphonate Ibandronate improves implant integration in Osteopenic Ovariectomized rats. *Bone* 37:204–210
- Lang H, Schüler N, Nolden R (1998) Attachment formation following replantation of cultured cells into periodontal defects – a study in Minipigs. *J Dent Res* 77:393–405
- Le Guéhennec L, Soueidan A, Layrolle P, Amouriq Y (2007) Surface treatments of titanium dental implants for rapid Osseointegration. *Dent Mater* 23:844–854
- Lee D-J, Lee J-M, Kim E-J, Takata T, Abiko Y, Okano T, Green DW, Shimono M, Jung H-S (2017) Bio-implant as a novel restoration for tooth loss. *Sci Rep* 7:7414
- Lekholm U, Van Steenberghe D, Herrmann I, Bolender C, Folmer T, Gunne J, Henry P, Higuchi K, Laney WR, Lindén U (1994) Osseointegrated implants in the treatment of partially edentulous jaws: A prospective 5-year multicenter study. *Int J Oral Max Impl* 9:627–635
- Lekovic V, Camargo PM, Klokkevold PR, Weinlaender M, Kenney EB, Dimitrijevic B, Nedic M (1998) Preservation of alveolar bone in extraction sockets using bioabsorbable membranes. *J Periodontol* 69:1044–1049
- Li J, Li Y, Ma S, Gao Y, Zuo Y, Hu J (2010) Enhancement of bone formation by bmp-7 transduced Mscs on biomimetic Nano-hydroxyapatite/polyamide composite scaffolds in repair of mandibular defects. *J Biomed Mater Res A* 95:973–981
- Li R, Guo W, Yang B, Guo L, Sheng L, Chen G, Li Y, Zou Q, Xie D, An X (2011) Human treated dentin matrix as a natural scaffold for complete human dentin tissue regeneration. *Biomaterials* 32:4525–4538
- Lin Y, Gallucci GO, Buser D, Bosshardt D, Belser U, Yelick PC (2011) Bioengineered periodontal tissue formed on titanium dental implants. *J Dent Res* 90:251–256
- Lindquist LW, Rockler B, Carlsson GE (1988) Bone Resorption around fixtures in edentulous patients treated with mandibular fixed tissue-integrated prostheses. *J Prosthet Dent* 59:59–63
- Liu Y, Enggist L, Kuffer AF, Buser D, Hunziker EB (2007) The influence of bmp-2 and its mode of delivery on the Osteoconductivity of implant surfaces during the early phase of Osseointegration. *Biomaterials* 28:2677–2686
- Liu Y, Zheng Y, Ding G, Fang D, Zhang C, Bartold PM, Gronthos S, Shi S, Wang S (2008) Periodontal ligament stem cell-mediated treatment for periodontitis in miniature swine. *Stem Cells* 26:1065–1073
- Lops D, Ferroni L, Gardin C, Ricci S, Guazzo R, Sbricoli L, Romeo E, Calvo-Guirado JL, Bressan E, Zavan B (2014) Osteoproperties of polyethylene glycol hydrogel material. *J Osseointegration* 6:61–65
- Luiz De Oliveira Da Rosa W, Machado Da Silva T, Fernando Demarco F, Piva E, Fernandes Da Silva A (2017) Could the application of bioactive molecules improve vital pulp therapy success? A systematic review. *J Biomed Mater Res A* 105:941–956
- Marco F, Milena F, Gianluca G, Vittoria O (2005) Peri-implant Osteogenesis in health and osteoporosis. *Micron* 36:630–644
- Marei MK, Saad MM, El-Ashwah AM, El-Backly RM, Al-Khodary MA (2009) Experimental formation of periodontal structure around titanium implants utilizing bone marrow Mesenchymal stem cells: A pilot study. *J Oral Implantol* 35:106–129
- Marin E, Briceño MI, Caballero-George C (2013) Critical evaluation of biodegradable polymers used in Nanodrugs. *Int J Nanomedicine* 8:3071
- Mina M, Kollar E (1987) The induction of Odontogenesis in non-dental mesenchyme combined with early murine mandibular arch epithelium. *Arch Oral Biol* 32:123–127
- Miron RJ, Sculean A, Cochran DL, Froum S, Zucchelli G, Nemcovsky C, Donos N, Lyngstadaas SP, Deschner J, Dard M (2016) Twenty years of enamel matrix derivative: The past, the present and the future. *J Clin Periodontol* 43:668–683
- Misch CE (2004) Dental implant prosthetics-E-book. Elsevier Health Sciences, St. Louis, MO
- Modino SA, Sharpe PT (2005) Tissue engineering of teeth using adult stem cells. *Arch Oral Biol* 50:255–258
- Mooney DJ, Powell C, Piana J, Rutherford B (1996) Engineering dental pulp-like tissue in vitro. *Biotechnol Prog* 12:865–868

- Na S, Zhang H, Huang F, Wang W, Ding Y, Li D, Jin Y (2016) Regeneration of dental pulp/dentine complex with a three-dimensional and scaffold-free stem-cell sheet-derived pellet. *J Tissue Eng Regen Med* 10:261–270
- Nair LS, Laurencin CT (2007) Biodegradable polymers as biomaterials. *Prog Polym Sci* 32:762–798
- Nakahara T, Nakamura T, Kobayashi E, Kuremoto K-I, Matsuno T, Tabata Y, Eto K, Shimizu Y (2004) In situ tissue engineering of periodontal tissues by seeding with periodontal ligament-derived cells. *Tissue Eng* 10:537–544
- Nakao K, Morita R, Saji Y, Ishida K, Tomita Y, Ogawa M, Saitoh M, Tomooka Y, Tsuji T (2007) The development of a bioengineered organ germ method. *Nat Methods* 4:227
- Nakashima M (2005) Bone morphogenetic proteins in dentin regeneration for potential use in endodontic therapy. *Cytok Growth Factor Rev* 16:369–376
- Nakashima M, Iohara K (2017) Recent Progress in translation from bench to a pilot clinical study on Total pulp regeneration. *J Endod* 43:S82–S86
- Nakashima M, Iohara K, Murakami M, Nakamura H, Sato Y, Arijji Y, Matsushita K (2017) Pulp regeneration by transplantation of dental pulp stem cells in pulpitis: A pilot clinical study. *Stem Cell Res Ther* 8:61
- Nanci A (2017) Ten Cate's Oral histology-E-book: Development, structure, and function. Elsevier Health Sciences, St. Louis, MO
- O'Brien FJ (2011) Biomaterials & Scaffolds for tissue engineering. *Mater Today* 14:88–95
- Ohara T, Itaya T, Usami K, Ando Y, Sakurai H, Honda MJ, Ueda M, Kagami H (2010) Evaluation of scaffold materials for tooth tissue engineering. *J Biomed Mater Res A* 94:800–805
- Ohazama A, Modino S, Miletich I, Sharpe P (2004) Stem-cell-based tissue engineering of murine teeth. *J Dent Res* 83:518–522
- Ong G (1998) Periodontal disease and tooth loss. *Int Dent J* 48:233–238
- Orchardson R, Cadden S (1998) Mastication. In: *The scientific basis of eating*. Karger Publishers, New York
- Orsini G, Pagella P, Putignano A, Mitsiadis TA (2018) Novel biological and technological platforms for dental clinical use. *Front Physiol* 9:1102
- Oryan A, Alidadi S, Moshiri A, Maffulli N (2014) Bone regenerative medicine: Classic options, novel strategies, and future directions. *J Orthop Surg Res* 9:18
- Osburn R (1974) Preservation of the alveolar ridge: A simplified technique for retaining teeth beneath removable appliances. *J Indiana State Dent Assoc* 53:8–11
- Oshima M, Mizuno M, Imamura A, Ogawa M, Yasukawa M, Yamazaki H, Morita R, Ikeda E, Nakao K, Takano-Yamamoto T (2011) Functional tooth regeneration using a bioengineered tooth unit as a mature organ replacement regenerative therapy. *PLoS One* 6:E21531
- Pagni G (2016) Stem cells for periodontal regeneration. In: *Dental Stem Cells: Regenerative Potential*. Springer, Cham
- Pandey LM, Pattanayek SK (2011) Hybrid surface from self-assembled layer and its effect on protein adsorption. *Appl Surf Sci* 257:4731–4737
- Park K, Heo S, Koak J, Kim S, Lee J, Kim S, Lim Y (2007) Osseointegration of anodized titanium implants under different current voltages: A rabbit study. *J Oral Rehabil* 34:517–527
- Peleg M, Sawatari Y, Marx RN, Santoro J, Cohen J, Bejarano P, Malinin T (2010) Use of corticocancellous allogeneic bone blocks for augmentation of alveolar bone defects. *Int J Oral Max Impl* 25:153–162
- Petrokovski J, Massler M (1967) Alveolar ridge Resorption following tooth extraction. *J Prosthet Dent* 17:21–27
- Pihlstrom BL, Michalowicz BS, Johnson NW (2005) Periodontal diseases. *Lancet* 366:1809–1820
- Pilipchuk SP, Monje A, Jiao Y, Hao J, Kruger L, Flanagan CL, Hollister SJ, Giannobile WV (2016) Integration of 3d printed and micropatterned Polycaprolactone scaffolds for guidance of oriented collagenous tissue formation in vivo. *Adv Healthc Mater* 5:676–687
- Plachokova AS, Nikolidakis D, Mulder J, Jansen JA, Creugers NH (2008) Effect of platelet-rich plasma on bone regeneration in dentistry: A systematic review. *Clin Oral Impl Res* 19:539–545

- Qu T, Jing J, Jiang Y, Taylor RJ, Feng JQ, Geiger B, Liu X (2014) Magnesium-containing nanostructured hybrid scaffolds for enhanced dentin regeneration. *Tissue Eng Part A* 20:2422–2433
- Quattlebaumr JB, Mellonig JT, Hensel NF (1988) Antigenicity of freeze-dried cortical bone allograft in human periodontal osseous defects. *J Periodontol* 59:394–397
- Raphel J, Karlsson J, Galli S, Wennerberg A, Lindsay C, Haugh MG, Pajarinen J, Goodman SB, Jimbo R, Andersson M (2016) Engineered protein coatings to improve the Osseointegration of dental and Orthopaedic implants. *Biomaterials* 83:269–282
- Reynolds MA, Aichelmann-Reidy ME, Branch-Mays GL (2010) Regeneration of periodontal tissue: Bone replacement grafts. *Dent Clin* 54:55–71
- Rocuzzo M, Ramieri G, Spada MC, Bianchi SD, Berrone S (2004) Vertical alveolar ridge augmentation by means of a titanium mesh and autogenous bone grafts. *Clin Oral Impl Res* 15:73–81
- Roumanas ED (2009) The social solution – denture esthetics, phonetics, and function. *J Prosthodont: Implant, Esthetic and Reconstructive Dentistry* 18:112–115
- Russell J, Scarborough N, Chesmel K (1997) Re: Ability of commercial demineralized freeze-dried bone allograft to induce new bone formation (1996; 67: 918–26). *J Periodontol* 68:804–806
- Sagar N, Pandey AK, Gurbani D, Khan K, Singh D, Chaudhari BP, Soni VP, Chattopadhyay N, Dhawan A, Bellare JR (2013) In-vivo efficacy of compliant 3d Nano-composite in critical-size bone defect repair: A six month preclinical study in rabbit. *PLoS One* 8:E77578
- Sakai V, Zhang Z, Dong Z, Neiva K, Machado M, Shi S, Santos C, Nör J (2010) Shed differentiate into functional Odontoblasts and endothelium. *J Dent Res* 89:791–796
- Sartori S, Silvestri M, Forni F, Icaro Cornaglia A, Tesei P, Cattaneo V (2003) Ten-year follow-up in a maxillary sinus augmentation using Anorganic bovine bone (bio-Oss). A case report with Histomorphometric evaluation. *Clin Oral Impl Res* 14:369–372
- Schallhorn RG (1977) Present status of osseous grafting procedures. *J Periodontol* 48:570–576
- Schei O, Waerhaug J, Lovdal A, Arno A (1959) Alveolar bone loss as related to Oral hygiene and age. *J Periodontol* 30:7–16
- Schepers E, Clercq MD, Ducheyne P, Kempeneers R (1991) Bioactive glass particulate material as a filler for bone lesions. *J Oral Rehabil* 18:439–452
- Sculean A, Nikolidakis D, Schwarz F (2008) Regeneration of periodontal tissues: Combinations of barrier membranes and grafting materials–biological foundation and preclinical evidence: A systematic review. *J Clin Periodontol* 35:106–116
- Sekula M, Zuba-Surma EK (2018) Biomaterials and stem cells: Promising tools in tissue engineering and biomedical applications. *Biomaterials in Regenerative Medicine*. Intech
- Selvig KA, Sorensen RG, Wozney JM, Wikesjö UM (2002) Bone repair following recombinant human bone morphogenetic Protein-2 stimulated periodontal regeneration. *J Periodontol* 73:1020–1029
- Seo B-M, Miura M, Gronthos S, Bartold PM, Batouli S, Brahim J, Young M, Robey PG, Wang CY, Shi S (2004) Investigation of multipotent postnatal stem cells from human periodontal ligament. *Lancet* 364:149–155
- Shetty V, Han T (1991) Alloplastic materials in reconstructive periodontal surgery. *Dent Clin N Am* 35:521–530
- Shillingburg HT, Sather DA, Wilson EL, Cain JR, Mitchell DL, Blanco LJ, Kessler JC (2012) Fundamentals of fixed prosthodontics. Quintessence Publishing Company, Hanover Park, IL
- Smith DE, Zarb GA (1989) Criteria for success of Osseointegrated Endosseous implants. *J Prosthet Dent* 62:567–572
- Song JH, Kim HE, Kim HW (2007) Collagen-apatite Nanocomposite membranes for guided bone regeneration. *J Biomed Mater Res B: Applied Biomaterials: An Official Journal of the Society for Biomaterials, the Japanese Society for Biomaterials, and the Australian Society for Biomaterials and the Korean Society for Biomaterials* 83:248–257
- Sonoyama W, Liu Y, Fang D, Yamaza T, Seo B-M, Zhang C, Liu H, Gronthos S, Wang C-Y, Shi S (2006) Mesenchymal stem cell-mediated functional tooth regeneration in swine. *PLoS One* 1: E79

- Suba Z, Takács D, Gyulai-Gaál S, Kovács K (2004) Facilitation of β -Tricalcium phosphate-induced alveolar bone regeneration by platelet-rich plasma in beagle dogs: A histologic and Histomorphometric study. *Int J Oral Max Impl* 19:158–165
- Sumita Y, Honda MJ, Ohara T, Tsuchiya S, Sagara H, Kagami H, Ueda M (2006) Performance of collagen sponge as a 3-D scaffold for tooth-tissue engineering. *Biomaterials* 27:3238–3248
- Sutton D, Lewis B, Patel M, Cawood J (2004) Changes in facial form relative to progressive atrophy of the edentulous jaws. *Int J Oral Max Surg* 33:676–682
- Tatakis DN, Promsudthi A, Wikesjö UM (1999) Devices for periodontal regeneration. *Periodontology* 2000(19):59–73
- Taylor TD (1998) Prosthodontic problems and limitations associated with Osseointegration. *J Prosthet Dent* 79:74–78
- Ten Heggeler J, Slot D, Van Der Weijden G (2011) Effect of socket preservation therapies following tooth extraction in non-molar regions in humans: A systematic review. *Clin Oral Impl Res* 22:779–788
- Thesleff I, Hurmerinta K (1981) Tissue interactions in tooth development. *Differentiation* 18:75–88
- Tomlin EM, Nelson SJ, Rossmann JA (2014) Suppl 1: Ridge preservation for implant therapy: A review of the literature. *Open Dent J* 8:66
- Tonomura A, Mizuno D, Hisada A, Kuno N, Ando Y, Sumita Y, Honda MJ, Satomura K, Sakurai H, Ueda M (2010) Differential effect of scaffold shape on dentin regeneration. *Ann Biomed Eng* 38:1664–1671
- Allen PF, McMillan AS (2003) A review of the functional and psychosocial outcomes of Edentulousness treated with complete replacement dentures. *J Can Dent Assoc* 69:662
- Urabe M, Hosokawa R, Chiba D, Sato Y, Akagawa Y (2000) Morphogenetic behavior of Periodontium on inorganic implant materials: An experimental study of canines. *J Biomed Mater Res: An Official Journal of the Society for Biomaterials, the Japanese Society for Biomaterials, and the Australian Society for Biomaterials and the Korean Society for Biomaterials* 49:17–24
- Villar CC, Cochran DL (2010) Regeneration of periodontal tissues: Guided tissue regeneration. *Dent Clin* 54:73–92
- Vining KH, Scherba JC, Bever AM, Alexander MR, Celiz AD, Mooney DJ (2018) Synthetic light-curable polymeric materials provide a supportive niche for dental pulp stem cells. *Adv Mater* 30:1704486
- Vittorini Orgeas G, Clementini M, De Risi V, De Sanctis M (2013) Surgical techniques for alveolar socket preservation: A systematic review. *Int J Oral Max Impl* 28:1049–1061
- Vroman I, Tighzert L (2009) Biodegradable Polymers. *Dent Mater* 2:307–344
- Wang W, Dang M, Zhang Z, Hu J, Eyster TW, Ni L, Ma PX (2016) Dentin regeneration by stem cells of apical papilla on injectable Nanofibrous microspheres and stimulated by controlled bmp-2 release. *Acta Biomater* 36:63–72
- Warrer K, Karring T, Gotfredsen K (1993) Periodontal ligament formation around different types of dental titanium implants. I. the self-tapping screw type implant system. *J Periodontol* 64:29–34
- Wei F, Song T, Ding G, Xu J, Liu Y, Liu D, Fan Z, Zhang C, Shi S, Wang S (2013a) Functional tooth restoration by allogeneic Mesenchymal stem cell-based bio-root regeneration in swine. *Stem Cells Dev* 22:1752–1762
- Wei X, Yang X, Han Z-P, Qu F-F, Shao L, Shi Y-F (2013b) Mesenchymal stem cells: A new trend for cell therapy. *Acta Pharmacol Sin* 34:747
- Weigel T, Schinkel G, Lendlein A (2006) Design and preparation of polymeric scaffolds for tissue engineering. *Expert Rev Med Devices* 3:835–851
- Wiens JP (1990) Acquired maxillofacial defects from motor vehicle accidents: A statistics and Prosthodontic considerations. *J Prosthet Dent* 63:172–181
- Wikesjö UM, Guglielmoni P, Promsudthi A, Cho KS, Trombelli L, Selvig KA, Jin L, Wozney JM (1999) Periodontal repair in dogs: Effect of Rhbmp-2 concentration on regeneration of alveolar bone and periodontal attachment. *J Clin Periodontol* 26:392–400
- Willis RD, Dicosimo CJ (1979) The absence of proprioceptive nerve endings in the human periodontal ligament: The role of periodontal mechanoreceptors in the reflex control of mastication. *Oral Surg Oral Med Oral Pathol Oral Radiol* 48:108–115

- Wu Y, Xia H, Zhang B, Zhao Y, Wang Y (2018) Assessment of Polyglycolic acid scaffolds for periodontal ligament regeneration. *Biotechnol Biotech Eq* 32:701–706
- Xiao Y, Qian H, Young WG, Bartold PM (2003) Tissue engineering for bone regeneration using differentiated alveolar bone cells in collagen scaffolds. *Tissue Eng* 9:1167–1177
- Yamada Y, Ueda M, Naiki T, Takahashi M, Hata K-I, Nagasaka T (2004) Autogenous injectable bone for regeneration with Mesenchymal stem cells and platelet-rich plasma: Tissue-engineered bone regeneration. *Tissue Eng* 10:955–964
- Yang X, Yang F, Walboomers XF, Bian Z, Fan M, Jansen JA (2010) The performance of dental pulp stem cells on Nanofibrous Pcl/gelatin/Nha scaffolds. *J Biomed Mater Res A: An Official Journal of the Society for Biomaterials, the Japanese Society for Biomaterials, and the Australian Society for Biomaterials and the Korean Society for Biomaterials* 93:247–257
- Yang F, Zhao S-F, Zhang F, He F-M, Yang G-L (2011a) Simvastatin-loaded porous implant surfaces stimulate Preosteoblasts differentiation: An in vitro study. *Oral Surg Oral Med Oral Pathol Oral Radiol Endod* 111:551–556
- Yang X, Han G, Pang X, Fan M (2011b) Chitosan/collagen scaffold containing bone morphogenetic protein-7 DNA supports dental pulp stem cell differentiation in vitro and in vivo. *J Biomed Mater Res A*. <https://doi.org/10.1002/jbm.a.34064>
- Yang B, Chen G, Li J, Zou Q, Xie D, Chen Y, Wang H, Zheng X, Long J, Tang W (2012) Tooth root regeneration using dental follicle cell sheets in combination with a dentin matrix-based scaffold. *Biomaterials* 33:2449–2461
- Yar M, Farooq A, Shahzadi L, Khan AS, Mahmood N, Rauf A, Chaudhry AA, Ur Rehman I (2016) Novel meloxicam releasing electrospun polymer/ceramic reinforced biodegradable membranes for periodontal regeneration applications. *Mater Sci Eng C* 64:148–156
- Yen AH-H, Sharpe PT (2008) Stem cells and tooth tissue engineering. *Cell Tissue Res* 331:359–372
- Yoshida M, Kikutani T, Okada G, Kawamura T, Kimura M, Akagawa Y (2009) The effect of tooth loss on body balance control among community-dwelling elderly persons. *Int J Prosthodont* 22:136–139
- Young CS, Terada S, Vacanti JP, Honda M, Bartlett JD, Yelick PC (2002) Tissue engineering of complex tooth structures on biodegradable polymer scaffolds. *J Dent Res* 81:695–700
- Young CS, Abukawa H, Asrican R, Ravens M, Troulis MJ, Kaban LB, Vacanti JP, Yelick PC (2005) Tissue-engineered hybrid tooth and bone. *Tissue Eng* 11:1599–1610
- Yuan Z, Nie H, Wang S, Lee CH, Li A, Fu SY, Zhou H, Chen L, Mao JJ (2011) Biomaterial selection for tooth regeneration. *Tissue Eng Part B Rev* 17:373–388
- Zara JN, Siu RK, Zhang X, Shen J, Ngo R, Lee M, Li W, Chiang M, Chung J, Kwak J (2011) High doses of bone morphogenetic protein 2 induce structurally abnormal bone and inflammation in vivo. *Tissue Eng Part A* 17:1389–1399
- Zeng X-T, Luo W, Huang W, Wang Q, Guo Y, Leng W-D (2013) Tooth loss and head and neck cancer: A meta-analysis of observational studies. *PLoS One* 8:E79074
- Zerbo IR, Bronckers AL, De Lange GL, Burger EH, Van Beek GJ (2001) Histology of human alveolar bone regeneration with a porous Tricalcium phosphate: A report of two cases. *Clin Oral Impl Res* 12:379–384
- Zhang Y, Song J, Shi B, Wang Y, Chen X, Huang C, Yang X, Xu D, Cheng X, Chen X (2007) Combination of scaffold and adenovirus vectors expressing bone morphogenetic Protein-7 for alveolar bone regeneration at dental implant defects. *Biomaterials* 28:4635–4642
- Zhao G, Zinger O, Schwartz Z, Wieland M, Landolt D, Boyan BD (2006) Osteoblast-like cells are sensitive to submicron-scale surface structure. *Clin Oral Impl Res* 17:258–264
- Zheng Y, Wang X, Wang Y, Liu X, Zhang C, Hou B, Wang S (2012) Dentin regeneration using deciduous pulp stem/progenitor cells. *J Dent Res* 91:676–682



Antifouling Peptoid Bionterfaces

3

Varun Saxena, Martyn G. L. Merrilees, and King Hang Aaron Lau

Abstract

Recent advances in synthetic chemistry has led to the increasingly sophisticated design and preparation of biofunctional polymeric surfaces and materials. In this regard, synthetic poly-(*N*-substituted glycine) “peptoids” which mimic the structure and function of peptides play an important role, since they may attain functionalities similar to natural biopolymers. This chapter reviews efforts by our group and others to develop “antifouling” peptoid coatings that resist the nonspecific and undesired adsorption of proteins and attachment of mammalian and microbial cells. We have found that the simplest peptoid—polysarcosine—has been found to be well hydrated and therefore well-suited for antifouling applications. We show that the synthetic convenience of peptoids in general greatly facilitates studies on how polymer chain length, chain density, sidechain chemistry, and specific peptoid sequences may control surface interactions. Indeed, specific peptoids and sequence arrangements have been found to exhibit long-term antifouling properties and excellent resistance against different strains of bacteria. Addition of simple sugar groups to peptoid chains may further enhance resistance against bacterial attachment. Combined with peptoid’s resistance against enzymatic degradation, antifouling peptoids have excellent potential in biomedical applications. These range from coatings of catheters and other biological devices to biosensing and nanomedicine that require a non-fouling interface to achieve improved device performance.

V. Saxena

Department of Pure & Applied Chemistry, University of Strathclyde, Glasgow, UK

Department of Biosciences and Bioengineering, Indian Institute of Technology Guwahati, Guwahati, Assam, India

M. G. L. Merrilees · K. H. A. Lau (✉)

Department of Pure & Applied Chemistry, University of Strathclyde, Glasgow, UK

e-mail: aaron.lau@strath.ac.uk

© Springer Nature Singapore Pte Ltd. 2020

P. Chandra, L.M. Pandey (eds.), *Biointerface Engineering: Prospects in Medical Diagnostics and Drug Delivery*, https://doi.org/10.1007/978-981-15-4790-4_3

55

Keywords

Peptoids · Bio-mimetic · Sequence-specific · Antifouling · Antibacterial · Chain length and density

3.1 Introduction

Recent research has focused on the design of biofunctional surfaces using polymeric materials. Poly-(*N*-substituted glycine) “peptoids” are structural isomers of peptides, differing only in the attachment position of the functional sidechain. These are located on the backbone α -carbon in peptides while they are instead located at the α -nitrogen in peptoids. This rearrangement is not recognized in nature and accounts for the protease resistance of the peptoids (Knight et al. 2015). Sidechain attachment at the amide group also removes chirality and hydrogen-bond (H-bond) donors from the peptoid backbone, promoting increased backbone conformation flexibility. This sidechain shift further enables a versatile synthetic route (the “submonomer” method) to install a diverse array of functional groups through commercially available building blocks (Lau 2014). The conformational flexibility and lack of intra- and inter-backbone H-bonds also increase thermal processability, solubility in common organic solvents, as well as hydration (Lau 2014, Knight et al. 2015, Prakash et al. 2018). Overall, the combination of biomimetic properties, resistance to enzymatic degradation, and material processability makes peptoids a potential candidate for various biomedical as well as technological applications (Lau 2014, Knight et al. 2015, Gangloff et al. 2016).

Analogous to synthetic peptides, there are two fundamental approaches to synthesizing peptoids: solid-phase submonomer synthesis (Zuckermann 2011) and ring-opening bulk polymerization (ROP) (Gangloff et al. 2016, Tao et al. 2018). The former enables sequence-specific design—the complex properties of the polymer are determined by the sequence in which simple monomer units are ordered along a linear chain. The latter enables production of bulk quantities of the polymer but can only produce sequences with averaged monomer compositions and less-specific functionalities.

Antifouling organic biointerfaces are surfaces grafted with small organic molecules or polymers that resist biofouling—the undesired surface adsorption of proteins, other biomolecules, and cell attachment. The search for surfaces that resist protein adsorption began several decades ago when it was recognized that surface-immobilized biomolecules mediated a number of biological and biomedically important processes (Vroman 1962, Prime and Whitesides 1991, Szleifer 1997a). In particular, polymer chains grafted by their chain ends on surfaces at high densities, defined as antifouling polymer “brushes”, are advantageous because their chemical properties can be tailored by chemical techniques and the brush arrangement exert an additional entropic and steric penalties against protein adsorption (de Gennes 1987, Szleifer 1997b, Halperin 1999). Polyethylene glycol (PEG) has been the “gold standard” antifouling polymer and indeed displays excellent short-term antifouling performance suitable for biosensing and cell patterning applications (Prime and Whitesides 1991, Unsworth

et al. 2005). However, significant effort has been devoted to discovering other antifouling polymers because PEG has not shown long-term stability and can exhibit complement activity (Toda et al. 2010, Lau et al. 2012b, 2015). The Messersmith group first reported antifouling surfaces composed of peptoids in 2005 (Statz et al. 2005), and we as well as other groups have expanded upon the initial study (Statz et al. 2008a, b, 2009, Lau et al. 2012a, b, 2015, van Zoelen et al. 2012, 2014, Ham et al. 2013, Ryu et al. 2014, Hörtz et al. 2015, Huesmann et al. 2015, Leng et al. 2015a, Tao et al. 2018, Cheung and Lau 2019).

This review highlights the potential advantages of applying peptoids as antifouling polymer brushes. These include the ability to conveniently prepare different peptoids exhibiting different monomer sidechain chemical groups, as well as sequences with different specific ordering of monomers to tailor the antifouling property with unparalleled control of chemical properties. It has also been reported that the conformational flexibility and high hydration of the peptoid backbone may be especially advantageous in resisting biofouling (Cheung and Lau 2019). Furthermore, the method of peptoid solid phase synthesis also lends itself to convenient attachment of antibacterial agents to combine antifouling and antibacterial performances. Access to higher molecular weight polypeptoids with ROP also provides excellent opportunities toward practical applications. Overall, peptoids provide a versatile platform to both study the molecular origins of the antifouling effect and to prepare sophisticated antifouling surfaces for potential biomedical applications.

3.2 Methods of Preparing Peptoids

The synthesis of peptoids is tackled by two main routes (Fig. 3.1): solid-phase submonomer synthesis (SPSS) to target sequence specificity, and ROP to achieve high molecular weight and larger quantities of material. ROP of N-substituted

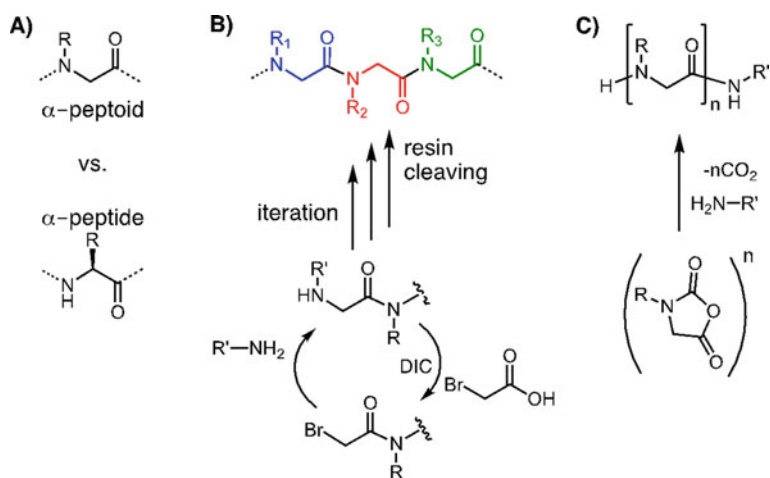


Fig. 3.1 (a) Peptoid chemical structure as compared to peptides. (b) Solid-phase synthesis procedure of sequence-specific peptoids. (c) Method to obtain peptoids by ring-opening polymerization (ROP). Reproduced with permission from Lau (2014). Copyright the Royal Society of Chemistry

N-carboxyanhydrides (NNCAs) was the first method reported (Goodman and Fried 1967, Sisido et al. 1977). High molecular weight low polydispersity peptoids in various block and branching architectures have been reported (Lahasky et al. 2011, Fetsch and Luxenhofer 2012, Jin et al. 2019). NNCA monomers are small organic molecules that polymerize through the nucleophilic ring-opening mechanism (Fig. 3.1c). Early studies in peptoid ROP were motivated by the need to understand the basic ROP mechanism, which is also used to produce poly(α -peptide)s (Habraken et al. 2011). Due to the sidechain attachment at the nitrogen, the NNCA propagating species produced is a neutral secondary amino and as such, the steric effects of substituents on the nitrogen significantly influence the reaction and the rate at which polymerization proceeds (Goodman and Fried 1967, Goodman et al. 1973, Fetsch et al. 2011). These effects are so great that polymerization rates can vary by several orders of magnitude depending upon the substituent group (Ballard and Bamford 1956, Luxenhofer et al. 2013). Synthesis of polypeptoids with bulky sidechains is particularly limited. Successful reports focus predominantly on poly(N-methylglycine) (i.e., polysarcosine, the simplest peptoid), poly(N-ethylglycine), and poly(N-propylglycine). Another general drawback of NNCA polymerization is the requirements of inert and dry conditions during both storage and polymerization. In light of this, catalytic polymerization of less-reactive N-thio-carboxyanhydride monomers has recently been developed to enable unprotected polymerization in air (Tao et al. 2014, 2017a, b, 2018).

SPSS is a more widely employed approach that focuses on sequence specificity and functional group control. This approach had evolved from Merrifield solid-phase peptide synthesis (SPPS): each residue is coupled in a sequence-specific manner from a high number of coupling sites inside porous crosslinked polymer “micro-sponges,” a.k.a. chemical resins. The submonomer method is distinguished from regular peptide SPPS by the fact that each peptoid residue is formed from two readily available units instead of from specially synthesized intact monomers (Kruijtzter and Liskamp 1995, Zuckermann 2011). This speeds up the development of bioactive sequence-specific peptoids with nonnatural sidechains (around 300 have already been demonstrated) (Culf and Ouellette 2010, Culf 2019). Each submonomer cycle is composed of an acylation step to extend the chain/monomer (for example, bromoacetic acid) followed by nucleophilic displacement to couple the sidechain functionality (Fig. 3.1b). As in peptide SPPS, peptoid SPSS can also be facilitated by microwave irradiation to reduce the time required per addition step (Yu et al. 1992, Olivos et al. 2002, Gorske et al. 2005). With or without microwave heating, SPSS peptoid sequences 15–30 residues in length are routine, and 50 residue chains have been demonstrated (Lau et al. 2012b, Murnen et al. 2012). A 100-mer sequence has also been demonstrated by fragment condensation (Murnen et al. 2012).

3.3 Antifouling Peptoid Design

3.3.1 Sidechain Chemistry

Control of the nonspecific biomolecular adsorption and cell attachment is important for biomedical devices in order to prevent, for example, bacterial infection and fibrotic encapsulation of devices. Statz et al. was the first to study the antifouling properties resulting from different peptoid sidechains (Fig. 3.2) (Statz et al. 2008a). Peptoids containing methoxyethyl sidechain groups (PMP1) were compared with hydroxyethyl (PMP2) and 2-hydroxypropyl (PMP3) sidechains. Lower fibrinogen adsorption was observed on PMP1 than on PMP2 and PMP3. However, PMP1 alone showed longer term prevention of mammalian cell attachment. All the peptoids studied showed good resistance against *E. coli* attachment but PMP1 and 2 showed significantly lower attachment of *S. epidermidis*, a species important in hospital complications. As the backbone of all the peptoids studied was same, the differences in protein adsorption, bacterial and mammalian cell attachment were attributed to the differences in sidechain chemistry.

We had further compared the ability of PMP1 to prevent biomolecular adsorption with that of PEG (Ryu et al. 2014). Both polymers were grafted on TiO₂, to simulate the effect on naturally oxidized surfaces of titanium-based biomedical devices. Single-molecule fluorescence imaging was used to quantify the amount of adsorbed

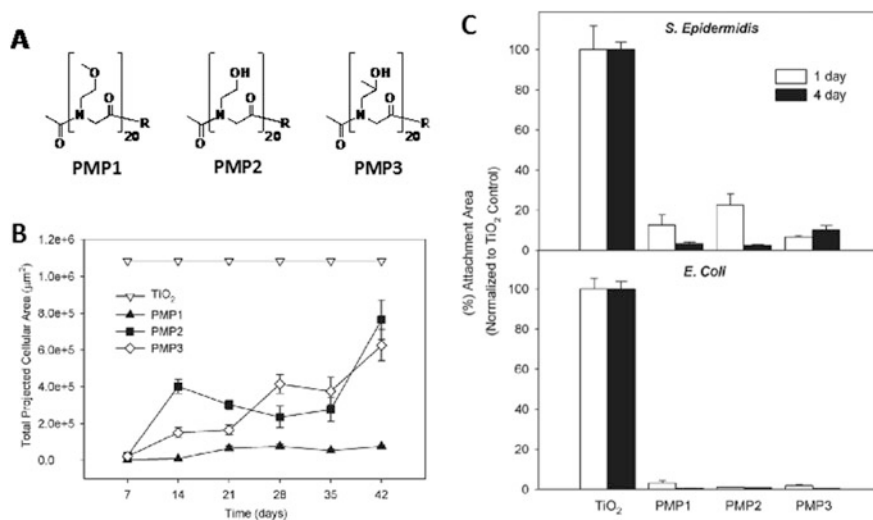


Fig. 3.2 (a) Chemical structures of the peptoids PMP1, PMP2, and PMP3. The R-group is a pentameric peptide with special adhesive properties to graft the 20-mer peptoid chain onto a TiO₂ surface. (b) The amount of fibroblast attached on the peptoid surfaces over 6 weeks. (c) The amount of *S. epidermidis* and *E. coli* attached on the peptoid surfaces after 1 and 4 days. Adapted with permission from Statz et al. (2008a). Copyright the Royal Society of Chemistry

DNA (single stranded) and immunoglobulin G (IgG). In most antifouling studies, measurements of protein adsorption rely on surface techniques such as surface plasmon resonance (SPR) spectroscopy, ellipsometry, and total internal reflection fluorescence (TIRF) microscopy. However, their limit of detection (LOD) is ca. 1 ng/cm^2 (for regular commercial instruments), which translates to ca. $40 \text{ IgG per } \mu\text{m}^2$, or $40 \times 10^6 \text{ IgG/mm}^2$. Therefore, some antifouling surfaces can appear to be “zero” fouling because the relatively low amount of adsorption may be below the LOD (Yang et al. 2009), even though the amount is still sufficient for cells to respond. Measuring adsorption by attenuated total reflection-fourier transform infrared (ATR-FTIR) spectroscopy or by assaying the amount of proteins left in a solution give even worse LOD. In our study, over an imaging area of $50 \mu\text{m}^2$, 5 ± 3 vs. 36 ± 10 molecules were adsorbed from a 10-nM DNA solution, on PMP1 vs. PEG-coated TiO_2 , respectively. Lower IgG adsorption could also be observed on PMP1 than on PEG, with 37 ± 12 vs. 431 ± 143 IgG adsorbed from a concentrated 0.5 mM IgG solution. These values on PMP1 translate to ca. 0.0005 ng/cm^2 DNA and 0.0025 ng/cm^2 IgG adsorbed, while those on PEG were an order of magnitude higher.

3.3.2 Effects of Chain Length and Chain Density

Antifouling polymer brushes attain their resistance against protein adsorption and cell attachment only at sufficiently high coverages of polymeric material over a surface (Raynor et al. 2009, Lau et al. 2012b, 2015). The chemical nature of the antifouling polymer should minimize van der Waals and other attractive intermolecular forces with biomolecules and cell surfaces (Prime and Whitesides 1993, Chapman et al. 2000). Interaction of the polymer with water molecules, i.e., hydration, should be significantly more favorable than interaction with proteins and other biomolecules (Raynor et al. 2009). Furthermore, the use of flexible polymer chains possessing high translational entropy may enforce a large penalty to adsorbing proteins because these would limit the conformational space of the grafted polymers (de Gennes 1987, Szleifer 1997b, Halperin 1999).

We had studied the effect of varying the chain length of PMP1 from 10 to 50 residues with corresponding brush thickness ranging from ca. 3 nm (10-mer at 1 chain/nm^2) to ca. 12 nm (50-mer at 0.5 chain/nm^2) (Fig. 3.3) (Lau et al. 2011). Other methods of grafting antifouling brushes, namely surface-initiated polymerization techniques, could only provide chain densities up to ca. 0.1 chain/nm^2 (Hong et al. 2017). To achieve sufficiently high overall polymer chain densities for antifouling applications, the lower density should be compensated by grafting of polymers of higher molecular weight to obtain a higher brush thickness (typically $>20 \text{ nm}$ in thickness).

For PMP1, we found that the peptoid exhibited an advancing water contact angle of 39° irrespective of chain length at sufficiently high brush densities (e.g., $>0.3 \text{ nm}^{-2}$ for PMP1-20 and $>0.1 \text{ nm}^{-2}$ for PMP1-50) (Lau et al. 2012a). This compares to almost complete wetting (i.e., $\sim 0^\circ$) on plasma cleaned TiO_2 . This indicated that

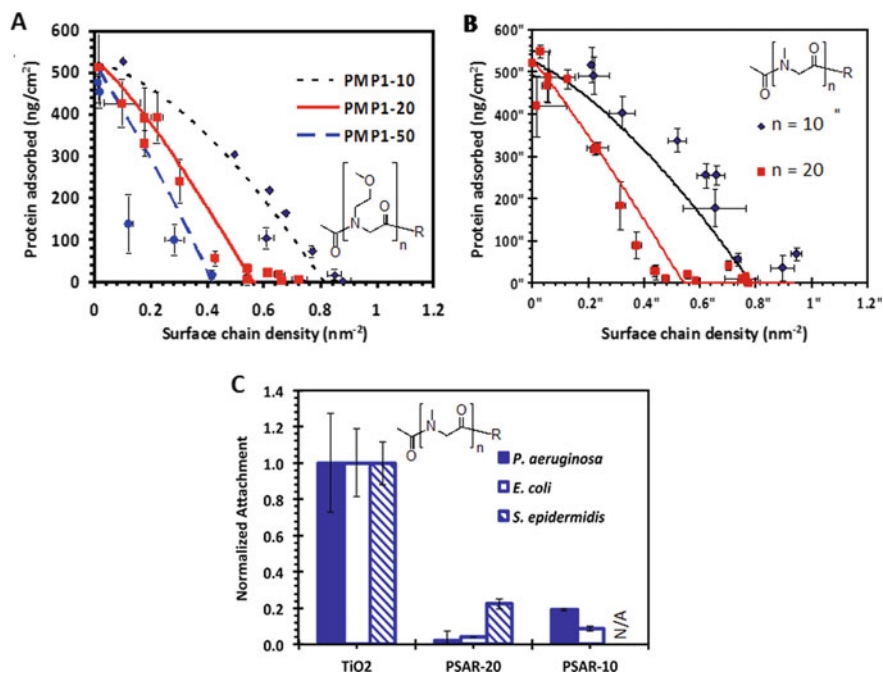


Fig. 3.3 The amount of irreversible adsorption of fibrinogen (i.e., after rinsing with buffer) at different grafted densities of (a) PMP1 and (b) polysarcosine chains of different chain lengths. The R-group is a pentameric peptide with special adhesive properties to graft the peptoid chains onto a TiO₂ surface, the same as used in earlier studies (see Fig. 3.2). The critical density is the density identified when the amount of adsorption falls to below the sensitivity limit of detection (ca. 10 ng/cm²). (c) Resistance against bacteria attachment on polysarcosine brushes. Adapted with permission from Lau et al. (2012a) and (2012b). Copyright the American Chemical Society

above the specified polymer grafting densities, the surfaces were completely covered by the PMP1 chains so that water molecules essentially interacted with the peptoid instead of partially with the peptoid and the underlying TiO₂. This coverage was a necessary but insufficient requirement for preventing irreversible protein adsorption (i.e., the amount adsorbed after rinsing). Figure 3.3a shows that a critical surface grafted chain density was needed: up to this critical density, the amount of protein adsorption decreased within increasing chain density; above this critical density, the amount adsorbed is very small and essentially below the measurement uncertainty. A molecular model theory was also developed to corroborate the change in critical density with different chain lengths (Lau et al. 2012a), which was confirmed by experimental measurements (Fig. 3.3a). The critical density was found to range from 0.88 nm⁻² for a relatively short 10-mer to 0.42 nm⁻² for a 50-mer. Table 3.1 summarizes the effects of chain length, chain densities, and sidechain chemistry on the water contact angles and critical brush densities to suppress fibrinogen adsorption for the peptoid species we have studied in detail.

Table 3.1 Summary of peptoid brush parameters relevant to their surface hydration and resistance against protein adsorption

Peptoid species	Sidechain	Chain lengths tested	Critical chain densities	Adv. contact angle	References
PMP1	Methoxyethyl	10/20/50	0.88/0.5/0.4 nm ⁻²	39°	See Sect. 3.2 and Lau et al. (2012a)
Polysarcosine	Methyl	10/20	0.5/1.0 nm ⁻²	13–20°	See Sect. 3.3 and Lau et al. (2012b)
PMKE/PMEK	Arrangements of methoxyethyl, carboxyethyl, aminoethyl.	20/36	0.5/0.32 nm ⁻²	30°	See Sect. 3.4 and Lau et al. (2015)
Glycocalyx-terminated PMP1	Glucose, β -D-maltose, methylethyl	20+	0.65 chain nm ⁻²	<30°	Ham et al. (2013)

3.3.3 Polysarcosine, the Simplest Peptoid, and Related Polymers

Sarcosine (N-methyl glycine) is the peptoid analog of alanine and, as an intermediate in the metabolism of choline and creatine (Smith-Palmer 2019), as well as a glycine transporter inhibitor (Cioffi et al. 2010), is the only naturally occurring peptoid. Alanine, and polyalanine in particular, is often considered a hydrophobic peptide because of intra- and inter-backbone H-bonding of the amide backbone polar groups to form α -helical or β -sheet secondary structures, promoted exactly by alanine residues, instead of H-bonding with water. However, since the amide hydrogens in peptoids are replaced by the sidechains (Fig. 3.1), intra- and inter-backbone H-bonding is not possible, and the peptoids backbone is completely free to interact with water.

After realizing the potential of polysarcosine, we showed by water contact angle measurements (Lau et al. 2012b) and molecular dynamics modeling (Cheung and Lau 2019) that surface grafted polysarcosine is highly hydrophilic, and we first reported the excellent antifouling properties of this peptoid in 2012 (Lau et al. 2012b). Furthermore, a particular advantage of using polysarcosine is the fact that the polymer may be prepared by both solid-phase SPSS to control the exact chain length for basic studies and by ROP polymerization to obtain bulk quantities of material (Gangloff et al. 2016, Tao et al. 2018)

In our measurements, polysarcosine 20-mers surface grafted at >0.5 chain/nm² exhibited an advancing water contact angle of ca. 15° and a receding angle of 5° at the high surface chain coverages. These values are as low as many zwitterionic charged polymer surfaces (see Sect. 3.4) and indicate excellent hydration of the peptoid (Lau et al. 2012b). When challenged with fibrinogen at its physiological concentration (3 mg/mL), we obtained critical densities of 1 nm⁻² for a chain length of 10 sarcosine units and ~ 0.5 nm⁻² for a chain length of 20 units (Fig. 3.3b).

Moreover, the 20-mer showed excellent resistance against the attachment of the mammalian fibroblasts for repeated challenges over 7 week, as well as against *P. aeruginosa* and *E. coli* in a 24 h attachment assay (Fig. 3.3c). These levels of antifouling performance are actually indistinguishable from those of PMP1 (compare Fig. 3.3a and b, and see further data from Lau et al. (2012a) and (2015)).

Other groups also examined polysarcosine brushes for antifouling applications. For example, Zhu et al. applied a polysarcosine coating on gold nanorods (AuNRs) for photothermal tumor nanomedicine therapy (Zhu et al. 2017). The polysarcosine-coated NR exhibited excellent stability in a wide range of pH, and no toxic effect or NR accumulation was found in the major organs such as heart, lung, spleen, kidney, and liver. With near-IR laser excitation, the tumors dissipated in treated mice. Barz and Schmidt also proposed to use polysarcosine to a core-shell cylindrical brush polymer complex for the sequestration and delivery of RNA molecules for gene therapy. In a study with AML-12 hepatocytes, a 70% knock-down efficiency of ApoB100 mRNA was measured with application of the polysarcosine complex (Hörtz et al. 2015).

Interestingly, before the antifouling properties of polysarcosine were recognized, other groups had already used the peptoid as the hydrophilic segment in block copolymer designs that self-assemble into micelles for drug delivery applications (Kidchob et al. 1998). In fact, it has been recognized that the solution properties of polysarcosine (e.g., hydrophilicity, critical aggregation concentration, and hydrodynamic radii) are similar to those of PEG (Huesmann et al. 2015). At the same time, close structural relatives of polysarcosine, namely poly(2-methyl-2-oxazoline) (PMOXA) (Wiesbrock et al. 2005, Hoogenboom and Schlaad 2017, Lorson et al. 2018) and the hydrophilic β -peptoid poly(N-methyl- β -alanine) (Lin et al. 2011), have shown very good antifouling properties. PMOXA, like polysarcosine, also possesses similar hydrophilicity to PEG. In other studies, however, increasing the alkyl sidechain length beyond the single methylene unit of sarcosine and its mimics decreases the solubility in water, which leads to differences in block copolymer microphase separation and degradation behavior under various pH conditions (Lambermont-Thijs et al. 2009). These results reinforce the point that the side chain chemistry can be tuned to govern antifouling properties and also the degradation, solubility, and stability of peptoids (for biomedical applications).

3.3.4 Sequence-Specific Design

It has been reported that zwitterionic polymers having both cationic and anionic entities exhibit improved antifouling properties compared with neutral brushes or those with cationic or anionic functional groups (Yang et al. 2009, Serrano et al. 2013). We therefore applied the capability of solid-phase synthesis to produce sequence-specific zwitterionic peptoids and study the detailed interfacial properties, including hydration, charge neutrality, and flexibility in molecular packing, of this antifouling design (Lau et al. 2015). Our peptoids consisted of alternating lysine and glutamic acid residues (i.e., Nlys and Nglu residues) spaced by specific numbers of

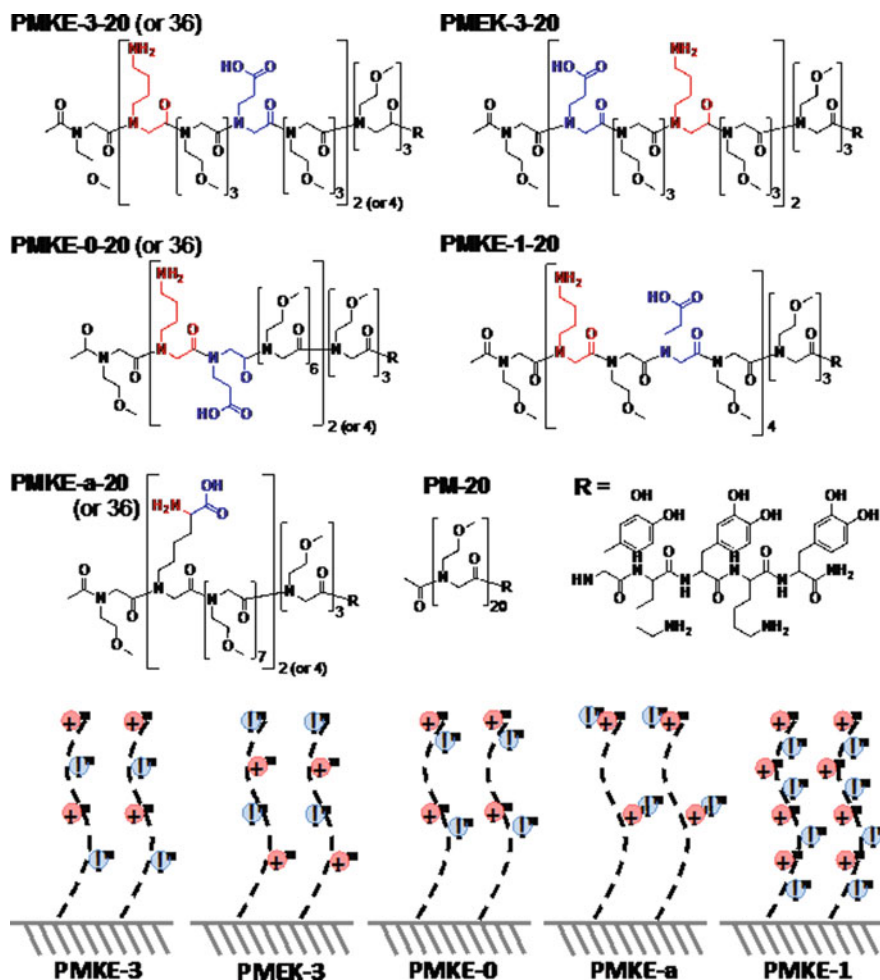


Fig. 3.4 Chemical structures of zwitterionic peptoid model polymers and schematics of the grafted charge arrangement (bottom row). The peptoids are named according to the nature of the residue design: P—peptoid; M—uncharged spacer residues with methoxyethyl sidechains; K—peptoid analog of lysine (red); E—peptoid analog of glutamic acid (blue). The number of M residues between the oppositely charged sidechains is indicated by the numeral following the letter designation (0, 1, 3, and a). The last numeral specifies the total number of residues in the peptoid brush segment (20 or 36). As in previous studies, The R-group is a pentameric peptide with special adhesive properties to graft the 20-mer peptoid chain onto a TiO₂ surface. Reproduced from Lau et al. (2015). Copyright Lau et al. Creative Commons license CC BY-NC 4.0

uncharged residues with methoxyethyl sidechains (i.e., the same Nme residues as in PMP1), to tune the spatial separation between the charged sidechains as well as the overall charge densities (Fig. 3.4). Therefore, the overall set of sequence designs tested the potential advantage of adding zwitterionic charged groups to the PMP1

brush design with already impressive antifouling performance (see Sects. 3.1 and 3.2).

The set of zwitterionic peptoids exhibited overall excellent resistance against protein adsorption and cell attachment similar to or slightly surpassing the levels exhibited by PMP1 (Fig. 3.5). Significantly, it was observed that a separation of <1.7 nm between charged groups was required to enable a charge-neutral zwitterionic character to the antifouling brush. Otherwise, individual charged groups on a protein and the polymer brush may directly interact electrostatically to cause higher adsorption (Fig. 3.5d). Furthermore, at intermediate grafting densities, the zwitterionic designs were able to suppress protein adsorption more than PMP1 by ca. 10–20%, although all antifouling peptoid brushes studied exhibited the same critical chain density for preventing protein adsorption (Fig. 3.5a and b). More importantly, the zwitterionic peptoids were able to suppress protein adsorption over the entire pH range studied from pH 5 to 7.4, whereas 5–8 times more protein adsorption occurred on PMP1 at pH 5 and 6 (Fig. 3.5c and d). Acidic pH is encountered in several biomedically important environments, including cancer tumors and lysosomes (for drug delivery). Therefore zwitterionic (peptoid) brushes could be advantageous in biomedical applications. All zwitterionic species, like the uncharged PMP1, were able to suppress fibroblast attachment. On the other hand, the resistance against bacteria attachment were more varied (Fig. 3.5e), with high resistance against *E. coli*, *S. aureus*, and *S. epidermidis*, but not *P. aeruginosa*. Some subtle differences between the different charge group arrangements were also observed.

Recently, we further studied the charge and hydration behavior of our zwitterionic peptoids using atomistic molecular dynamics (MD) (Cheung and Lau 2019). Previous modeling of polyvinyl-based zwitterionic polymers, PEG, and other antifouling polymers have already shown that polymer designs favoring H-bonding with water result in longer living hydration layers and enhance antifouling performance (Leng et al. 2015b, 2018). Our simulations further showed that charged residues of zwitterionic peptoids are segregated to the exterior of the brush layer which minimizes the electrostatic dipole of the brush structure, potentially leading to reduced electrostatic interaction with proteins. Moreover, we were able to verify that at intermediate to high densities (0.37 and 0.56 chain/nm⁻²), the zwitterionic peptoid brushes are organized as relatively uniform layers. Interestingly, and perhaps contrary to expectations, at any chain density, the mobilities of the zwitterionic peptoid chains at high grafting densities remain higher than both the same peptoids at lower densities and the uncharged PMP1 as well as polysarcosine (see Sect. 3.3). One might expect the bulkier charged groups to limit the space available for chain fluctuations. However, the high chain mobilities observed could be due to the strong interaction of the charged groups with water molecules and the constant chain rearrangements required to accommodate the highly mobile water molecules contained within a high-density zwitterionic brush structure.

The Segalman group had also prepared a set of sequence-specific polystyrene-*block*-peptoid copolymers to investigate the effects of chain hydration and chain segregation on antifouling properties against spores of marine organisms (van

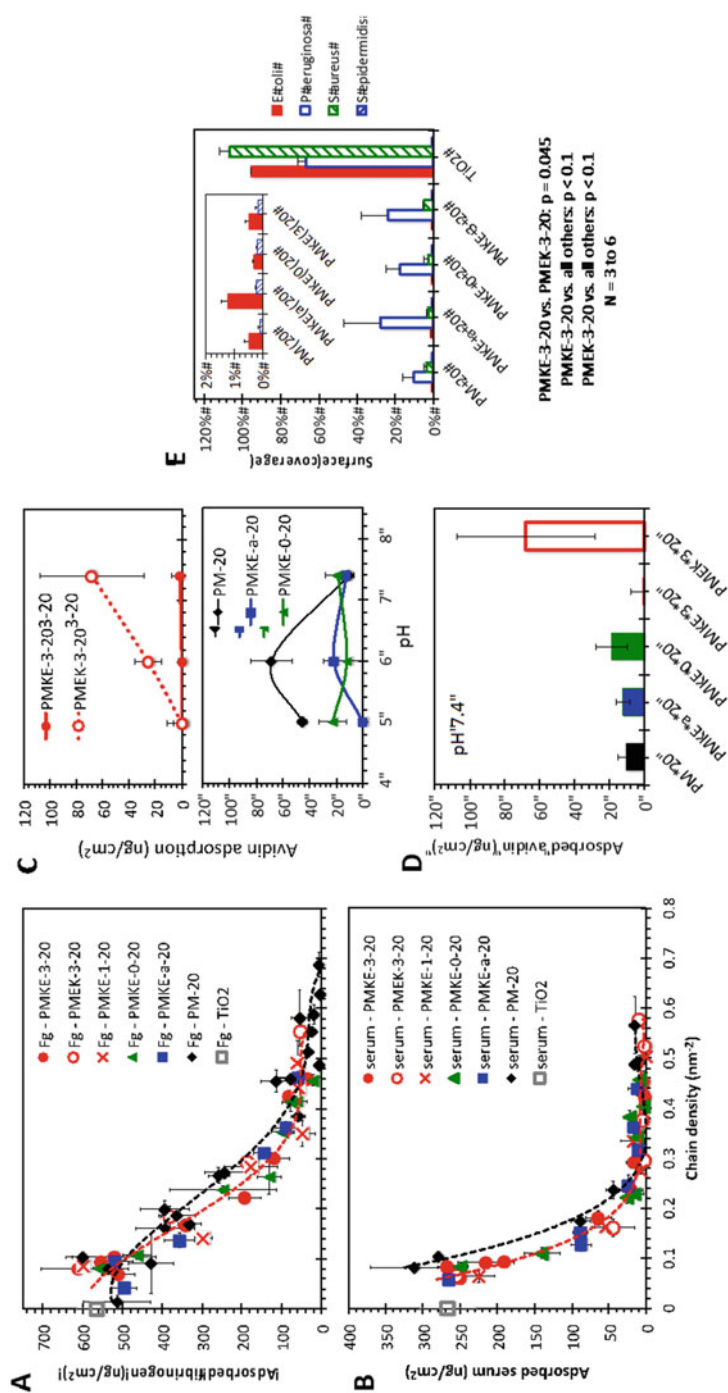


Fig. 3.5 Adsorption of fibrinogen protein (a) and 10% bovine calf serum (b) on zwitterionic peptoid brushes grafted at different chain densities. The peptoid nomenclature references those shown in Fig. 3.4. (c) Avidin adsorption on the peptoid brushes and the TiO₂ control at different pH. The peptoid surface chain density was $0.31 \pm 0.03 \text{ nm}^{-2}$ for all brushes. (d) Summary of the adsorption results at pH 7.4. Error bars for all panels indicate $\pm 1 \text{ SD}$. $N \geq 3$. (e) The amount of bacteria attached on the various peptoids. Adapted from Lau et al. (2015). Copyright Lau et al. Creative Commons license CC BY-NC 4.0

Zoelen et al. 2012, 2014, Leng et al. 2015a). Residues with fluorinated sidechains were incorporated to enhance the ability of the brushes to release the fraction of spores that had been adsorbed. Sum frequency generation (SFG) vibrational spectroscopy and X-ray spectroscopy were used to measure the surface hydration and monomer segregation, respectively. Interestingly, while fouling-release properties are found to be controlled mainly by the number of fluorinated residues, the surface chemistry and antifouling performance were controlled mainly by the position of the fluorinated units along the chains (van Zoelen et al. 2014). Further studies showed that fluorinated residues that reside toward the surface increases the water contact angle and decreases the hydration, and hence increases the amount of adsorption. However, this also had the effects of enhancing the speed of polymer chain restructuring at the air interface and spore release (Leng et al. 2015a).

3.3.5 Addition of Antimicrobial Peptoids and Other Functional Groups

Antimicrobial resistance, lack of broad spectrum activity, as well as side effects of conventional antibiotics have led to the search for new or modified antimicrobial agents (Molchanova et al. 2017, Hasan et al. 2018, Saxena et al. 2018). A plethora of antimicrobial peptides occur in nature, but their susceptibility to enzymatic degradation has hindered their application. Hence peptoids, which are resistant to proteolysis, are considered a plausible molecular platform for the development of novel antimicrobial agents (Ryge and Hansen 2005, Vedel et al. 2007, Uchida et al. 2009, Eggimann et al. 2015, Corson et al. 2016, Molchanova et al. 2019). However, the cytotoxic effects of current antimicrobial peptoids as well as the general problem of rising antimicrobial resistance with environmental release of antimicrobials remain.

In an attempt to apply antimicrobial peptoids but mitigate their problems, Statz et al. grafted antimicrobial peptoids to the tips of antifouling PMP1 brushes (Statz et al. 2008b). This strategy should limit antimicrobial release as well as reduce cytotoxicity since the antimicrobial is localized to the material surface (e.g., the surface of a biomedical device where infection might take place). The antifouling peptoid segment should also reduce the amount of bacteria that attaches to cause an infection in the first place. In this initial study, however, both the antimicrobial and antifouling effects were lowered in the combined peptoid design after grafting on a surface, as compared to the antimicrobial peptoid in solution before surface grafting and PMP1 grafted by itself. In fact, significantly higher water contact angles were measured as compared to PMP1, indicating decreased hydration of the combined peptoid surfaces. The consequent increase in protein adsorption was probably due to the number of hydrophobic residues (ca. two-thirds of the chain) contained within the antimicrobial peptoid segment. However, recent preliminary work in our group shows that these problems could be mitigated with careful control of the specific linker spacings placed between the antimicrobial sequence and the device surface (data not shown).

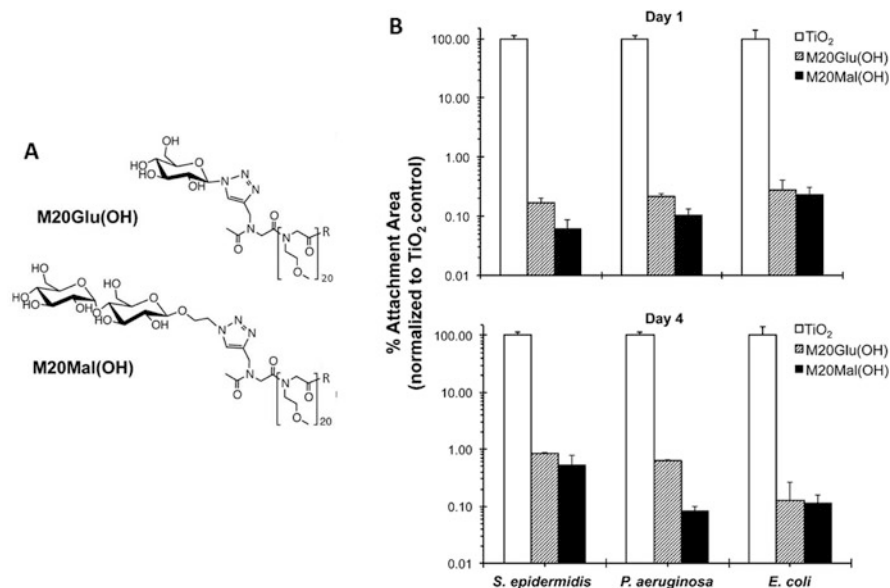


Fig. 3.6 (a) Chemical structure of the antifouling glycopeptoids (peptoids with sugar groups attached). As in previous studies, the R-group is a pentameric peptide with special adhesive properties to graft the 20-mer peptoid chain onto a TiO₂ surface. (b) Suppression in the attachment of various bacterial strains by the glycopeptoids after 1 day and 4 days. Adapted with permission from Ham et al. (2013). Copyright the American Chemical Society

To enhance the antifouling effect of peptoid brushes, especially against bacteria, Ham et al. also coupled additional units to the tips of a PMP1 brush (Ham et al. 2013). Indeed, to further the theme of biomimicry, the researchers added simple sugar groups (glucose and maltose) to create surface grafted glycopeptoids that resemble the glycocalyx of the mammalian outer cell membrane (Fig. 3.6), in an attempt to capture the ability of cells to inhibit nonspecific biomolecular interactions. Encouraging results were obtained. The attachment of *P. aeruginosa* and *E. coli* on the glycopeptoids decreased to 0.1% of the surface coverage on modified TiO₂ surfaces, while the attachment of *S. epidermidis* decreased to 1% of the TiO₂ control (Fig. 3.6b). Significantly, when compared with PMP1, complementary nuclear magnetic resonance (NMR) spectroscopy and molecular dynamics (MD) studies showed that the number of H-bonds made with water increased by ca. five times on glucose-functionalized PMP1 and by ca. ten times on maltose-functionalized PMP1. These results further highlight the role of hydration on the antifouling performance of antifouling (peptoid) designs, as well as the ability to use the peptoid platform to (conveniently) achieve sophisticated molecular designs with biofunctionality.

3.4 Conclusion

The convenience of solid-phase submonomer peptoid synthesis has enabled the investigation of a variety of peptoid designs, both as homopolymers and as sequence-specific chains, for their potential antifouling properties against protein adsorption, fibroblast attachment, as well as bacteria attachment (both gram positive and negative). We have demonstrated excellent antifouling performance for PMP1, its zwitterionic derivative PMKE, and polysarcosine, the simplest peptoid. Interestingly, polysarcosine appears to exhibit similar antifouling performance as the more “sophisticated” PMP1. The possibility of obtaining polysarcosine in bulk quantities by ROP polymerization also makes this peptoid particularly attractive from an application point of view, and various groups have proposed to use it as an alternative to PEG.

We have also used the sequence specificity of peptoids to investigate in detail how the spatial distribution of charge groups of zwitterionic polymers directs antifouling properties. With the appropriate charge spacing, PMKE appears to offer some performance gain over PMP1, in particular, the ability of the zwitterionic design to resist biofouling in more varied pH environments and potentially in corresponding biomedically relevant niches. Peptoid synthesis in general also enables the convenient coupling of additional functional groups to the chain. Addition of simple sugars to the end of a peptoid, e.g., maltose, especially enhanced the resistance against bacteria attachment by up to an order of magnitude. Overall, peptoids constitute an unparalleled platform to investigate the chemical design of antifouling polymers and to obtain coated surfaces with excellent resistance against the fouling of proteins and biological cells.

Acknowledgments VS thanks the Commonwealth Scholarship Commission for a Split Site award (INCN-2018-129). The work of MM and KHAL were supported by a young investigator grant from the Human Frontier Science Program (RGY0074/2016).

References

- Ballard D, Bamford C (1956) Reactions of N-carboxy- α -amino-acid anhydrides catalysed by tertiary bases. *J Chem Soc (Resumed)* 9:381–387
- Chapman RG, Ostuni E, Takayama S, Holmlin RE, Yan L, Whitesides GM (2000) Surveying for surfaces that resist the adsorption of proteins. *J Am Chem Soc* 122:8303–8304
- Cheung DL, Lau KHA (2019) Atomistic study of zwitterionic peptoid antifouling brushes. *Langmuir* 35:1483–1494
- Cioffi CL, Liu S, Wolf MA (2010) Chapter 2—recent developments in glycine transporter-1 inhibitors. *Annual reports in medicinal chemistry*. J E Macor, Academic Press 45:19–35
- Corson AE, Armstrong SA, Wright ME, McClelland EE, Bicker KL (2016) Discovery and characterization of a peptoid with antifungal activity against *Cryptococcus neoformans*. *ACS Med Chem Lett* 7:1139–1144
- Culf AS (2019) Peptoids as tools and sensors. *Biopolymers* 110:e23285
- Culf AS, Ouellette RJ (2010) Solid-phase synthesis of N-substituted glycine oligomers (α -peptoids) and derivatives. *Molecules* 15:5282–5335

- de Gennes PG (1987) Polymers at an interface; a simplified view. *Adv Colloid Interf Sci* 27:189–209
- Eggimann GA, Bolt HL, Denny PW, Cobb SL (2015) Investigating the anti-leishmanial effects of linear peptoids. *ChemMedChem* 10:233–237
- Fetsch C, Luxenhofer R (2012) Highly defined multiblock copolypeptoids: pushing the limits of living nucleophilic ring-opening polymerization. *Macromol Rapid Commun* 33:1708–1713
- Fetsch C, Grossmann A, Holz L, Nawroth JF, Luxenhofer R (2011) Polypeptoids from N-substituted glycine N-carboxyanhydrides: hydrophilic, hydrophobic, and amphiphilic polymers with poisson distribution. *Macromolecules* 44:6746–6758
- Gangloff N, Ulbricht J, Lorson T, Schlaad H, Luxenhofer R (2016) Peptoids and polypeptoids at the frontier of supra- and macromolecular engineering. *Chem Rev* 116:1753–1802
- Goodman M, Fried M (1967) Conformational aspects of polypeptide structure. XX. Helical poly-N-methyl-L-alanine. Experimental results. *J Am Chem Soc* 89:1264–1267
- Goodman M, Chen F, Prince FR (1973) Conformational aspect of polypeptide structure. XLIV. Conformational transitions of poly (N-methyl-alanines) induced by trifluoroacetic acid. *Biopolymers* 12:2549–2561
- Gorske BC, Jewell SA, Guerard EJ, Blackwell HE (2005) Expedient synthesis and design strategies for new peptoid construction. *Org Lett* 7:1521–1524
- Habraken GJ, Wilsens KH, Koning CE, Heise A (2011) Optimization of N-carboxyanhydride (NCA) polymerization by variation of reaction temperature and pressure. *Polym Chem* 2:1322–1330
- Halperin A (1999) Polymer brushes that resist adsorption of model proteins: design parameters. *Langmuir* 15:2525–2533
- Ham HO, Park SH, Kurutz JW, Szeleifer IG, Messersmith PB (2013) Antifouling glycolyx-mimetic peptoids. *J Am Chem Soc* 135:13015–13022
- Hasan A, Waibhaw G, Saxena V, Pandey LM (2018) Nano-biocomposite scaffolds of chitosan, carboxymethyl cellulose and silver nanoparticle modified cellulose nanowhiskers for bone tissue engineering applications. *Int J Biol Macromol* 111:923–934
- Hong D, Hung H-C, Wu K, Lin X, Sun F, Zhang P, Liu S, Cook KE, Jiang S (2017) Achieving ultralow fouling under ambient conditions via surface-initiated atrop of carboxybetaine. *ACS Appl Mater Interfaces* 9:9255–9259
- Hoogenboom R, Schlaad H (2017) Thermoresponsive poly (2-oxazoline) s, polypeptoids, and polypeptides. *Polym Chem* 8:24–40
- Hörtz C, Birke A, Kaps L, Decker S, Wächtersbach E, Fischer K, Schuppan D, Barz M, Schmidt M (2015) Cylindrical brush polymers with polysarcosine side chains: a novel biocompatible carrier for biomedical applications. *Macromolecules* 48:2074–2086
- Huesmann D, Sevenich A, Weber B, Barz M (2015) A head-to-head comparison of poly(sarcosine) and poly(ethylene glycol) in peptidic, amphiphilic block copolymers. *Polymer* 67:240–248
- Jin H, Jian T, Ding Y-H, Chen Y, Mu P, Wang L, Chen C-L (2019) Solid-phase synthesis of three-armed star-shaped peptoids and their hierarchical self-assembly. *Biopolymers* 110:e23258
- Kidchob T, Kimura S, Imanishi Y (1998) Amphiphilic poly(Ala)-b-poly(Sar) microspheres loaded with hydrophobic drug. *J Control Release* 51:241–248
- Knight AS, Zhou EY, Francis MB, Zuckermann RN (2015) Sequence programmable peptoid polymers for diverse materials applications. *Adv Mater* 27:5665–5691
- Kruijtzter JA, Liskamp RM (1995) Synthesis in solution of peptoids using Fmoc-protected N-substituted glycines. *Tetrahedron Lett* 36:6969–6972
- Lahasky SH, Serem WK, Guo L, Garno JC, Zhang D (2011) Synthesis and characterization of cyclic brush-like polymers by N-heterocyclic carbene-mediated zwitterionic polymerization of N-propargyl N-carboxyanhydride and the grafting-to approach. *Macromolecules* 44:9063–9074
- Lambermont-Thijs HML, Hoogenboom R, Fustin C-A, Bomal-D'Haese C, Gohy J-F, Schubert US (2009) Solubility behavior of amphiphilic block and random copolymers based on 2-ethyl-2-oxazoline and 2-nonyl-2-oxazoline in binary water–ethanol mixtures. *J Polym Sci A Polym Chem* 47:515–522

- Lau KHA (2014) Peptoids for biomaterials science. *Biomaterials Science* 2:627–633
- Lau KA, Ren C, Park SH, Szleifer I, Messersmith PB (2011) An experimental–theoretical analysis of protein adsorption on peptidomimetic polymer brushes. *Langmuir* 28:2288–2298
- Lau KHA, Ren C, Park SH, Szleifer I, Messersmith PB (2012a) An experimental–theoretical analysis of protein adsorption on peptidomimetic polymer brushes. *Langmuir* 28:2288–2298
- Lau KHA, Ren C, Sileika TS, Park SH, Szleifer I, Messersmith PB (2012b) Surface-grafted polysarcosine as a peptoid antifouling polymer brush. *Langmuir* 28:16099–16107
- Lau KHA, Sileika TS, Park SH, Sousa AM, Burch P, Szleifer I, Messersmith PB (2015) Molecular design of antifouling polymer brushes using sequence-specific peptoids. *Adv Mater Interfaces* 2:1400225
- Leng C, Buss HG, Segalman RA, Chen Z (2015a) Surface structure and hydration of sequence-specific amphiphilic polypeptides for antifouling/fouling release applications. *Langmuir* 31:9306–9311
- Leng C, Hung H-C, Sieggreen OA, Li Y, Jiang S, Chen Z (2015b) Probing the surface hydration of nonfouling zwitterionic and poly (ethylene glycol) materials with isotopic dilution spectroscopy. *J Phys Chem C* 119:8775–8780
- Leng C, Huang H, Zhang K, Hung H-C, Xu Y, Li Y, Jiang S, Chen Z (2018) Effect of surface hydration on antifouling properties of mixed charged polymers. *Langmuir* 34:6538–6545
- Lin S, Zhang B, Skoumal MJ, Ramunno B, Li X, Wesdemiotis C, Liu L, Jia L (2011) Antifouling Poly(β -peptoids). *Biomacromolecules* 12:2573–2582
- Lorson T, Lübtow MM, Wegener E, Haider MS, Borova S, Nahm D, Jordan R, Sokolski-Papkov M, Kabanov AV, Luxenhofer R (2018) Poly (2-oxazoline) s based biomaterials: a comprehensive and critical update. *Biomaterials* 178:204–280
- Luxenhofer R, Fetsch C, Grossmann A (2013) Polypeptides: a perfect match for molecular definition and macromolecular engineering? *J Polym Sci A Polym Chem* 51:2731–2752
- Molchanova N, Hansen PR, Franzyk H (2017) Advances in development of antimicrobial peptidomimetics as potential drugs. *Molecules* 22:1430
- Molchanova N, Wang H, Hansen PR, Højby N, Nielsen HM, Franzyk H (2019) Antimicrobial activity of α -peptide/ β -peptoid lysine-based peptidomimetics against colistin-resistant *Pseudomonas aeruginosa* isolated from cystic fibrosis patients. *Front Microbiol* 10:275
- Murnen HK, Khokhlov AR, Khalatur PG, Segalman RA, Zuckermann RN (2012) Impact of hydrophobic sequence patterning on the coil-to-globule transition of protein-like polymers. *Macromolecules* 45:5229–5236
- Olivos HJ, Alluri PG, Reddy MM, Salony D, Kodadek T (2002) Microwave-assisted solid-phase synthesis of peptoids. *Org Lett* 4:4057–4059
- Prakash A, Baer MD, Mundy CJ, Pfaendtner J (2018) Peptoid backbone flexibility dictates its interaction with water and surfaces: a molecular dynamics investigation. *Biomacromolecules* 19:1006–1015
- Prime K, Whitesides G (1991) Self-assembled organic monolayers: model systems for studying adsorption of proteins at surfaces. *Science* 252:1164–1167
- Prime KL, Whitesides GM (1993) Adsorption of proteins onto surfaces containing end-attached oligo(ethylene oxide)—a model system using self-assembled monolayers. *J Am Chem Soc* 115:10714–10721
- Raynor JE, Capadona JR, Collard DM, Petrie TA, García AJ (2009) Polymer brushes and self-assembled monolayers: versatile platforms to control cell adhesion to biomaterials (review). *Biointerphases* 4:FA3–FA16
- Ryge TS, Hansen PR (2005) Novel lysine-peptoid hybrids with antibacterial properties. *J Pept Sci: Offi Pub Eur Pept Soc* 11:727–734
- Ryu JY, Song IT, Lau KA, Messersmith PB, Yoon T-Y, Lee H (2014) New antifouling platform characterized by single-molecule imaging. *ACS Appl Mater Interfaces* 6:3553–3558
- Saxena V, Hasan A, Sharma S, Pandey LM (2018) Edible oil nanoemulsion: an organic nanoantibiotic as a potential biomolecule delivery vehicle. *Int J Polym Mater Polym Biomater* 67:410–419

- Serrano Á, Sterner O, Mieszkina S, Zürcher S, Tosatti S, Callow ME, Callow JA, Spencer ND (2013) Nonfouling response of hydrophilic uncharged polymers. *Adv Funct Mater* 23:5706–5718
- Sisido M, Imanishi Y, Higashimura T (1977) Molecular weight distribution of polysarcosine obtained by NCA polymerization. *Die Makromolekulare Chemie: Macromol Chem Phys* 178:3107–3114
- Smith-Palmer T (2019) Clinical analysis I sarcosine, creatine, and creatinine. In: Worsfold P, Poole C, Townshend A, Miró M (eds) *Encyclopedia of analytical science*, 3rd edn. Academic Press, Oxford, pp 163–172
- Statz AR, Meagher RJ, Barron AE, Messersmith PB (2005) New peptidomimetic polymers for antifouling surfaces. *J Am Chem Soc* 127:7972–7973
- Statz AR, Barron AE, Messersmith PB (2008a) Protein, cell and bacterial fouling resistance of polypeptoid-modified surfaces: effect of side-chain chemistry. *Soft Matter* 4:131–139
- Statz AR, Park JP, Chongsiriwatana NP, Barron AE, Messersmith PB (2008b) Surface-immobilised antimicrobial peptoids. *Biofouling* 24:439–448
- Statz AR, Kuang J, Ren C, Barron AE, Szeleifer I, Messersmith PB (2009) Experimental and theoretical investigation of chain length and surface coverage on fouling of surface grafted polypeptoids. *Biointerphases* 4:FA22–FA32
- Szeleifer I (1997a) Polymers and proteins: interactions at interfaces. *Curr Opin Solid State Mater Sci* 2:337–344
- Szeleifer I (1997b) Protein adsorption on surfaces with grafted polymers: a theoretical approach. *Biophys J* 72:595–612
- Tao X, Deng C, Ling J (2014) PEG-amine-initiated polymerization of sarcosine n-thiocarboxyanhydrides toward novel double-hydrophilic peg-b-polysarcosine diblock copolymers. *Macromol Rapid Commun* 35:875–881
- Tao X, Zheng B, Bai T, Zhu B, Ling J (2017a) Hydroxyl group tolerated polymerization of N-substituted glycine N-thiocarboxyanhydride mediated by aminoalcohols: a simple way to α -Hydroxyl- ω -aminotelechelic polypeptoids. *Macromolecules* 50:3066–3077
- Tao X, Zheng B, Kricheldorf HR, Ling J (2017b) Are N-substituted glycine N-thiocarboxyanhydride monomers really hard to polymerize? *J Polym Sci A Polym Chem* 55:404–410
- Tao X, Li M-H, Ling J (2018) α -Amino acid N-thiocarboxyanhydrides: a novel synthetic approach toward poly(α -amino acids). *Eur Polym J* 109:26–42
- Toda M, Arima Y, Iwata H (2010) Complement activation on degraded polyethylene glycol-covered surface. *Acta Biomater* 6:2642–2649
- Uchida M, McDermott G, Wetzler M, Le Gros MA, Myllys M, Knoechel C, Barron AE, Larabell CA (2009) Soft X-ray tomography of phenotypic switching and the cellular response to antifungal peptoids in *Candida albicans*. *Proc Natl Acad Sci* 106:19375–19380
- Unsworth LD, Sheardown H, Brash JL (2005) Polyethylene oxide surfaces of variable chain density by chemisorption of PEO-thiol on gold: adsorption of proteins from plasma studied by radiolabelling and immunoblotting. *Biomaterials* 26:5927–5933
- van Zoelen W, Zuckermann RN, Segalman RA (2012) Tunable surface properties from sequence-specific polypeptoid–polystyrene block copolymer thin films. *Macromolecules* 45:7072–7082
- van Zoelen W, Buss HG, Ellebracht NC, Lynd NA, Fischer DA, Finlay J, Hill S, Callow ME, Callow JA, Kramer EJ, Zuckermann RN, Segalman RA (2014) Sequence of hydrophobic and hydrophilic residues in amphiphilic polymer coatings affects surface structure and marine antifouling/fouling release properties. *ACS Macro Lett* 3:364–368
- Vedel L, Bonke G, Foged C, Ziegler H, Franzky H, Jaroszewski JW, Olsen CA (2007) Antiplasmodial and prehemolytic activities of α -peptide– β -peptoid chimeras. *ChemBioChem* 8:1781–1784
- Vroman L (1962) Effect of adsorbed proteins on the wettability of hydrophilic and hydrophobic solids. *Nature* 196:476–477
- Wiesbrock F, Hoogenboom R, Leenen M, van Nispen SFGM, van der Loop M, Abeln CH, van den Berg AMJ, Schubert US (2005) Microwave-assisted synthesis of a 42-membered library of

- diblock copoly(2-oxazoline)s and chain-extended homo poly(2-oxazoline)s and their thermal characterization. *Macromolecules* 38:7957–7966
- Yang W, Xue H, Li W, Zhang J, Jiang S (2009) Pursuing “zero” protein adsorption of poly (carboxybetaine) from undiluted blood serum and plasma. *Langmuir* 25:11911–11916
- Yu HM, Chen ST, Wang KT (1992) Enhanced coupling efficiency in solid-phase peptide synthesis by microwave irradiation. *J Organ Chem* 57:4781–4784
- Zhu H, Chen Y, Yan F-J, Chen J, Tao X-F, Ling J, Yang B, He Q-J, Mao Z-W (2017) Polysarcosine brush stabilized gold nanorods for in vivo near-infrared photothermal tumor therapy. *Acta Biomater* 50:534–545
- Zuckermann RN (2011) Peptoid origins. *Pept Sci* 96:545–555



Structure and Rheology of Hydrogels: Applications in Drug Delivery

4

Sai Geetha Marapureddy and Prachi Thareja

Abstract

Hydrogels are 3D network like structures comprising of hydrophilic polymers having copious amounts of water in their interstitial spaces and thus promising materials for the drug delivery platforms. Physical and chemical methods are employed to synthesize the hydrogels. Rheology provides the structure–property relationships to understand the various mechanisms of hydrogels which can tune the cross-linking density to assess the mechanical strength. Stimuli-responsive, in situ, and injectable hydrogels are being explored at different scales for the delivery of drugs, proteins, and biomolecules. This chapter provides an extensive overview of the different methods of fabrication, swelling properties, rheology, and developments in drug delivery applications of hydrogels.

Keywords

Cross-linking · Swelling · Rheology · Diffusion · Drug delivery

Abbreviations

BAG	Bioactive glass
CGT	Critical gelation temperature
DRF	Tris (4-isocyanatophenyl) thiophosphate
LCST	Lower critical solution temperature
McH ⁺	Merocyanine-H ⁺
PBA	Phenyl boronic acid
PEG	Poly ethylene glycol

S. G. Marapureddy · P. Thareja (✉)
Chemical Engineering, Indian Institute of Technology (IIT) Gandhinagar, Palaj, Gujarat, India
e-mail: marapu.reddy@iitgn.ac.in; prachi@iitgn.ac.in

PEO	Poly ethylene oxide
PMVE/MA	Poly methylvinylether/maleic acid
PNIPAM	Poly n-isopropylacrylamide
PPO	Poly propylene oxide
PVA	Poly vinyl alcohol
PVP	Poly vinyl pyrrolidene
SAOS	Small angle oscillatory shear
UCST	Upper critical solution temperature

4.1 Introduction

Hydrogels are water-insoluble cross-linked hydrophilic network polymers which are capable of holding a copious amount of water in their swollen state, about 30–40 times of their dry weight. The cross-linking can be either physical/chemical or can be a combination of both (Ahmadi et al. 2015). Hydrophilic functional groups such as amine (NH_2), hydroxyl ($-\text{OH}$), amide ($-\text{CONH}-$, $-\text{CONH}_2$), and sulfate ($-\text{SO}_3\text{H}$) present on the polymeric backbone are the main reason to hold water in the matrix where cross-links prevent the dissolution of the network (Ahmed 2015; Gerlach and Arndt 2009). In 1959, Lim and his coworkers prepared a copolymer of triethyleneglycol monomethacrylate with triethyleneglycol dimethacrylate in which methacrylate esters were the cross-linking agents of ethylene glycol polymer (Kopeček 2009) and noticed its hydrogel nature and later explored its application in contact lenses.

The evolution of hydrogels has been reported in four stages by Buwalda et al. The first-generation hydrogels came in the early 1950s where the hydrogels were prepared by chemical cross-linking and some irradiation methods. The second-generation hydrogels focused on the stimuli-responsive gels where external stimuli of pH, temperature, and light, etc., control the swelling. The third-generation hydrogels emerged in the early 1980s with click chemistry—physical interactions such as metal coordination complex formations and stereocomplex formations. The fourth-generation hydrogels, i.e., smart hydrogels, encompass nanocomposite hydrogels and double network hydrogels (Buwalda et al. 2014; Roy 2015).

Rheological studies showed that a solution of water-soluble polymers show Newtonian behavior where no considerable entanglements are present, but when cross-linked networks were introduced, they started to show viscoelastic behavior (Akhtar et al. 2016). These unique and versatile properties attracted many researchers to explore the applications of hydrogels in the fields of agriculture, biomedical, cosmetics, personal care products such as adult diapers and protein separation (Maitra and Shukla 2014). Drug delivery is one such platform where hydrogels are being taken, the leverage of controlled and continuous delivery of the therapeutics. There are various drug delivery platforms being explored other than the hydrogels such as metallic nanoparticles (Thirumurugan et al. 2018), emulsions (Saxena et al. 2018), polymeric films (Hasan et al. 2017), dendrimers (Palmerston Mendes et al. 2017), liposomes (Alavi et al. 2017), bio-inspired drug delivery

vehicles where bacterial ghosts, micro-bots, virus-like nanoparticles are the carriers of drug (Maelys et al. 2018), fullerenes (Wissing et al. 2004), quantum dots such as zinc oxide (Cai et al. 2016) and zinc selenide (Zhao et al. 2017), etc., with different success rates.

However, the main advantage of hydrogels is the drug release kinetics, which can be controlled by tuning the density of cross-linking (Zhao et al. 2015). Hydrogels can achieve targeted drug delivery as they are sensitive to external stimuli (Xu et al. 2018). Polymers such as polyethylene glycol (PEG) and chitosan give stealth properties against phagocytosis and increase the retention time of the drug (Amoozgar et al. 2012). Hydrogels also have good tunable biocompatible and biodegradable properties compared to the other bio-materials (Chai et al. 2017). This chapter summarizes the different methods of synthesis of hydrogels, swelling properties, and different stimuli that affect the swelling in hydrogels. Rheology of hydrogels has been explained to understand the mechanism of their gelation with time and temperature, structural recovery after applying cyclic shear strain and the mechanical properties of hydrogels. Different routes of drug delivery and the release mechanism through hydrogels have also been discussed in detail.

4.2 Different Interactions Responsible for the Formation of Hydrogels

4.2.1 Chemical Cross-linking

Chemical cross-linking can be performed in two ways. In the first approach, multi/unifunctional monomer cross-links the monomers during the copolymerization. Bulk, solution, and suspension polymerization techniques are applied to achieve this cross-linking. In the second approach, polymers are cross-linked by simply mixing the preformed polymers by adding chemical cross-linkers or by using irradiation methods (Ahmed 2015).

Hydrophilic groups (NH_2 , COOH , OH) on the polymeric matrix are subjected to covalent bonding by low molecular weight cross-linkers. The cross-linkers are small molecules which have at least two functional groups to form the connection between polymeric chains. Aldehyde such as glutaraldehyde with two aldehyde groups at the ends are used to cross-link the $-\text{NH}_2$ groups of chitosan, $-\text{OH}$ groups of polyvinyl alcohol (PVA) to form Schiff bases as shown in Fig. 4.1a (Arguk Elles-Monal et al. 1998; Kumar Parida et al. 2011; Jamnongkan and Kaewpirom 2010). Genipin derived from Gardenia fruit is a natural and biocompatible chemical cross-linker which has replaced the use of aldehydes. Yu et al. synthesized a thermoresponsive hydrogel composed of carboxymethyl chitosan and poloxamer 407 using genipin as a cross-linker for drug delivery vehicle of baicalin (Yu et al. 2018). Dimida et al. synthesized chitosan scaffolds for tissue engineering using Genipin as a cross-linker, as shown in Fig. 4.1c (Dimida et al. 2017; Muzzarelli et al. 2015). Higher functional groups such as 1,6-hexamethylene diisocyanate and hexanedibromide cross-link

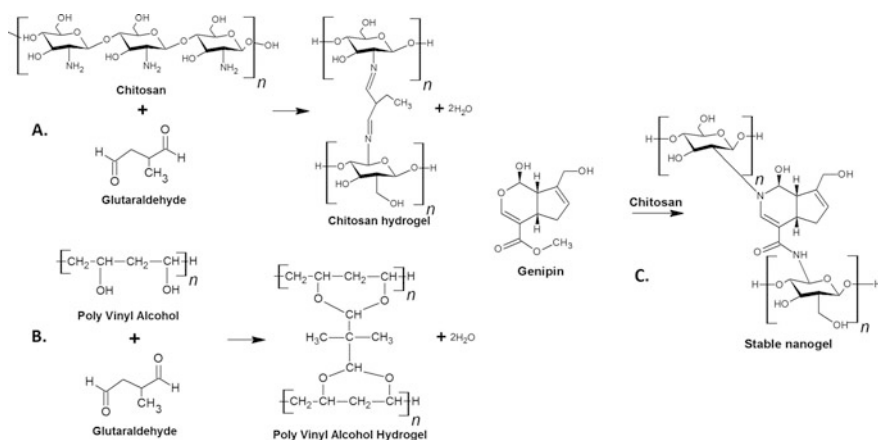


Fig. 4.1 (a) Chitosan and (b) polyvinyl alcohol chemically cross-linked with glutaraldehyde, reproduced from Jammongkan and Kaewpirom (2010) (c) Chitosan cross-linked with genipin, reproduced from Muzzarelli et al. (2015)

with dextran (Simonsen et al. 1995) and scleroglucan (Coviello et al. 1999) polymers, respectively.

Chemically cross-linked hydrogels also have significant mechanical strength and long degradation times, depending on the structure of cross-linking agents and covalent bonds in gels (Aoyagi et al. 1992). Unreacted chemical cross-linking agents have to be removed entirely from the hydrogel to prevent undesirable side effects in biomedical applications. This use of chemical cross-linking can be entirely avoided by using irradiation techniques to cross-link the polymers (Hennink and van Nostrum 2012). PVA and polyvinylpyrrolidone (PVP) are cross-linked by irradiating the mixture with γ radiation (Razzak et al. 2001). Collagen hydrogels generally get cross-linked at neutral pH, but irradiating with γ rays can cross-link the hydrogel at acidic pH (Inoue et al. 2006).

4.2.2 Physical Cross-linking

Unlike chemical cross-linking, physically cross-linked gel network is temporary. Some of the physically formed networks are readily deformable and can be reformed without a hysteresis. Ionic, hydrophobic, crystallization, and stereocomplex formations are the primary physical interactions which can lead to the formation of physically cross-linked hydrogels.

4.2.2.1 Ionic Interactions

These interactions involve the electrostatic attraction between oppositely charged molecules or ions. Incorporation of an oppositely charged polymer/ion to that of the primary polymeric matrix induces an electrostatic interaction that forms bridges

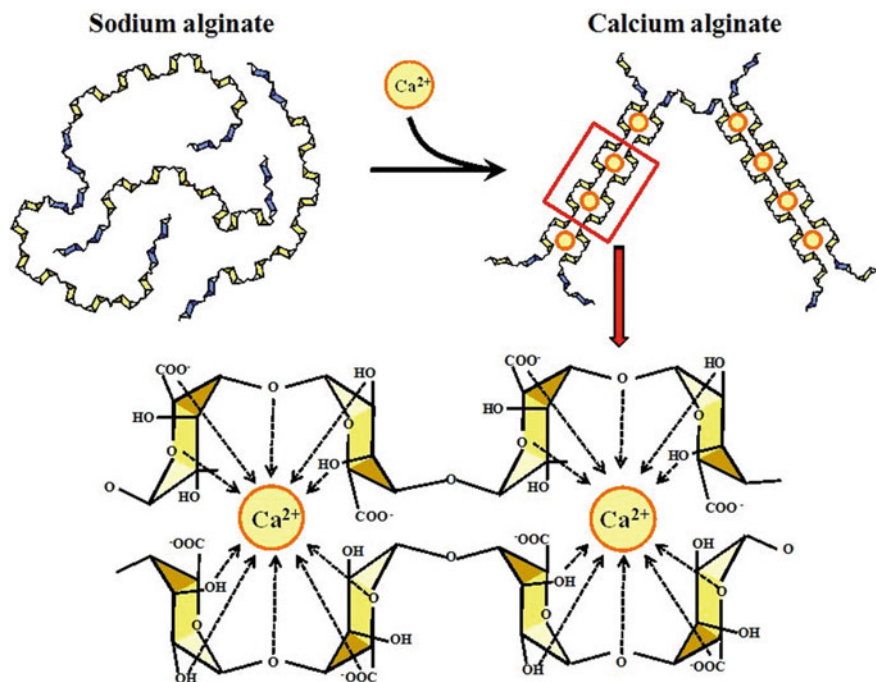


Fig. 4.2 Sodium alginate cross-linked with calcium chloride salt due to ionic interactions reproduced from Kashima and Imai (2012)

between the polymer chains resulting in the formation of a gel (Berger et al. 2004). For example, sodium alginate, an anionic polymer, treated with calcium or aluminum chloride forms a stable hydrogel as shown in Fig. 4.2 (Kashima and Imai 2012); PVA treated with borax (Tsong and Burgess 2012); and chitosan cross-linked with tripolyphosphate (TPP) (Jätariu et al. 2011).

4.2.2.2 Hydrophobic Interactions

Amphiphilic molecules consisting of short hydrophobic chains associate through hydrophobic interactions to form self-assemblies and bridge the hydrophilic chains resulting in a non-permanent network (Papadakis and Tsitsilianis 2017). These interactions create reversible cross-links, which make them flowable with external stimuli such as temperature and pH. Jung et al. developed thermoresponsive pluronic hydrogels by physically mixing hyaluronic acid and a triblock copolymer comprising of hydrophilic polyethylene oxide (PEO), and hydrophobic polypropylene oxide (PPO) arranged in an A–B–A manner (PEO–PPO–PEO) for drug delivery studies. The pluronics are known to form micelles with an increase in temperature. The hydrophobic interactions between methyl groups on pluronics and acetyl groups on hyaluronic acid caused the gelation and formed a densely packed network of

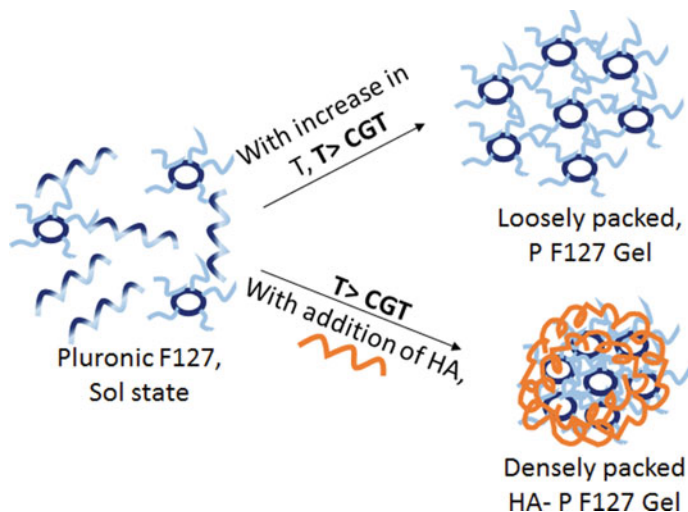


Fig. 4.3 Schematic of densely packed PF127 and hyaluronic acid by hydrophobic interactions (Jung et al. 2017)

micelles upon reaching critical gelation temperature (CGT) as shown in Fig. 4.3 (Jung et al. 2017).

4.2.2.3 Hydrogen Bonding

Hydrogen bonding is an interaction existing between an electronegative element and a hydrogen attached to the other electronegative element. Intra- or inter-hydrogen bonding between the polymeric chains can form a reversible network which can lead to the formation of a hydrogel (Arunan et al. 2011).

Song et al. explored the fabrication of a tough hydrogel by heating acrylamide in the presence of PVP under an inert atmosphere to form an interpolymer complex by hydrogen bonding as shown in Fig. 4.4 (Song et al. 2013). Kimura et al. investigated the network formation of a mixture of two water-soluble phospholipids poly (2-methacryloyloxyethyl phosphorylcholine-co-methacrylic acid) and poly (2-methacryloyloxyethyl phosphorylcholine-co-n-butyl methacrylate).

They concluded that the instant dimer formation due to hydrogen bonding was the reason for the formation of hydrogel (Kimura et al. 2004).

4.2.2.4 Crystallization

The crystallization process induces gelation among some polymers where some parts of polymeric chains grow into crystallites, and the other amorphous part is arranged disorderly (Stenekes et al. 2001). Semi-crystalline PVA forms a gel when it undergoes freeze–thaw cycles alternatively. The hydrogen bond formed between PVA polymeric chains form an entangled network. When PVA goes through the freezing cycle, ice forms in an amorphous region and during the thawing cycle, PVA crystallites grow until their facets meet other crystallites and result in the formation

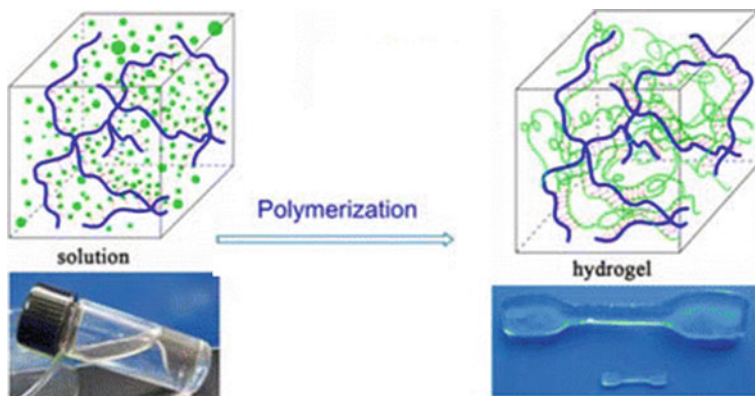


Fig. 4.4 Schematic of PVP and acrylamide hydrogel formed due to hydrogen bonding reproduced from Song et al. (2013)

of a porous network (Gupta et al. 2011). PVA crystallites formed in the gel acted as physical cross-linking sites in the network (Peppas and Scott 1992).

A stronger gel was formed than that of chemically cross-linked as the mechanical load is distributed along the crystallites (Hassan and Peppas 2000; Peppas and Merrill 1976). Similarly, dextran also forms a hydrogel by crystallization process as the aggregates formed at higher concentration due to intermolecular hydrogen bonding form crystallites by nucleation (Stenekes et al. 2001).

4.2.2.5 Stereocomplex Formation

A polymer consisting of two enantiomers lead to the stereocomplex formation and in turn, developed into cross-links in the hydrogel matrix (Maitra and Shukla 2014).

For instance, enantiomeric lactic acid oligomers grafted on dextran form cross-links due to the stereocomplex formation, as shown in Fig. 4.5. This hydrogel system is completely biodegradable as the lactic acid oligomers are attached to dextran via a hydrolytically sensitive carbonate ester bond (Hennink et al. 2004). The synthesis process was straightforward as the hydrogel could be formed by simply blending two aqueous solutions. However, a limited number of polymeric compositions can be used in this strategy of formation of hydrogels (Aoyagi et al. 1992).

4.3 Swelling of Hydrogels

Swelling is the main characteristic of hydrogels. Polymer–water interactions, ionic interactions, and osmotic forces control the swelling in a hydrogel. The elastic forces originating from the network cross-linking balance out the swelling forces to prevent the dissolution of hydrogels (Omidian and Park 2010). Swelling and deswelling depend on various factors such as ionic strength and pH of the medium, polymer

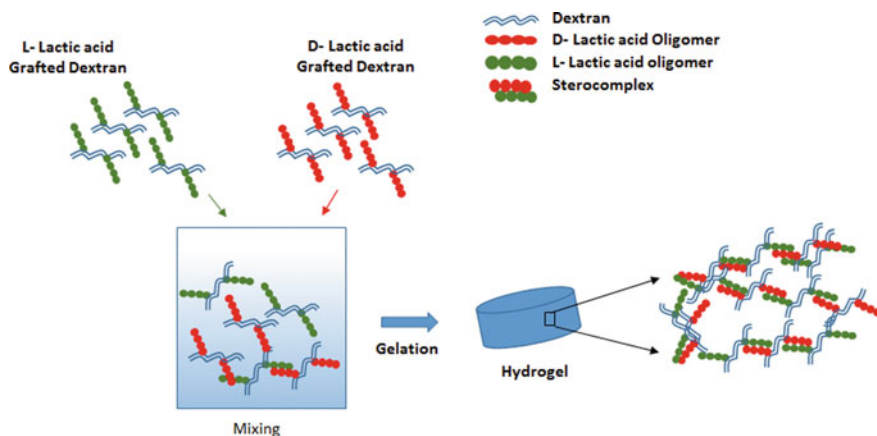


Fig. 4.5 Formation of the hydrogel by cross-linking enantiomers of lactic acid with dextran (Hennink et al. 2004)

concentration, mode of cross-linking, cross-linker concentration, and drying techniques (Kim and Matsunaga 2017).

The most critical factor that influences the swelling is cross-link density. The cross-link density determines the length between two cross-links on the same polymer chain. Cross-linking is higher if the length is small and vice versa (Choi et al. 2015). When cross-linking density is low, swelling is initially diffusion controlled, and slowly, the polymer chains relax to allow more water into the network, as shown in Fig. 4.6. As the cross-link density increases, only the diffusion mechanism dominates and the rate of swelling decreases (Omidian and Park 2010).

The swelling involves a transition in the mass, volume, and dimensions of hydrogels. The swelling ratio is expressed either as weight swelling ratio (gm/gm) or volume swelling ratio (ml/ml) (Amri et al. 2018).

$$\text{Weight swelling ratio, } (Q_t) = \frac{W_w - W_d}{W_d}$$

where W_w is the wet weight, W_d is the dry weight of the hydrogel. Q_t is measured in some cases, for instance, swelling in diapers (Prasad et al. 2004). If the swelling is pressure-driven, volume change can be noted by pressure sensors.

4.3.1 External Stimuli-Controlled Swelling

4.3.1.1 pH-Controlled Swelling

Anionic hydrogels consisting of a polymer having sulfonic or carboxylic groups ionize at a pH higher than their pK_b values and swell due to electrostatic repulsion as shown in Fig. 4.7.

Cationic hydrogels consist of a polymer having amino groups which get protonated at lower pH and repel with H^+ ions leading to swelling (Schwarte et al. 1999). Cationic polymers like chitosan and polyethylene amine swell at lower pH as

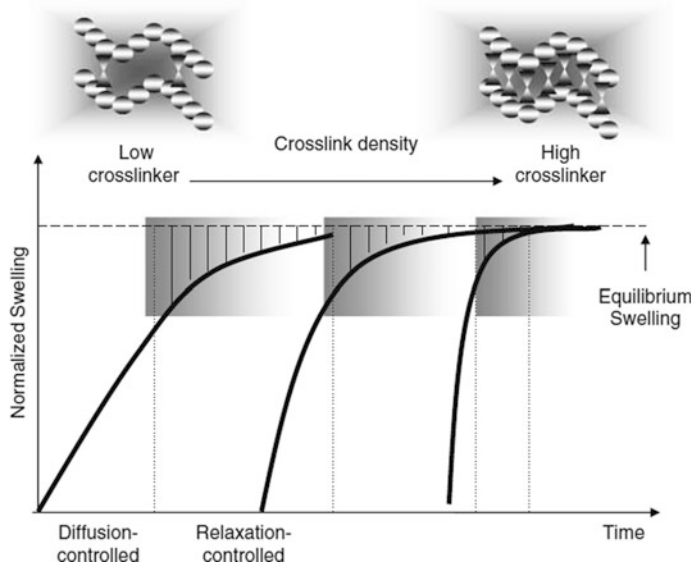


Fig. 4.6 Swelling kinetics of hydrogels reproduced from Omidian and Park (2010)

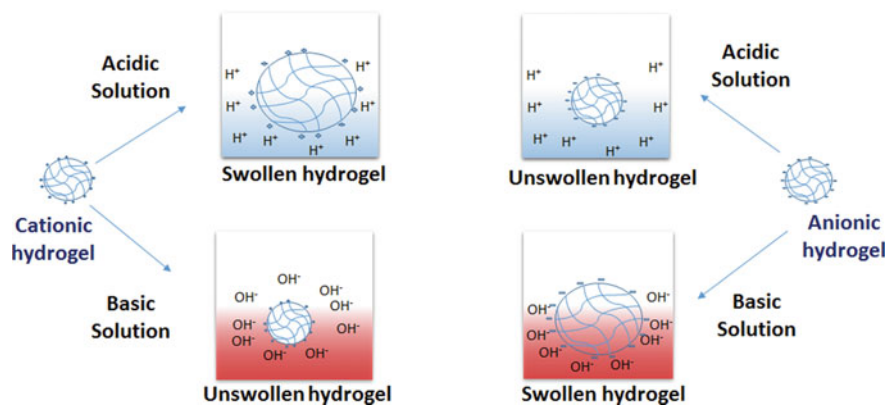


Fig. 4.7 Schematic of swelling of cationic and anionic hydrogels (Gupta et al. 2002)

amino groups present on them gets protonated in an acidic medium (Papadakis and Tsiilianis 2017).

Thus swelling depends on factors such as ionic charge, the concentration, the hydrophobicity, pK_a , and pK_b value of the polymers and pH of the swelling medium (Rizwan et al. 2017). Xu et al. fabricated a pH-responsive biodegradable hydrogel with pentablock copolymer poly (L-lactide)-co-polyethyleneglycol-co-poly (L-lactide) dimethacrylates as degradable polymeric cross-linker along with the monomers acrylic acid and N-isopropylacrylamide (NIPAM) for drug release applications. When the hydrogel was transferred to pH 1.2, hydrogel collapsed and

swelled when transferred to pH 7. This transition could be repeated for several cycles (Xu et al. 2018). Similarly, two copolymers, poly (methacrylic acid-co-methacryloxyethyl glucoside) and poly (methacrylic acid-g-ethylene glycol), were used to synthesize an anionic hydrogel by radical polymerization. The pK_a of this polymer was 5, and thus hydrogel swelled by 25-folds at pH 7 (Kim et al. 2003).

4.3.1.2 Temperature-Controlled Swelling

Some hydrogels show a sol–gel transition behavior when heated or cooled to a certain temperature. There are two main volume transitions: lower critical solution temperature (LCST) and upper critical solution temperature (UCST) (Kim and Matsunaga 2017). Polymers having LCST are soluble below this temperature, and above this temperature, they become hydrophobic and insoluble. Upon heating, hydrophobic chains lead to the formation of a hydrogel. Polymers possessing UCST are insoluble below this temperature as polymer–polymer interactions become stronger than polymer–solvent interactions (Augé and Zhao 2016). This type of behavior draws attention to many biomedical applications (Echeverria et al. 2018).

Poly(N-isopropylacrylamide) (PNIPAM) is extensively used as a temperature-responsive hydrogel (Han et al. 2018). LCST of PNIPAM is 32–34 °C. When PNIPAM gel cools down from 50 to 10 °C, swelling ratio drastically increases, and this swelling and deswelling can be repeated many times (see Fig. 4.8a). During this, the diameter also changed as shown in Fig. 4.8b (Shah et al. 2008).

Bhattarai et al. developed thermoresponsive biodegradable hydrogel made up of chitosan grafted with PEG. At low temperatures, the hydrogen bonds between PEG and chitosan get disrupted as the water molecules come between PEG and chitosan. At high temperatures, chitosan and PEG interactions increased and led to the formation of gel because of prevailing hydrophobic interactions and hydrogen bonding between –OH of PEG molecules and –NH₂ of chitosan (Bhattarai et al. 2005). This hydrogel showed a thermoreversible behavior between 30 to 40 °C and a

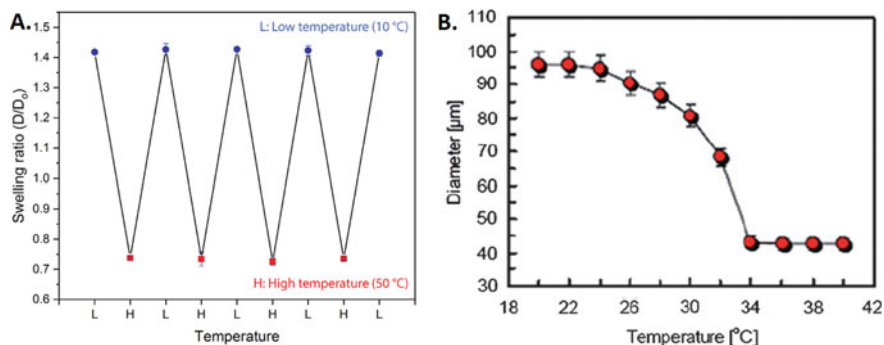


Fig. 4.8 (a) Change in the swelling ratio with a change in temperature of PNIPAM hydrogel up to several cycles reproduced from Han et al. (2018) (b) An increase in diameter with temperature after reaching LCST of PNIPAM microgel reproduced from Shah et al. (2008)

pH-responsive swelling with an increase in pH (Ju et al. 2001). These types of hydrogels are useful in drug delivery as they form a gel as soon as they are injected into the human body (above LCST) and deliver the drug at the corresponding pH.

4.3.1.3 Light Responsive Swelling

Schiphorst et al. synthesized a dual light and temperature responsive cotton fabric functionalized with PNIPAM hydrogel using surface-initiated activators regenerated by electron transfer atom transfer radical polymerization method. NIPAM, acrylic acid, and an alkyl acrylate functionalized spiropyran monomers were used to instigate the light-responsive properties to the hydrogel as shown in Fig. 4.9a. The hydrogel grafted cotton when placed in an excess humidity chamber in the dark conditions, an immediate swelling was observed in the cotton fibers as spiropyran isomerizes to hydrophilic merocyanine- H^+ (MCH^+) and when the swollen sample was illuminated to white light, a decrement in the diameter of the fibers was noticed as light isomerizes MCH^+ back to hydrophobic (Schiphorst et al. 2016).

Zhao et al. attached trans-azobenzene units of the polyacrylic acid (see Fig. 4.9b.3) to the hydrophobic units of deoxycholic acid modified cyclodextrin (see Fig. 4.9b.2) to form a light-responsive hydrogel as shown in Fig. 4.9b.1 where trans-azobenzene isomerized to less stable cis form when it was photo-irradiated with the UV light and vice versa when irradiated with visible light (Zhao and Stoddart 2009).

4.3.1.4 Analyte Responsive Swelling

Analyte responsive hydrogels are prepared when specific molecules or templates that can recognize the analyte molecules are embedded in the hydrogel (Echeverria et al. 2018). The interactions between analyte and template lead to swelling and deswelling, and this may involve a change in the volume and refractive index

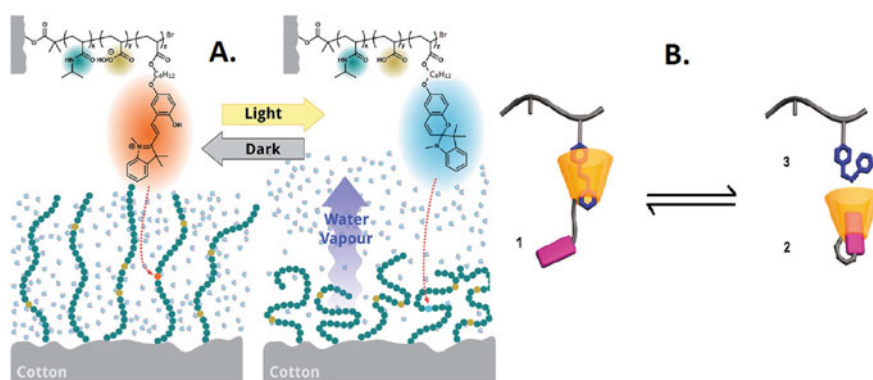


Fig. 4.9 Light-induced swelling behavior of (a) PNIPAM hydrogel functionalized cotton reproduced from Schiphorst et al. (2016), and (b) 1. Super inclusion complex formed by 2. deoxycholic acid-modified cyclodextrin and 3. azobenzene-modified polyacrylic acid reproduced from Zhao and Stoddart (2009)

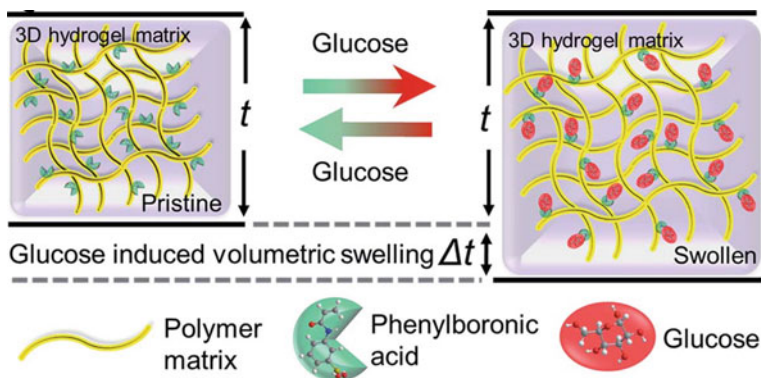


Fig. 4.10 Swelling and deswelling due to glucose concentration reproduced from Bajgrowicz-Cieslak et al. (2017)

which provide a platform for sensing and drug delivery (Byrne et al. 2002). For example, glucose-responsive hydrogels are such sensor-based hydrogels where the swelling was induced by glucose concentration. Cieslak et al. fabricated a simple optical sensor using a glucose-responsive hydrogel. Acrylamide and *N,N'*-methylene bisacrylamide were used as a polymeric matrix and 3-(acrylamide) phenylboronic acid (PBA) as a template molecule. PBA in the hydrogel reacted with glucose and forms a reversible boronate linkage which leads to swelling and the optical sensor attached measure the change in diffraction patterns and in turn measure the change in glucose concentration as shown in Fig. 4.10 (Bajgrowicz-Cieslak et al. 2017). This type of hydrogels can help in sensing the fluctuations of glucose levels in the body of diabetic patients (Lin et al. 2010).

Apart from good water absorbance and retention capacity of hydrogels, mechanical properties also play a crucial role in applications. A hydrogel should be capable of freely standing and should have a high modulus for cell growth and motility in tissue engineering applications (Zuidema et al. 2014). The drug delivery application expects a network relaxation in a hydrogel for the drug release, which is controlled by cross-linker and polymer concentration and their environmental conditions.

4.4 Rheology of Hydrogels

Ideal viscous liquids show Newtonian behavior and follow Newton's law of viscosity, whereas ideal elastic materials show a quick deformation on the application of stress and recover as soon as the stress is removed and exhibit a Hookean behavior. Hydrogels are the viscoelastic materials whose behavior falls between viscous and elastic material. A polymer flows freely like a liquid when it is not cross-linked, and thus it is called a hydrosol. When cross-links are introduced, there is a sol-gel transition, viscosity builds up, and the movement is restricted (Thakur et al. 2018). Cross-linking also introduces inhomogeneities in the network structure, as shown in

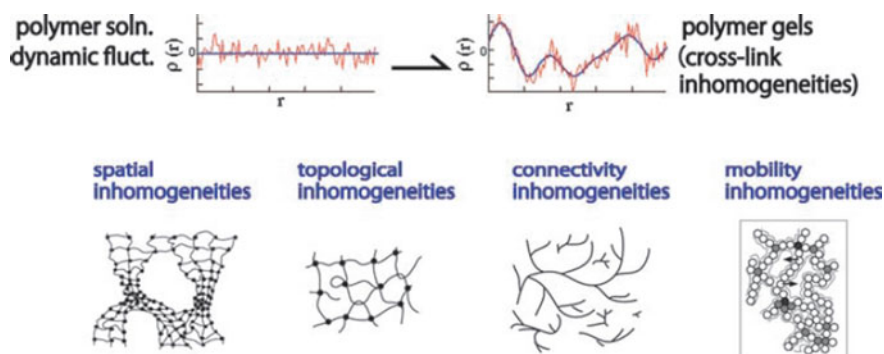


Fig. 4.11 Different types of inhomogeneities developed while cross-linking of hydrogels reproduced from Shibayama and Norisuye (2002)

Fig. 4.11, which in turn leads to the weak mechanical behavior of the gel (Shibayama and Norisuye 2002). Physical cross-links are so random and have more chances for the presence of inhomogeneities in the network in comparison to chemically cross-linked. Homogeneity can be developed in preformed polymers rather than the monomers (Shibayama and Sakai 2012).

Rheology is a quick method with high sensitivity to assess the gelation time, temperature, and structural inhomogeneities of hydrogels. The advantage is that a minute sample is required (Choi et al. 2015). Rheological properties are determined by small perturbations under which the material particles of the hydrogel are displaced relative to each other resulting in strain. These perturbations are ensured to be under the linear viscoelastic region where the mechanical properties are independent of applied or measured stress or strain (Yan and Pochan 2010). Small angle oscillatory shear (SAOS) and creep relaxations are the main techniques to evaluate the mechanical properties of hydrogels. In the experiments, either stress or strain is given as a sinusoidal input. If the rheometer is stress controlled, the input will be $\tau(t) = \tau_o(\sin \omega t)$ and the resultant output will be $\gamma(t) = \gamma_o(\sin \omega t + \delta)$ where $\tau(t)$ is time-dependent shear stress, $\gamma(t)$ is the resultant shear strain, γ_o is the amplitude of strain response, ω is the angular frequency of oscillation, and δ is the phase difference between input and output response. If the phase lag, δ is 90° , the material is fully viscous and completely elastic if it is 0° (Mezger 2006; Choi et al. 2015). Parameters derived from the SAOS are written in the complex form. The complex shear modulus (G^*) of the tested material is represented as $G^* = G' + G''$. G' is the value that defines the energy stored during the material deformation, also known as the storage modulus. G'' is the value that defines the energy dissipated when the material undergoes shear and is also known as the loss modulus. Therefore G' and G'' represents the elastic behavior and viscous behavior of the material, respectively. Loss tangent $\tan \delta$ is defined as a ratio of loss modulus to the storage modulus. If $\tan \delta > 1$, the sample behaves more like a viscous liquid while, if $\tan \delta < 1$, the sample behaves more like an elastic solid (Mezger 2006; Yan and Pochan 2010).

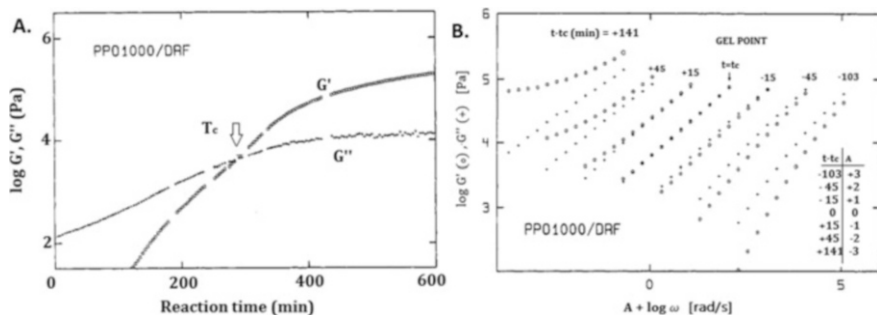


Fig. 4.12 (a) Temporal evolution of G' (open circles) and G'' (closed circles) during the crosslinking reaction of PPO1000 and DRF at 30 °C and $\omega = 0.5$ rad/s. (b) Frequency sweep of PPO/DRF reaction at distinct times with a shifting factor A, reproduced from Chambon et al. (1986)

Figure 4.12a shows the temporal evolution of the reaction of PPO and tris (4-isocyanatophenyl) thiophosphate (DRF). It shows that as the reaction proceeds, G' increases with an increase in the crosslinking density whereas the G'' goes through a slight maximum and reaches an equilibrium (Chambon et al. 1986).

The moduli cross over point ($t = t_c$) cannot be considered as an exact gel point due to external phenomenon such as vitrification and found to be a function of frequency (Winter and Chambon 1986). The moduli are measured across a frequency range to check the behavior at short and large time scales. Frequency sweep of PPO/DRF reaction at different times was plotted (see Fig. 4.12b) and observed that before reaching the gel point, $G'' > G'$ at all frequencies showing the liquid-like behavior and reaches a transition gel point where G' and G'' follow a power law, $G' = G'' = k\omega^n$ (Montembault et al. 2005).

For stoichiometrically balanced gels $n = 0.5$, $n < 0.5$ when the excess crosslinker is present and $n > 0.5$ for vice versa (Winter 1987). Further cross-linking leads to $G' > G''$ and the slopes of both G' and G'' decrease and eventually become frequency-independent (Salehiyan and Hyun 2013).

Nguyen et al. investigated the effect of molecular weight of PNIPAM polymer on the gelation temperature and noticed that H4P7 (average molar mass (AMM):192000 g/mol) became a gel at a lower temperature to P7 (AMM:7000 g/mol) and TP7 (AMM:17000 g/mol) as shown in Fig. 4.13a (Nguyen et al. 2015). Kocen et al. elucidated the effect of adding inorganic bioactive glass (BAG) particles to gellan gum hydrogels on their G' , G'' , and gelation temperature.

It was concluded that on the addition of 4 wt% particles, G' and G'' increased and the gelation temperature increased from 40 to 70 °C as shown in Fig. 4.13b (Kocen et al. 2017). Flow properties are essential to study self-healing and shear thinning of hydrogels for drug delivery and tissue engineering applications. Shear thinning hydrogels are preformed hydrogels whose viscosity decreases when an external shear is applied and restores its shape as soon as the load is released (Samimi Gharaie et al. 2018). Chen et al. fabricated a hydrogel of hyaluronic acid whose assembly and disassembly were controlled by the interactions between cyclodextrin

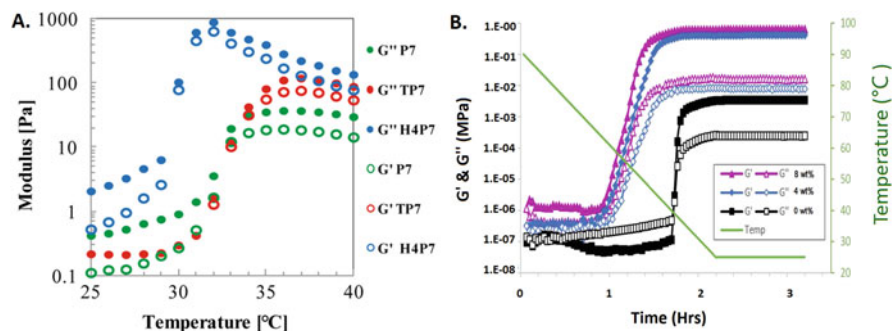


Fig. 4.13 (a) G' and G'' evolution of different molecular weight PNIPAM hydrogels with temperature, reproduced from Nguyen et al. (2015). (b) Temperature sweep of guar gum hydrogels loaded with different weight % of BAG particles from 90 to 25 °C, reproduced from Kocen et al. (2017)

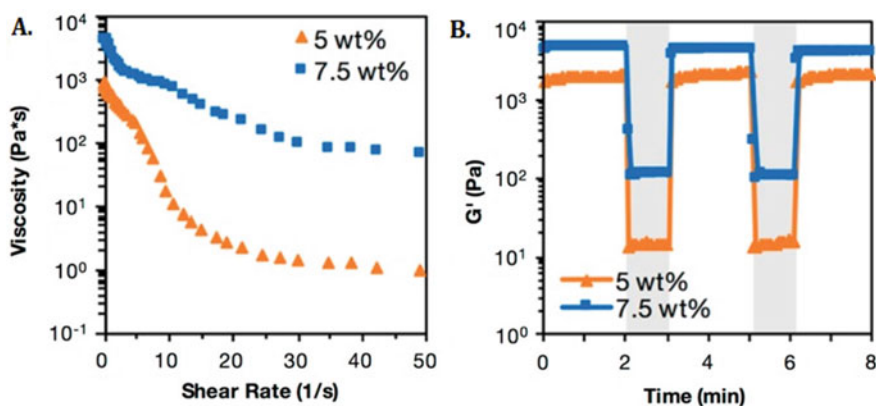


Fig. 4.14 Continuous flow experiments and cyclic strain sweeps of 5 and 7.5 wt% of hyaluronic acid hydrogels reproduced from Chen et al. (2017)

and adamantane molecules. Shear thinning hydrogels show a decrease in viscosity with an increase in strain. Cyclic strain sweeps conducted on hydrogels at 500% and 0.2% alternatively, as shown in Fig. 4.14. A 100% recovery was established after decreasing the load (Chen et al. 2017).

4.5 Application of Hydrogels in Drug Delivery

Hydrogels are good drug delivery vehicles because of their biocompatibility having lots of water in them. They are promising agents for controlled drug delivery as the cross-linking system controls the release of a drug.

Generally, hydrogels are classified into three categories based on their possible shapes such as macroscopic hydrogels, micro and nano hydrogels (Li and Mooney 2016). Macroscopic hydrogels size ranges from the few millimeters to centimeters. These gels are impenetrable to epithelial barriers, but the drug may cross the barrier depending on its properties. Polymers having mucoadhesive properties such as chitosan, alginate, gelatin, and carbohydrate derivatives are preferred for transdermal delivery (Mythri et al. 2011). Microgels and nanogels are injected either orally or directly injected at the site.

Diffusion is the primary mechanism for the drug absorption and the release in hydrogels having a porous structure. Diffusion is rapid in case of hydrogels due to the presence of water content in them, and particularly hydrophilic drugs get released in a short period. Various mechanisms restrict this rapid release such as introducing a higher cross-linking, selective release, or by enhancing the interactions between the drug and the polymer. Mesh size decreases with an increase in a cross-linking agent and so as the diffusivity of the drug. Drugs mainly interact with the polymer via physical interactions such as hydrogen bonding, hydrophilic, and electrostatic interactions. Some drugs are covalently bonded to polymeric backbones to increase the payload (Hoare and Kohane 2008).

4.5.1 Drug Loading in Hydrogels

Hydrogels have a significant advantage of localized drug delivery where the drug can be released directly at the infected or damaged part of the body. Hydrogels can deliver a wide variety of drugs, biomolecules such as peptides, proteins, and nucleic acids. The release profile of this payload also alters depending on the method of loading of a drug in the hydrogel.

A drug can be loaded directly either before the cross-linking of polymers or after the cross-linking. In the first approach, the drug is just added to the polymers and cross-linkers simultaneously (Amoozgar et al. 2012). In the second approach, a drug is loaded by diffusion into the already cross-linked hydrogels. Typically, a 70% of the drug can undergo a burst release during the initial swelling in both the methods which can be controlled by varying the cross-linking density that reduces the burst release to 20–25% (Bhattarai et al. 2010).

4.5.2 Release Kinetics in Hydrogels

Different kinetic models are developed to describe the drug release from the hydrogels. Models based on the rate-limiting step are categorized as drug release through diffusion or swelling (Lin and Metters 2006). In the diffusion-controlled release, unsteady state unidirectional drug diffusion from the slab-shaped hydrogel matrix of thickness l can be described by Fick's second law of diffusion with appropriate boundary conditions under the assumption of uniform distribution of the drug in the matrix, and a constant diffusion coefficient (D).

$$\frac{dC}{dt} = D \frac{d^2C}{dx^2} \quad (4.1)$$

where C is the concentration of drug in mg/ml, t is a time in seconds, x is the position

The solution of Eq. 4.1 in the form of trigonometric series is as follows:

$$\frac{M_t}{M_\infty} = 1 - \sum_{n=0}^{\infty} \frac{8}{(2n+1)^2 \pi^2} \exp \left[\frac{-D(2n+1)^2 \pi^2 t}{l^2} \right] \quad (4.2)$$

where M_t is defined as the mass of drug release at time t and M_∞ as the mass of drug release when the time approaches infinity.

For small values of times, Eq. 4.2 is approximated to

$$\frac{M_t}{M_\infty} = 4 \left[\frac{Dt}{\pi l^2} \right]^{1/2} \quad (4.3)$$

Equation 4.3 is valid for the first 60% of drug release. Peppas et al. deduced a generalized expression for both Fickian and non-Fickian release as Eq. 4.4.

$$\frac{M_t}{M_\infty} = kt^n \quad (4.4)$$

where k is a constant indicating the characteristic of the polymeric network, and n is a diffusional exponent which indicates the transport mechanism (Ritger and Peppas 1987).

Swelling-controlled drug release accompanies diffusion and macromolecular polymer relaxation. So this empirical relation of Eq. 4.4 is restricted to swelling of 25% of its original volume. If $n = 0.5$, the diffusion is completely Fickian and if $0.5 < n < 1$, the release is controlled by both diffusion and the network relaxation ($D_{\text{diff}} > D_{\text{rel}}$). If $n = 1$, the release is completely non-Fickian where polymer relaxation and diffusion are comparable ($D_{\text{diff}} \sim D_{\text{rel}}$) (Siepmann and Peppas 2011; Bajpai and Shrivastava 2002).

4.5.3 Different Routes for Drug Delivery

4.5.3.1 Drug Delivery Through Macro Hydrogels

Hydrogel patches are readily used to deliver a drug transdermally where the drug passes through the skin to reach the targeted organs through the systemic circulation. Transdermal drug delivery can be achieved by active route (iontophoresis, sonophoresis, and electroporation) or by a passive route where the concentration difference of the drug-loaded patch and skin leads to the drug release (Tan and Pfister 1999). Figueroa and Mendez investigated the transdermal delivery by polyacrylamide hydrogel cross-linked by methylene bisacrylamide through active

(iontophoresis) and passive routes for psoriasis treatment. The *in vitro* studies showed that the amount of drug (Methotrexate) released through diffusion by iontophoresis delivered a more amount of drug compared to the passive route (Alvarez-Figueroa and Blanco-Méndez 2001).

A drug-loaded adhesive patch made of poly(methylvinylether/ maleic acid) (PMVE/MA) and tri-propylene glycol ether cast on microneedle array of PMVE/MA and PEG cross-linked by heating at 80 °C using silicone micro mold templates. The *in vivo* studies of insulin delivery on diabetic rat model showed that microneedle-attached patch showed a sustained delivery, and glucose level in the body also dropped to a reasonable extent (Donnelly et al. 2012; Hardy et al. 2016).

Hydrogels can also be inserted directly into the human body by surgery without contacting the epithelial barriers, but the risks and side effects with surgery may cause discomfort. Alternatively, hydrogels can be directly injected at the affected site in the sol form and can undergo gelation after entering the body due to external stimuli (Singh et al. 2011). Kinetics of gel formation plays a crucial role in injectable hydrogels (Loebel et al. 2017). For example, Gupta et al. synthesized a hydrogel of guar gum and chitosan, which forms a gel *in situ* on contacting with teardrops as they consist of electrolytes. Transcorneal permeation of timolol maleate drug is higher in case of guar gum and chitosan hydrogel in comparison to guar gum and direct loading.

A minimum invasive drug-loaded injectable hydrogel composed of ureido-pyrimidinone modified PEG formed the gel after coming in contact with body pH and temperature (Bastings et al. 2015). Qu et al. fabricated an injectable electro-responsive chitosan-grafted polyaniline hydrogel using oxidized dextran as a cross-linker which was also responsive to pH. *In vitro* studies show that drug release can be changed with the voltage (Qu et al. 2018).

4.5.3.2 Micro and Nano Hydrogels for Drug Delivery

Micro and nano-sized hydrogels have the advantage to get injected into the body parts whose size is less than 1 mm. Foreign particles having less than 5 μm have a chance to get cleared by macrophages. Antiglaucoma drugs such as brimonidine and timolol maleate attached polylactic-co-glycolic acid nanoparticles were added to polydopamine dendrimer and were UV cross-linked to form a hydrogel. The study shows that drug-loaded hydrogel tested on rabbit's eye immediately decreased and stabilized the intraocular pressure within 30 min (Yang et al. 2012). Methotrexate-loaded chitin nanogels were investigated for transdermal drug delivery, and it exhibited an excellent transdermal flux in stratum corneum and other epidermal layers compared to the drug-loaded saline solution (Panonnummal and Sabitha 2018). These drug-loaded micro or nano gels are predicted to increase the retention time of drug and get degraded in tiny size particles such that they are quickly eliminated by various tissues and organs (Gao et al. 2008).

Merkel et al. developed deformable low moduli micro hydrogel resembling red blood cells to increase the circulation time using perfluoropolyether polymer by non-wetting templates technique (Merkel et al. 2011). The authors reported that an 8-fold decrease in elastic moduli could lead to an increase in 30-fold circulation time.

Sherbiny et al. synthesized biodegradable mucoadhesive micro hydrogels of PEG-grafted chitosan and pluronics (40 wt%) whose aerodynamic diameter is $11.13 \pm 0.23 \mu\text{m}$ which increased when it entered the lung cavity to increase the adhesiveness and prevention against phagocytosis. In vitro macrophage uptake studies suggest that PEG brushes on the microgels provide stealth and sustained drug delivery (El-Sherbiny et al. 2010). Cellular uptake of the drug is necessary to deliver the drug at a selective site, and positively charged particles readily enter the negatively charged cellular membrane (Yim et al. 2013). The cisplatin drug-loaded cationic poly ethylenimine-coated polyacrylamide nano hydrogels showed good cytocompatibility and an enhanced cellular uptake (Shirakura et al. 2016).

Yang et al. explored the pH-based drug delivery at the malignant tissues having less pH than the healthy tissues. Poly(oligo (ethylene glycol) methacrylates-ss-acrylic acid) nanogels change from hydrophilic to hydrophobic state at acidic pH, and hence they deliver doxorubicin drug at the affected site selectively (Yang et al. 2015).

4.6 Available Hydrogel Products in Market

S. no	Hydrogel product	Manufacturing company	Application	Reference
1.	Moraxen®	CeNes pharmaceuticals	For the sustained release of morphine to reduce severe cancer pain	https://adisinsight.springer.com/drugs/800010172
2.	Chitosan-based formulation	Kiomed Pharma	To restore the rheological properties of healthy synovial fluid	http://kiomedpharma.com/products/arthrovisc/
3.	BeadBlock® (PVA hydrogel cross-linked with acrylic polymer)	BTG plc	To embolize the hypervascular renal tumors in combination therapy by injecting it directly through the catheter	https://btgplc.com/en-US/Bead-Block/Home
4.	Cervidil (a PEO and polyurethane-based hydrogel)	Ferring Pharmaceuticals	Vaginal insert to deliver dinoprostone to induce the labor	http://www.cervidil.com/resources/
5.	Sular® (a PEG-based hydrogel)	Covia Pharmaceuticals	A hydrogel layer is added to control the release of nisoldipine	https://www.covispharma.com/#home-products
6.	Hydromer® (a PVP-based hydrogel)	Hydromer Inc.	A hydrogel foam for hemostasis of heaving bleeding	https://www.hydromer.com/medical_hydrogels_foams.html

4.7 Conclusions and Outlook

A wide variety of new responsive and injectable hydrogels are fabricated using many biodegradable and biocompatible polymers with different cross-linking agents and cross-linking methods. A structure–property evaluation is also a significant concern, along with development in the fabrication of different hydrogels. Thus, rheology is a simple technique to study the temporal evolution of gelation and the effect of cross-linker, and polymer concentration, ionic strength, pH of the solvent to tune the mechanical strength of the hydrogels. Hydrogels are synthesized in macro, micro, and nano-shaped hydrogels depending on the drug delivery application. A significant number of in vitro and in vivo experiments have been done on hydrogels to investigate the controlled and sustained drug delivery. Hydrogels loaded with tumor receptive ligands are used for selective drug delivery. Despite the fact that a handful of patents have been filed on many hydrogels, only a few released in the market as biodegradability is still an issue. One of the drawbacks of a hydrogel is the lack of mechanical strength. Nanocomposite hydrogels and interpenetrating double network hydrogels are being explored to improve the strength of gels. The mechanical strength of the hydrogels can be increased by incorporating the nanofillers in the polymer matrix. Different types of organic and inorganic nanoparticles are integrated into the polymer to acquire the benefits of stimuli-responsive and better mechanical properties of nanoparticles (Thoniyot et al. 2015). The degradation of hydrogel needs to be tailored for the complete removal of hydrogel after releasing the drug or can be reused for refilling the drug. Memory imprinted/sensor-based hydrogels are explored to a limited extent, which can be used for controlled drug delivery.

References

- Ahmadi F, Oveisi Z, Samani M, Amoozgar Z (2015) Chitosan based hydrogels: Characteristics and pharmaceutical applications. *Res Pharm Sci* 10:1–16
- Ahmed EM (2015) Hydrogel: Preparation, characterization, and applications: A review. *J Adv Res* 6:105–121
- Akhtar MF, Hanif M, Ranjha NM (2016) Methods of synthesis of hydrogels ... a review. *Saudi Pharm J* 24:554–559
- Alavi M, Karimi N, Safaei M (2017) Application of various types of liposomes in drug delivery systems. *Adv Pharm Bull* 7:3–9
- Alvarez-Figueroa MJ, Blanco-Méndez J (2001) Transdermal delivery of methotrexate: Iontophoretic delivery from hydrogels and passive delivery from microemulsions. *Int J Pharm* 215:57–65
- Amoozgar Z, Park J, Lin Q, Yeo Y (2012) Low molecular-weight chitosan as a pH-sensitive stealth coating for tumor-specific drug delivery. *Mol Pharm* 9:1262–1270
- Amri N, Ghemati D, Bouguettaya N, Aliouche D (2018) The swelling kinetics and rheological behavior of chitosan-PVA/Montmorillonite hybrid polymers. *Period Polytech Chem Eng* 63:179–189
- Aoyagi M, Kim Y, Hoffman JM (1992) Smart biomaterials. *Membr Technol* 1992:4
- Arguk Elles-Monal W, Goycoolea FM, Peniche C, Higuera-Ciajara I (1998) Rheological study of the chitosan/glutaraldehyde chemical gel system. *Polym Gels Netw* 6:429–440

- Arunan E, Desiraju GR, Klein RA et al (2011) Definition of the hydrogen bond (IUPAC recommendations 2011). *Pure Appl Chem* 83:1637–1641
- Augé A, Zhao Y (2016) What determines the volume transition temperature of UCST acrylamide-acrylonitrile hydrogels? *RSC Adv* 6:70616–70623
- Bajgrowicz-Cieslak M, Alqurashi Y, Elshereif MI et al (2017) Optical glucose sensors based on hexagonally-packed 2.5-dimensional photonic concavities imprinted in phenylboronic acid functionalized hydrogel films. *RSC Adv* 7:53916–53924
- Bajpai AK, Shrivastava M (2002) Swelling kinetics of a hydrogel of poly(ethylene glycol) and poly(acrylamide-co-styrene). *J Appl Polym Sci* 85:1419–1428
- Bastings MM, Koudstaal S, Agostoni P et al (2015) An injectable and drug-loaded Supramolecular hydrogel for local catheter injection into the pig heart. *J Vis Exp* 100:52450
- Berger J, Reist M, Mayer JM et al (2004) Structure and interactions in covalently and ionically crosslinked chitosan hydrogels for biomedical applications. *Eur J Pharm Biopharm* 57:19–34
- Bhattarai N, Matsen FA, Zhang M (2005) PEG-grafted chitosan as an injectable thermoreversible hydrogel. *Macromol Biosci* 5:107–111
- Bhattarai N, Gunn J, Zhang M (2010) Chitosan-based hydrogels for controlled, localized drug delivery. *Adv Drug Deliv Rev* 62:83–99
- Buwalda SJ, Boere KWM, Dijkstra PJ et al (2014) Hydrogels in a historical perspective: From simple networks to smart materials. *J Control Release* 190:254–273
- Byrne ME, Park K, Peppas NA (2002) Molecular imprinting within hydrogels. *Adv Drug Deliv Rev* 54:149–161
- Cai X, Luo Y, Zhang W et al (2016) pH-sensitive ZnO quantum dots–doxorubicin nanoparticles for lung cancer targeted drug delivery. *ACS Appl Mater Inter* 8:22442–22450
- Chai Q, Jiao Y, Yu X (2017) Hydrogels for biomedical applications: Their characteristics and the mechanisms behind them. *Gels* 3:6
- Chambon F, Petrovic ZS, MacKnight WJ, Winter HH (1986) Rheology of model polyurethanes at the gel point. *Macromolecules* 19:2146–2149
- Chen MH, Wang LL, Chung JJ et al (2017) Methods to assess shear-thinning hydrogels for application as injectable biomaterials. *ACS Biomater Sci Eng* 3:3146–3160
- Choi B, Loh XJ, Tan A et al (2015) Introduction to in situ forming hydrogels for biomedical applications. In: Loh XJ (ed) *BioEngineering in-situ gelling polymers*, 1st edn. Springer Singapore, Singapore, pp 5–35
- Coviello T, Grassi M, Rambone G et al (1999) Novel hydrogel system from scleroglucan: Synthesis and characterization. *J Control Release* 60:367–378
- Dimida S, Barca A, Cancelli N et al (2017) Effects of Genipin concentration on cross-linked chitosan scaffolds for bone tissue engineering: Structural characterization and evidence of biocompatibility features. *Int J Polym Sci* 2017:1–8
- Donnelly RF, Singh TRR, Garland MJ et al (2012) Hydrogel-forming microneedle arrays for enhanced transdermal drug delivery. *Adv Funct Mater* 22:4879–4890
- Echeverria C, Fernandes S, Godinho M et al (2018) Functional stimuli-responsive gels: Hydrogels and microgels. *Gels* 4:54
- El-Sherbiny IM, McGill S, Smyth HDC (2010) Swellable microparticles as carriers for sustained pulmonary drug delivery. *J Pharm Sci* 99:2343–2356
- Gao D, Hao X, Philbert MA, Kopelman R (2008) Bioeliminable nanohydrogels for drug delivery. *Nano Lett* 8:3320–3324
- Gerlach G, Arndt K-F (2009) Hydrogel sensors and actuators. *Springer Ser Chem Sensors Biosens* 6:1–15
- Gupta P, Vermani K, Garg S (2002) Hydrogels: From controlled release to pH-responsive drug delivery. *Drug Discov Today* 7:569–579
- Gupta S, Webster TJ, Sinha A (2011) Evolution of PVA gels prepared without crosslinking agents as a cell adhesive surface. *J Mater Sci Mater Med* 22:1763–1772

- Han D, Lu Z, Chester SA, Lee H (2018) Micro 3D printing of a temperature-responsive hydrogel using projection micro-Stereolithography. *Sci Rep* 8:1963
- Hardy JG, Larrañeta E, Donnelly RF et al (2016) Hydrogel-forming microneedle arrays made from light-responsive materials for on-demand transdermal drug delivery. *Mol Pharm* 13:907–914
- Hasan A, Waibhaw G, Tiwari S et al (2017) Fabrication and characterization of chitosan, polyvinylpyrrolidone, and cellulose nanowhiskers nanocomposite films for wound healing drug delivery application. *J Biomed Mater Res Part A* 105:2391–2404
- Hassan CM, Peppas NA (2000) Structure and applications of poly(vinyl alcohol) hydrogels produced by conventional crosslinking or by freezing/thawing methods. In: *Biopolymers · PVA Hydrogels. Anionic Polymerisation Nanocomposites*. Springer, Berlin Heidelberg, Berlin, Heidelberg, pp 37–65
- Hennink WE, van Nostrum CF (2012) Novel crosslinking methods to design hydrogels. *Adv Drug Deliv Rev* 64:223–236
- Hennink W, De Jong S, Bos G et al (2004) Biodegradable dextran hydrogels crosslinked by stereocomplex formation for the controlled release of pharmaceutical proteins. *Int J Pharm* 277:99–104
- Hoare TR, Kohane DS (2008) Hydrogels in drug delivery: Progress and challenges *. *Polym with aligned carbon Nanotub Act Compos Mater* 49:1993–2007
- Inoue N, Bessho M, Furuta M et al (2006) A novel collagen hydrogel cross-linked by gamma-ray irradiation in acidic pH conditions. *J Biomater Sci Polym Ed* 17:837–858
- Jamnongkan T, Kaewpirom S (2010) Potassium release kinetics and water retention of controlled-release fertilizers based on chitosan hydrogels. *J Polym Environ* 18:413–421
- Jătăriu AN, Popa M, Curteanu S, Peptu CA (2011) Covalent and ionic co-cross-linking-an original way to prepare chitosan-gelatin hydrogels for biomedical applications. *J Biomed Mater Res – Part A* 98(A):342–350
- Ju HK, Kim SY, Lee YM (2001) pH/temperature-responsive behaviors of semi-IPN and comb-type graft hydrogels composed of alginate and poly(N-isopropylacrylamide). *Polymer (Guildf)* 42:6851–6857
- Jung Y, Park W, Park H et al (2017) Thermo-sensitive injectable hydrogel based on the physical mixing of hyaluronic acid and Pluronic F-127 for sustained NSAID delivery. *Carbohydr Polym* 156:403–408
- Kashima K, Imai M (2012) Advanced membrane material from marine biological polymer and sensitive molecular-size recognition for promising separation technology. In: *Advancing desalination*. InTech, p 64
- Kim Y-J, Matsunaga YT (2017) Thermo-responsive polymers and their application as smart biomaterials. *J Mater Chem B* 5:4307
- Kim B, La Flamme K, Peppas NA (2003) Dynamic swelling behavior of pH-sensitive anionic hydrogels used for protein delivery. *J Appl Polym Sci* 89:1606–1613
- Kimura M, Fukumoto K, Watanabe J, Ishihara K (2004) Hydrogen-bonding-driven spontaneous gelation of water-soluble phospholipid polymers in aqueous medium. *J Biomater Sci Polym Ed* 15:631–644
- Kocen R, Gasik M, Gantar A, Novak S (2017) Viscoelastic behaviour of hydrogel-based composites for tissue engineering under mechanical load. *Biomed Mater* 12:025004
- Kopeček J (2009) Hydrogels from soft contact lenses and implants to self-assembled nanomaterials. *J Polym Sci A Polym Chem* 47:5929–5946
- Kumar Parida U, Nayak AK, Binhani BK, Nayak PL (2011) Synthesis and characterization of chitosan-polyvinyl alcohol blended with Cloisite 30B for controlled release of the anticancer drug Curcumin. *J Biomater Nanobiotechnol* 2:414–425
- Li J, Mooney DJ (2016) Designing hydrogels for controlled drug delivery. *Nat Rev Mater* 1:16071
- Lin CC, Metters AT (2006) Hydrogels in controlled release formulations: Network design and mathematical modeling. *Adv Drug Deliv Rev* 58:1379–1408
- Lin G, Chang S, Hao H et al (2010) Osmotic swelling pressure response of smart hydrogels suitable for chronically implantable glucose sensors. *Sensors Actuators B Chem* 144:332–336

- Loebel C, Rodell CB, Chen MH, Burdick JA (2017) Shear-thinning and self-healing hydrogels as injectable therapeutics and for 3D-printing. *Nat Protoc* 12:1521–1541
- Maelys G, Neubi N, Opoku-Damoah Y et al (2018) Bio-inspired drug delivery systems: An emerging platform for targeted cancer therapy. *Biomater Sci* 6:958
- Maitra J, Shukla VK (2014) Cross-linking in Hydrogels – A Review. *Am J Polym Sci* 4:25–31
- Merkel TJ, Jones SW, Herlihy KP et al (2011) Using mechanobiological mimicry of red blood cells to extend circulation times of hydrogel microparticles. *Proc Natl Acad Sci* 108:586–591
- Mezger TG (2006) *The rheology handbook*, 2nd edn. Vincentz, Hannover, p 180
- Montebault A, Viton C, Domard A (2005) Rheometric study of the gelation of chitosan in a hydroalcoholic medium. *Biomaterials* 26:1633–1643
- Muzzarelli R, El Mehtedi M, Bottegoni C et al (2015) Genipin-Crosslinked chitosan gels and scaffolds for tissue engineering and regeneration of cartilage and bone. *Mar Drugs* 13:7314–7338
- Mythri G, Kavitha K, Kumar MR, Jagadeesh Singh SD (2011) Novel mucoadhesive polymers – a review. *J Appl Pharm Sci* 1:37–42
- Nguyen HH, Payré B, Fitremann J et al (2015) Thermoresponsive properties of PNIPAM-based hydrogels: Effect of molecular architecture and embedded gold nanoparticles. *Langmuir* 31:4761–4768
- Omidian H, Park K (2010) Introduction to hydrogels. In: Ottenbrite RM, Park K, Okano T (eds) *Biomedical applications of hydrogels handbook*. Springer New York, New York, NY, pp 1–16
- Palmerston Mendes L, Pan J, Torchilin V (2017) Dendrimers as Nanocarriers for nucleic acid and drug delivery in cancer therapy. *Molecules* 22:1401
- Panonnnummal R, Sabitha M (2018) Anti-psoriatic and toxicity evaluation of methotrexate loaded chitin nanogel in imiquimod induced mice model. *Int J Biol Macromol* 110:245–258
- Papadakis C, Tsitsilianis C (2017) Responsive hydrogels from associative block copolymers: Physical gelling through Polyion Complexation. *Gels* 3:3
- Peppas NA, Merrill EW (1976) Differential scanning calorimetry of crystallized PVA hydrogels. *J Appl Polym Sci* 20:1457–1465
- Peppas NA, Scott JE (1992) Controlled release from poly (vinyl alcohol) gels prepared by freezing-thawing processes. *J Control Release* 18:95–100
- Prasad HRY, Srivastava P, Verma KK (2004) Diapers and skin care: Merits and demerits. *Indian J Pediatr* 71:907–908
- Qu J, Zhao X, Ma PX, Guo B (2018) Injectable antibacterial conductive hydrogels with dual response to an electric field and pH for localized “smart” drug release. *Acta Biomater* 72:55–69
- Razzak MT, Darwis D, Zainuddin S (2001) Irradiation of polyvinyl alcohol and polyvinyl pyrrolidone blended hydrogel for wound dressing. *Radiat Phys Chem* 62:107–113
- Ritger PL, Peppas NA (1987) A simple equation for description of solute release I. Fickian and non-Fickian release from non-swelling devices in the form of slabs, spheres, cylinders or discs. *J Control Release* 5:23–36
- Rizwan M, Yahya R, Hassan A et al (2017) pH sensitive hydrogels in drug delivery: Brief history, properties, swelling, and release mechanism, material selection and applications. *Polymers (Basel)* 9:137
- Roy B (2015) *J Biomed Sci* 2:20–21
- Salehiyan R, Hyun K (2013) Effect of organoclay on non-linear rheological properties of poly(lactic acid)/poly(caprolactone) blends. *Korean J Chem Eng* 30:1013–1022
- Samimi Gharraie S, Dabiri S, Akbari M (2018) Smart shear-thinning hydrogels as injectable drug delivery systems. *Polymers (Basel)* 10:1317
- Saxena V, Hasan A, Sharma S, Pandey LM (2018) Edible oil nanoemulsion: An organic nanoantibiotic as a potential biomolecule delivery vehicle. *Int J Polym Mater Polym Biomater* 67:410–419
- Schwarte LM, Podual K, Peppas NA (1999) Cationic hydrogels for controlled release of proteins and other macromolecules. *Tailored Polym Mater Control Deliv Syst* 709:56–66

- Shah RK, Kim J-W, Agresti JJ et al (2008) Fabrication of monodisperse thermosensitive microgels and gel capsules in microfluidic devices. *Soft Matter* 4:2303
- Shibayama M, Norisuye T (2002) Gel formation analyses by dynamic light scattering. *Bull Chem Soc Jpn* 75:641–659
- Shibayama M, Sakai T (2012) CHAPTER 2. Fabrication, structure, mechanical properties, and applications of tetra-PEG hydrogels. In: Loh XJ, Scherman OA (eds) *Polymeric and self assembled hydrogels: From fundamental understanding to applications*. Royal Society of Chemistry, Cambridge, pp 7–38
- Shirakura T, Ray A, Kopelman R (2016) Polyethylenimine incorporation into hydrogel nanomaterials for enhancing nanoparticle-assisted chemotherapy. *RSC Adv* 6:48016–48024
- Siepmann J, Peppas NA (2011) Higuchi equation: Derivation, applications, use and misuse. *Int J Pharm* 418:6–12
- Simonsen L, Hovgaard L, Mortensen PB, Brøndsted H (1995) Dextran hydrogels for colon-specific drug delivery. V. Degradation in human intestinal incubation models. *Eur J Pharm Sci* 3:329–337
- Singh V, Bushetti SS, Raju SA et al (2011) Polymeric ocular hydrogels and ophthalmic inserts for controlled release of timolol maleate. *J Pharm Bioallied Sci* 3:280–285
- Song G, Zhang L, He C et al (2013) Facile fabrication of tough hydrogels physically cross-linked by strong cooperative hydrogen bonding. *Macromolecules* 46:7423–7435
- Stenekes RJH, Talsma H, Hennink WE (2001) Formation of dextran hydrogels by crystallization. *Biomaterials* 22:1891–1898
- Tan HS, Pfister WR (1999) Pressure-sensitive adhesives for transdermal drug delivery systems. *Pharm Sci Technol Today* 2:60–69
- ter Schiphorst J, van den Broek M, de Koning T et al (2016) Dual light and temperature responsive cotton fabric functionalized with a surface-grafted spiropyran–NIPAAm-hydrogel. *J Mater Chem A* 4:8676–8681
- Thakur G, Rodrigues FC, Dathathri E et al (2018) Protein-based gels. *Polymeric Gels*. Elsevier, In, pp 31–54
- Thirumurugan A, Blessy V, Karthikeyan M (2018) Comparative study on doxorubicin loaded metallic nanoparticles in drug delivery against MCF-7 cell line. In: *Applications of nanomaterials*. Elsevier, pp 303–313
- Thoniyot P, Tan MJ, Karim AA et al (2015) Nanoparticle-hydrogel composites: Concept, design, and applications of these promising, multi-functional materials. *Adv Sci* 2:1400010
- Tsung J, Burgess DJ (2012) Biodegradable polymers in drug delivery systems. In: *Fundamentals and applications of controlled release drug delivery*. Springer US, Boston, MA, pp 107–123
- Winter HH (1987) Can the gel point of a cross-linking polymer be detected by the $G' - G''$ Crossover? *Polym Eng Sci* 27:1698–1702
- Winter HH, Chambon F (1986) Analysis of linear viscoelasticity of a crosslinking polymer at the gel point. *J Rheol (N Y N Y)* 30:367–382
- Wissing S, Kayser O, Müller R (2004) Solid lipid nanoparticles for parenteral drug delivery. *Adv Drug Deliv Rev* 56:1257–1272
- Xu L, Qiu L, Sheng Y et al (2018) Biodegradable pH-responsive hydrogels for controlled dual-drug release. *J Mater Chem B* 510:510
- Yan C, Pochan DJ (2010) Rheological properties of peptide-based hydrogels for biomedical and other applications. *Chem Soc Rev* 39:3528–3540
- Yang H, Tyagi P, Kadam RS et al (2012) Hybrid dendrimer hydrogel/PLGA nanoparticle platform sustains drug delivery for one week and antiglaucoma effects for four days following one-time topical administration. *ACS Nano* 6:7595–7606
- Yang H, Wang Q, Chen W et al (2015) Hydrophilicity/hydrophobicity reversible and redox-sensitive nanogels for anticancer drug delivery. *Mol Pharm* 12:1636–1647
- Yim H, Park SJ, Bae YH, Na K (2013) Biodegradable cationic nanoparticles loaded with an anticancer drug for deep penetration of heterogeneous tumours. *Biomaterials* 34:7674–7682

- Yu Y, Feng R, Li J, et al (2018) A hybrid genipin-crosslinked dual-sensitive hydrogel/nanostructured lipid carrier ocular drug delivery platform. *Asian J Pharm Sci*
- Zhao Y-L, Stoddart JF (2009) Azobenzene-based light-responsive hydrogel system. *Langmuir* 25:8442–8446
- Zhao F, Yao D, Guo R et al (2015) Composites of polymer hydrogels and Nanoparticulate Systems for Biomedical and Pharmaceutical Applications. *Nano* 5:2054–2130
- Zhao T, Liu X, Li Y et al (2017) Fluorescence and drug loading properties of ZnSe:Mn/ZnS-paclitaxel/SiO₂ nanocapsules templated by F127 micelles. *J Colloid Interface Sci* 490:436–443
- Zuidema JM, Rivet CJ, Gilbert RJ, Morrison FA (2014) A protocol for rheological characterization of hydrogels for tissue engineering strategies. *J Biomed Mater Res – Part B Appl Biomater* 102:1063–1073



Surface Engineering in Wearable Sensors for Medical Diagnostic Applications

5

Devin Schmidt, Anil Mahapatro, and Kim Cluff

Abstract

In a time of rising average population and complex illnesses, the healthcare system is strained and struggling to keep costs low. Wearable devices are a potential solution to detecting the onset of sickness allowing for early treatment as well as continuous monitoring to prevent readmittance. Utilization of sensors to monitor patients will allow them to return to the comfort of their home while still under physician supervision remotely in case treatment is necessary, freeing up hospital space and staff to treat those in need of direct care. Additionally, in the consumer market, wearable devices are utilized by millions of users to monitor their vital signs and general health. In this manuscript, various wearable device, biosensors, and their applications are presented, as well as methods such as surface engineering, a powerful tool to incorporate materials into devices to result in increased functionality. Current challenges and the future outlook of the wearables industry are also discussed.

Keywords

Wearable sensors · Surface engineering · Biosensors · Medical diagnostics · Healthcare

5.1 Introduction

The human body is a complex system in which many variables can alter mental and physical performance. Having the ability to monitor multiple physiological parameters through the use of wearable sensors can play a vital role in personal

D. Schmidt · A. Mahapatro (✉) · K. Cluff
Department of Biomedical Engineering, Wichita State University, Wichita, KS, USA
e-mail: anil.mahapatro@wichita.edu

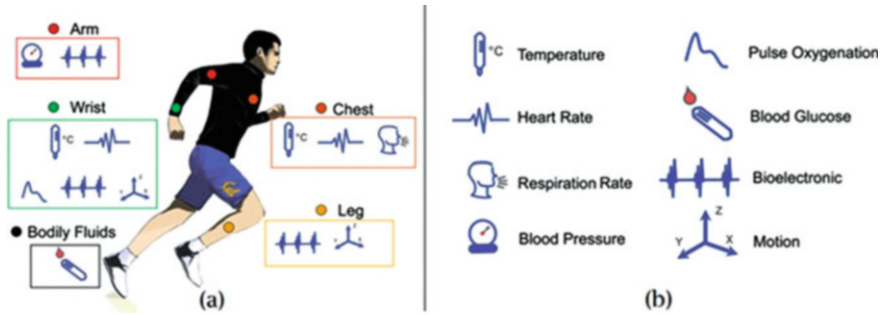


Fig. 5.1 Sensing locations and associated biosignals that could be monitored (a). Legend of symbols and biosignals (b). Adapted from Ref Khan et al. (2016). Open access article distributed under the Creative Common Attribution License

healthcare as well as aiding medical diagnostics. In modern-day wearable technology, a variety of instruments such as accelerometers, gyroscopes, optical, force, temperature, and magnetometers have been incorporated into clothing, watches, and eyewear (Lee and Chung 2009; Zhang et al. 2006; Park and Jayaraman 2003; Sungmee and Jayaraman 2003) for the detection of location, movement, and health-related criteria. As displayed in Fig. 5.1, the sensor must be designed with location in mind to acquire a specific biosignal (Khan et al. 2016). While current consumer market device measurements consist of physical activity and vital signs, developments are being made to analyze biofluids such as saliva (Soukup et al. 2012; Tekus et al. 2012; Kim et al. 2014), sweat (Bandodkar et al. 2014; Anastasova et al. 2017; Mena-Bravo and Luque de Castro 2014; Gao et al. 2016; Salvo et al. 2010), and tears (Elsherif et al. 2018; Kudo et al. 2006; La Belle et al. 2016; Yao et al. 2011). The real-time monitoring of these parameters allows for an improved understanding of the user's body conditions which can prompt early intervention of a serious health condition if abnormalities are detected.

In the medical setting, wearable sensors are the standard to monitor vital signs of the patients. A pulse oximeter can regularly be found clasped to the fingertip of a patient or foot of an infant, monitoring the person's blood oxygen saturation in addition to pulse. With the use of a light emitter, the device uses the different absorbance levels of oxygenated hemoglobin and deoxyhemoglobin in a calculation to determine the peripheral blood oxygen saturation level (Chan et al. 2013). While this value is not always identical to the arterial oxygen saturation level, the convenience and safety of acquiring the information in a noninvasive method for a near accurate reading has shown its value in clinical use. Other wearables seen in clinical use allow for the monitoring of body temperature, brain activity, and muscle motion (Edwards 2012). In combination, these sensors allow for a significant understanding of the patient's body condition, monitoring physiological parameters the individual may not express physically or be able to verbally explain when seeking proper treatment. When adapted to functioning with a network, the sensors also permit the patient to return to the comfort of their home while still being monitored by

physicians remotely. This is beneficial towards conserving resources and workload on the medical team, resulting in improved care for those requiring close supervision and on-site treatment.

While wearable devices continue to provide an important role in the clinical setting, the consumer market is currently undergoing tremendous growth. In 2016, the global wearable sensors market was valued at \$146 million and is expected to reach \$2.86 billion by 2025 (Research 2018). With this estimated expansion, both the industry and the research community will continue to push the boundaries of healthcare innovation within wearable technology to provide real-time monitoring of physiological parameters and activity.

One of the most recent advancements to reach the consumer market headlines is the inclusion of electrodes capable of performing electrocardiography (ECG) on the Apple Watch (Apple 2018). While this ECG function is not of the same efficacy of a traditional 12-lead ECG as seen in clinical use, it does let users easily detect critical information such as a rapid, skipped, or irregular heartbeat that may be associated with atrial fibrillation from the convenience of a wristwatch.

Traditionally, wearable sensors for the general population are tailored towards fitness. However, for many users, there is little understanding of the underlying technology involved in the smart device that is relaying information such as heart rate to their phone or computer. Researchers with novel ideas in the form of smaller, cheaper, and more capable sensors for detection of multiple physiological parameters will significantly benefit the health monitoring of the general population by providing access to a wealth of information about their body's status. One tool that engineers are utilizing to achieve innovative functionality in wearable sensors is the application of surface engineering.

5.2 Surface Engineering

Surface engineering is the process of modifying the surface of a component by utilizing a treatment, coating, or layer to enhance its properties. The purpose is to retain the key bulk properties of the component's material, while offering improved functionality. These properties may include the elasticity, hardness, Young's modulus, and yield, fatigue, and tensile strength necessary to perform the components duty (Funatani 2000). In surface engineering, the engineered surface undergoes a process that can vary from a simple finishing method such as abrasive blasting and thermal treatments (Davis 2002) to intricate chemical and plating surface coatings. Within these methods, the result can be a change to the surface metallurgy, chemistry, or an additional material layer to be exposed to the object's functioning environment. The various methods used in surface engineering can be seen in Fig. 5.2.

The utilization of surface modification applies to a vast number of fields, scaling from nanoscale coatings in the biomedical field (Mahapatro 2015) to large-scale wind turbines (Slot et al. 2015). In each of these scenarios, a component needs to be constructed to meet a variety of requirements which may not be possible from a single material. Ideally, the replacement material should mimic the natural

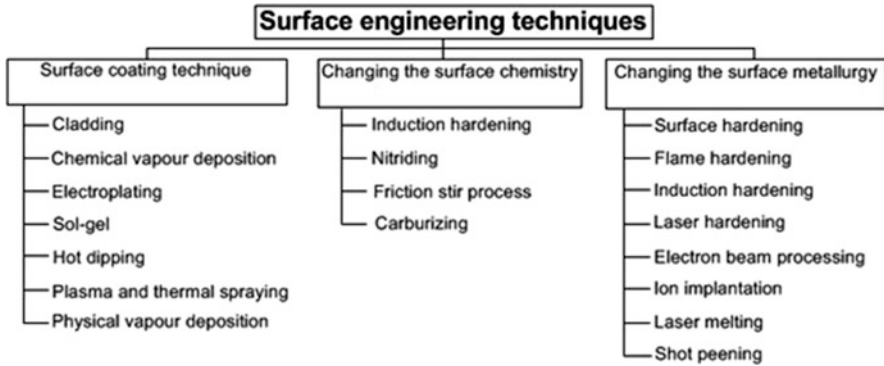


Fig. 5.2 Overview of the surface engineering applications and methods. Adapted from Ref. Gupta et al. (2017). Open access article distributed under the Creative Common Attribution License

component material it is replacing from a mechanical, chemical, biological, and functional point of view. In the biomedical field, surface engineering has been applied on implantable devices to allow for components to be surrounded by biological tissue and fluids while remaining bioinert, biocompatible, or even biodegradable (Huang et al. 2010; Zhang et al. 2002; Shen et al. 1993; Yu et al. 2008; Lee et al. 2006; Kievit and Zhang 2011; Habibovic et al. 2002; Chen et al. 2006; Woodard et al. 2007; Schmidmaier et al. 2001; Stemberger et al. 2003; Song et al. 2008; Yang et al. 2004; Ishihara 1997) depending on the application requirements. Biocompatible in that there is limited adverse response to surrounding tissue while limiting the intentional function of the device. Biodegradable in which it can be broken down by natural biological processes for the needed duration of the treatment.

5.2.1 Implant Treatments

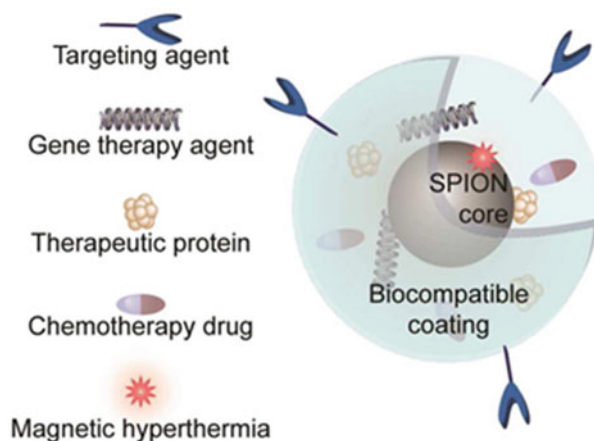
One example of surface engineering developments in the biomedical research field would be magnesium-based orthopedic implants. On its own, magnesium is lightweight while still providing suitable mechanical properties in addition to stimulatory effects on bone growth (Staiger et al. 2006; Zeng et al. 2008). However, the high corrosion rate and hydrogen evolution in the degradation of magnesium has limited its viability in clinical use. By incorporating a polymer coating consisting of polycaprolactone to the implant, the corrosion rate is able to be controlled, allowing for the component to fulfill its function for the prescribed healing period (Wong et al. 2010). In another study, a hydroxyapatite coating was electrodeposited on AZ91D magnesium alloy to improve its biodegradable performance (Song et al. 2008). With hydroxyapatite's bioactive properties that have shown to improve bone tissue growth (Habibovic et al. 2002; Chen et al. 2006; Woodard et al. 2007), it continues to be a material of interest in research for orthopedic implant coatings. In a similar

study by Behera et al., hydroxyapatite was incorporated with a titanium alloy for implant applications to promote strong bonding between tissue and material (Behera et al. 2018a, b). Titanium alloys, especially Ti-6Al-4V, have become of great interest to the medical field due to the excellent corrosion resistance, biocompatibility, and suitable mechanical properties (Elias et al. 2008; Khan et al. 1999; Niinomi 1998).

5.2.2 Drug Delivery

On a smaller scale, surface engineering is being applied in drug delivery and cancer targeting systems as well. The body utilizes many physiological and cellular barriers to hinder the traveling of a foreign object; however, they can be bypassed by a well-designed polymer coating or simply size. In cancer targeting research, groups are using superparamagnetic iron oxide nanoparticles (SPION) in conjunction with a therapeutic agent and magnetic resonance imaging to detect and monitor cancer cells within the body in a noninvasive fashion (Huang et al. 2010; Zhang et al. 2002; Shen et al. 1993; Yu et al. 2008; Lee et al. 2006; Kievit and Zhang 2011). The architecture of these nanoparticles can be seen in Fig. 5.3. These particles are able to circulate throughout the body and accumulate at the tumor site to provide physicians with monitoring abilities over prolonged periods of time. Several polymers have been engineered on the surface of the SPION, including dextran (Shen et al. 1993), polyethylene glycol (Zhang et al. 2002), and polyvinylpyrrolidone (Huang et al. 2010). With iron oxide and the designated coating's biodegradable properties, the particles can eventually be degraded and enter the body's natural iron transport (Kievit and Zhang 2011). As nanoparticle research continues to advance alongside polymeric coatings, future drugs will be able to cure diseases that are currently thought to be untreatable.

Fig. 5.3 Simplified architecture of surface-engineered superparamagnetic iron oxide nanoparticles (SPION) with treatment agent. Adapted from Ref. Kievit and Zhang (2011). Copyright American Chemical Society



5.3 Biosensors

Surface engineering innovations have been incorporated into sensors to begin a new development in detection and monitoring. Biosensors are devices that contain a receptor that detects and reacts to analytes in the application's setting, resulting in a generated signal that is sent to a processing unit to record a measurement in a desirable format (Goode et al. 2015), as seen in Fig. 5.4. The very first biosensor was developed in 1962 to continuously monitor blood glucose levels during cardiovascular surgeries (Clark Lc Jr Fau-Lyons and Lyons 1962). Since then, biosensors have made tremendous advancements and span from the use in the food and agriculture industry (Verma and Bhardwaj 2015; McGrath et al. 2013) to defense systems (Paddle 1996) to integrated health monitoring and treatment (Sershen and West 2003; Cao et al. 2001; Uhrich et al. 1999; Singh et al. 2016; Zhao et al. 2013; Tothill 2009). With the versatility of selectively quantifying specific compounds from a small and effective device, biosensors have gained considerable attention from the research community. As expected, the biosensor industry has grown tremendously, amounting to an estimated \$300 million annual worldwide investment and a continuously increasing number of publications and patents (Co. 2004). However, the commercialization of these devices has not followed the same path. Over 50 years after the biosensor to detect blood glucose levels was developed,

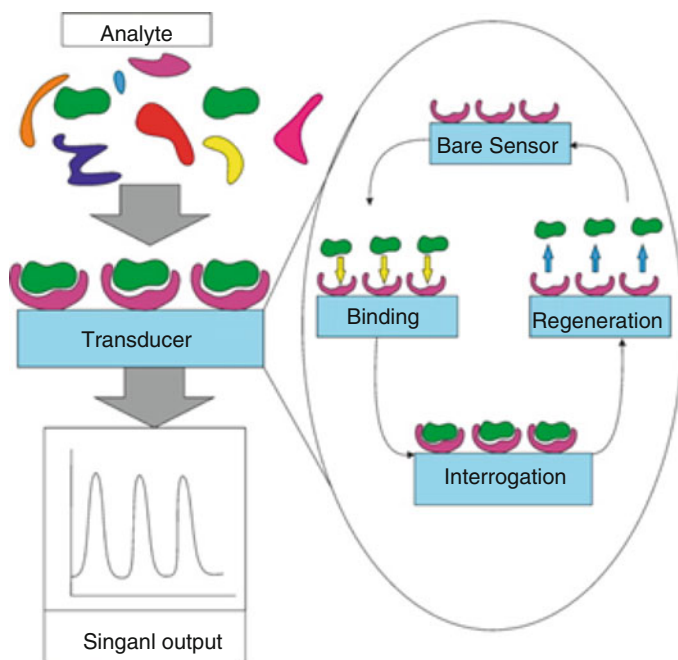


Fig. 5.4 Simplified illustration of biosensor design and operation. Adapted from Ref. Goode et al. (2015). Copyright American Chemical Society

handheld devices based on the same technology remain one of the only biosensors available to the consumer. This gap of progression is due to the lack of reliability of the sensor outside of a laboratory environment. The body is a complex system and the sensor needs to be able to acquire data accurately in a changing environment of chemical concentrations. Once accomplished, biosensors will have the potential to provide real-time results, replacing traditional testing procedures done in the hospital or appointment settings.

Cost is another factor limiting the widespread application of these devices. With the aging population and rise of healthcare cost, the collective goal of the healthcare industry is to treat patients with minimized cost. For these sensors, there is significant investment needed for the required supplementary instruments, chemicals, and transducer. However, once proven to be a successful analytical tool in practical situations, biosensors will inevitably be a more viable option versus making a clinical visit, as seen today by those affected by diabetes monitoring their blood sugar levels at their own convenience. Additionally, once optimized and at lower cost, the widespread utilization of biosensors in developing areas of the world with food and water safety risks as well as high mortality rates to preventable diseases would be of incredible value (Rodriguez-Mozaz et al. 2005). Currently in the consumer market, wearable devices able to monitor heart rate can be had for as little as \$25. With more features included such as calories burned, distance traveled, sleep monitoring, and most recently ECG in the Apple Watch, devices can reach over \$400. However, for the proactive individuals implementing a healthier lifestyle with the continuous monitoring of a wearable device, this cost would be marginal compared to clinical treatment.

The following sections will highlight the implanted and wearable biosensor technology currently in development within the health monitoring and medical diagnostic field.

5.3.1 Implanted

Within the biosensor developments, integrated devices have the potential to drastically improve point-of-care diagnostics, patient monitoring, and treatment. With the ability to monitor specific metabolites or drug concentrations in real time, treatments will be able to be optimized for maximum efficacy. Due to ineffective detection methods, many diseases, especially forms of cancer, are only discovered after it has metastasized through the body, which is often times beyond the point of treatment. Biosensors designed to target specific biomarkers such as those from tumors in the body would allow for early intervention before the disease progressed (Tothill 2009). In one study, a group designed a sensor with an immobilized sequence-specific peptide for the detection of extracellular hydrogen peroxide, a by-product released from breast cancer cells (Zhao et al. 2013). With a detection sensitivity down to 0.03 μM , the biosensor could be valuable for selectively detecting H_2O_2 in physiological systems. In another publication, carbon nanomaterials were utilized in the detection of lung cancer biomarker, hTERT, in incredibly low concentrations in

the attogram and femtogram scale (Singh et al. 2016). With the continuous innovations occurring in nanomaterial research, the future forms of cancer detection and treatment will be unmatched.

One of the most popular surface chemistry methods utilized on biosensors is the application of antibodies. Due to the significant research behind antibody's binding physics and reversible interactions with a wide selection of analytes, antibodies provided a reliable surface for bioreceptors, especially for rapid and sensitive analysis of pathogens and toxins (Goode et al. 2015; Karlsson et al. 1991; Omidfar et al. 2013).

Drug release systems are another area of great interest for biosensor researchers. With an implanted sensor to monitor the levels of a specific analyte, drugs can directly be released to the area of interest with maximum efficiency. For nearly two decades, groups have been working to develop a self-dosing implantable device to therapeutic agents (Sershen and West 2003; Cao et al. 2001). This would be beneficial in that less drugs will be needed due to direct site treatment or by skipping the ingestion stage entirely, while still receiving the necessary amount. Additionally, this would allow a controlled drug release to the therapeutic site over a time period (Uhrich et al. 1999).

5.3.2 Wearables

In addition to the biosensors imbedded within the body to provide continuous data on the targeted component, biosensors are also in development as wearable sensors for the analysis of body fluids such as saliva, tears, urine, and perspiration. For a potential user, a noninvasive option to monitor the status of their body will be preferred if able to perform the same function, as introducing a foreign object to the body can trigger an inflammatory and wound healing response (Anderson et al. 2008). One area still seeking improvements is the monitoring of blood glucose for those with diabetes. With the current finger pricking method, users are forced to manually check their blood sugar, which is inconvenient and also dependent upon time after eating (Moebus et al. 2011). Developments have been made for the continuous analysis of tear glucose concentrations (Elsherif et al. 2018; Kudo et al. 2006; La Belle et al. 2016; Yao et al. 2011). The contact lens sensor fabricated by Yao et al. demonstrated a fast response, high sensitivity, and repeatability, providing optimism of a future wearable contact lens capable of chemical analysis. In 2018, further improvements were made in the contact lens development by Elsharif et al. with the integration of a photonic glucose sensor on a contact lens that operates within physiological parameters and maintains a rapid response (Elsherif et al. 2018).

One particular area of interest, especially in the exercise science industry, is the analysis of sweat. The great advantage of evaluating sweat is that it is easily accessible at many locations on the body and has the potential to provide valuable physiological information (Bandodkar et al. 2014; Mena-Bravo and Luque de Castro 2014; Anastasova et al. 2017; Raiszadeh et al. 2012; Salvo et al. 2010) as well as

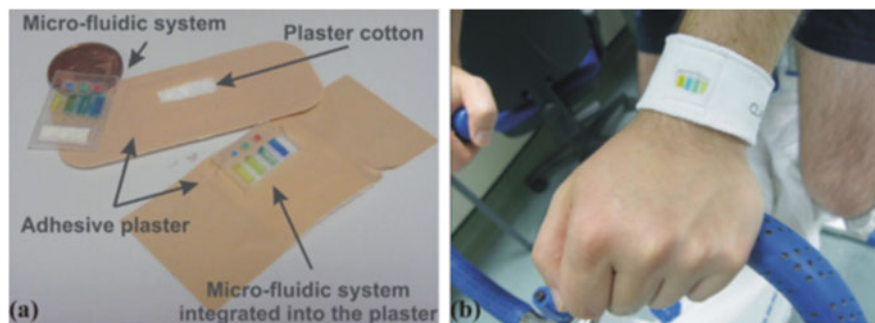


Fig. 5.5 Micro-fluidic system integrated into a plaster (a) and into a wristband (b). Adapted from Anastasova et al. (2017). Open access article distributed under the Creative Common Attribution License

detecting genetic disorders such as cystic fibrosis (Rock et al. 2014). Different routes are being approached in this area of research, such as sensing pH, metabolites, or proteins. In athletics, this could be especially valuable information to understand the fluid and electrolyte loss of the individuals. With the ability to track these parameters in parallel with vital signs, the mental and physical well-being of an individual under physical exertion can be tracked for prevention of injury or health risk. To analyze the sweat, different methods are being used to approach the challenge. Curto et al. incorporated ionic liquids into polymer gels and pH indicators to monitor and display the sweat pH level by simple observation. This idea was incorporated into a wristband, as seen in Fig. 5.5.

While this electronic-free device allows for the user to inspect during physical activity, the pH values are predictions based on the color change of the pH indicator dyes, which could be subject to error. However, the convenience and ability to incorporate this sensing technology into a simple patch or clothing could be useful. In other developments, electrochemical sensors are being fabricated to detect the sodium and lactate concentrations in parallel while wireless communicating data (Anastasova et al. 2017). This publication utilized microfluidic channels to guide sweat to the pH-sensing iridium oxide membrane and lactate-sensing doped enzyme deposit. Additionally, the sensor was adapted with Bluetooth technology to wirelessly transmit the data to an android application. With a response time of approximately 90 seconds and coefficient of variation under 10% for each parameter, this work has potential to provide clinically important information from the convenience of a wireless skin sensor.

Another body fluid that is under investigation in the biosensor research community is saliva. Just like perspiration, saliva is continuously available in convenient manner and it does not require physical activity to produce in measurable amounts. With the correlation between saliva and blood analytes (Soukup et al. 2012; Tekus et al. 2012), a mouthguard was developed to monitor metabolites in saliva (Kim et al. 2014). In this study, lactate was specifically targeted for measurement by entrapping a lactate-oxidase layer on the working electrode. By monitoring lactate, this

wearable biosensor could be used to monitor the status of a user's endurance during physical activity. While wearing a mouthpiece may not be the most comfortable scenario for the common person, athletes could benefit from the protection a mouthpiece provides while also acquiring real-time data on their body status. Indications of high lactate levels could inform elite athletes that they are not in peak physical condition and need to adjust their training regimen.

These biosensors are a brief insight of what the research community is currently developing to further the monitoring and treatment process for individuals. On the clinical side, the goal is to get patients out of the hospital setting and back to the comfort of their home while still being under remote physician supervision. For consumer use, these wearable devices will allow for a better understanding of the body's status, potentially leading to a desire to exceed goals for a healthier lifestyle.

5.4 Temperature Monitoring

One important physiological parameter to maintain body functionality includes sustaining a core body temperature (CBT) of about 37°C (98°F). For humans and animals, the body utilizes thermoregulatory functions to maintain homeostasis during rest and exercise (Abizaid et al. 2001). Studies have shown that a slightly elevated CBT results in improved working memory, alertness, visual attention, and quicker reaction time (Wright et al. 2002). For many individuals, having your temperature taken is almost exclusively tied to illness or a visit to see a doctor, yet temperature monitoring is not a parameter often thought about on a day-to-day basis.

5.4.1 Health Complications

It is well documented that when deviating significantly from baseline body temperature conditions, bodily health issues can arise. Falling below 35°C induces hypothermia, where complications occur such as respiratory depression, cardiac arrhythmia, impaired mental function, muscle dysfunction, and can progress to cardiac arrest or coma if untreated (Coleshaw 1983; Cheshire 2016). Alternatively, rising and maintaining a CBT above 40°C results in a state of hyperthermia which can cause sweating, fatigue, lightheadedness, headache, muscle cramps, low blood pressure, and paresthesia, which can lead to loss of consciousness, seizures, and coma (Cheshire 2016). At both extremes of body temperature, these symptoms and illnesses can hinder an individual's ability to perform day-to-day tasks as well as threaten their life.

In microgravity, these small health complications can pose a significant threat to the health of the crew. In spaceflight, a recent study has shown there is a gradual increase in CBT during long duration space missions of about 1°C (1.8°F). The lack of gravity limits evaporation and convection, preventing the body from cooling as effectively (Stahn et al. 2017). Additionally, when wearing the extravehicular mobility unit, the user will be under mental and physical strain which can raise the

body temperature even further (Oka 2015). Monitoring the physiological parameters of the crew is necessary for proper personal health and mission safety. However, the instruments to measure these parameters take up more capacity than desired, and in space transportation, weight and size are at an absolute premium (Advanced Space Transportation Program: Paving the Highway to Space 2008). This limitation drives the need to develop a thin sensor that can passively monitor multiple physiological parameters and communicate the data wirelessly in real time.

5.4.2 Temperature Sensors

In the current market, the population is familiar with the traditional temperature probes that are inserted in the mouth, rectum, or under the armpit to collect the respective data. These thermometers make use of a thermistor, an electrical resistor with temperature-dependent resistance. While simple, affordable, and effective, these instruments can provide false readings if food or drink has been consumed within 15 minutes or if the individual has been frequently breathing through the mouth. For some users, this may be an unpleasant experience or inconvenient to monitor their body temperature. The goal would be to have a sensor to monitor the temperature in real time without having to go through preparation or specific placement.

In recent years, researchers have been working on innovative projects to noninvasively monitor body temperature in various ways. One route several groups have went is the utilization of RFID (Vaz et al. 2010; Yu-Shiang et al. 2008; Zhou and Wu 2007; Milici et al. 2014; Opasjumruskit et al. 2006) to wirelessly transmit data at ultralow power consumption, allowing for wireless temperature monitoring system. One commercially available skin temperature sensor that uses RFID, the ThermoSENSOR by Cadi, was compared against a digital clinical thermometer as well as ear thermometer and found to be within 0.5°C (Ng et al. 2010). However, with its high cost, lack of flexibility, need for a battery, and size protruding from the site of temperature detection, progress can still be made.

One new and unique approach to monitoring the body temperature using a wearable device is a 3D printed hearing aid with the addition of an infrared sensor to measure the temperature of the ear drum (Ota et al. 2017). While the use of tympanic thermometers has been around for two decades (Shinozaki et al. 1988) and they are commercially available, the presence of ear wax or a curved ear canal can interfere with accuracy. For a typical consumer, this device may seem unappealing due to having an object inside the ear canal and attached to the surrounding area; however the dual functionality in addition to the personalized design could lead to more multi-function wearable devices, especially for infants, elderly, or at-risk patients.

5.5 Electromagnetic RF Resonator Sensor

As a research group, the goal is to design and fabricate an innovative skin patch sensor that monitors multiple physiological parameters in a wireless and noninvasive fashion. This allows for maximum functionality with less required resources, a desire that spans across all industries. In recent developments with the use of an electromagnetic radiofrequency resonating sensor, Dr. Kim Cluff's research group has developed innovative sensors to measure limb hemodynamics (Cluff et al. 2018), intracranial fluid volume shifts (Griffith et al. 2018), and volume changes in the heart (Alruwaili et al. 2018) in a noninvasive manner. The open-circuit electromagnetic resonant skin patch sensor was tailored to biomedical applications after originally being proposed to detect surface damage on aircraft (Woodard 2011). When powered using external oscillating magnetic fields, a loop antenna becomes electrically excited, and couples to the sensor, which is a simple spiral copper trace. The energized sensor then forms its own electromagnetic fields that can penetrate into surrounding materials, as seen in Fig. 5.6. These fields interact with nearby substrates, and changes in the electrical impedance cause changes to the resonant response of the sensor, allowing it to detect permittivity changes associated with the substrate using s-parameters. Figure 5.7 is an example of an electromagnetic resonating sensor fabricated for studying limb hemodynamics being applied to a tissue phantom. The sensor uses polyimide film as sensor substrate on both sides of the conductive copper trace.

With an understanding of the sensor's functionality with surrounding materials, one method to add functionality to the SansEC sensor is to incorporate surface engineering into the design. The following sections will go into detail of how

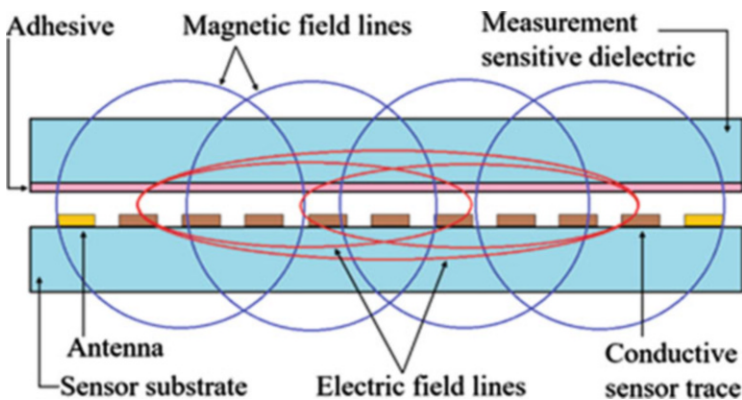


Fig. 5.6 Cross section side view of resonant open-circuit sensor that illustrates the antenna coupling to the spiral trace and interactions with the dielectric material within the electromagnetic field lines (Woodard 2011)

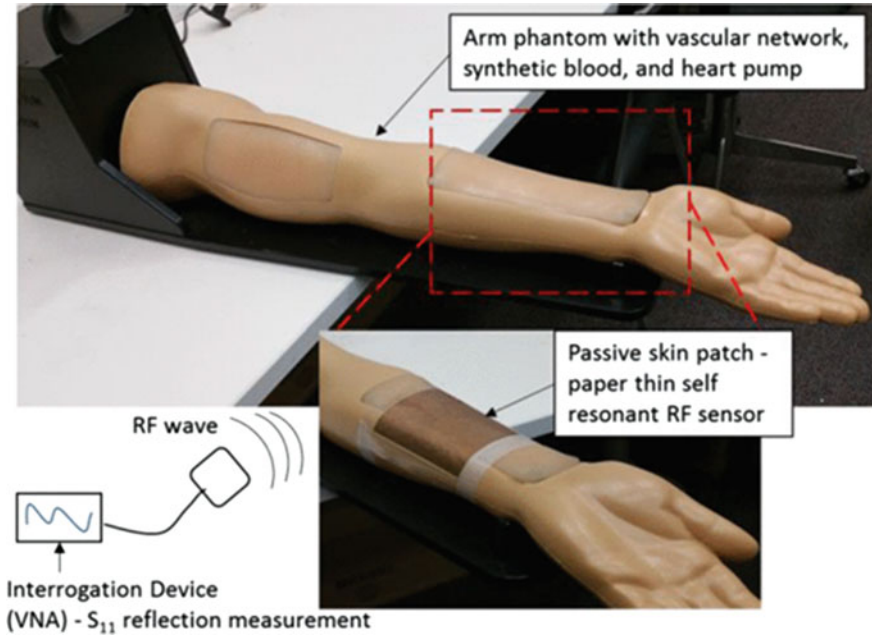


Fig. 5.7 Open circuit RF resonator sensor used to detect limb hemodynamics. Adapted from Ref. Cluff et al. (2018). Copyright IEEE

thermoreponsive polymers and dielectric materials could be utilized with this sensor technology to add temperature-sensing ability to its current physiological monitoring.

5.5.1 Thermoresponsive Materials

Thermoresponsive polymers are a class of “smart” polymers with the property to respond to changes in temperature (Stuart et al. 2010; Roy et al. 2013; Schmaljohann 2006; Gandhi et al. 2015; Ward and Georgiou 2011). In aqueous solutions, these materials undergo solubility changes at a critical temperature. Among the dozens of polymers and copolymers that exhibit thermoresponsive behavior, poly (N-isopropylacrylamide) (PNIPAM) is the most extensively investigated polymers due to its transition temperature being in between room temperature and body temperature at 32C. At room temperature, PNIPAM is soluble and transparent when in water. However, as the temperature rises above its lower critical solution temperature, the intra- and intermolecular hydrogen bonding dominates, resulting in a collapse of the polymer and changing of the solubility (Roy et al. 2013). This transition results in clouding, but upon cooling, the polymer response reverses and becomes soluble again.

What makes thermoresponsive polymers attractive is that the temperature at which the transition takes place is tunable. Introducing hydrophobic or hydrophilic groups allows for the adjustment of the transition temperature to increase or decrease, as well as manipulate the temperature range at which response occurs to be a slow or sharp transition. Studies have shown there is a dielectric permittivity change in the aqueous solution containing thermoresponsive polymers (Füllbrandt et al. 2013, 2014; Su et al. 2014; Nakano et al. 2012). By incorporating a microgel coating containing a thermoresponsive polymer in solution that transitions near physiological temperatures to the electromagnetic RF resonating sensor, a sensor with biomedical applications could be developed. However, this complicated method would result in a complex sensor fabrication as well as potential misreading due to volume shifts in the microgel.

5.5.2 Dielectric Materials

For the electromagnetic RF resonator sensor to measure temperature, surface modification will need to be implemented to use a dielectrically sensitive film that can increase selectivity of the sensor frequency response to changes in skin temperature. In preliminary studies, the feasibility was explored for application of polyvinylidene fluoride (PVDF) as a potential substrate and measurement sensitive dielectric material to be incorporated into the skin temperature sensor (Schmidt et al. 2019).

PVDF is a corrosion-resistant thermoplastic that has displayed dielectric properties that are strongly dependent on temperature and frequency. Previous studies have been conducted at lower frequencies in the Hz to MHz range which indicates the ability of the polymer to show variations in dielectric permittivity with variations in temperature (Yadav et al. 2010; Dang et al. 2005; Fu et al. 2015; Thomas et al. 2010) and frequency (Yadav et al. 2010; Dang et al. 2005; Fu et al. 2015; Thomas et al. 2010; Wang et al. 2013; Zhai et al. 2014; Niu et al. 2015). This relationship can be seen in Fig. 5.8.

However, no report exists that elaborates on the effects of temperature on dielectric properties of PVDF in the 10 MHz to 3 GHz range, which is the frequency range the sensor uses for physiological measurements. By utilizing the temperature-dependent dielectric properties of PVDF with the functionality of the electromagnetic resonating sensor, it is envisioned that an innovative passive, wireless temperature sensor can be developed. In addition to the advantageous dielectric properties of PVDF, the flexibility and durability of PVDF will further benefit the proposed skin temperature sensor and help in creating a more robust device.

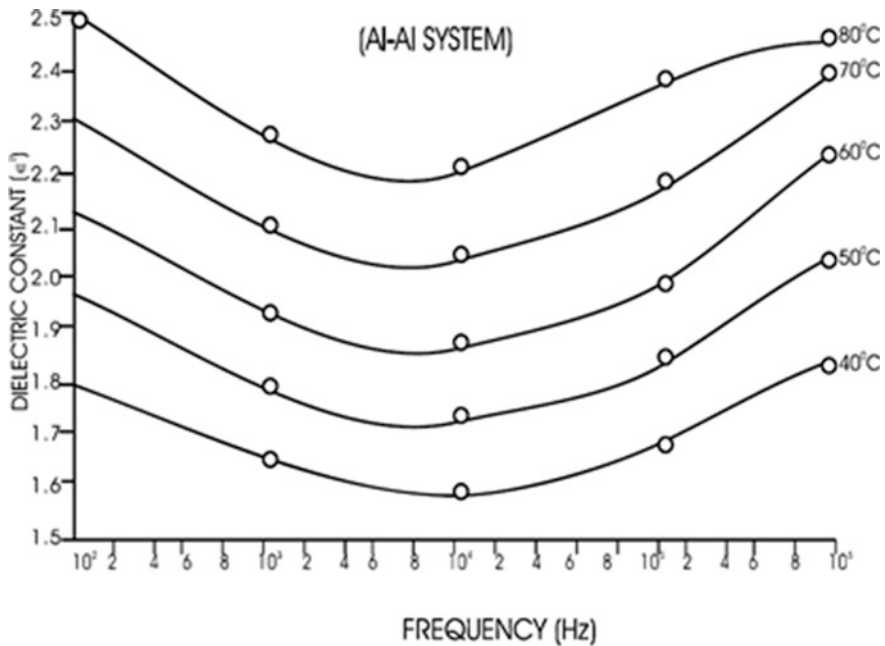


Fig. 5.8 Frequency and temperature-dependent dielectric permittivity of PVDF. Adapted from Ref. Yadav et al. (2010). Open access article distributed under the Creative Common Attribution License

5.6 Future Outlook and Challenges

As our population ages and the healthcare system is strained, there is a demand to monitor individuals without being on site to lower costs and provide suitable attention to those in need. Ongoing challenges being targeted in sensor research consists of real-time accurate monitoring, cost, comfort, power consumption, and reliable information transmission (Dunn et al. 2018). For flexibility, comfort, and sensitivity, one promising avenue for advances in sensor development is the incorporation of nanotechnology, another research topic of immense interest (Chae and Lee 2014; Kim et al. 2016). Nano-carbon materials are being considered to replace traditional silicon for computing to allow for flexible and stretchable devices. Additionally, nanomaterials high surface to volume ratio allows for improved sensitivity. With healthcare cost being the underlying motivation behind the development of wearable, this challenge will take care of itself over time (Saracco 2017). New technologies initial high cost and exclusivity will become more affordable and available with advancements in fabrication methods and material availability.

Another challenge with the acceptance of wearable devices to substitute point of care testing is the reliability of the device to deliver accurate data for all users. In

order to do so, calibration is of great importance and must be done with multiple devices across a diverse user group to develop algorithms and continuously improve with the ability to monitor specific types of activity (Bassett et al. 2012). Additionally, with continued development and the increasing adoption of wearable technology monitoring our body's activity, the disposal of consumer electronics is also of concern. E-waste is one of the fastest growing waste industries, and while precious metals used in the fabrication of the devices can be gathered, the presence of harmful chemicals makes it challenging. The devices of the future need to be designed and manufactured with this in mind to limit the environmental footprint of this industry (Gu et al. 2016; Kumar et al. 2017; Lepawsky et al. 2017).

5.7 Conclusion

This review presents and discusses wearable devices, their current application, and the potential they could provide to improved healthcare monitoring and treatment. With the tremendous growth that is expected in the wearable devices field, diagnostic and monitoring instruments used in clinical and research applications will slowly trickle into the consumer market. To be effective, these wearable devices will need to be safe, comfortable, and be able to provide clinical grade information to replace the current instruments used in healthcare.

References

- Abizaid A, Costa MA, Centemero M, Abizaid AS, Legrand VM, Limet RV, Schuler G, Mohr FW, Lindeboom W, Sousa AG, Sousa JE, van Hout B, Hugenholtz PG, Unger F, Serruys PW (2001) Clinical and economic impact of diabetes mellitus on percutaneous and surgical treatment of multivessel coronary disease patients: insights from the Arterial Revascularization Therapy Study (ARTS) trial. *Circulation* 104(5):533–538
- Advanced Space Transportation Program: Paving the Highway to Space (2008) National Aeronautics and Space Administration (NASA). <https://www.nasa.gov/centers/marshall/news/background/facts/astp.html>.
- Alruwaili F, Cluff K, Griffith J, Farhoud H (2018) Passive self resonant skin patch sensor to monitor intraventricular volume using electromagnetic properties of fluid volume changes. *IEEE J Transl Eng Health Med*:1–1. <https://doi.org/10.1109/JTEHM.2018.2870589>
- Anastasova S, Crewther B, Bembnowicz P, Curto V, Ip HMD, Rosa B, Yang G-Z (2017) A wearable multisensing patch for continuous sweat monitoring. *Biosens Bioelectron* 93:139–145. <https://doi.org/10.1016/j.bios.2016.09.038>
- Anderson JM, Rodriguez A, Fau-Chang DT (2008) Foreign body reaction to biomaterials (1044–5323 (Print))
- Apple (2018) ECG app and irregular heart rhythm notification available today on Apple Watch. <https://www.apple.com/newsroom/2018/12/ecg-app-and-irregular-heart-rhythm-notification-available-today-on-apple-watch/>
- Bandodkar AJ, Molinnus D, Mirza O, Guinovart T, Windmiller JR, Valdés-Ramírez G, Andrade FJ, Schöning MJ, Wang J (2014) Epidermal tattoo potentiometric sodium sensors with wireless signal transduction for continuous non-invasive sweat monitoring. *Biosens Bioelectron* 54:603–609. <https://doi.org/10.1016/j.bios.2013.11.039>

- Bassett DR Jr, Rowlands A, Trost SG (2012) Calibration and validation of wearable monitors. *Med Sci Sports Exerc* 44(1 Suppl 1):S32–S38. <https://doi.org/10.1249/MSS.0b013e3182399cf7>
- Behera RR, Das A, Pamu D, Pandey LM, Sankar MR (2018a) Mechano-tribological properties and in vitro bioactivity of biphasic calcium phosphate coating on Ti-6Al-4V. *J Mech Behav Biomed Mater* 86:143–157. <https://doi.org/10.1016/j.jmbbm.2018.06.020>
- Behera RR, Hasan A, Sankar MR, Pandey LM (2018b) Laser cladding with HA and functionally graded TiO₂-HA precursors on Ti-6Al-4V alloy for enhancing bioactivity and cytocompatibility. *Surf Coat Technol* 352:420–436. <https://doi.org/10.1016/j.surfcoat.2018.08.044>
- Cao X, Lai S, James Lee L (2001) Design of a self-regulated drug delivery device. *Biomed Microdevices* 3(2):109–118. <https://doi.org/10.1023/A:1011494008729>
- Chae SH, Lee YH (2014) Carbon nanotubes and graphene towards soft electronics. (2196–5404 (Print))
- Chan ED, Chan MM, Chan MM (2013) Pulse oximetry: understanding its basic principles facilitates appreciation of its limitations. *Respir Med* 107(6):789–799. <https://doi.org/10.1016/j.rmed.2013.02.004>
- Chen W, Liu Y, Courtney HS, Bettenga M, Agrawal CM, Bumgardner JD, Ong JL (2006) In vitro anti-bacterial and biological properties of magnetron co-sputtered silver-containing hydroxyapatite coating. *Biomaterials* 27(32):5512–5517. <https://doi.org/10.1016/j.biomaterials.2006.07.003>
- Cheshire WP Jr (2016) Thermoregulatory disorders and illness related to heat and cold stress. *Auton Neurosci Basic Clin* 196:91–104. <https://doi.org/10.1016/j.autneu.2016.01.001>
- Clark LC Jr Fau-Lyons, Lyons C (1962) Electrode systems for continuous monitoring in cardiovascular surgery. (0077–8923 (Print))
- Cluff K, Becker R, Jayakumar B, Han K, Condon E, Dudley K, Szatkowski G, Pipinos II, Amick RZ, Patterson J (2018) Passive wearable skin patch sensor measures limb hemodynamics based on electromagnetic resonance. *IEEE Trans Biomed Eng* 65(4):847–856. <https://doi.org/10.1109/TBME.2017.2723001>
- Co. F-KM (2004) U.S. and worldwide: biosensor market, R&D, applications and commercial implication. New York
- Coleshaw SRK (1983) Impaired memory registration and speed of reasoning caused by low body temperature. *J Appl Physiol* 55:27
- Dang Z-M, Wang L, Wang H-Y, Nan C-W, Xie D, Yin Y, Tjong SC (2005) Rescaled temperature dependence of dielectric behavior of ferroelectric polymer composites. *Appl Phys Lett* 86(17):172905. <https://doi.org/10.1063/1.1920408>
- Davis JR (2002) Surface hardening of steels: understanding the basics. ASM International
- Dunn J, Runge R, Snyder M (2018) Wearables and the medical revolution. *Per Med* 15(5):429–448. <https://doi.org/10.2217/pme-2018-0044>
- Edwards J (2012) Wireless sensors relay medical insight to patients and caregivers [special reports]. *IEEE Signal Process Mag* 29(3):8–12. <https://doi.org/10.1109/MSP.2012.2183489>
- Elias CN, Lima JHC, Valiev R, Meyers MA (2008) Biomedical applications of titanium and its alloys. *JOM* 60(3):46–49. <https://doi.org/10.1007/s11837-008-0031-1>
- Elsharif M, Hassan MU, Yetisen AK, Butt H (2018) Wearable contact lens biosensors for continuous glucose monitoring using smartphones. *ACS Nano* 12(6):5452–5462
- Funatani K (2000) Emerging technology in surface modification of light metals. *Surf Coat Technol* 133-134:264–272
- Fu J, Hou Y, Zheng M, Wei Q, Zhu M, Yan H (2015) Improving dielectric properties of PVDF composites by employing surface modified strong polarized BaTiO₃ particles derived by molten salt method. *ACS Appl Mater Interfaces* 7(44):24480–24491. <https://doi.org/10.1021/acsami.5b05344>
- Füllbrandt M, von Klitzing R, Schönhals A (2013) The dielectric signature of poly (N-isopropylacrylamide) microgels at the volume phase transition: dependence on the crosslinking density. *Soft Matter* 9(17):4464–4471. <https://doi.org/10.1039/C3SM27762C>

- Füllbrandt M, Ermilova E Fau-Asadujjaman A, Asadujjaman A Fau-Holzel R, Holzel R Fau-Bier FF, Bier Ff, Fau-von Klitzing R, von Klitzing R, Fau-Schonhals A (2014) Dynamics of linear poly(N-isopropylacrylamide) in water around the phase transition investigated by dielectric relaxation spectroscopy. (1520–5207 (Electronic))
- Gandhi A, Paul A, Sen SO, Sen KK (2015) Studies on thermoresponsive polymers: phase behaviour, drug delivery and biomedical applications. *Asian J Pharm Sci* 10(2):99–107. <https://doi.org/10.1016/j.ajps.2014.08.010>
- Gao W, Emaminejad S, Nyein HYY, Challa S, Chen K, Peck A, Fahad HM, Ota H, Shiraki H, Kiriya D, Lien D-H, Brooks GA, Davis RW, Javey A (2016) Fully integrated wearable sensor arrays for multiplexed in situ perspiration analysis. *Nature* 529:509. <https://doi.org/10.1038/nature16521>. <https://www.nature.com/articles/nature16521#supplementary-information>
- Goode JA, Rushworth JVH, Millner PA (2015) Biosensor regeneration: a review of common techniques and outcomes. *Langmuir* 31(23):6267–6276. <https://doi.org/10.1021/la503533g>
- Griffith J, Cluff K, Eckerman B, Aldrich J, Becker R, Moore-Jansen P, Patterson J (2018) Non-invasive electromagnetic skin patch sensor to measure intracranial fluid–volume shifts. *Sensors* 18(4):1022
- Gu Y, Wu Y, Xu M, Mu X, Zuo T (2016) Waste electrical and electronic equipment (WEEE) recycling for a sustainable resource supply in the electronics industry in China. *J Clean Prod* 127:331–338. <https://doi.org/10.1016/j.jclepro.2016.04.041>
- Gupta V, Choudhary B, Morgan A, Bansal A, Singh M, Singh H (2017) A review on surface engineering modifications obtained using inconel-625, vol 8.
- Habibovic P, Barrère F, Van Blitterswijk CA, de Groot K, Layrolle P (2002) Biomimetic hydroxyapatite coating on metal implants. *J Am Ceram Soc* 85(3):517–522. <https://doi.org/10.1111/j.1151-2916.2002.tb00126.x>
- Huang J, Bu L, Xie J, Chen K, Cheng Z, Li X, Chen X (2010) Effects of nanoparticle size on cellular uptake and liver MRI with polyvinylpyrrolidone-coated iron oxide nanoparticles. *ACS Nano* 4(12):7151–7160. <https://doi.org/10.1021/nn101643u>
- Ishihara K (1997) Novel polymeric materials for obtaining blood-compatible surfaces, vol. 5.
- Karlsson R, Michaelsson A, Mattsson L (1991) Kinetic analysis of monoclonal antibody-antigen interactions with a new biosensor based analytical system. *J Immunol Methods* 145(1):229–240. [https://doi.org/10.1016/0022-1759\(91\)90331-9](https://doi.org/10.1016/0022-1759(91)90331-9)
- Khan MA, Williams RL, Williams DF (1999) The corrosion behaviour of Ti–6Al–4V, Ti–6Al–7Nb and Ti–13Nb–13Zr in protein solutions. *Biomaterials* 20(7):631–637. [https://doi.org/10.1016/S0142-9612\(98\)00217-8](https://doi.org/10.1016/S0142-9612(98)00217-8)
- Khan Y, Ostfeld AE, Lochner CM, Pierre A, Arias AC (2016) Monitoring of vital signs with flexible and wearable medical devices. *Adv Mater* 28(22):4373–4395. <https://doi.org/10.1002/adma.201504366>
- Kievit FM, Zhang M (2011) Surface engineering of iron oxide nanoparticles for targeted cancer therapy. *Acc Chem Res* 44(10):853–862. <https://doi.org/10.1021/ar2000277>
- Kim J, Valdes-Ramirez G Fau-Bandodkar AJ, Bandodkar Aj, Fau-Jia W, Jia W, Fau-Martinez AG, Martinez Ag, Fau-Ramirez J, Ramirez J, Fau-Mercier P, Mercier P, Fau-Wang J, Wang J (2014) Non-invasive mouthguard biosensor for continuous salivary monitoring of metabolites. (1364–5528 (Electronic))
- Kim J, Lee J, Son D, Choi MK, Kim D-H (2016) Deformable devices with integrated functional nanomaterials for wearable electronics. *Nano Convergence* 3(1):4. <https://doi.org/10.1186/s40580-016-0062-1>
- Kudo H, Sawada T, Kazawa E, Yoshida H, Iwasaki Y, Mitsubayashi K (2006) A flexible and wearable glucose sensor based on functional polymers with Soft-MEMS techniques. *Biosens Bioelectron* 22(4):558–562. <https://doi.org/10.1016/j.bios.2006.05.006>
- Kumar A, Holuszko M, Espinosa DCR (2017) E-waste: an overview on generation, collection, legislation and recycling practices. *Resour Conserv Recycl* 122:32–42. <https://doi.org/10.1016/j.resconrec.2017.01.018>

- La Belle JT, Adams A, Lin C-E, Engelschall E, Pratt B, Cook CB (2016) Self-monitoring of tear glucose: the development of a tear based glucose sensor as an alternative to self-monitoring of blood glucose. *Chem Commun* 52(59):9197–9204. <https://doi.org/10.1039/C6CC03609K>
- Lee Y-D, Chung W-Y (2009) Wireless sensor network based wearable smart shirt for ubiquitous health and activity monitoring. *Sensors Actuators B Chem* 140(2):390–395. <https://doi.org/10.1016/j.snb.2009.04.040>
- Lee H, Lee E, Kim DK, Jang NK, Jeong YY, Jon S (2006) Antibiofouling polymer-coated superparamagnetic iron oxide nanoparticles as potential magnetic resonance contrast agents for in vivo cancer imaging. *J Am Chem Soc* 128(22):7383–7389. <https://doi.org/10.1021/ja061529k>
- Lepawsky J, Araujo E, Davis J-M, Kahhat R (2017) Best of two worlds? Towards ethical electronics repair, reuse, repurposing and recycling. *Geoforum* 81:87–99. <https://doi.org/10.1016/j.geoforum.2017.02.007>
- Mahapatro A (2015) Bio-functional nano-coatings on metallic biomaterials. *Mater Sci Eng C* 55:227–251. <https://doi.org/10.1016/j.msec.2015.05.018>
- McGrath TF, Andersson K, Fau-Campbell K, Campbell K, Fau-Fodey TL, Fodey TI, Fau-Elliott CT (2013) Development of a rapid low cost fluorescent biosensor for the detection of food contaminants. (1873–4235 (Electronic))
- Mena-Bravo A, Luque de Castro MD (2014) Sweat: a sample with limited present applications and promising future in metabolomics. *J Pharm Biomed Anal* 90:139–147. <https://doi.org/10.1016/j.jpba.2013.10.048>
- Milici S, Amendola S, Bianco A, Marrocco G (2014) Epidermal RFID passive sensor for body temperature measurements. In: 2014 IEEE RFID technology and applications conference (RFID-TA), 8–9 Sept. 2014. pp 140–144. 10.1109/RFID-TA.2014.6934216
- Moebus S, Göres L, Lösch C, Jöckel K-H (2011) Impact of time since last caloric intake on blood glucose levels. *Eur J Epidemiol* 26(9):719–728. <https://doi.org/10.1007/s10654-011-9608-z>
- Nakano S, Sato Y, Kita R, Shinyashiki N, Yagihara S, Sudo S, Yoneyama M (2012) Molecular dynamics of poly(N-isopropylacrylamide) in protic and aprotic solvents studied by dielectric relaxation spectroscopy. *J Phys Chem B* 116(2):775–781. <https://doi.org/10.1021/jp210376u>
- Ng K-G, Wong S-T, Lim S-M, Goh Z (2010) Evaluation of the Cadi ThermoSENSOR wireless skin-contact thermometer against ear and axillary temperatures in children. *J Pediatr Nurs* 25(3):176–186. <https://doi.org/10.1016/j.pedn.2008.12.002>
- Niinomi M (1998) Mechanical properties of biomedical titanium alloys. *Mater Sci Eng A* 243(1):231–236. [https://doi.org/10.1016/S0921-5093\(97\)00806-X](https://doi.org/10.1016/S0921-5093(97)00806-X)
- Niu Y, Yu K, Bai Y, Wang H (2015) Enhanced dielectric performance of BaTiO₃/PVDF composites prepared by modified process for energy storage applications. *IEEE Trans Ultrason Ferroelectr Freq Control* 62(1):108–115. <https://doi.org/10.1109/TUFFC.2014.0066666>
- Oka T (2015) Psychogenic fever: how psychological stress affects body temperature in the clinical population. *Temperature (Austin, Tex)* 2(3):368–378. <https://doi.org/10.1080/23328940.2015.1056907>
- Omidfar K, Khorsand F, Darziani Azizi M (2013) New analytical applications of gold nanoparticles as label in antibody based sensors. *Biosens Bioelectron* 43:336–347. <https://doi.org/10.1016/j.bios.2012.12.045>
- Opasjumruskit K, Thanthipwan T, Sathusen O, Sirinamarattana P, Gadmanee P, Pootarapan E, Wongkomet N, Thanachayanont A, Thamsirianunt M (2006) Self-powered wireless temperature sensors exploit RFID technology. *IEEE Pervas Comput* 5(1):54–61. <https://doi.org/10.1109/MPRV.2006.15>
- Ota H, Chao M, Gao Y, Wu E, Tai L-C, Chen K, Matsuoka Y, Iwai K, Fahad HM, Gao W, Nyein HYY, Lin L, Javey A (2017) 3D printed “Earable” smart devices for real-time detection of core body temperature. *ACS Sensors* 2(7):990–997. <https://doi.org/10.1021/acssensors.7b00247>
- Paddle BM (1996) Biosensors for chemical and biological agents of defence interest. *Biosens Bioelectron* 11(11):1079–1113. [https://doi.org/10.1016/0956-5663\(96\)82333-5](https://doi.org/10.1016/0956-5663(96)82333-5)

- Park S, Jayaraman S (2003) Smart textiles: wearable electronic systems. *MRS Bull* 28(8):585–591. <https://doi.org/10.1557/mrs2003.170>
- Raiszadeh MM, Ross MM, Russo PS, Schaepper MA, Zhou W, Deng J, Ng D, Dickson A, Dickson C, Strom M, Osorio C, Soeprono T, Wulfkuhle JD, Petricoin EF, Liotta LA, Kirsch WM (2012) Proteomic analysis of eccrine sweat: implications for the discovery of schizophrenia biomarker proteins. *J Proteome Res* 11(4):2127–2139. <https://doi.org/10.1021/pr2007957>
- Research GV (2018) Wearable sensors market size, share & trends analysis report by sensor type, by device (smart watch, fitness band, smart glasses, smart fabric), by vertical, by region, and segment forecast, 2018–2025.
- Rock MJ, Makhholm L, Eickhoff J (2014) A new method of sweat testing: the CF Quantum®sweat test. *J Cyst Fibros* 13(5):520–527. <https://doi.org/10.1016/j.jcf.2014.05.001>
- Rodriguez-Mozaz S, Alda Mj Fau-Marco M-P, Marco Mp Fau-Barcelo D, Barcelo D (2005) Biosensors for environmental monitoring a global perspective. (1873–3573 (Electronic))
- Roy D, Brooks Wl, Fau-Sumerlin BS (2013) New directions in thermoresponsive polymers. (1460–4744 (Electronic))
- Salvo P, Francesco FD, Costanzo D, Ferrari C, Trivella MG, Rossi DD (2010) A wearable sensor for measuring sweat rate. *IEEE Sensors J* 10(10):1557–1558. <https://doi.org/10.1109/JSEN.2010.2046634>
- Saracco R (2017) A never ending decrease of technology cost. *IEEE Future Directions*. Available at: <http://sites.ieee.org/futuredirections/2017/10/18/a-never-ending-decrease-of-technology-cost/>
- Schmaljohann D (2006) Thermo- and pH-responsive polymers in drug delivery. *Adv Drug Deliv Rev* 58(15):1655–1670. <https://doi.org/10.1016/j.addr.2006.09.020>
- Schmidmaier G, Wildemann B, Stemberger A, Haas NP, Raschke M (2001) Biodegradable poly(D, L-lactide) coating of implants for continuous release of growth factors. *J Biomed Mater Res* 58(4):449–455. <https://doi.org/10.1002/jbm.1040>
- Schmidt D, Mahapatro A, Loffin B, Cluff K (2019) Investigating the effect of temperature and frequency on dielectric properties of polyvinylidene fluoride (PVDF) for its application in a skin temperature sensor. Paper presented at the ANTEC, Detroit, MI
- Sershen S, West J (2003) Implantable, polymeric systems for modulated drug delivery. (0169–409X (Print))
- Shen T, Weissleder R Fau-Papisov M, Papisov M Fau-Bogdanov A, Jr, Bogdanov A, Jr, Fau-Brady TJ (1993) Monocrystalline iron oxide nanocompounds (MION): physicochemical properties. (0740–3194 (Print))
- Shinozaki T, Deane R Fau-Perkins FM (1988) Infrared tympanic thermometer: evaluation of a new clinical thermometer. (0090–3493 (Print))
- Singh A, Choudhary M, Kaur S, Singh SP, Arora K (2016) Molecular functionalization of carbon nanomaterials for immuno-diagnosis of cancer. *Mater Today Proc* 3(2):157–161. <https://doi.org/10.1016/j.matpr.2016.01.050>
- Slot HM, Gelinck ERM, Rentrop C, van der Heide E (2015) Leading edge erosion of coated wind turbine blades: review of coating life models. *Renew Energy* 80:837–848. <https://doi.org/10.1016/j.renene.2015.02.036>
- Song YW, Shan DY, Han EH (2008) Electrodeposition of hydroxyapatite coating on AZ91D magnesium alloy for biomaterial application. *Mater Lett* 62(17):3276–3279. <https://doi.org/10.1016/j.matlet.2008.02.048>
- Soukup M, Biesiada I Fau-Henderson A, Henderson A Fau-Idowu B, Idowu B Fau-Rodeback D, Rodeback D Fau-Ridpath L, Ridpath L Fau-Bridges EG, Bridges Eg, Fau-Nazar AM, Fau-Bridges KG (2012) Salivary uric acid as a noninvasive biomarker of metabolic syndrome. (1758–5996 (Electronic))
- Stahn AC, Werner A, Opatz O, Maggioni MA, Steinach M, von Ahlefeld VW, Moore A, Crucian BE, Smith SM, Zwart SR, Schlabs T, Mendt S, Trippel T, Koralewski E, Koch J, Choukèr A, Reitz G, Shang P, Röcker L, Kirsch KA, Gunga H-C (2017) Increased core body temperature in

- astronauts during long-duration space missions. *Sci Rep* 7(1):16180. <https://doi.org/10.1038/s41598-017-15560-w>
- Staiger MP, Pietak AM, Huadmai J, Dias G (2006) Magnesium and its alloys as orthopedic biomaterials: a review. *Biomaterials* 27(9):1728–1734
- Stemberger A, Gollwitzer H, Meyer H, Ibrahim K, Busch R, Mittelmeier W (2003) Antibacterial poly(D,L-lactic acid) coating of medical implants using a biodegradable drug delivery technology. *J Antimicrob Chemother* 51(3):585–591. <https://doi.org/10.1093/jac/dkg105>
- Stuart MAC, Huck WTS, Genzer J, Müller M, Ober C, Stamm M, Sukhorukov GB, Szleifer I, Tsukruk VV, Urban M, Winnik F, Zauscher S, Luzinov I, Minko S (2010) Emerging applications of stimuli-responsive polymer materials. *Nat Mater* 9:101. <https://doi.org/10.1038/nmat2614>
- Su W, Zhao K, Wei J, Ngai T (2014) Dielectric relaxations of poly(N-isopropylacrylamide) microgels near the volume phase transition temperature: impact of cross-linking density distribution on the volume phase transition. *Soft Matter* 10(43):8711–8723. <https://doi.org/10.1039/C4SM01516A>
- Sungmee P, Jayaraman S (2003) Enhancing the quality of life through wearable technology. *IEEE Eng Med Biol Magazine* 22(3):41–48. <https://doi.org/10.1109/EMEMB.2003.1213625>
- Tekus E, Kaj M, Szabó E, Lilla Szénási N, Kerepesi I, Figler M, Gabriel R, Wilhelm M (2012) Comparison of blood and saliva lactate level after maximum intensity exercise 63 (Suppl 1). <https://doi.org/10.1556/ABiol.63.2012.Suppl.1.9>
- Thomas P, Varughese K, Dwarakanath K, Varma K (2010) Dielectric properties of poly(vinylidene fluoride)/CaCu₃Ti₄O₁₂ composites, vol. 70. <https://doi.org/10.1016/j.compscitech.2009.12.014>
- Tothill IE (2009) Biosensors for cancer markers diagnosis. (1084–9521 (Print))
- Uhrich KE, Cannizzaro SM, Langer RS, Shakesheff KM (1999) Polymeric systems for controlled drug release. *Chem Rev* 99(11):3181–3198. <https://doi.org/10.1021/cr940351u>
- Vaz A, Ubarretxena A, Zalbide I, Pardo D, Solar H, Garcia-Alonso A, Berenguer R (2010) Full passive UHF tag with a temperature sensor suitable for human body temperature monitoring. *IEEE Trans. Circuits Syst II Exp Briefs* 57(2):95–99. <https://doi.org/10.1109/TCSII.2010.2040314>
- Verma N, Bhardwaj A (2015) Biosensor technology for pesticides—a review. *Appl Biochem Biotechnol* 175(6):3093–3119. <https://doi.org/10.1007/s12010-015-1489-2>
- Wang FF, Wang YJ, Ren ZB (2013) Dielectric properties of CCTO/PVDF composite films. *Adv Mater Res* 816–817:276–279. <https://doi.org/10.4028/www.scientific.net/AMR.816-817.276>
- Ward MA, Georgiou TK (2011) Thermoresponsive polymers for biomedical applications. *Polymers* 3(3). <https://doi.org/10.3390/polym3031215>
- Wong HM, Yeung KWK, Lam KO, Tam V, Chu PK, Luk KDK, Cheung KMC (2010) A biodegradable polymer-based coating to control the performance of magnesium alloy orthopaedic implants. *Biomaterials* 31(8):2084–2096. <https://doi.org/10.1016/j.biomaterials.2009.11.111>
- Woodard SE (2011) Sensing technology—a new tool for designing space systems and components. In: 2011 Aerospace conference, 5–12 March 2011. pp 1–11. <https://doi.org/10.1109/AERO.2011.5747495>
- Woodard JR, Hilldore AJ, Lan SK, Park CJ, Morgan AW, Eurell JAC, Clark SG, Wheeler MB, Jamison RD, Wagoner Johnson AJ (2007) The mechanical properties and osteoconductivity of hydroxyapatite bone scaffolds with multi-scale porosity. *Biomaterials* 28(1):45–54. <https://doi.org/10.1016/j.biomaterials.2006.08.021>
- Wright KP, Hull JT, Czeisler CA (2002) Relationship between alertness, performance, and body temperature in humans. *Am J Phys Regul Integr Comp Phys* 283(6):R1370–R1377. <https://doi.org/10.1152/ajpregu.00205.2002>
- Yadav VS, Sahu DK, Singh Y, Kumar M, Dhukarya DC (2010) Frequency and temperature dependence of dielectric properties of pure poly vinylidene fluoride (PVDF) thin films. *AIP Conf Proc* 1285(1):267–278. <https://doi.org/10.1063/1.3510553>

- Yang SY, Lee D, Cohen RE, Rubner MF (2004) Bioinert solution-cross-linked hydrogen-bonded multilayers on colloidal particles. *Langmuir* 20(14):5978–5981. <https://doi.org/10.1021/la0490442>
- Yao H, Shum AJ, Cowan M, Lähdesmäki I, Parviz BA (2011) A contact lens with embedded sensor for monitoring tear glucose level. *Biosens Bioelectron* 26(7):3290–3296. <https://doi.org/10.1016/j.bios.2010.12.042>
- Yu MK, Jeong YY, Park J, Park S, Kim JW, Min JJ, Kim K, Jon S (2008) Drug-loaded superparamagnetic iron oxide nanoparticles for combined cancer imaging and therapy in vivo. *Angew Chem* 120(29):5442–5445. <https://doi.org/10.1002/ange.200800857>
- Yu-Shiang L, Sylvester D, Blaauw D (2008) An ultra low power 1V, 220nW temperature sensor for passive wireless applications. In: 2008 IEEE custom integrated circuits conference, 21–24 Sept. 2008. pp 507–510. <https://doi.org/10.1109/CICC.2008.4672133>
- Zeng R, Dietzel W, Witte F, Hort N, Blawert C (2008) Progress and challenge for magnesium alloys as biomaterials. *Adv Eng Mater* 10(8):B3–B14. <https://doi.org/10.1002/adem.200800035>
- Zhai JW, Wang YJ, Deng JL, Feng CG (2014) Preparation and dielectric properties of Cu/PVDF composite films. *Adv Mater Res* 1035:417–421. <https://doi.org/10.4028/www.scientific.net/AMR.1035.417>
- Zhang Y, Kohler N, Fau-Zhang M (2002) Surface modification of superparamagnetic magnetite nanoparticles and their intracellular uptake. (0142–9612 (Print))
- Zhang Y, Poon CCY, Chan C, Tsang MWW, Wu K (2006) A health-shirt using e-textile materials for the continuous and cuffless monitoring of arterial blood pressure. In: 2006 3rd IEEE/EMBS international summer school on medical devices and biosensors, 4–6 Sept. 2006. pp 86–89. <https://doi.org/10.1109/ISSMDBS.2006.360104>
- Zhao J, Yan Y, Zhu L, Li X, Li G (2013) An amperometric biosensor for the detection of hydrogen peroxide released from human breast cancer cells. *Biosens Bioelectron* 41:815–819. <https://doi.org/10.1016/j.bios.2012.10.019>
- Zhou S, Wu N (2007) A novel ultra low power temperature sensor for UHF RFID tag chip. In: 2007 IEEE Asian solid-state circuits conference, 12–14 Nov. 2007. pp 464–467. <https://doi.org/10.1109/ASSCC.2007.4425731>



Modulation of Physicochemical Properties of Polymers for Effective Insulin Delivery Systems

6

Prateek Ranjan Yadav and Sudip K. Pattanayek

Abstract

Defect in insulin secretion or insulin action in the body leads to a chronic health disease known as diabetes mellitus (DM). Current therapy for diabetes through subcutaneous insulin administration leads to occasional hypoglycemia in patients and bolus. Non-invasive means of insulin delivery, including transdermal, ocular, buccal, oral, and nasal, are currently being explored. However, the various factors limit these new insulin delivery routes, including degradation and structure deformation of insulin due to the presence of harsh body conditions like temperature and pH. The insulin drug should reach the specific site of action at the required physiological concentration in a definite time interval. In noninvasive means of insulin delivery systems, polymers of characteristics properties are used. Natural polymers such as chitosan, alginate, starch, pectin, casein, dextran, gelatin, and cyclodextrin and their derivatives are used frequently. In this chapter, we have reviewed the present status of ongoing research on the various polymers and their characteristics for insulin delivery in transdermal, oral, and nasal delivery methods.

Keywords

Insulin · Transdermal · Stimuli-responsive

P. R. Yadav · S. K. Pattanayek (✉)

Department of Chemical Engineering, Indian Institute of Technology Delhi, New Delhi, India

e-mail: sudip@chemical.iitd.ac.in

© Springer Nature Singapore Pte Ltd. 2020

P. Chandra, L.M. Pandey (eds.), *Biointerface Engineering: Prospects in Medical Diagnostics and Drug Delivery*, https://doi.org/10.1007/978-981-15-4790-4_6

123

6.1 Introduction

Diabetes mellitus is a common metabolic disorder that involves hyperglycemia or an excess of glucose in the bloodstream due to insulin deficiency or abnormality in the use of insulin. The beta cells, which are distributed in a cluster of cells in the pancreas (also named as the Islets of Langerhans), produce insulin to maintain blood glucose levels in the body. The required level of insulin allows other cells present in the body to transform glucose into energy.

Additionally, when the level of glucose in the bloodstream increases significantly, insulin allows the storage of glucose as glycogen inside the body. The stored glucose is used later in the higher energy requirements. In the absence of insulin, the body cells are unable to utilize glucose as energy properly. As a result, the glucose remains in the bloodstream leading to hyperglycemia. Chronic hyperglycemia is characteristic of diabetes mellitus, which is related to severe complications, such as damage to the nervous system, eyes, and kidneys (Alberti and Zimmet 1998). It is increasingly recognized as a serious, worldwide public health concern. According to the International Diabetic Federation (IDF) report, about 463 million adults are living with diabetes, and it is going to rise to 700 million by 2045.

There are three types of diabetes mellitus: type 1, type 2, and gestational diabetes. In type 1 diabetes mellitus (T1DM), the pancreas makes a little or no insulin. In type 2 diabetes mellitus (T2DM), the pancreas produces insufficient insulin, or the insulin works improperly. In gestational diabetes (GDM), high blood glucose during pregnancy and subsequent complications to both mother and child are observed. The GDM usually disappears after pregnancy but the affected women and their children may develop type 2 diabetes later in life. According to IDF, the proportion of type 2 diabetes is around 90%, while type 1 diabetes is about 10% of all diabetes cases. Patients with diabetes often rely on insulin to regulate their blood glucose levels.

The most commonly used route of insulin administration among diabetic patients is subcutaneous insulin injections. This route of administration has inherent poor patient compliance with injections, in addition to several demerits, such as occasional hypoglycemia and a risk of infection at the injection sites (Swift et al. 2002; Yumlu et al. 2009; Shikama et al. 2010; Nilsson 2016). Therefore, the scientist has been trying to develop a minimally invasive or noninvasive method of insulin delivery. Many alternative routes of insulin delivery which have been explored over the last two decades are nasal, buccal, dermal, oral, ocular, pulmonary, and intraperitoneal (Illum 2002; Owens 2002; Cefalu 2003; Goldberg and Gomez-Orellana 2003). A polymer with the route-specific characteristics properties is needed to take care of the environmental conditions, biocompatibility, and biodegradability. In addition, the controlled release of insulin in the body requires either a constant dose over a long period or a cyclic dosage of insulin. The controlled release of insulin is also required to be monitored through the physicochemical properties of the polymer (Ramkissoon-Ganorkar et al. 1999; Brown et al. 1986).

The processing of the combination of polymer and insulin may require temperature, contacts with a hydrophobic surface, extreme pH conditions, and the presence of organic solvents. The activity of insulin may decrease in the presence of the above

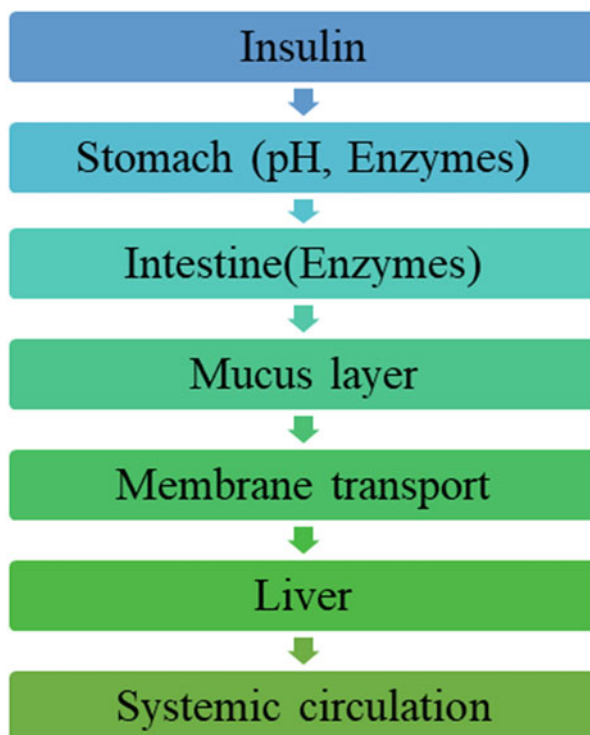
severe conditions for a protein and be avoided (Brange et al. 1997). To protect insulin from these unfavorable conditions, an appropriate polymer or polymer blend should be used as a protective layer over the insulin molecules. The polymer used should be compliant to the recommendation of drug regulatory bodies like the Food and Drugs Administration (FDA) and the European Medicines Agency (EMA).

This chapter aims to provide unique coverage of the field of various polymers used in insulin delivery systems, addressing the recent developments in responsive polymers. We will look into three distinct routes of insulin delivery system, i.e., oral, transdermal, and nasal, and subsequently find out the effectiveness of various insulin-loaded polymer matrix developed to date.

6.2 Oral Insulin Delivery

Due to convenience, oral administration is the most preferred delivery route (Plapiet et al. 2011, 2014). The medicine directly goes from the digestive tract to the liver before going to the systemic bloodstream (Fig. 6.1). (Chen et al. 2011; Chaturvedi et al. 2013; Herrero et al. 2012). However, the oral delivery of insulin remains a challenge as it is to be protected from the harsh medium condition of the digestive tract (stomach and intestine). Besides, other challenges are the presence of mucus

Fig. 6.1 Oral absorption of insulin into the bloodstream



and the low permeability of insulin across the intestinal epithelium during its passage through the gastrointestinal tract.

The stability and bioavailability of insulin is the primary concern in the oral delivery system. The native structure of insulin is damaged upon exposure to an extreme acidic condition of the stomach (pH of gastric acid is 1.5–3.5). Oral polymeric based insulin delivery systems should have the capability to protect the encapsulated insulin from getting disrupted by harsh acidic and proteolytic enzymes (Hosseinasab et al. 2014).

6.3 Polymers Used in Oral Insulin Delivery

Over the past few decades, various polymers (biodegradable and nonbiodegradable) have been studied extensively by many researchers for carrying out oral insulin delivery (Delie and Blanco-Prieto 2005). Slow degradation of polymers gives rise to the sustained and controlled release of the loaded insulin. It has also been reported that these polymer molecules may cross the intestine wall in small quantities. The most common polymers used in oral insulin drug delivery are chitosan, dextran, alginate, cyclodextrin, poly(lactic-co-glycolic acid)(PLGA), etc. (see Fig. 6.2 for the structure of polymers and no. of papers on various polymers for oral insulin delivery as reported in google scholar in different years). Despite some promising research outcomes, a polymeric-based oral insulin delivery system has not been introduced in the market yet due to the inability of microcapsule to give the desired protection and subsequent insulin absorption. Besides, there is a lag between the intake of the capsule and the absorption of insulin. The promising result has been reported for the phase IIb trial of ORMD-0801 in patients with T2DM.

Chitosan (CS), a natural polysaccharide, is utilized in the maximum number of researches. Its biodegradability, antimicrobial activity, and biocompatibility have attracted researchers in the field of pharmaceuticals. It is a copolymer of β (1–4) linked glucosamine and N-acetyl glucosamine, as shown in Fig. 6.2a. The presence of many OH and amine groups, which are capable of the formation of intermolecular hydrogen bonding, helps it in the formation of gel with high viscosity. Besides, the chitosan polymer can be modified due to the presence of reactive functional groups. Physical properties of chitosan are controlled by the chemical modification of the primary hydroxyl and amine groups present on its backbone. Chitosan molecule conjugated with hydrophobic moiety results in forming amphiphile self-assembled nanoparticles, which can encapsulate drugs and deliver them to a desired target. Several hydrophobic derivatives of chitosan have been investigated, as given in Table 6.1. The entrapment of insulin is reported at around 50%. Chitosan enhances the intestinal absorption of insulin when it is structured in the form of nanoparticles. The orally administered insulin-loaded particles to diabetic Wistar rats resulted in a reduction in its body sugar level (BSL). Recently researchers have improved the entrapment efficiency of chitosan carriers up to 90% leading to effective insulin delivery without much loss (Urimi et al. 2019; Mumuni et al. 2020).

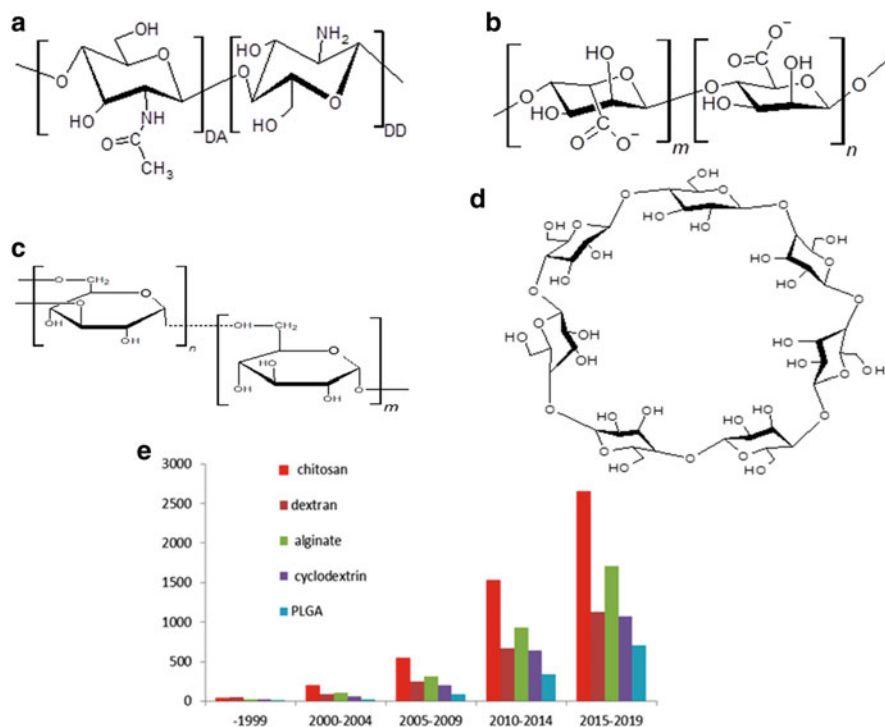


Fig. 6.2 Oral delivery of insulin using various polymers. Chemical structures of (a) chitosan, (b) alginate, (c) dextran, and (d) β -cyclodextrin, (e) no of papers on various polymers for oral insulin delivery as reported in google scholar in different years (Accessed on 13/03/2020)

Dextran, a natural water-soluble polysaccharide, is used as a polymeric carrier in novel drug delivery systems as it improves water solubility of less soluble drugs. It consists of linear 1, 6-linked glucopyranose units, with some degree of branching at 1,3 locations, as shown in Fig. 6.2b. Dextran conjugation is used as a blend with other polymers, which helps in designing new customized polymers with different structures, molecular weights, and shapes. The useful functional groups are required for coupling at the ideal positions in the chain.

The dextran is conjugated with insulin molecules. This system has been studied extensively due to its excellent pharmacokinetic and pharmacodynamic properties. The entrapment efficiency of the dextran composite (see Table 6.1) is reported to be about 60%, which is higher than that with chitosan. In vivo studies showed that there is a reduction in body glucose level in rabbit or rats after oral administration of the dextran-based insulin composite. The reported BSL decrease may widely vary depending on the formulation of the composite. The best results are reported for the nanoparticle surface conjugated with vitamin B12, a specific target legend. The entrapment efficiency is reported to be between 45 and 70%. The composite could protect 65–83% of insulin from getting degraded in the gastrointestinal tract. In vivo

Table 6.1 Various polymeric carriers used for oral insulin delivery formulation

Carrier	Method of synthesis	Components	Physical analysis	Entrapment efficiency	Animal model	In vivo observation	Dose	References
Chitosan	Ionic gelation	88.9% deacetylated chitosan + poloxamer188 + TPP	120 nm, 350 nm, 1000 nm	50.4–91.5%	Alloxan-induced male Wistar rats (220–280 g, 13.9–16.7 mmol/L glucose)	BSL remarkably decreased at 15 h (60%)	Oral: 10 IU/kg	Pan et al. (2002)
	Ionic gelation	85% deacetylated chitosan (MW: 280 kDa) + γ -PGA (60 kDa)	198.4 nm, 27.8 mV	55.1 \pm 3.3%	Streptozotocin-induced diabetic adult male Wistar rats	50% BSL reduction at 4 h maintained at the same level for at least 6 h	Oral: 30 IU/kg	Lin et al. (2007)
	Ionotropic gelation	85% deacetylated chitosan (MW: 270 kDa) + Lauryl succinyl chitosan + TPP	315 nm–1.09 μ m, negative zeta potential	48.1%	Streptozotocin-induced diabetic adult male Wistar rats	Sustained reduction in body sugar level for 6 h	Oral: 60 IU/kg	Rekha and Sharma (2009)
	Ionotropic gelation	75–85% deacetylated chitosan (MW: 50–190 kDa) + PSS (MW: ~70,000) + γ -PGA	210 \pm 2.8 nm, 55.1 \pm 3.3	85.9 \pm 0.28%	Streptozotocin-induced Sprague-Dawley male diabetic rats (250 \pm 30 g)	70% drop in BGL after 4 h and effect lasted for 24 h	Oral: 50 IU/kg	Urimi et al. (2019)
	Self-gelation	85% deacetylated chitosan (MW: 200–300 kDa) + Snail mucin	479.6 nm and 504.1 nm, 22.1–31.2 mV	88.6–92.5%	Alloxan-induced Wistar rats (125–2.11 g)	Slow reduction in BGL but effect sustained for 8 h	Oral: 501 U/kg	Mumuni et al. (2020)

Dextran	Emulsion	Dextran (MW: 10,000, 70,000 and 200,00) + vitamin B12	164–251 nm	45.37–71.19%	Streptozotocin-induced female Wistar rats (150–200 g)	70–75% decrease in BGL and reaching basal level in 8–10 h and this effect prolonged for 54 h	Oral: 20 IU/kg	Chalasan et al. (2007)
	Iontropic pregelation	Dextran sulfate (500 kDa) + 15% deacetylated LMW chitosan (50 kDa)	527 nm, irregular spherical, –20.6 mV	69.3%	Streptozotocin-induced male Wistar rats (200–250 g)	50 IU/kg: 22% decrease in BSL; 100 IU/kg: 60% BSL reduction; Effect continued after 24 h	Oral: 50 or 100 IU/kg	Sarmento et al. (2007a)
	Layer-by-layer assembly	Dextran sulfate (MW: 500 kDa) + 75–85% deacetylated chitosan (400 kDa)	3–12 μ m, irregularly shaped particles	65%	Chinchilla male rabbits (2.5–3.5 kg); Streptozotocin induced diabetic male Wistar rats	Rabbit: Blood sugar level reduced to 40% in 1 h Rats: 50% reduction, 10 h of hypoglycemic effect	Rabbit: Oral (4 IU/kg) Rats: Oral (25 IU/kg)	Pechenkin et al. (2011)
	Direct hydration method	Dextran (MW: 5 kDa) + PLGA (50/50) (MW 13 kDa)	100–200 nm	> 90%	Streptozotocin induced diabetic mice	BGL came to normal after 4 h and the effect sustained up to 12 h	Oral: 100 IU/kg	Alibolandi et al. (2016)

(continued)

Table 6.1 (continued)

Carrier	Method of synthesis	Components	Physical analysis	Entrapment efficiency	Animal model	In vivo observation	Dose	References
Alginate	Piezoelectric ejection process with ionotropic gelation	Alginate + Calcium chloride + WGA	1–20 μm	–	Streptozotocin-induced diabetic Sprague-Dawley rats	60% reduction in BSL in 4 h	Oral: 50 IU/kg	Kim et al. (2005)
	Emulsification/internal gelation	Sodium alginate + span 801 + calcium carbonate	2.67 nm–2.76 μm , spherical	80%	–	–	–	Reis et al. (2007)
	Ionotropic pregelation and polyelectrolyte complexation	Guluronic alginate + chitosan (50 kDa) + calcium chloride	748 nm, –5.6 mV	72.8%	Streptozotocin-induced male Wistar rats (250–300 g, 250 mg/dL glucose)	50 IU/kg: 59% reduction 100 IU/kg: 55% BSL reduction; Effect prolonged for 18 h	Oral: 50 and 100 IU/kg	Sarmento et al. (2007b)
	Coacervation, diffusion filling	Sodium alginate + mucin	260–680 μm , round, smooth	88%	Alloxan-induced diabetic rabbits (1.8–2.5 kg, 120 mg/dl)	Maximum BSL reduction in 5 h after oral administration	Oral: 50 IU/kg	Builders et al. (2008)
	Complex coacervation	Alginate + chitosan (50 kDa)	551 nm, +25.7 mV	52.48%	Streptozotocin-induced adult albino rats (150–250 g)	47% BSL reduction at 5 h, Prolonged hypoglycemic effect over 4 h	Oral: 10 IU/kg	Sahu (2013)
	Modified emulsification/internal gelation technique	Sodium alginate + dextran sulfate + poloxamer 188	48–293 nm, –53.4 to –60.4 mV	99.3 \pm 0.5%	Streptozotocin-induced male Wistar rats (250–300 g, 250 mg/dL glucose)	Rapid decrease in BSL reaching 20% of the initial value in 2 h	Oral: 50 IU/kg	Lopes et al. (2015)

β-cyclodextrin	Spray drying	β-cyclodextrin + hydroxypropyl methylcellulose acetate succinate + ethyl cellulose	0.8 μm, 3.57 mV, uniform surface morphology	94.9%	Streptozotocin-induced Sprague-Dawley male diabetic rats (100–150 g)	60% BSL reduction after 12 h	Oral: 4 IU/kg	D'Souza et al. (2014)
	Layer by layer technique	Cyclodextrin + PEGylated phospholipid + dextran sulfate	109 ± 9 nm, -25 ± 3 mV	71.4 ± 3.37%	Diabetic Male Wistar rats (294–353 g)	60% BSL reduction after 1 h and effect last for 6 h	Oral: 50 IU/kg	Presas et al. (2018)
	Ionic crosslinking	β-cyclodextrin (MW: 1.5 kDa) + 90–95% deacetylated chitosan (MW: 46 kDa)	144–297 nm,	57.0 ± 1.38%	Alloxan-induced diabetic mice	BGL sharply dropped to 29.33% of initial value within 1 h and this effect lasted only a short time	Oral: 50 IU/kg	Song et al. (2018)
PLGA	Emulsion solvent diffusion method	PLGA (50/50) (MW: 16.5 kDa) + Hp55 (Hypromellose phthalate, HPMCP-55) (MW 84000)	169 ± 16 nm	65.41 ± 2.3%	Streptozotocin-induced male Wistar rats (180–220 g)	60% reduction in BSL in 6 h	Oral: 20 IU/kg	Cui et al. (2007)
	Double emulsion solvent evaporation	PLGA (50/50) (MW: 10,000 and 50,000) + PVA (99% hydrolyzed) (MW: 73,500)	615 ± 50 nm	72.6%	Streptozotocin induced diabetic mice	60% decrease in body sugar level with effect lasting for 24 h	Oral: 20 IU/kg	Liu et al. (2007)

(continued)

Table 6.1 (continued)

Carrier	Method of synthesis	Components	Physical analysis	Entrapment efficiency	Animal model	In vivo observation	Dose	References
	w/o/w solvent evaporation	PLGA 50/50 (MW: 15,000) + 91.1% deacetylated chitosan (MW 250 kDa) + Pluronic 188	134.4 nm, +43.1 mV	52.76%	Alloxan-induced Sprague-Dawley male diabetic rats (190–210 g)	45.7% BSL reduction at 8 h	Oral: 15 IU/kg	Zhang et al. (2012)
	Double emulsion solvent evaporation	PLGA 50/50 (MW: 20 kDa) + 85% deacetylated N-Trimethyl chitosan + polyvinyl alcohol	247.6 ± 7.2 nm, 45.2 ± 4.6 mV	47 ± 2.9%	Streptozotocin-induced male Wistar rats (180–220 g)	70% drop in body sugar level with effect lasted for 12 h	Oral: 20 IU/kg	Sheng et al. (2015)

Reference: *BSL* Body sugar level; *MW* Molecular weight; *TPP* Triphosphosphate; γ -*PGA* Poly(γ -glutamic acid); *PSS* Poly(sodium 4-styrenesulfonate); *PVA* Polyvinyl alcohol; *WGA* Wheat germ agglutinin; *PLGA* Poly(lactic-co-glycolic) acid

studies showed that the plasma glucose level decreases significantly in the range 70–75% of basal levels in 8–10 h (Chalasanani et al. 2007).

Alginate, which is a high molecular weight hydrophilic polysaccharide, is widely used in biomedical applications owing to its mucoadhesive, biodegradable, low immunogenicity, and biocompatible nature. Alginate is composed of linear anionic block copolymers of α -L-guluronic acids (G) and β -D-mannuronic acid (M) residues, as depicted in Fig. 6.2c. These residues are spread as blocks of G and M or blocks of alternating G and M residues. Unlike chitosan, alginate is soluble in high pH and insoluble in lower pH conditions (Chaudhury and Das 2010). Another significant property of alginate gel is the occurrence of sol-gel transition without alteration of temperature. This sole-gel transition creates pores in the polymer whose dimensions depend on the nature, concentration, and conformation of the alginate. Due to this, it improves the rate of flow of excipients in drug delivery systems.

The alginate is blended with other polymers like chitosan and dextran sulfate to improve the drug encapsulation efficiency of alginates (Reis et al. 2007; Sonia and Sharma 2012). The entrapment of insulin is found to be as high as 88%, which is the maximum reported value in the presence of alginate-based materials. The method of preparation of nano-particles controls insulin entrapment efficiency. After five hours of oral administration, *in vivo* studies showed that microparticles could reduce the body glucose level very effectively.

Cyclodextrins (CDs) is a class of macrocyclic oligosaccharides that are linked by α -1,4 glycosidic bonds (shown in Fig. 6.2d). They have been studied extensively for engineering novel functional materials for various biomedical applications as it improves the solubility of hydrophobic drugs and the stabilization of drugs against dehydration, hydrolysis, oxidation, and photodecomposition. This property also inhibits the adsorption or absorption of drugs to container walls. The most common cyclodextrins are α , β , and γ , based on the number of glucose units in a truncated cone shape having a hydrophobic interior cavity, and a relatively hydrophilic external surface. The hydrophobic inner cavities interact with various hydrophobic guest molecules or their hydrophobic domains and form non-covalent inclusion complexes. These internal cavities are hydrophobic, which facilitates the inclusion of compounds ranging from small molecules, ions, and proteins. Due to their drug loading capacity, cyclodextrins and their derivatives have been explored extensively by the researchers for oral administration of various peptides and protein drugs.

Cyclodextrin (CD) complexation has a unique ability to improve insulin therapy. It stabilizes the insulin molecule against forming aggregation, thermal denaturation, and degradation. Insulin aggregation and denaturation activate by the presence of hydrophobic residues in the protein molecules, which result in a reduction of biological activity (Sluzky et al. 1991). It is reported that CD can form a complex with the hydrophobic cavities present in insulin molecules which stabilizes the structure of insulin molecules and further improves the absorption in GI (Irie 1999). D'Souza et al. have used a spray drying method to produce β -cyclodextrin microparticles, which improves the bioavailability of insulin (D'Souza et al. 2015).

β -Cyclodextrin microparticles could ensure a minimum amount of insulin release when it comes in contact with the simulated gastric fluid (D'Souza et al. 2014).

Poly-lactic-co-glycolic (PLGA) is FDA-approved biocompatible, biodegradable synthetic polymer, which has tunable mechanical properties. The hydrophobic interactions between insulin and PLGA molecules lead to entrapment of insulin in PLGA nanoparticles (Lassalle and Ferreira 2010). The mixture of insulin-loaded PLGA microparticles and polyvinyl alcohol (PVA) hydrogels has shown the entrapment efficiency of 72.6% (Liu et al. 2007). This nanoparticle-based insulin delivery can reduce the body sugar level of infected mice by 60%. Attempts have also been made to modify the negative charge on the surface of PLGA nanoparticles as it reduces oral bioavailability by limiting the insulin diffusion across the mucus layer. Chitosan polymer has been used for coating the PLGA nanoparticles. The positive charge of chitosan polymer reverses the effect of negative charge on PLGA and exhibits the strong bioadhesive potency with increased pharmacological availability (Zhang et al. 2012).

From the above discussion, it can be seen that various polymeric carriers have been developed for oral insulin delivery. Despite a few promising reports of oral insulin delivery systems, further study is required before clinical testing. They are not able to compete with SC insulin injection due to the low bioavailability of oral insulin. The main reasons behind low bioavailability are uneven size distribution, poor reproducibility, and degradability. The natural polymers are extracted from various sources which compromise the purity and physicochemical properties. Therefore, the well-defined study of polymer insulin behavior must be undertaken to make oral insulin delivery a reality in the market.

6.4 Transdermal Insulin Delivery

The problem of severe conditions faced by drugs during oral delivery and painful subcutaneous drug delivery can be eliminated through transdermal delivery. The skin has mainly three layers, namely, epidermis, dermis, and hypodermis, as shown in Fig. 6.3. The outermost layer of the skin, which is known as stratum corneum (SC), provides a significant barrier for any drug transdermal delivery. It becomes difficult for compounds, like drugs and vaccines, to cross the barrier and reach the systemic circulation in the therapeutically relevant amount. To improve drug delivery, various methods such as chemical or biochemical enhancers (Karande et al. 2004; He et al. 2009), iontophoresis (Djabri et al. 2012), electroporation (Zorec et al. 2013), sonophoresis (Mitrugotri et al. 1996), sonoporation (van Wamel et al. 2006), magnetophoresis (Murthy et al. 2010), microwave (Wong and Nor Khaizan 2012), thermal (Park et al. 2008) and laser (Chen et al. 2012) ablation, microscission (Herndon et al. 2004), the needleless jet injector (Engwerda et al. 2011), and microneedle (MN) (Davis et al. 2005) have been tested. Among all of them, microneedle-based delivery systems have gained widespread interest.

Microneedle array consists of micron-sized needles with a height varying from 100 to 2000 μm and a width of 10 to 50 μm , which could penetrate the upper layer of

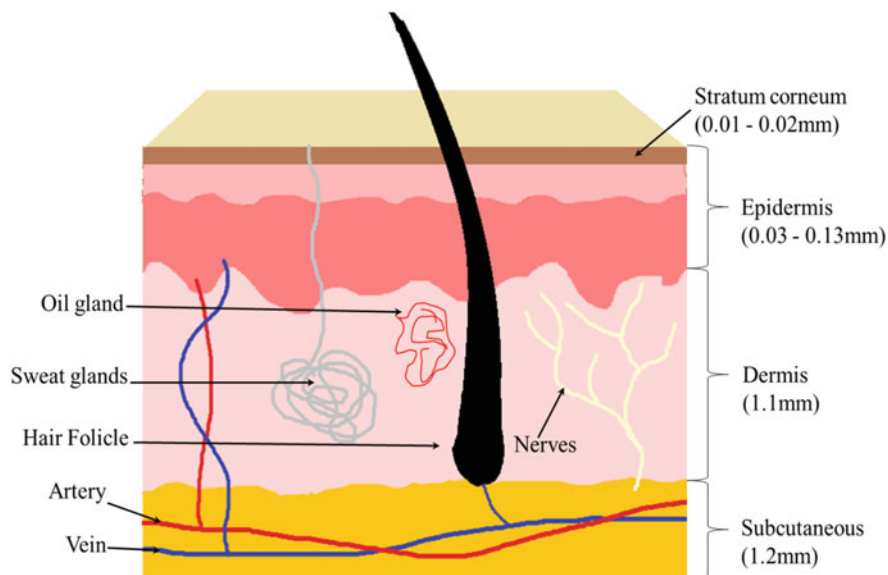


Fig. 6.3 Schematics of skin with a thickness of various layers

the skin without causing pain. It can create pores on the skin, which enable the drug to flow through the epidermis layer to the dermal tissues directly. Due to this, microneedles can deliver a right amount of drug with the relatively high delivery efficiency in comparison to other transdermal delivery methods.

6.5 Polymer Used in Transdermal Insulin Delivery

Microneedles (MNs) can be made from various materials, which are broadly divided into three types: metal materials, inorganic materials, and polymer materials. Metal and inorganic materials are not preferred as their transdermal drug delivery efficiency is influenced by the shape, size, and pore density of the microneedles. Additionally, the breakage of the microneedles inside the skin may lead to safety problems and may cause skin infection. Polymeric material-based microneedles are considered to be most promising for drug delivery. The nature of polymers is being modulated to prepare different varieties of microneedles like solid, coated, dissolving, hollow tip, and hollow microneedles. The polymer-based microneedles are single-use and can be used to load an acceptable amount of drug in the formulation. Many polymers have been used to fabricate microneedles for insulin delivery, which we will discuss in this section (see Table 6.2).

The most important property needed for microneedle is mechanical strength, geometry (e.g., shape tip radius, pitch, and base radius), and its composition. These are directly affected by the type of polymer used. Ideal polymeric microneedles possess the following characteristics:

Table 6.2 Properties of polymer used in polymeric microneedle-based insulin delivery system

Polymer	Components	Animal species	Observation	Dose	Ref.
PVA	PVA + CMC + Dextran	Bama pigs (10–12 kg)	Pigs receiving two patches (2 IU/kg) showed similar profile as injection pen, except the initial response delayed for about 20 min	1 IU/kg	Yang et al. (2015)
	PVA (MW = 6000), PVP (MW = 1000) + γ -PGA	Streptozotocin induced male Sprague Dawley (SD) rats (200 \pm 25 g)	90% drop in blood glucose level in 6 h	0.2 IU/kg	Chen et al. (2015)
	PVA + Silk fibroin	Female mice	60% decrease in BGL in 2 h	1 mg	Lau et al. (2017)
PMVE/MA	PVA (MW 2000, 1000 and 31,000)	Female Balb/c mice weighing 20 \pm 1 g	80% drop in blood glucose level, time varied with different polymer MW used	0.3 IU/kg	Chen et al. (2018)
	PMVE/MA + PEG	Streptozotocin induced male Sprague Dawley (SD) rats (240 \pm 10 g)	90% drop in blood glucose level	5 mg/cm ² of patch	Donnelly et al. (2012)
	Gelatin + (FITC-dextran) (MW 2000 kDa)	Streptozotocin induced diabetic male Sprague Dawley (SD) rat (200 \pm 25 g)	60% drop in BGL after 3 h	0.2 IU/kg	Ling and Chen (2013)
Gelatin	Gelatin (MW: 5.78 kDa + Calcium sulfate hemihydrate	Streptozotocin induced diabetic male Sprague Dawley (SD) rat (200 \pm 20 g)	60% drop in BGL in 1 h	20 IU	Yu et al. (2017a)
	Gelatin + CMC	Streptozotocin-induced diabetic mice	80% drop in BGL after 6 h	2 IU/kg	Chen et al. (2018a)
Hyaluronic acid (HA)	Hyaluronic acid	Streptozotocin-induced diabetic male Wistar rat, weighing (220–270 g)	43%–88% drop in plasma glucose level depending on the dose in 1 h	0.13–0.44 IU/kg	Liu et al. (2012)

HA (300 kDa)	Streptozotocin-induced diabetic mice (200 ± 20 g)	Blood glucose reduced to nearly 200 mg/dL within 30 min and maintained a normal glycemic state (<200 mg/dL) for up to 4 h	10 mg/kg	Yu et al. (2015)
Alginate + HA	Streptozotocin-induced diabetic mice (200 ± 20 g)	BGLs is reduced to 200 mg/dL from 500 mg/dL after 2 h treatment and effect continued for 12 h	10 IU/kg	Yu et al. (2017b)
HA + PEG	Streptozotocin-induced diabetic mice (200 ± 20 g)	Body glucose level rapidly reduced to 90 mg/dL within 1 h	10 mg/kg	Hu et al. (2017)
HA + PEG	Streptozotocin-induced diabetic mice	BGLs reduced to 200 mg/dL after 2 h	10 IU/kg	Yu et al. (2017d)

Reference: FITC Fluorescent isothiocyanate-dextran; HA Hyaluronic acid; PMVE/MA Poly(methyl vinyl ether-co-maleic acid); PEG Polyethylene glycol; PVP Polyvinylpyrrolidone; PGA Polyglycolide

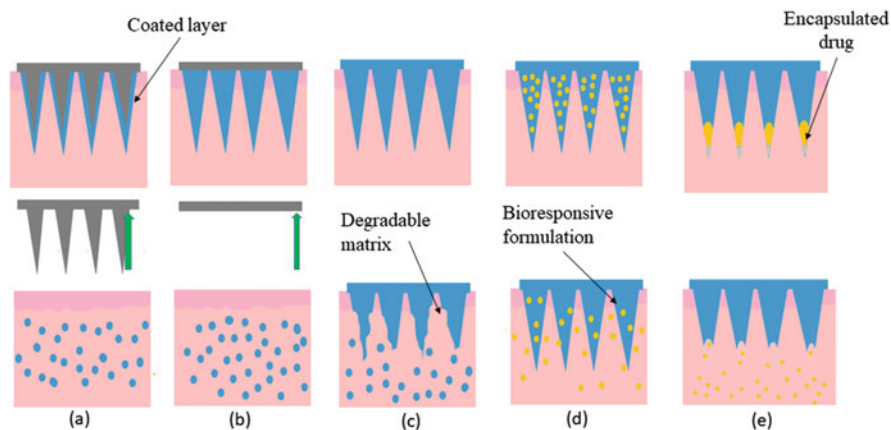


Fig. 6.4 Schematics of various polymeric microneedles: (a) coated MN (b) dissolvable MN (c) degradable MN, (d) bioresponsive MN, and (e) tip-hollow MN

- Biocompatibility with the skin
- Physical strength to penetrate through the SC
- The careful fabrication process for controlled delivery of drugs inside the skin

Each type of microneedle follows a different approach for delivering the drug through the skin, as illustrated in Fig. 6.4. The first one is a coated microneedle in which drug formulation is coated on the surface of the microneedle. The coated microneedle is inserted into the skin and left for the time till all the drug is released into the skin (Fig. 6.4a). Next is dissolvable microneedle, which is made of polymer loaded with the drug inside its matrix. These types of microneedles are inserted into the skin and drug moves inside the skin with the dissolution of the polymer matrix (Fig. 6.4b). The third one is degradable microneedles, which allows for the delivery of payloads by the degradation of the polymer matrix (Fig. 6.4c). They are different from dissolving microneedles in the way that degradable microneedles release the drug without getting dissolved in the skin. So, they can be removed from the skin once the drug delivery process is complete. The fourth approach shows bio-responsive microneedle, which involves tuning of drug release in a bioresponsive manner like change in pH or temperature (Fig. 6.4d). This is the most advanced technique of drug delivery as it offers opportunities for on-demand release of drugs in a controlled manner (Yu et al. 2015). Recently Ye et al. have come up with a new design of microneedle called “Tip hollow” microneedle in which drug is encapsulated at the tip of microneedle (Fig. 6.4e). It has good mechanical strength like solid microneedles and delivery is expected to be optimized using Tip-hollow MN (Ye et al. 2020).

The main polymers which have been used in the fabrication of polymeric microneedle are polyvinyl alcohol (PVA), gelatin, cysteine, poly(methyl vinyl ether-co-maleic acid) (PMVE/MA), hyaluronic acid (HA), carboxymethyl cellulose

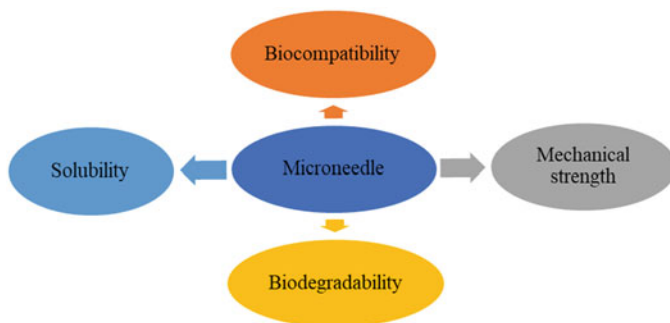


Fig. 6.5 Essential properties required in transdermal drug delivery through microneedles

(CMC), etc. To get the desired properties of an MN, a combination of polymers is used as a single polymer substance cannot fulfill all requirements. The most important properties required for microneedle based transdermal delivery is shown in Fig. 6.5. In this section, we will discuss in brief about these polymeric materials and their properties which make them suitable for using a transdermal insulin delivery system.

Polyvinyl alcohol (PVA) is a water-soluble, biodegradable polymer that makes it suitable for fabricating microneedles (Chang et al. 2000). Its chemical formula is $(C_2H_4O)_n$, where the value of n for commercially available materials varies from 500 and 5000. PVA is first heated to dissolve in water, followed by the freezing and thawing process. This leads to the formation of a highly elastic thermoreversible gel (Watase and Nishinari 1988). The material resulting from this treatment has excellent rubbery nature with high mechanical strength. PVA gel remains stable at room temperature and retains its original shape, but it has a tendency to swell in contact with water. Properties of the gel formed may depend on the degree of polymerization, the concentration of an aqueous solution, and the number of freezing-thawing cycles (Gao et al. 2009). PVA has also been used as a stabilizer in the fabrication of nanoparticles in oral insulin delivery systems (Czuba et al. 2018). The properties mentioned above make it compatible for use as a microneedle material for insulin delivery.

Yang et al. used polyvinyl alcohol for preparing a swellable microneedle for insulin delivery (Yang et al. 2015). A mixture of PVA, dextran, and carboxymethyl cellulose (CMC) in a solvent is used to fabricate the microneedle patch. As discussed in the oral delivery section, CMC increases the water absorption capacity and improves the drug release kinetics of the microneedle array patch. Compared to other hydrophilic microneedles (Lee et al. 2008), the PVA microneedles would not dissolve in the skin but swell. The swelling opens the diffusion channels for loaded insulin to release inside the skin (Yang et al. 2015). Microneedles generally have the problem of incomplete insertion into the skin due to skin viscoelasticity. Most of the drug does not come out from the needle due to incomplete insertion. To solve this problem, Chen et al. fabricated fully insertable insulin-loaded poly-glutamic acid microneedle with supporting structure made up of polyvinyl alcohol/poly-vinyl pyrrolidone (PVA/PVP). The supporting structure provided the mechanical strength

with complete microneedle insertion into the skin. The whole insulin is released into the skin in 4 min (Chen et al. 2015).

Lau et al. have fabricated microneedles by mixing polyvinyl alcohol with silk fibroin for creating a multilayered microneedle patch. A fast release of insulin (1.0 mg in 3 h) was achieved with an improved insulin dissolution rate (Lau et al. 2017). In another study, Chen et al. fabricated polymeric microneedle using a different molecular weight of polyvinyl alcohol for the delivery of insulin. The different drug release rate was observed in different molecular weight of polyvinyl alcohol-based microneedles leading to a different decrease in body sugar level. The results of *in vivo* drug release indicated that the absorption of insulin decreased with an increase in the molecular weight of PVA due to the formation of hydrogen bonding (Chen et al. 2018).

Gelatin is another naturally occurring polymer that has been tested in this application due to its properties like biocompatibility, biodegradability, and hydrophilicity (Santoro et al. 2014). It tends to absorb a large amount of water, which results in a very fast release profile (Lu 2004). Drug-release profiles are expected to depend on the molecular weight and degree of crosslinking (Young et al. 2005). New synthesis techniques for gelatin-natural as well as gelatin-synthetic polymer mixtures have been proposed to enable desired water uptake and swelling behavior (Foux and Zilberman 2015). Chen et al. have made a dissolving microneedle patch by using gelatin and sodium carboxymethyl cellulose (CMC). It showed an 80% drop in body glucose level (BGL) in 6 h in diabetic mice after giving a dose of 2 IU/kg (Chen et al. 2018a). This study verified the potential of using gelatin/CMC microneedle patch for insulin delivery which can be further used for delivering other poor permeable protein drugs. Ling et al. prepared a strong composite for dissolving insulin-loaded microneedle by blending starch and gelatin to improve its processability.

Starch is a naturally occurring low-cost, bio-degradable polysaccharide, used as an excipient for solid dosage formulations (Rodrigues and Emeje 2012, Zhang and Sun 2004). It is generally blended with other biomaterials like gelatin to improve its properties such as inflexible, brittleness, and poor film-forming capability to be used for the transdermal drug delivery system. In another study, Yu et al. prepared microneedle using calcium sulfate and gelatin with a high aspect ratio (6:1) for the delivery of insulin (Yu et al. 2017a). Donnelly et al. used poly(methyl vinyl ether-co-maleic acid) (PMVE/MA), commonly known with name Gantrez[®] AN-139 for preparing an insulin-loaded microneedle (Donnelly et al. 2012). Films made from aqueous blends of PMVE/MA are very brittle and are not a desired property. A suitable plasticizer like FDA-approved polyethylene glycol (PEG) is mixed to plasticize bioadhesive films.

6.5.1 Smart Insulin Microneedles Using Polymeric Microneedles

The polymer is engineered in developing smart insulin delivery patches, wherein the insulin is delivered only at the necessary condition. The rate of insulin administration

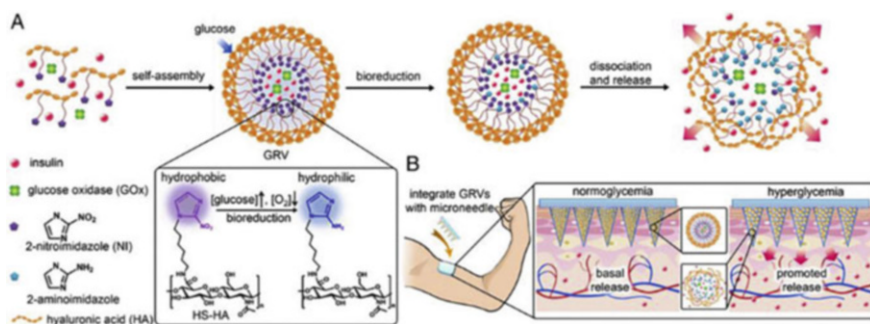


Fig. 6.6 Hypoxia-sensitive vesicle-loaded microneedle array patches. (a) GRVs were formed through the self-assembly of the amphipathic grafted HA, (b) Response-release mechanism of microneedles. Adapted with permission from Yu et al. (2015)

is controlled by incorporating bioresponsive material in the microneedle. Recently, the focus on bioresponsive insulin microneedles has increased due to their controlled and glucose-regulated delivery (Hu et al. 2017; Ma and Wu 2017; Chen et al. 2018b; Hovorka 2011; Mo et al. 2014; Wu et al. 2011; Yu et al. 2016, 2017c). The controlled insulin administration limits the potential for excessively low blood glucose levels, which may arise due to excessive insulin dosing (Veisoh et al. 2015).

Yu et al. have developed a “smart insulin patch” consisting of three components: insulin, the enzyme glucose oxidase (GO_x), and a polymer. This array patch releases insulin in response to a hyperglycemic state (a schematic is shown in Fig. 6.6). GO_x acts as a glucose sensor and the polymer acts as an actuator for insulin release. GO_x and insulin-loaded glucose-responsive vesicles (GRVs) are composed of hyaluronic acid conjugated 2-nitroimidazole (NI). Hyaluronic acid is hypoxia-sensitive and NI converts into hydrophilic 2-aminoimidazoles in hypoxic conditions. The GRVs would dissociate and release insulin. In vivo studies have shown that transcutaneous microneedles containing the GRVs have caused a quick decrease in body glucose level to around 200 mg/dL within thirty minutes of treatment. Recently, he has published another paper related to bioresponsive microneedles made up of diblock copolymers consisting of polyethylene glycol (PEG) and 2-nitroimidazole-modified polyserine. This system forms vesicles, which is hypoxia and H_2O_2 dual-sensitive (Yu et al. 2017d). Rapid consumption of oxygen and generation of H_2O_2 increase water solubility of such copolymers and dissociation of the vesicles. This leads to the release of insulin inside the skin. The in vivo studies show that the insulin patch can regulate the body glucose level in a diabetic mouse for 10 h.



In another microneedle-based study, GO_x and insulin-loaded vesicles, which are composed of polyethylene glycol (PEG) and phenylboronic ester (PBE) conjugated poly-serine (mPEG-b-P(Ser-PBE)) (Hu et al. 2017), are used. The pendant PBE in block copolymer not only has the ability of H_2O_2 -mediated degradation at

physiological conditions but also eliminates the excess H_2O_2 . This approach provides a basis for the clinical treatment of diabetes.

In addition to the delivery of insulin, Ye et al. have used the microneedle for glucose-responsive regulation of insulin secretion from exogenous pancreatic β -cells without implantation. The glucose-signal amplifiers were composed of GO_x , β -amylase, and glucoamylase. When the blood glucose levels elevated, the GO_x could accelerate material dissociate and release the enzymes, which could hydrolyze β -amylose and generate a local glucose-concentrated site. The “amplified” glucose effectively stimulated β -cell capsules and promoted the release of insulin into the blood vascular. This smart microneedle patch proved more important from a fundamental perspective for transporting insulin for diabetes therapy.

6.6 Nasal Insulin Delivery

Nasal administration of insulin offers an exciting alternative to the inconvenient parenteral route or oral administration. Insulin administered through nasal path protects it from enzymatic degradation and increase its dissolution rate. The columnar epithelium present in bronchi can act as a controlled release system. However, several factors remain a concern to deliver insulin: Mucociliary clearance, enzymatic degradation, and low bioavailability. To overcome these limitations, various nasal particulate systems have been developed using mucoadhesive polymers as carriers. These micro- and nano-sized particles effectively transfer insulin into the systemic circulation for the effective glycemic control. The polysaccharides such as are alginate, starch, and cellulose are used as mucoadhesive nasal drug delivery systems. In this section, we have listed various polymers used in the nasal delivery of insulin and their performance *in vivo*.

Morimoto et al. were the first one to study the effect of insulin in the aqueous gel of poly(acrylic acid) on a rat model (Morimoto et al. 1985). Subsequently, Agrawal et al. prepared a thermosensitive gel of chitosan and polyvinyl alcohol used in the nasal formulation of insulin. This formulation exhibited a prolonged hypoglycemic effect when administered *in vivo*. The reported (Agrawal et al. 2010) *in vivo* studies showed a 40% reduction in the BGL after 4 h of administration. Wu et al. also formulated a thermosensitive hydrogel of N-[(2-hydroxyl-3-trimethylammonium) propyl] chitosan chloride and β -glycerophosphate for nasal insulin delivery. There *in vivo* experiments showed a decrease in BGL by 40–50% for at least 4–5 h after administration (Wu et al. 2007). In another study, Chung et al. prepared a thermo-responsive gel of glutaraldehyde mediated crosslinked chitosan, poloxamer, and glycine. The gel is used in the formulation of nasal insulin. *In vivo* studies performed on diabetic mice showed prolonged hyperglycemic effect for three hours with pharmacological efficiency of 18% (Chung et al. 2010). Jain et al. have used starch nanoparticles as a mucoadhesive carrier in the formulation of nasal insulin. The nanoparticles formulation of insulin showed a rapid and sustained hypoglycemic action until 6 h (Jain et al. 2008). In addition to this, dextran microspheres have also been used to carry out nasal insulin delivery (Pereswetoff-Morath and Edman 1995).

Nasal insulin delivery is still not able to act as an alternative to subcutaneous insulin delivery due to low bioavailability and inability to provide prolonged glucose control. The concentration of insulin blood increases more rapidly and declines more quickly during nasal administration than the subcutaneous administration. There is also a possibility of physical loss of the dosage form into other parts of the respiratory tract like lungs. Further, the maximum loading of insulin is limited to about 150 μl (Liu et al. 2007). Intensive research and development are required for carrying out effective nasal insulin delivery.

6.7 Conclusions and Future Prospects

The management of blood glucose levels in patients suffering from diabetes has improved a lot since the introduction of insulin therapy. Several noninvasive methods of insulin delivery, e.g., oral, transdermal, and nasal, have been tested. These noninvasive methods may provide better control over blood glucose levels and offer lesser other complications like weight gain, peripheral hyperinsulinemia, hypoglycemic events, and late diabetic complications. Many clinical studies have been done and most of them have shown reasonably good clinical results. Further improvements are needed before these alternative routes for insulin delivery are utilized.

The main limitations in oral insulin delivery include the low intestinal permeability and enzymatic degradation, which results in lower insulin bioavailability. To overcome these complications, biopolymers of various characteristics are being investigated to encapsulate insulin. These polymers are derived from various sources. To preserve the insulin's stability, bioavailability, mucoadhesion, and controlled release using these polymers, a detailed study is required. Further research on the formulation front is required to optimize the nature of the polymer in terms of surface charge, particle size, the thickness of protective polymer coating, and the permeability of insulin. The physicochemical properties of insulin carrier will decide its oral absorption and therapeutic effect in diabetes treatment.

The other mode of insulin delivery is the transdermal route. It has also attracted the researchers due to the possibility of flexible dosing using a painless administration. Physicochemical properties of insulin play a significant role in its transport through the skin layer. The lower flux of insulin in the skin and its retention in the polymeric patch are the major hurdles for its application. A relationship between the loaded and the final release amounts of insulin is to be developed to guide the clinical application. The amount of drug that can be loaded in the polymeric microneedle is less. Detailed research is required to improve the drug loading. Besides, the development of a smart glucose-responsive microneedle is the future direction of research.

As discussed earlier, the nasal administration also has several limitations. The drug substances and their constituents added to the dosage forms can irreversibly damage the cilia on the nasal mucosa. Thus, it requires a lot of clinical investigations before it can be used by the patients. All the delivery systems discussed above have a profound capability to act as an alternative to subcutaneous insulin delivery. But

they lack in certain aspects which require further research before it can be used in clinical practice safely and effectively.

References

- Agrawal AK, Gupta PN, Khanna A et al (2010) Development and characterization of in situ gel system for nasal insulin delivery. *Die Pharm Int J Pharm Sci* 65:188–193
- Alberti KGMM, Zimmet PZ (1998) Definition, diagnosis and classification of diabetes mellitus and its complications. Part 1: Diagnosis and classification of diabetes mellitus. Provisional report of a WHO consultation. *Diabet Med* 15:539–553. [https://doi.org/10.1002/\(sici\)1096-9136\(199807\)15:7<539::aid-dia668>3.0.co;2-s](https://doi.org/10.1002/(sici)1096-9136(199807)15:7<539::aid-dia668>3.0.co;2-s)
- Alibolandi M, Alabdollah F, Sadeghi F, Mohammadi M, Abnous K, Ramezani M, Hadizadeh F (2016) Dextran-b-poly (lactide-co-glycolide) polymersome for oral delivery of insulin: In vitro and in vivo evaluation. *J Control Release* 227:58–70
- Brange J, Andersen L, Laursen ED et al (1997) Toward understanding insulin fibrillation. *J Pharm Sci* 86:517–525
- Brown L, Munoz C, Siemer L et al (1986) Controlled release of insulin from polymer matrices: Control of diabetes in rats. *Diabetes* 35:692–697
- Builders PF, Kunle OO, Okpaku LC et al (2008) Preparation and evaluation of mucinated sodium alginate microparticles for oral delivery of insulin. *Eur J Pharm Biopharm* 70:777–783. <https://doi.org/10.1016/j.ejpb.2008.06.021>
- Cefalu WT (2003) Concept, strategies, and feasibility of noninvasive insulin delivery. *Diabetes Care* 27:239–246. <https://doi.org/10.2337/diacare.27.1.239>
- Chalasanani KB, Russell-Jones GJ, Jain AK et al (2007) Effective oral delivery of insulin in animal models using vitamin B12-coated dextran nanoparticles. *J Control Release* 122:141–150. <https://doi.org/10.1016/j.jconrel.2007.05.019>
- Chang JY, Godovsky DY, Han MJ, et al (2000) Biopolymers· PVA hydrogels anionic polymerisation Nanocomposites. Springer Science & Business Media
- Chaturvedi K, Ganguly K, Nadagouda MN, Aminabhavi TM (2013) Polymeric hydrogels for oral insulin delivery. *J Control Release* 165:129–138. <https://doi.org/10.1016/j.jconrel.2012.11.005>
- Chaudhury A, Das S (2010) Recent advancement of chitosan-based nanoparticles for Oral controlled delivery of insulin and other therapeutic agents. *AAPS PharmSciTech* 12:10–20. <https://doi.org/10.1208/s12249-010-9561-2>
- Chen M-C, Sonaje K, Chen K-J, Sung H-W (2011) A review of the prospects for polymeric nanoparticle platforms in oral insulin delivery. *Biomaterials* 32:9826–9838. <https://doi.org/10.1016/j.biomaterials.2011.08.087>
- Chen X, Shah D, Kosiratna G et al (2012) Facilitation of transcutaneous drug delivery and vaccine immunization by a safe laser technology. *J Control Release* 159:43–51. <https://doi.org/10.1016/j.jconrel.2012.01.002>
- Chen M-C, Ling M-H, Kusuma SJ (2015) Poly- γ -glutamic acid microneedles with a supporting structure design as a potential tool for transdermal delivery of insulin. *Acta Biomater* 24:106–116. <https://doi.org/10.1016/j.actbio.2015.06.021>
- Chen BZ, Ashfaq M, Zhang XP, Zhang JN, Guo XD (2018) In vitro and in vivo assessment of polymer microneedles for controlled transdermal drug delivery. *J Drug Target* 26(8):720–729
- Chen C-H, Shyu V, Chen C-T (2018a) Dissolving microneedle patches for transdermal insulin delivery in diabetic mice: Potential for clinical applications. *Materials (Basel)* 11:1625. <https://doi.org/10.3390/ma11091625>
- Chen G, Yu J, Gu Z (2018b) Glucose-responsive microneedle patches for diabetes treatment. *J Diabetes Sci Technol* 13:41–48. <https://doi.org/10.1177/1932296818778607>

- Chung TW, Liu DZ, Yang JS (2010) Effects of interpenetration of thermo-sensitive gels by crosslinking of chitosan on nasal delivery of insulin: In vitro characterization and in vivo study. *Carbohydr Polym* 82(2):316–322
- Cui F, Tao A, Cun D et al (2007) Preparation of insulin loaded PLGA-Hp55 nanoparticles for oral delivery. *J Pharm Sci* 96:421–427. <https://doi.org/10.1002/jps.20750>
- Czuba E, Diop M, Mura C, Schaschkow A, Langlois A, Bietiger W et al (2018) Oral insulin delivery, the challenge to increase insulin bioavailability: Influence of surface charge in nanoparticle system. *Int J Pharm* 542(1–2):47–55
- D'Souza B, Bhowmik T, Uddin MN et al (2014) Development of β -cyclodextrin-based sustained release microparticles for oral insulin delivery. *Drug Dev Ind Pharm* 41:1288–1293. <https://doi.org/10.3109/03639045.2014.947507>
- D'Souza B, Bhowmik T, Uddin MN, Oettinger C, D'Souza M (2015) Development of β -cyclodextrin-based sustained release microparticles for oral insulin delivery. *Drug Dev Ind Pharm* 41(8):1288–1293
- Davis SP, Martanto W, Allen MG, Prausnitz MR (2005) Hollow metal microneedles for insulin delivery to diabetic rats. *IEEE Trans Biomed Eng* 52:909–915
- Delie F, Blanco-Prieto M (2005) Polymeric particulates to improve Oral bioavailability of peptide drugs. *Molecules* 10:65–80. <https://doi.org/10.3390/10010065>
- Djabri A, Guy RH, Delgado-Charro MB (2012) Transdermal iontophoresis of ranitidine: An opportunity in paediatric drug therapy. *Int J Pharm* 435:27–32. <https://doi.org/10.1016/j.ijpharm.2012.03.006>
- Donnelly RF, Singh TRR, Garland MJ et al (2012) Hydrogel-forming microneedle arrays for enhanced transdermal drug delivery. *Adv Funct Mater* 22:4879–4890. <https://doi.org/10.1002/adfm.201200864>
- Engwerda EEC, Abbink EJ, Tack CJ, de Galan BE (2011) Improved pharmacokinetic and Pharmacodynamic profile of rapid-acting insulin using needle-free jet injection technology. *Diabetes Care* 34:1804–1808. <https://doi.org/10.2337/dc11-0182>
- Foxx M, Zilberman M (2015) Drug delivery from gelatin-based systems. *Expert Opin Drug Deliv* 12:1547–1563. <https://doi.org/10.1517/17425247.2015.1037272>
- Gao H-W, Yang R-J, He J-Y, Yang L (2009) Rheological behaviors of PVA/H₂O solutions of high-polymer concentration. *J Appl Polym Sci NA-NA*. <https://doi.org/10.1002/app.31677>
- Goldberg M, Gomez-Orellana I (2003) Challenges for the oral delivery of macromolecules. *Nat Rev Drug Discov* 2:289–295. <https://doi.org/10.1038/nrd1067>
- He W, Guo X, Xiao L, Feng M (2009) Study on the mechanisms of chitosan and its derivatives used as transdermal penetration enhancers. *Int J Pharm* 382:234–243. <https://doi.org/10.1016/j.ijpharm.2009.07.038>
- Herndon TO, Gonzalez S, Gowrishankar TR et al (2004) Transdermal microconduits by microscission for drug delivery and sample acquisition. *BMC Med* 2. <https://doi.org/10.1186/1741-7015-2-12>
- Herrero EP, Alonso MJ, Csaba N (2012) Polymer-based oral peptide nanomedicines. *Ther Deliv* 3:657–668. <https://doi.org/10.4155/tde.12.40>
- Hosseinasab S, Pashaei-Asl R, Khandaghi AA et al (2014) Retracted: Synthesis, characterization, and in vitro studies of PLGA-PEG Nanoparticles for Oral insulin delivery. *Chem Biol Drug Des* 84:307–315. <https://doi.org/10.1111/cbdd.12318>
- Hovorka R (2011) Closed-loop insulin delivery: From bench to clinical practice. *Nat Rev Endocrinol* 7:385–395. <https://doi.org/10.1038/nrendo.2011.32>
- Hu X, Yu J, Qian C et al (2017) H₂O₂-responsive vesicles integrated with transcutaneous patches for glucose-mediated insulin delivery. *ACS Nano* 11:613–620. <https://doi.org/10.1021/acsnano.6b06892>
- Illum L (2002) Nasal drug delivery: New developments and strategies. *Drug Discov Today* 7:1184–1189
- Irie T (1999) Cyclodextrins in peptide and protein delivery. *Adv Drug Deliv Rev* 36:101–123. [https://doi.org/10.1016/s0169-409x\(98\)00057-x](https://doi.org/10.1016/s0169-409x(98)00057-x)

- Jain AK, Khar RK, Ahmed FJ, Diwan PV (2008) Effective insulin delivery using starch nanoparticles as a potential trans-nasal mucoadhesive carrier. *Eur J Pharm Biopharm* 69:426–435. <https://doi.org/10.1016/j.ejpb.2007.12.001>
- Karande P, Jain A, Mitragotri S (2004) Discovery of transdermal penetration enhancers by high-throughput screening. *Nat Biotechnol* 22:192–197. <https://doi.org/10.1038/nbt928>
- Kim B-Y, Jeong JH, Park K, Kim J-D (2005) Bioadhesive interaction and hypoglycemic effect of insulin-loaded lectin–microparticle conjugates in oral insulin delivery system. *J Control Release* 102:525–538. <https://doi.org/10.1016/j.jconrel.2004.10.032>
- Lassalle V, Ferreira ML (2010) PLGA based drug delivery systems (DDS) for the sustained release of insulin: Insight into the protein/polyester interactions and the insulin release behavior. *J Chem Technol Biotechnol* 85:1588–1596. <https://doi.org/10.1002/jctb.2470>
- Lau S, Fei J, Liu H et al (2017) Multilayered pyramidal dissolving microneedle patches with flexible pedestals for improving effective drug delivery. *J Control Release* 265:113–119
- Lee JW, Park J-H, Prausnitz MR (2008) Dissolving microneedles for transdermal drug delivery. *Biomaterials* 29:2113–2124. <https://doi.org/10.1016/j.biomaterials.2007.12.048>
- Lin Y-H, Chen C-T, Liang H-F et al (2007) Novel nanoparticles for oral insulin delivery via the paracellular pathway. *Nanotechnology* 18:105102. <https://doi.org/10.1088/0957-4484/18/10/105102>
- Ling M-H, Chen M-C (2013) Dissolving polymer microneedle patches for rapid and efficient transdermal delivery of insulin to diabetic rats. *Acta Biomater* 9:8952–8961. <https://doi.org/10.1016/j.actbio.2013.06.029>
- Liu J, Zhang SM, Chen PP, Cheng L, Zhou W, Tang WX et al (2007) Controlled release of insulin from PLGA nanoparticles embedded within PVA hydrogels. *J Mater Sci Mater Med* 18 (11):2205–2210
- Liu S, Jin M, Quan Y et al (2012) The development and characteristics of novel microneedle arrays fabricated from hyaluronic acid, and their application in the transdermal delivery of insulin. *J Control Release* 161:933–941. <https://doi.org/10.1016/j.jconrel.2012.05.030>
- Lopes MA, Abrahim-Vieira B, Oliveira C, Fonte P, Souza AM, Lira T, Seica R (2015) Probing insulin bioactivity in oral nanoparticles produced by ultrasonication-assisted emulsification/internal gelation. *Int J Nanomedicine* 10:5865
- Lu Z (2004) Paclitaxel-loaded gelatin nanoparticles for Intravesical bladder cancer therapy. *Clin Cancer Res* 10:7677–7684. <https://doi.org/10.1158/1078-0432.ccr-04-1443>
- Ma G, Wu C (2017) Microneedle, bio-microneedle and bio-inspired microneedle: A review. *J Control Release* 251:11–23. <https://doi.org/10.1016/j.jconrel.2017.02.011>
- Mitragotri S, Blankshtein D, Langer R (1996) No title. *Pharm Res* 13:411–420. <https://doi.org/10.1023/a:1016096626810>
- Mo R, Jiang T, Di J et al (2014) Emerging micro- and nanotechnology based synthetic approaches for insulin delivery. *Chem Soc Rev* 43:3595. <https://doi.org/10.1039/c3cs60436e>
- Morimoto K, Morisaka K, Kamada A (1985) Enhancement of nasal absorption of insulin and calcitonin using polyacrylic acid gel. *J Pharm Pharmacol* 37:134–136. <https://doi.org/10.1111/j.2042-7158.1985.tb05024.x>
- Mumuni MA, Kenechukwu FC, Ofokansi KC, Attama AA, Díaz DD (2020) Insulin-loaded mucoadhesive nanoparticles based on mucin-chitosan complexes for oral delivery and diabetes treatment. *Carbohydr Polym* 229:115506
- Murthy SN, Sammeta SM, Bowers C (2010) Magnetophoresis for enhancing transdermal drug delivery: Mechanistic studies and patch design. *J Control Release* 148:197–203. <https://doi.org/10.1016/j.jconrel.2010.08.015>
- Nilsson MR (2016) Insulin amyloid at injection sites of patients with diabetes. *Amyloid* 23:139–147
- Owens DR (2002) New horizons – alternative routes for insulin therapy. *Nat Rev Drug Discov* 1:529–540. <https://doi.org/10.1038/nrd836>
- Pan Y, Zheng J-M, Zhao H-Y et al (2002) Relationship between drug effects and particle size of insulin-loaded bioadhesive microspheres. *Acta Pharmacol Sin* 23:1051–1056

- Park J-H, Lee J-W, Kim Y-C, Prausnitz MR (2008) The effect of heat on skin permeability. *Int J Pharm* 359:94–103. <https://doi.org/10.1016/j.ijpharm.2008.03.032>
- Pechenkin MA, Balabushevich NG, Zorov IN (2011) Design in vitro and in vivo characterization of chitosan-dextran sulfate microparticles for Oral delivery of insulin. *J Bioequiv Availab* 03. <https://doi.org/10.4172/jbb.1000094>
- Pereswetoff-Morath L, Edman P (1995) Dextran microspheres as a potential nasal drug delivery system for insulin – in vitro and in vivo properties. *Int J Pharm* 124:37–44. [https://doi.org/10.1016/0378-5173\(95\)00070-y](https://doi.org/10.1016/0378-5173(95)00070-y)
- Plapied L, Duhem N, des Rieux A, Pr eat V (2011) Fate of polymeric nanocarriers for oral drug delivery. *Curr Opin Colloid Interface Sci* 16:228–237. <https://doi.org/10.1016/j.cocis.2010.12.005>
- Presas E, McCartney F, Sultan E, Hunger C, Nellen S, Alvarez CV, O'Driscoll CM (2018) Physicochemical, pharmacokinetic and pharmacodynamic analyses of amphiphilic cyclodextrin-based nanoparticles designed to enhance intestinal delivery of insulin. *J Control Release* 286:402–414
- Pridgen EM, Alexis F, Farokhzad OC (2014) Polymeric nanoparticle Technologies for Oral Drug Delivery. *Clin Gastroenterol Hepatol* 12:1605–1610. <https://doi.org/10.1016/j.cgh.2014.06.018>
- Ramkissoon-Ganorkar C, Liu F, Baudy s M, Kim SW (1999) Modulating insulin-release profile from pH/thermosensitive polymeric beads through polymer molecular weight. *J Control Release* 59:287–298
- Reis CP, Ribeiro AJ, Hounɡ S et al (2007) Nanoparticulate delivery system for insulin: Design, characterization and in vitro/in vivo bioactivity. *Eur J Pharm Sci* 30:392–397. <https://doi.org/10.1016/j.ejps.2006.12.007>
- Rekha MR, Sharma CP (2009) Synthesis and evaluation of lauryl succinyl chitosan particles towards oral insulin delivery and absorption. *J Control Release* 135:144–151. <https://doi.org/10.1016/j.jconrel.2009.01.011>
- Rodrigues A, Emeje M (2012) Recent applications of starch derivatives in nanodrug delivery. *Carbohydr Polym* 87:987–994. <https://doi.org/10.1016/j.carbpol.2011.09.044>
- Sahu SK (2013) Development and evaluation of insulin incorporated nanoparticles for oral administration. *ISRN Nanotechnol*:2013
- Santoro M, Tataro AM, Mikos AG (2014) Gelatin carriers for drug and cell delivery in tissue engineering. *J Control Release* 190:210–218. <https://doi.org/10.1016/j.jconrel.2014.04.014>
- Sarmento B, Ribeiro A, Veiga F et al (2007a) Alginate/chitosan nanoparticles are effective for Oral insulin delivery. *Pharm Res* 24:2198–2206. <https://doi.org/10.1007/s11095-007-9367-4>
- Sarmento B, Ribeiro AJ, Veiga F et al (2007b) Insulin-loaded nanoparticles are prepared by alginate Iontropic pre-gelation followed by chitosan polyelectrolyte Complexation. *J Nanosci Nanotechnol* 7:2833–2841. <https://doi.org/10.1166/jnn.2007.609>
- Sheng J, Han L, Qin J, Ru G, Li R, Wu L, Wang J (2015) N-trimethyl chitosan chloride-coated PLGA nanoparticles overcoming multiple barriers to oral insulin absorption. *ACS Appl Mater Interfaces* 7(28):15430–15441
- Shikama Y, Kitazawa J, Yagihashi N et al (2010) Localized amyloidosis at the site of repeated insulin injection in a diabetic patient. *Intern Med* 49:397–401
- Sluzky V, Tamada JA, Klibanov AM, Langer R (1991) Kinetics of insulin aggregation in aqueous solutions upon agitation in the presence of hydrophobic surfaces. *Proc Natl Acad Sci* 88:9377–9381. <https://doi.org/10.1073/pnas.88.21.9377>
- Song M, Wang H, Chen K, Zhang S, Yu L, Elshazly EH, Gong R (2018) Oral insulin delivery by carboxymethyl-β-cyclodextrin-grafted chitosan nanoparticles for improving diabetic treatment. *Artifi Cells Nanomed Biotechnol* 46(sup3):S774–S782
- Sonia TA, Sharma CP (2012) An overview of natural polymers for oral insulin delivery. *Drug Discov Today* 17:784–792. <https://doi.org/10.1016/j.drudis.2012.03.019>
- Swift B, Hawkins PN, Richards C, Gregory R (2002) Examination of insulin injection sites: An unexpected finding of localized amyloidosis. *Diabet Med* 19:881–882

- Urmi D, Agrawal AK, Kushwah V, Jain S (2019) Polyglutamic acid functionalization of chitosan nanoparticles enhances the therapeutic efficacy of insulin following oral administration. *AAPS PharmSciTech* 20(3):131
- van Wamel A, Kooiman K, Harteveld M et al (2006) Vibrating microbubbles poking individual cells: Drug transfer into cells via sonoporation. *J Control Release* 112:149–155. <https://doi.org/10.1016/j.jconrel.2006.02.007>
- Veisheh O, Tang BC, Whitehead KA, Anderson DG, Langer R (2015) Managing diabetes with nanomedicine: Challenges and opportunities. *Nat Rev Drug Discov* 14(1):45–57
- Watase M, Nishinari K (1988) No title. *Die Makromol Chemie* 189:871–880. <https://doi.org/10.1002/macp.1988.021890419>
- Wong TW, Nor Khaizan A (2012) Physicochemical modulation of skin barrier by microwave for transdermal drug delivery. *Pharm Res* 30:90–103. <https://doi.org/10.1007/s11095-012-0852-z>
- Wu J, Wei W, Wang L-Y et al (2007) A thermosensitive hydrogel based on quaternized chitosan and poly(ethylene glycol) for nasal drug delivery system. *Biomaterials* 28:2220–2232. <https://doi.org/10.1016/j.biomaterials.2006.12.024>
- Wu Q, Wang L, Yu H et al (2011) Organization of Glucose-Responsive Systems and Their Properties. *Chem Rev* 111:7855–7875. <https://doi.org/10.1021/cr200027j>
- Yang S, Wu F, Liu J et al (2015) Phase-transition microneedle patches for efficient and accurate transdermal delivery of insulin. *Adv Funct Mater* 25:4633–4641. <https://doi.org/10.1002/adfm.201500554>
- Ye R, Yang J, Li Y, Zheng Y, Yang J, Li Y, Jiang L (2020) Fabrication of tip-hollow and tip-dissolvable microneedle arrays for transdermal drug delivery. *ACS Biomater Sci Eng* 6(4):2487–2494
- Young S, Wong M, Tabata Y, Mikos AG (2005) Gelatin as a delivery vehicle for the controlled release of bioactive molecules. *J Control Release* 109:256–274. <https://doi.org/10.1016/j.jconrel.2005.09.023>
- Yu J, Zhang Y, Ye Y et al (2015) Microneedle-array patches loaded with hypoxia-sensitive vesicles provide fast glucose-responsive insulin delivery. *Proc Natl Acad Sci* 112:8260–8265. <https://doi.org/10.1073/pnas.1505405112>
- Yu J, Zhang Y, Bomba H, Gu Z (2016) Stimuli-responsive delivery of therapeutics for diabetes treatment. *Bioeng Transl Med* 1:323–337. <https://doi.org/10.1002/btm2.10036>
- Yu W, Jiang G, Liu D, Li L, Chen H, Liu Y et al (2017a) Fabrication of biodegradable composite microneedles based on calcium sulfate and gelatin for transdermal delivery of insulin. *Mater Sci Eng C* 71:725–734
- Yu W, Jiang G, Zhang Y, Liu D, Xu B, Zhou J (2017b) Polymer microneedles fabricated from alginate and hyaluronate for transdermal delivery of insulin. *Mater Sci Eng C* 80:187–196
- Yu J, Zhang Y, Kahkoska AR, Gu Z (2017c) Bioresponsive transcutaneous patches. *Curr Opin Biotechnol* 48:28–32. <https://doi.org/10.1016/j.copbio.2017.03.001>
- Yu J, Qian C, Zhang Y, Cui Z, Zhu Y, Shen Q et al (2017d) Hypoxia and H₂O₂ dual-sensitive vesicles for enhanced glucose-responsive insulin delivery. *Nano Lett* 17(2):733–739
- Yumlu S, Barany R, Eriksson M, Röcken C (2009) Localized insulin-derived amyloidosis in patients with diabetes mellitus: A case report. *Hum Pathol* 40:1655–1660
- Zhang J-F, Sun X (2004) Mechanical properties of poly(lactic acid)/starch composites Compatibilized by maleic anhydride. *Biomacromolecules* 5:1446–1451. <https://doi.org/10.1021/bm0400022>
- Zhang X, Sun M, Zheng A et al (2012) Preparation and characterization of insulin-loaded bioadhesive PLGA nanoparticles for oral administration. *Eur J Pharm Sci* 45:632–638. <https://doi.org/10.1016/j.ejps.2012.01.002>
- Zorec B, Becker S, Reberšek M et al (2013) Skin electroporation for transdermal drug delivery: The influence of the order of different square wave electric pulses. *Int J Pharm* 457:214–223. <https://doi.org/10.1016/j.ijpharm.2013.09.020>



Organization of Bio-Molecules in Bulk and Over the Nano-Substrate: Perspective to the Molecular Dynamics Simulations

7

Sunil Kumar and Trilochan Mishra

Abstract

The properties of bio-molecules are explicitly influenced by their organization in bulk and vicinity of substrate. Organization of bio-molecules can be of various kinds such as folded, unfolded, helix, swollen, globule, and so forth. These organizations of bio-molecule also depend on the local surrounding environmental conditions like temperature, solvency, adsorption, and encapsulation. Variation in environmental conditions helps to manipulate and control the organizations for the desired applications. Adsorption and encapsulation of bio-molecule over substrate have many applications in the area of drug delivery, design and development of bio-sensors, advance bio-separation process, etc. Molecular dynamics simulation is a very powerful tool to investigate the molecular structures, synthesis process and optimum properties, etc. A large number of efficient force field parameters and molecular dynamics simulators are available for large-scale simulation.

Keywords

Bio-molecule · Adsorption · Desorption · Graphene · SWCNT · Molybdenum disulfide · Molecular dynamics simulation

7.1 Introduction

The application of molecular dynamics simulations in the medical science and technology has expanded significantly in the recent years (Perricone et al. 2018; Marco et al. 2016; Hospital et al. 2015). It is widely used for the study of various

S. Kumar (✉) · T. Mishra
CSIR-National Metallurgical Laboratory, Jamshedpur, India
e-mail: sunil@nmlindia.org

properties of bio-molecules in the bulk and the vicinity of nano-substrate at a broad range of temperature and pressure. It is usually known that the combination of various bio-molecules and nano-substrate can be used to develop new drugs and its delivery systems. Significant enhancement in the simulation speed, accurateness, and accessibility has increased the demand of molecular dynamics simulations to predict the properties prior to real experiments. Molecular dynamics simulation methodology works on the Newton's equation of motions (Rapaport 2004; Allen and Tildesley 2017). It has three processing steps such as preprocessing, molecular dynamics simulator, and postprocessing as shown in the schematic in Fig. 7.1. Preprocessing step consists of information for the atomic structure of bio-molecules based on the quantum chemistry and physics (known as force-field parameters).

To define the atomic or molecular structure of the bio-molecules, various kinds of force fields parameters required to implement the inter- and intra-atomic interaction between the atoms. A large number of force-fields parameters and their models for the bio-molecules and nano-substrate have been developed recently such as Assisted Model Building with Energy Refinement (AMBER) (Case et al. 2005, 2006), CHARMM (Chemistry at HARvard Macromolecular Mechanics) (Brooks et al. 1983), GRONingen MOlecular Simulation (GROMOS) (Scott et al. 1999), reactive force field (ReaxFF) (Van Duin et al. 2001; Chenoweth et al. 2008; Senftle et al. 2016), Adaptive Intermolecular Reactive Empirical Bond Order (AIREBO) (O'Connor et al. 2015), and DREIDING force field (Mayo et al. 1990). These force fields are extremely accurate and based on the quantum chemistry and physics along with the experimental data and observations. Molecular dynamics simulator consists of simulation algorithm and it works according to input parameters from preprocessing steps. Fast, flexible, and accurate molecular dynamics simulators such as GRONingen MACHine for Chemical Simulations (GROMACS) (Van Der et al. 2005; Berendsen et al. 1995; Lindahl et al. 2001), Nanoscale Molecular Dynamics (NAMD) (Nelson et al. 1996; Phillips et al. 2005), Large-scale Atomic/Molecular Massively Parallel Simulator (LAMMPS) (Plimpton 1995), and DL-POLY (Smith et al. 2006) have been developed for realistic simulation of bio-molecules and nano-substrate. Postprocessing step consists of analysis of output simulation trajectory data for the visualization and characterization of final properties of simulated system. Simulation trajectories can be characterized by using open source software tools like Visual Molecular dynamics simulation (VMD) (Humphrey et al. 1996) and Open Visualization tool (OVITO) (Stukowski 2009) etc.

Nano-substrates (like carbon nanotubes, graphene, graphyne, nano-pillared graphite, silica, hybrid surfaces, etc.) and other 2D materials with the bio-molecules are extensively employed for the design of drug delivery systems, bio-sensors and other bio-medical devices (Georgakilas et al. 2016; Bitounis et al. 2013; Holzinger et al. 2017; Li et al. 2017; Yang et al. 2010; Mena et al. 2015). Nano-substrate facilitates unique organization of bio-molecules and enhances desirable properties for the abovementioned applications. Furthermore, the development of switchable surfaces, i.e., adsorption and desorption of bio-molecule which are responsive to a particular environmental conditions like hydrophobic/hydrophilic,

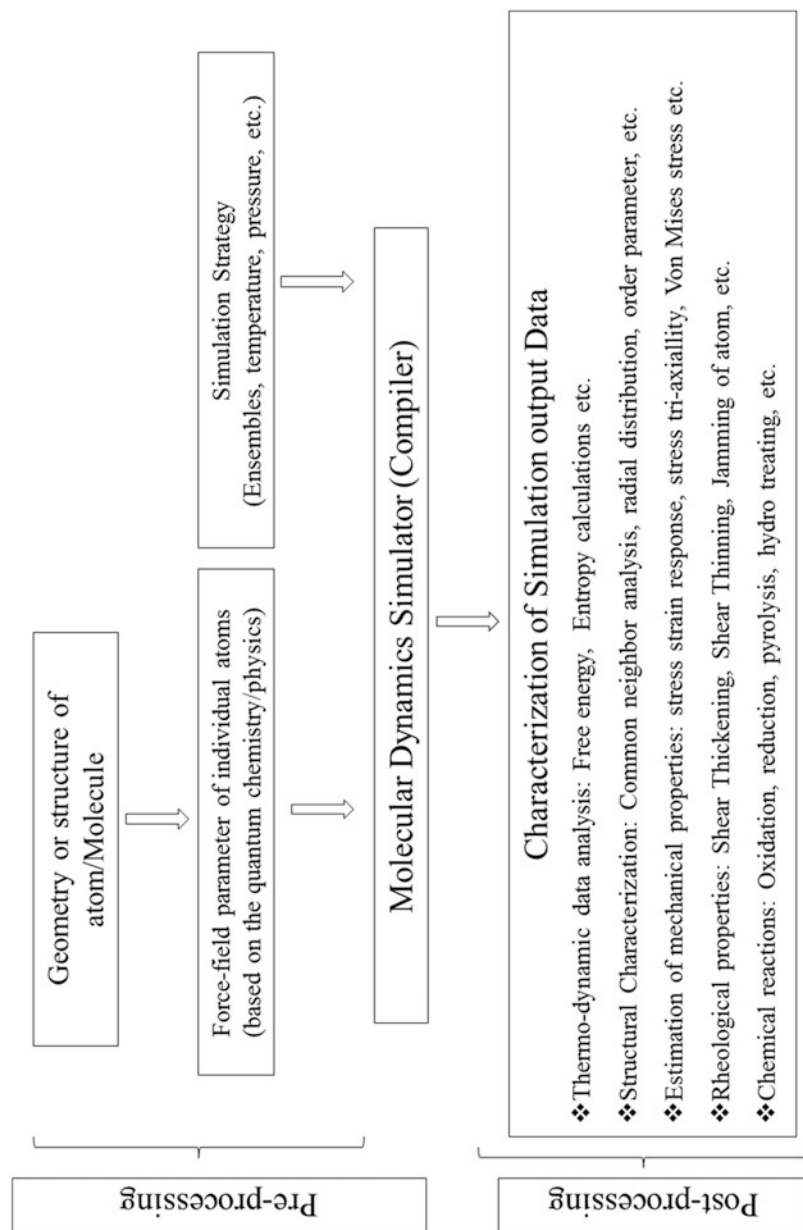


Fig. 7.1 Schematic of the molecular dynamics simulations methodology consist of pre- and postprocessing steps

depicts new and innovative process for bio-molecule operation. The mechanism of the adsorption and desorption of bio-molecules over the substrate is uniquely influenced by their chemical and physical characteristics along with the architecture (Vilhena et al. 2016; Gu et al. 2015; Zuo et al. 2011; Raffaini and Ganazzoli 2013; Moradi et al. 2016; Anselme and Bigerelle 2011; Viela et al. 2016; Kristensen et al. 2013; Pandey et al. 2013; Hasan et al. 2018a; Pandey and Pattanayek 2011, 2013; Hasan et al. 2018b). Explicitly, it is well known that the inert substrate can be functionalized, which facilitates or activates the desired characteristic of substrate. However, surface architecture imparts massive effect over the pattern or nature of adsorption and desorption behavior of bio-molecules.

7.2 Organization of Bio-Molecules in Bulk

Evolution of various organizations of bio-molecules manipulate many laboratory and industrial processes, such as drug delivery (Shi et al. 2004; Liu et al. 2007, 2008), bio-sensors (Wang et al. 2004; Besteman et al. 2003; Allen et al. 2007; Balavoine et al. 1999), material for medical implants (Calvert 1997; Park et al. 2017; Saito et al. 2009; He et al. 2013; Díez-Pascual and Díez-Vicente 2015), and bio-separation process (Nguyen et al. 2014; Chen et al. 2010, 2016; Shanmuganathan et al. 2019; Hasan et al. 2017). Organizations of bio-molecules are greatly influenced by the solvency conditions, inter-atomic interactions, and temperature. Bio-molecules, i.e., proteins and DNA, consist of complex atomic structures and multiple type of atoms and bonding pattern which are too difficult to design and carry out molecular dynamics simulations using ordinary computing resources. Therefore, simplistic models like united atom model (Tieleman et al. 2006; Paul et al. 1995) and coarse grain model (Shelley et al. 2001; Knotts et al. 2007; Lopez et al. 2002) have been developed for the simulation of polymer, protein, DNA/RNA, and other bio-molecules. These models consist of a group of atoms considered as a single bead, by freezing the quantum and atomic properties. United atom model has been extensively used to investigate the organization and mechanical properties of the chain-like molecules. Kavassalis and Sundararajan (1993, Sundararajan and Kavassalis 1997) demonstrated an explicit folding mechanism as globular to a folded crystalline structure of chain-like molecule during cooling process in implicit solvency conditions using united atom molecular dynamics simulations. Muthukumar (1986) has revealed that the long chain-like molecules first formed local crystalline regions as “baby nuclei,” which then gradually aggregates and forms a folded crystal. Kumar and Pattanayek (2018) have investigated the organization of long polymer chain with a wide range of persistent length in implicit solvent during cooling from 800 K to 300 K using united atom molecular dynamics simulations. They have observed four distinct organizations depending on the persistent length. These are the spherical globules, elongated globule, and cigar- and toroid-like organization in the bulk as shown in Fig. 7.2. The polymer chain of lower persistent length shows the spherical globules. In case of moderate persistent length, polymer chain segments make lamellar organization. The

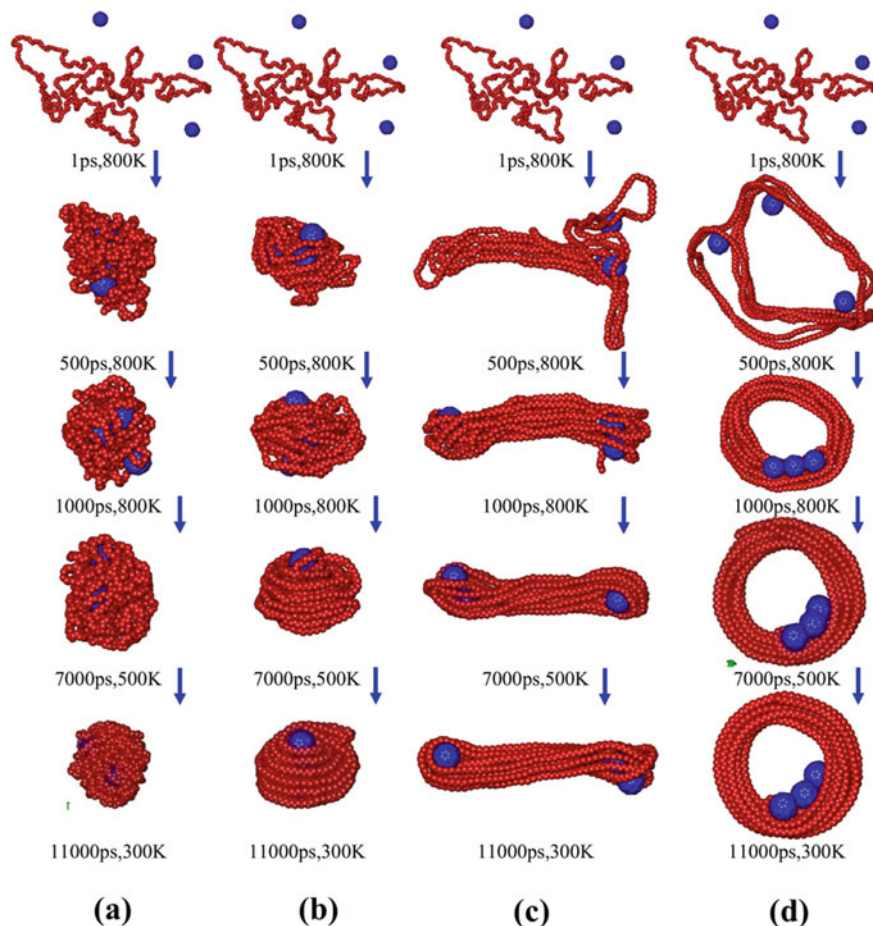


Fig. 7.2 The evolution of various folding and organization of polymer molecule (united atom model) as the simulation time increases during cooling from 800 K to 300 K: (a) $k_{\phi} = 0.02$, (b) $k_{\phi} = 0.2$, (c) $k_{\phi} = 0.5$, and (d) $k_{\phi} = 2$ eV. Adapted and reprinted from Kumar and Pattanayek (2018) with permission from Elsevier, Copyright (2018)

evolution of long cigar-like structure formed directly from lamellar aggregation of chain segments during the simulation. In case of high persistent length polymer chain segments make a circular-like organization, which looks like a toroid.

To demonstrate the organization of protein in explicit solvent, it is required to characterize all possible states as native, transition, intermediate, and denatured along with the mechanism of conversion. These characterizations are complicated using the only experimental technique due to the dynamic, heterogeneous, and transient nature of nonnative states of protein. Therefore, molecular dynamics simulation has been used to characterize the folding/unfolding proteins in various environments. The first few molecular dynamics simulation studies of the protein

folding based on the folding pathway and intermediate states (Daggett and Levitt 1992; Mark and van Gunsteren 1992). From these studies, it can be concluded that the transitional states and other related physical properties predicted by simulations are exactly the same as observed from the experiments. In the intermediates conformations, proteins are extended swollen state compared to the native state with hydrophobic core as predicted by molecular dynamics simulations.

The investigation of various properties of DNA and RNA is carried out explicitly to understand the genetic information at various levels of the cell. To understand the functional mechanism of DNA and RNA molecules, it is requisite to carry out molecular dynamics simulations at the atomistic level. The static and dynamic properties of DNA and RNA organizations are essential for their biochemical functions during the process transcription, replication, and translation. The organization of DNA/RNA in various solutions are generally flexible compared to the other bio-molecules like globular proteins. Therefore many experimental X-ray crystal structures of DNA/RNA have been explored. However molecular dynamics (MD) simulation is frequently employed for effective investigations of various organizations in DNA/RNA in the implicit/explicit solvent. Various inter- and intra-atomic interactions like nonbonded, bonded, and hydrogen bonding play fundamental roles to depict various unique organizations of DNA/RNA in bulk. The unique conformation of double-stranded DNA is stabilized by the condensation of the counter-ions due to nonbonded electrostatic and van der Waals interactions.

7.3 Adsorption Over Planner Substrate

Planner substrate like carbon allotropes (Geim 2009; Geim and Novoselov 2010; Kurapati et al. 2016), molybdenum di-sulfide (Venkata et al. 2016), black/red phosphorous (Tao et al. 2017), stannene (Dong et al. 2018), and so forth depicts huge applications in the area of bio-medical science and technology as shown in Fig. 7.3. Carbon allotrope mainly consists of carbon atom with hybridization states: sp^3 , sp^2 , and sp . The sp^2 hybridized carbon atom mostly formed in planner structure of graphene networks. Carbon triple bonds formed by sp -hybridized atoms construct graphdiyne 2D material.

Graphene has sp^2 -hybridized carbon atoms packed into a honeycomb lattice of a two-dimensional (2-D) sheet. Single-layer graphene depicts many exclusive properties, such as highly transparent to visible light, exceptional mechanical strength, extreme thermal stability, and large surface area. Due to these exceptional properties, graphene has attracted much attention of the bio-medical scientist and can be used as a filler or support for the bio-molecules to form nano-composites. The bio-molecules-graphene nano-composites depict surprising properties because not only individual properties, but they also demonstrate indication of further advantageous properties.

In particular, graphene-bio-molecules composites can be prepared by anchoring various types of bio-molecule to the graphene substrate through both in situ (e.g., growing bio-molecules on the graphene substrate) and ex situ (e.g., attaching

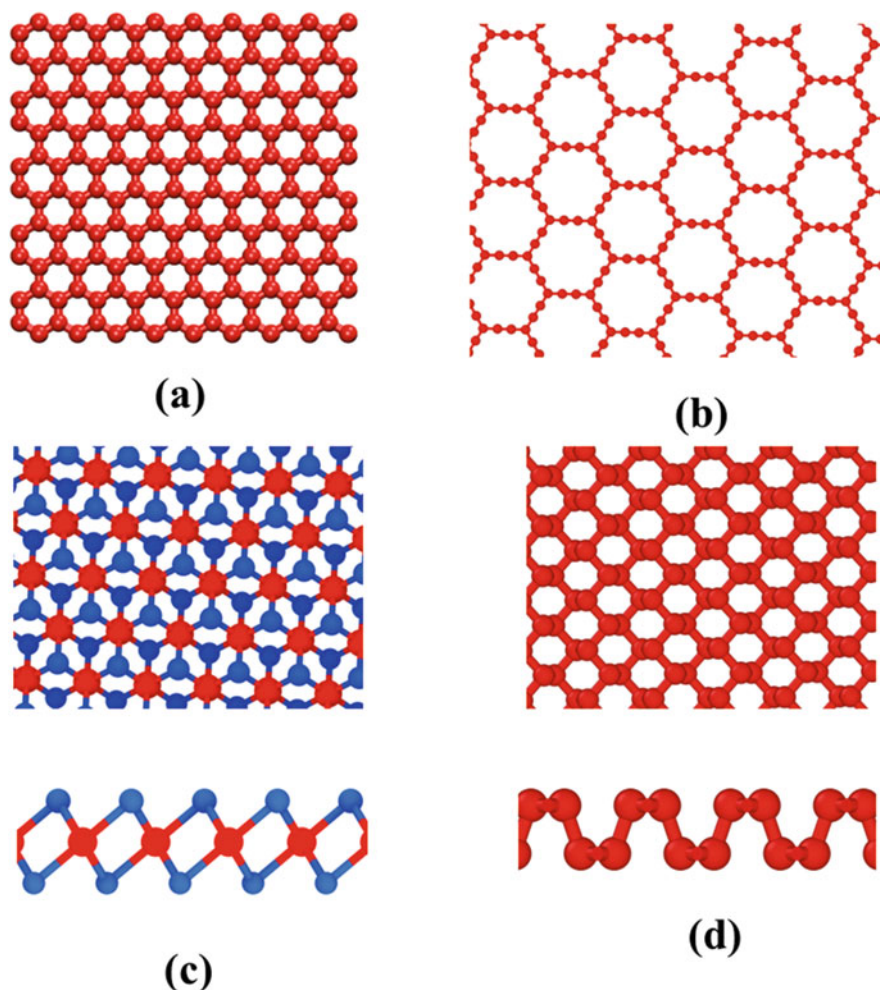


Fig. 7.3 Atomic structure of planner 2D substrate: (a) graphene, (b) graphdiyne, (c) molybdenum disulfide, and (d) black phosphorous

pre-synthesized bio-molecules to the graphene substrate) methods (Viela et al. 2016; Kristensen et al. 2013). A comprehensive atomistic understanding of bio-molecule-graphene interactions is not only important for the development and design of new drugs and bio-sensors but it may also provide information on the mechanisms such as molecular folding. The graphene substrate facilitates to achieve unique self-organization of bio-molecules, which depicts special properties and stability compared to the bulk. In most cases, the adsorption of bio-molecule is achieved through non-covalently, via the π - π interactions of the graphene substrate. During the adsorption process, the graphene substrate stabilizes the native structure of bio-molecules and forms a self-assembled structure. Ou et al. (2011) have performed

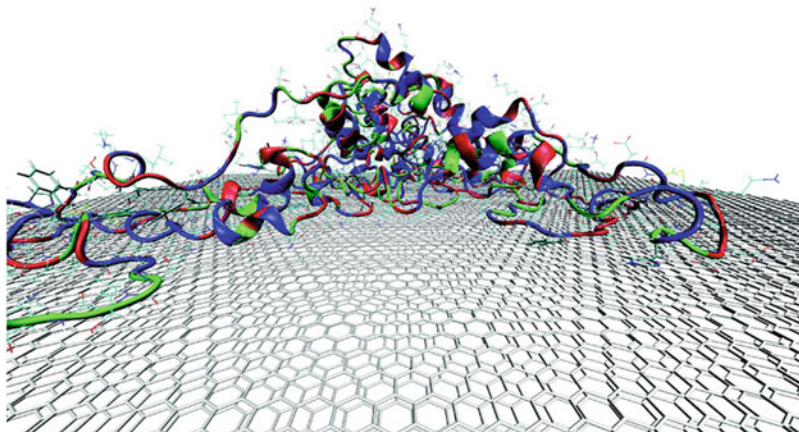


Fig. 7.4 Adsorption of protein over a graphene substrate using molecular dynamics simulations. Adapted and reprinted from Mücksch and Urbassek (2011) with permission from ACS, Copyright (2011)

molecular dynamics simulations for the study of adsorption, conformational dynamics, and dimerization of the α -helical peptide on a graphene substrate in explicit solvent at temperature $T = 310$ and 330 K. They have found that the two peptide chain turn into unfolded and assembled into an amorphous dimer on the graphene substrate. The C-terminal residue preferred to adsorb on the graphene substrate due to the strong interactions with the carbon atoms and lead to a unfolding of the α -helix starting from the C-terminal. The β -sheet conformation of protein has not observed any folding within the 15–200 nano seconds (ns) during molecular dynamics simulations, which depict that the α -helix to β -sheet transition for peptide is a very sluggish process.

Molecular dynamics simulation is able to recognize the regions of strong interatomic interaction between the peptide and the graphene and locate the starting point of the α -helix unfolding over the graphene substrate as shown in Fig. 7.4 (Mücksch and Urbassek 2011). The free and forced adsorption of various bio-molecules like bovine serum albumin (BSA) and other peptide molecules over graphitic substrate has largely been studied using molecular-dynamics simulation. In case of force adsorption, an AFM tip pushes the protein with constant force to the surface using molecular dynamics simulations. The adsorption dynamics and energetic is dependent on the environment conditions like implicit or explicit solvency conditions, temperatures, etc. Further, the adsorption of various bio-polymers is extensively influenced by the chemical modification of graphene substrate.

Similarly, all-atom molecular dynamics simulations are extensively used for the investigation of the adsorption and organization of DNA over the graphene or graphene oxide substrates in the presence of explicit solvent. The responsible factors for the adsorption are π - π stacking, electrostatic, van der Waals (vdW) interactions,

and hydrogen bonding. Through simulations, the adsorption and organization of two dsDNA segments onto the graphene oxide substrate has been investigated (Chen et al. 2014). It has been reported that the DNA segments can “stand up” with their helix axis perpendicular to the substrate due to energy penalty and other electrostatic repulsion between DNA and substrate. DNA segments cannot lie on the substrate with their helical axes parallel to substrate. The π - π stacking between base-pairs and the graphene oxide basal plane mainly contributes to their binding and organization. Molecular dynamics results reveal that the graphene oxide substrate behaves like an amphiphile. The hydrophobic π - π stacking interactions illustrate that the basal plane of graphene oxide is much more hydrophobic. However, the oxygen-containing groups of graphene oxide provide hydrophilic characteristic.

Other carbon allotropes, like graphdiyne and graphyne, are *sp*-hybridized carbon atoms with the planner structures (Srinivasu and Ghosh 2012; Peng et al. 2014; Inagaki and Kang 2014). Graphdiyne consists of a 2D structure with big triangular unit cell containing 18 carbon atoms. In each unit cell, there are two acetylenyl groups between neighboring benzene rings. Graphdiyne is the first synthetic carbon-based nano-material with the *sp*²-hybridized carbon atoms (benzene rings) and *sp*-hybridized carbon from acetylenyl groups. Graphdiyne has been reported to have promising applications in the fields of bio-science and technology. Applications of the graphdiyne and its derivatives have been reported in the bio-sensing, bio-imaging, cancer therapy, radiation protection, and so forth (Inagaki and Kang 2014; Banerjee 2016, 2018; Liu et al. 2019; Zhang and Wang 2015; Luan et al. 2016). In these bio-medical applications, graphdiyne exhibits better performance and higher stability compared to other carbon-based materials.

Various other kinds of 2D nanomaterials, such as hexagonal Boron Nitride (h-BN) (Watanabe et al. 2004), silicene (Lalmi et al. 2010), phosphorene (Liu et al. 2014), and molybdenum disulfide (MoS₂) (Coleman et al. 2011; Wang et al. 2015), have been employed to fabricate various kinds of bio-medical devices and its components. Molybdenum disulfide (MoS₂) has been demonstrating its bright prospects in biomedical applications. For example, MoS₂ is found to be an extremely efficient antimicrobial and antifungal 2D material. The MoS₂ can be used for the drug delivery through surface conjugation and coating. It has been reported that high-performance photo-thermal-triggered drug delivery platform can be constructed to utilize the strong near-infrared (NIR) adsorption over MoS₂. Furthermore, moderate direct band gap (1.8 eV) of MoS₂ shows its application in the biosensors for the detection of various proteins and DNA. MoS₂ has also been employed in the tomography imaging due to the X-ray adsorption of Mo element. Molecular dynamics simulations demonstrated that the MoS₂ monolayer has an exceptional ability to bind peptides in a quick and strong manner. Extremely strong interaction between protein and MoS₂ substrate helps to unfold the peptide despite the intra-peptide hydrogen bonds and subsequent secondary structures of α -helices (Gu et al. 2016, 2017; Saikia et al. 2013). This phenomenon leads to the nano-toxicity of MoS₂ when used in biological systems.

7.4 Adsorption and Encapsulation of Bio-Molecules over the Cylindrical Substrate

Adsorption and encapsulation of the bio-molecules over cylindrical substrate (such as single-wall carbon nanotubes (SWCNT)) is attracting much interest not only due to unusual properties but also because of the enhanced properties of this pseudo-one-dimensional morphology. For the illustration, in case of drug delivery applications, the SWCNT provides a protective layer against undesirable degradation of the encapsulated drug molecules. While sidewall can leave the active drug molecules open to attack from the nearby environment (Martincic and Tobias [2015](#); Roosta et al. [2016a, b](#)). Other important outcome of the encapsulating molecules within single-wall carbon nanotubes is that the resulting bio-molecule nano-composite modifies the properties of the fillers from those in the bulk. Encapsulation of chain-like molecules such as bio-polymers, DNA, graphene nano-ribbons, polymers, and so forth into a single-wall carbon nanotube has also attracted interest for their capability to produce novel, functionalized bio-molecular nano-composite materials (Gao et al. [2003](#); Zou et al. [2010](#)). Single-wall carbon nanotubes also can be used for the separation of biological molecules and microfluidic lab-on-a-chip applications.

To encapsulate a molecule into a single-wall carbon nanotube requires significant attractive energy between the molecule and carbon atom of nanotube. This is due to the confined region within the single-wall carbon nanotube that rigorously limits the number of conformations (loss in entropy) of the molecule. The loss in the entropy must be compensated by the gain of enthalpy during encapsulation process of bio-molecules into the single-wall carbon nanotube. The van der Waals interaction between single-wall carbon nanotube and bio-polymer played the dominant role in the encapsulation processes as investigated by using molecular dynamics simulations. After encapsulation, translocation of bio-polymer through nano-channels of single-wall carbon nanotube is due to more favorable van der Waals interaction energy. Based on the combination of molecular dynamics simulations and theory, it has been estimated that the translocation time for linear polymer chain is nearly 1 μs . However, it is extensively dependent on the solvency conditions and architecture and conformation state of bio-molecules inside a single-walled carbon nanotube. Yang et al. ([2006](#)) have been carrying out molecular dynamics simulation to study the translocation of alkane molecules into a single-walled carbon nanotube. They considered various chain lengths of alkane molecules and single-walled carbon nanotube diameters at 300 K. They found that the long polymer chains followed a cylindrical trajectory along the internal curved surface of the single-wall carbon nanotube. Kumar et al. ([2015](#)) and Kumar and Pattanayek ([2019](#)) have investigated encapsulation and translocation of chain-like polymer molecule into a single-wall carbon nanotube. They have characterized various organizations of polymer chain over the single-wall carbon nanotubes. At ambient temperature, polymer chain organization consists of a central stem surrounded by helically wrapped layers inside the short single-wall carbon nanotube. Polymer outside the single-wall carbon nanotube depicts helical conformations or circular arrangements as shown in Fig. [7.5](#). These organizations of polymer chain dictate similar conformations of the

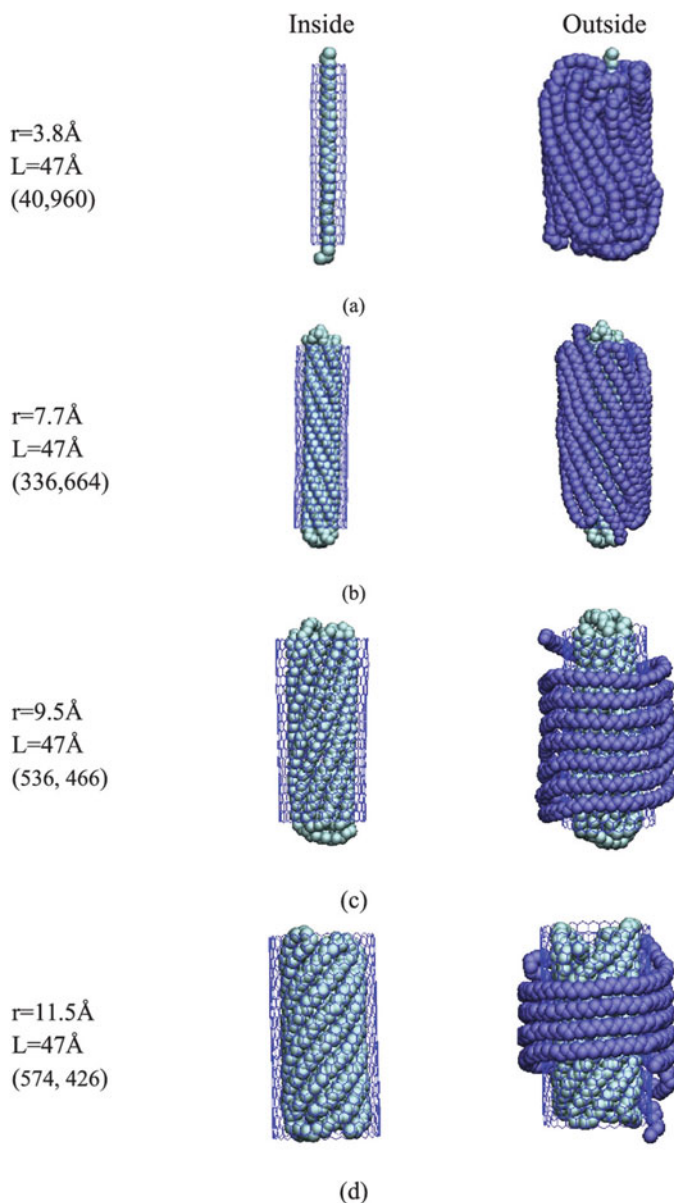


Fig. 7.5 Organization of chain-like molecule inside and outside of single-walled carbon nanotube at $T = 300\text{ K}$ using molecular dynamics simulations for different radius: (a) 3.8, (b) 7.7, (c) 9.5 and (d) 11.5 Angstrom. Adapted and reprinted from Kumar et al. (2015) with permission from AIP, Copyright (2015)

bio-molecule into the carbon nanotubes. Hence, large numbers of investigations pertaining to the conformation of various kinds of bio-molecules inside single-wall carbon nanotubes have been studied using large-scale molecular dynamics simulations.

The interactions between single-walled carbon nanotube and DNA provide driving force for the adsorption and encapsulation process. Single-stranded DNA can be helically adsorbed around a single-wall carbon nanotube due to π - π interactions between the nucleotide bases and the sidewall of nanotube (Zheng et al. 2003). However, double-stranded DNA depicts weak interaction with single-wall carbon nanotubes, because it interacts via groove and end. Okada et al. (2006) studied that a fully long ssDNA chain takes up a helical conformation inside the single-wall carbon nanotube. The reactivity of encapsulated ssDNA with other chemical compounds and reagents has been extremely controlled by the single-wall carbon nanotube. Further, aggregation, dispersion, and sorting of single-wall carbon nanotubes can be controlled by incorporation of DNA in aqueous medium. Pramanik and Maiti (2017) have investigated structure and stability of single-stranded DNA over the single-walled carbon nanotube by means of all-atom molecular dynamics simulation. It has been noticed that dispersion efficiency of single-walled carbon nanotubes depends on the types of nucleic bases of DNA. After adsorption of DNA over outer cylindrical substrate of single-wall carbon nanotube, another important phenomenon is the encapsulation and translocation of DNA through the single-walled carbon nanotube. Molecular dynamics simulation is extremely supportive to investigate encapsulations and translocation of DNA into the single-walled carbon nanotubes. Many novel investigations have reported the encapsulation/translocation of RNA/DNA inside single-walled carbon nanotubes of various diameters and chirality using all-atom molecular dynamics simulations with explicit solvent (Mogurampelly and Maiti 2013) as shown in Fig. 7.6. Various energetic factors like enthalpy, entropy, and free energy barrier are accountable for encapsulation and translocation. Molecular dynamics simulations show that the free energy gains by the molecules upon their encapsulations into the single-walled carbon nanotube provide stability of these molecules. The free energy profiles depict that all molecules can enter the single-walled carbon nanotube without facing any strong energy barrier but experience a strong energy barrier during their translocation. Strong energy barrier can be overcome by using plunger to make a nano-syringe for energetic of force-induced translocation of DNA into the single-walled carbon nanotube.

7.5 Conclusion

In this chapter, a brief outline has been emphasized during organization of bio-molecules in bulk and over the nano-substrate using molecular dynamics simulation. We have discussed different steps used in the molecular dynamics simulation along with the force fields and integration algorithms. Various molecular dynamics simulation software and other characterization tools are available as open source.

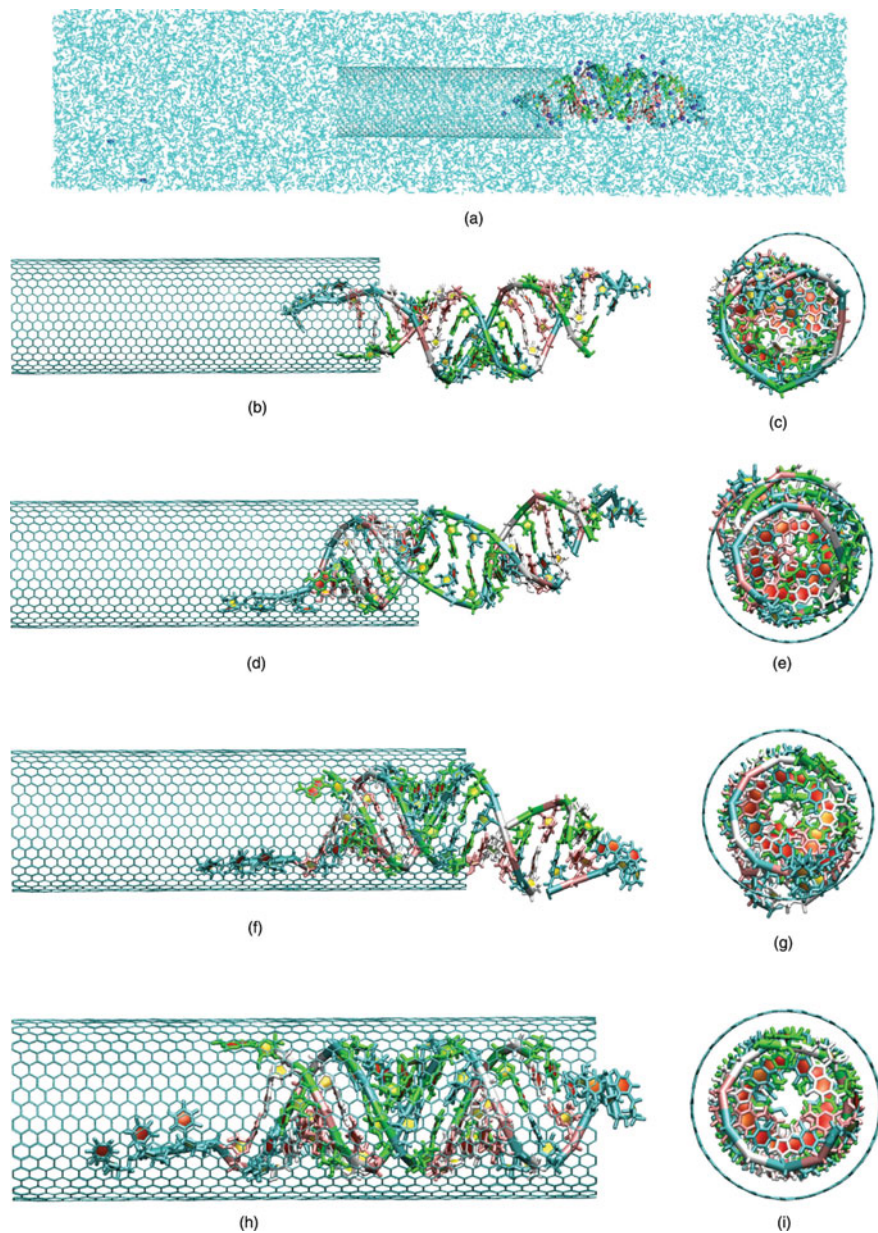


Fig. 7.6 Encapsulation, organization of RNA into a single-walled carbon nanotube by molecular dynamics simulations. (a)–(i) Snapshots of RNA at various time during MD simulations. Adapted and reprinted from Mogurampelly and Maiti (2013) with permission from AIP, Copyright (2013)

Finally, different application of molecular dynamics simulation in the area of organizations of bio-molecules functions in bulk and in the vicinity of nano-substrate has been described. Chain-like molecules adsorb over the planar and cylindrical substrate due to energy benefits. However, due to limited accessibility of conformation of bio-molecules, the entropic factor inhibits the adsorption process. From the molecular dynamics simulations, the amount of enthalpic and entropic factors for the adsorption and encapsulations process of bio-molecules can be estimated. After extensive simulations and data analysis it is shown that enthalpic energy dominates over the entropy. Therefore, enthalpic energy is responsible for adsorption and encapsulations. Various helical organizations of bio-molecules inside the single-walled carbon nanotube are due to favorable enthalpic energy of the simulation system. We believe that, brief description of organization of bio-molecules using molecular dynamics simulations may enhance the understanding of academician and researches toward the development of drugs and bio-medical devices.

References

- Allen MP, Tildesley DJ (2017) *Computer simulation of liquids*. Oxford University Press
- Allen BL, Kichambare PD, Star A (2007) Carbon nanotube field-effect-transistor-based biosensors. *Adv Mat* 19(11):1439–1451
- Anselme K, Bigerelle M (2011) Role of materials surface topography on mammalian cell response. *Int Mat Rev* 56(4):243–266
- Balavoine F, Schultz P, Richard C, Mallouh V, Ebbesen TW, Mioskowski C (1999) Helical crystallization of proteins on carbon nanotubes: a first step towards the development of new biosensors. *Angew Chem Int Ed* 38(13):1912–1915
- Banerjee AN (2016) Prospects and challenges of graphene-based nanomaterials in nanomedicine. *Glob J Nano* 1:555552
- Banerjee AN (2018) Graphene and its derivatives as biomedical materials: future prospects and challenges. *Int Foc* 8(3):20170056
- Berendsen HJC, Spoel D, Drunen R (1995) GROMACS: a message-passing parallel molecular dynamics implementation. *Comp Phys Comm* 91(1):43–56
- Besteman K, Lee J, Wiertz FG, Heering HA, Dekker C (2003) Enzyme-coated carbon nanotubes as single-molecule biosensors. *Nano Lett* 3(6):727–730
- Bitounis D, Ali-Boucetta H, Hong BH, Min D, Kostarelos K (2013) Prospects and challenges of graphene in biomedical applications. *Adv Mat* 25(16):2258–2268
- Brooks BR, Bruccoleri RE, Olafson BD, States DJ, Swaminathan SA, Karplus M (1983) CHARMM: a program for macromolecular energy, minimization, and dynamics calculations. *J Comp Chem* 4(2):187–217
- Calvert P (1997) Biopolymers: the structure of starch. *Nature* 389(6649):338
- Case DA, Cheatham TE, Darden T, Gohlke H, Luo R, Merz KM Jr, Onufriev A, Simmerling C, Wang B, Woods RJ (2005) The Amber biomolecular simulation programs. *J Comp Chem* 26(16):1668–1688
- Case DA, Darden TA, Cheatham TE, Simmerling CL, Wang J, Duke RE, Luo R, et al. (2006) AMBER 9. University of California, San Francisco 45.
- Chen R, Qin L, Jia M, He X, Li W (2010) Novel surface-modified molecularly imprinted membrane prepared with iniferter for permselective separation of lysozyme. *J Mem Sci* 363(1–2):212–220
- Chen J, Chen L, Wang Y, Chen S (2014) Molecular dynamics simulations of the adsorption of DNA segments onto graphene oxide. *J Phys D: App Phys* 47(50):505401

- Chen L, Wang X, Lu W, Wu X, Li J (2016) Molecular imprinting: perspectives and applications. *Chem Soc Rev* 45(8):2137–2211
- Chenoweth K, Van Duin ACT, Goddard WA (2008) ReaxFF reactive force field for molecular dynamics simulations of hydrocarbon oxidation. *J Phys Chem A* 112(5):1040–1053
- Coleman JN, Lotya M, O'Neill A, Bergin SD, King PJ et al (2011) Two dimensional nanosheets produced by liquid exfoliation of layered materials. *Science* 331:568–571
- Daggett V, Levitt M (1992) A model of the molten globule state from molecular dynamics simulations. *Proc Natl Acad Sci U S A* 89:5142–5146
- Díez-Pascual AM, Díez-Vicente AL (2015) Nano-TiO₂ reinforced PEEK/PEI blends as biomaterials for load-bearing implant applications. *ACS App Mat Int* 7(9):5561–5573
- Dong R, Zhang T, Feng X (2018) Interface-assisted synthesis of 2D materials: trend and challenges. *Chem Rev* 118(13):6189–6235
- Gao H, Kong Y, Cui D, Ozkan CS (2003) Spontaneous insertion of DNA oligonucleotides into carbon nanotubes. *Nano Lett* 3(4):471–473
- Geim AK (2009) Graphene: status and prospects. *Science* 324(5934):1530–1534
- Geim AK, Novoselov KS (2010) The rise of graphene. In: *Nanoscience and technology: a collection of reviews from nature journals*, pp 11–19
- Georgakilas V, Tiwari JN, Kemp KC, Perman JA, Bourlinos AB, Kim KS, Zboril R (2016) Noncovalent functionalization of graphene and graphene oxide for energy materials, biosensing, catalytic, and biomedical applications. *Chem Rev* 116(9):5464–5519
- Gu Z, Yang Z, Chong Y, Ge C, Weber JK, Bell DR, Zhou R (2015) Surface curvature relation to protein adsorption for carbon-based nanomaterials. *Sci Rep* 5:10886
- Gu Z, Li W, Hong L, Zhou R (2016) Exploring biological effects of MoS₂ nanosheets on native structures of α -helical peptides. *J Chem Phys* 144(17):175103
- Gu Z, Luna PD, Yang Z, Zhou R (2017) Structural influence of proteins upon adsorption to MoS₂ nanomaterials: comparison of MoS₂ force field parameters. *Phys Chem Chem Phys* 19(4):3039–3045
- Hasan A, Waibhaw G, Tiwari S, Dharmalingam K, Shukla I, Pandey LM (2017) Fabrication and characterization of chitosan, polyvinylpyrrolidone, and cellulose nanowhiskers nanocomposite films for wound healing drug delivery application. *J Bio Mat Res Part A* 105(9):2391–2404
- Hasan A, Saxena V, Pandey LM (2018a) Surface functionalization of Ti₆Al₄V via self-assembled monolayers for improved protein adsorption and fibroblast adhesion. *Langmuir* 34(11):3494–3506
- Hasan A, Waibhaw G, Pandey LM (2018b) Conformational and organizational insights into serum proteins during competitive adsorption on self-assembled monolayers. *Langmuir* 34(28):8178–8194
- He H, Pham-Huy LA, Dramou P, Xiao D, Zuo P, Pham-Huy C (2013) Carbon nanotubes: applications in pharmacy and medicine. *Bio Res Int*. <https://doi.org/10.1155/2013/578290>
- Holzinger M, Goff AL, Cosnier S (2017) Synergetic effects of combined nanomaterials for biosensing applications. *Sensors* 17(5):1010
- Hospital A, Goñi JR, Orozco M, Gelpí JL (2015) Molecular dynamics simulations: advances and applications. *Adv Appl Bio Chem AABC* 8:37
- Humphrey W, Dalke A, Schulten K (1996) VMD: visual molecular dynamics. *J Mol Grap* 14(1):33–38
- Inagaki M, Kang F (2014) Graphene derivatives: graphane, fluorographene, graphene oxide, graphyne and graphdiyne. *J Mat Chem A* 2(33):13193–13206
- Kavassalis TA, Sundararajan PR (1993) A molecular-dynamics study of polyethylene crystallization. *Macromolecules* 26(16):4144–4150
- Knotts TA, Rathore N, Schwartz DC, de Pablo JJ (2007) A coarse grain model for DNA. *J Chem Phys* 126(8):02B611
- Kristensen SH, Pedersen GA, Nejsun LN, Sutherland DS (2013) Protein adsorption at nanopatterned surfaces studied by quartz crystal microbalance with dissipation and surface plasmon resonance. *J Phys Chem B* 117(36):10376–10383

- Kumar S, Pattanayek SK (2018) Semi-flexible polymer engendered aggregation/dispersion of fullerene (C60) nano-particles: an atomistic investigation. *Chem Phys Lett* 701:22–29
- Kumar S, Pattanayek SK (2019) Force induced removal of an encapsulated semi-flexible polymer from single walled carbon nanotube. *Chem Phys* 516:22–27
- Kumar S, Pattanayek SK, Pereira GG (2015) Polymers encapsulated in short single wall carbon nanotubes: Pseudo-1D morphologies and induced chirality. *J Chem Phys* 142:114901
- Kurapati R, Kostarelos K, Prato M, Bianco A (2016) Biomedical uses for 2D materials beyond graphene: current advances and challenges ahead. *Adv Mat* 28(29):6052–6074
- Lalmi B, Oughaddou H, Enriquez H, Kara A, Vizzini S et al (2010) Epitaxial growth of a silicene sheet. *Appl Phys Lett* 97:223109
- Li S, Chen Y, Liu H, Wang Y, Liu L, Lv F, Li Y, Wang S (2017) Graphdiyne materials as nanotransducer for in vivo photoacoustic imaging and photothermal therapy of tumor. *Chem Mat* 29(14):6087–6094
- Lindahl E, Hess B, Spoel DVD (2001) GROMACS 3.0: a package for molecular simulation and trajectory analysis. *Mol Mod Annual* 7(8):306–317
- Liu Z, Sun X, Nakayama-Ratchford N, Dai H (2007) Supramolecular chemistry on water-soluble carbon nanotubes for drug loading and delivery. *ACS Nano* 1(1):50–56
- Liu Z, Robinson JT, Sun X, Dai H (2008) PEGylated nanographene oxide for delivery of water-insoluble cancer drugs. *J Am Chem Soc* 130(33):10876–10877
- Liu H, Neal AT, Zhu Z, Luo Z, Xu X et al (2014) Phosphorene: an unexplored 2d semiconductor with a high hole mobility. *ACS Nano* 8:4033–4041
- Liu J, Chen C, Zhao Y (2019) Progress and prospects of graphdiyne-based materials in biomedical applications. *Adv Mat*:1804386
- Lopez CF, Moore PB, Shelley JC, Shelley MY, Klein ML (2002) Computer simulation studies of biomembranes using a coarse grain model. *Comp Phys Comm* 147(1–2):1–6
- Luan B, Huynh T, Zhou R (2016) Potential interference of protein–protein interactions by graphyne. *J Phys Chem B* 120(9):2124–2131
- Marco DV, Masetti M, Bottegoni G, Cavalli A (2016) Role of molecular dynamics and related methods in drug discovery. *J Med Chem* 59(9):4035–4061
- Mark AE, van Gunsteren WF (1992) Simulation of the thermal denaturation of hen egg white lysozyme: trapping the molten globule state. *Biochemistry* 31:7745–7748
- Martincic M, Tobias G (2015) Filled carbon nanotubes in biomedical imaging and drug delivery. *Exp Opin Drug Del* 12(4):563–581
- Mayo SL, Olafson BD, Goddard WA (1990) DREIDING: a generic force field for molecular simulations. *J Phys Chem* 94(26):8897–8909
- Menaa F, Abdelghani A, Menaa B (2015) Graphene nanomaterials as biocompatible and conductive scaffolds for stem cells: impact for tissue engineering and regenerative medicine. *J Tiss Eng Reg Med* 9(12):1321–1338
- Mogurampelly S, Maiti PK (2013) Translocation and encapsulation of siRNA inside carbon nanotubes. *J Chem Phys* 138(3):034901
- Moradi S, Hadjesfandiari N, Toosi SF, Kizhakkedathu JN, Hatzikiriakos SG (2016) Effect of extreme wettability on platelet adhesion on metallic implants: from super hydrophilicity to super hydrophobicity. *ACS Appl Mat Int* 8(27):17631–17641
- Mücksch C, Urbassek HM (2011) Molecular dynamics simulation of free and forced BSA adsorption on a hydrophobic graphite surface. *Langmuir* 27(21):12938–12943
- Muthukumar M (1986) Thermodynamics of polymer solutions. *J Chem Phys* 85(8):4722–4728
- Nelson MT, Humphrey W, Gursoy A, Dalke A, Kalé LV, Skeel RD, Schulten K (1996) NAMD: a parallel, object-oriented molecular dynamics program. *Int J Sup Appl High Perf Comp* 10(4):251–268
- Nguyen P-D, Tran TB, Nguyen DTX, Min J (2014) Magnetic silica nanotube-assisted impedimetric immunosensor for the separation and label-free detection of Salmonella typhimurium. *Sen Act B: Chem* 197:314–320

- O'Connor TC, Andzelm J, Robbins MO (2015) AIREBO-M: a reactive model for hydrocarbons at extreme pressures. *J Chem Phys* 142(2):024903
- Okada T, Kaneko T, Hatakeyama R, Tohji K (2006) Electrically triggered insertion of single-stranded DNA into single-walled carbon nanotubes. *Chem Phys Lett* 417(4):288–292
- Ou L, Luo Y, Wei G (2011) Atomic-level study of adsorption, conformational change, and dimerization of an α -helical peptide at graphene surface. *J Phys Chem B* 115(32):9813–9822
- Pandey LM, Pattanayek SK (2011) Hybrid surface from self-assembled layer and its effect on protein adsorption. *Appl Surf Sci* 257(10):4731–4737
- Pandey LM, Pattanayek SK (2013) Relation between the wetting effect and the adsorbed amount of water-soluble polymers or proteins at various interfaces. *J Chem Eng Data* 58(12):3440–3446
- Pandey LM, Pattanayek SK, Delabouglise D (2013) Properties of adsorbed bovine serum albumin and fibrinogen on self-assembled monolayers. *J Phys Chem C* 117(12):6151–6160
- Park S, Lih E, Park K, Joung YK, Han DK (2017) Biopolymer-based functional composites for medical applications. *Prog Poly Sci* 68:77–105
- Paul W, Yoon DY, Smith GD (1995) An optimized united atom model for simulations of polymethylene melts. *J Chem Phys* 103(4):1702–1709
- Peng Q, Dearden AK, Crean J, Han L, Liu S, Wen X, De S (2014) New materials graphyne, graphdiyne, graphone, and graphane: review of properties, synthesis, and application in nanotechnology. *Nano Sci Appl* 7:1
- Perricone U, Gulotta MR, Lombino J, Parrino B, Cascioferro S, Diana P, Cirrincione G, Padova A (2018) An overview of recent molecular dynamics applications as medicinal chemistry tools for the undruggable site challenge. *Med Chem Comm* 9(6):920–936
- Phillips JC, Braun R, Wang W, Gumbart J, Tajkhorshid E, Villa E, Chipot C, Skeel RD, Kale L, Schulten K (2005) Scalable molecular dynamics with NAMD. *J Comp Chem* 26(16):1781–1802
- Plimpton S (1995) Fast parallel algorithms for short-range molecular dynamics. *J Comp Phys* 117(1):1–19
- Pramanik D, Maiti PK (2017) DNA-assisted dispersion of carbon nanotubes and comparison with other dispersing agents. *ACS App Mat Int* 9(40):35287–35296
- Raffaini G, Ganazzoli F (2013) Surface topography effects in protein adsorption on nanostructured carbon allotropes. *Langmuir* 29(15):4883–4893
- Rapaport DC (2004) *The art of molecular dynamics simulation*. Cambridge University Press
- Roosta S, Nikkhal SJ, Sabzali M, Hashemianzadeh SM (2016a) Molecular dynamics simulation study of boron-nitride nanotubes as a drug carrier: from encapsulation to releasing. *RSC Adv* 6(11):9344–9351
- Roosta S, Hashemianzadeh SM, Ketabi S (2016b) Encapsulation of cisplatin as an anti-cancer drug into boron-nitride and carbon nanotubes: Molecular simulation and free energy calculation. *Mat Sci Eng: C* 67:98–103
- Saikia N, Jha AN, Deka RC (2013) Dynamics of fullerene-mediated heat-driven release of drug molecules from carbon nanotubes. *J Phys Chem Lett* 4(23):4126–4132
- Saito N, Usui Y, Aoki K, Narita N, Shimizu M, Hara K, Ogiwara N et al (2009) Carbon nanotubes: biomaterial applications. *Chem Soc Rev* 38(7):1897–1903
- Scott WRP, Hünenberger PH, Tironi IG, Mark AE, Billeter SR, Fennen J, Torda AE, Huber T, Krüger P, van Gunsteren WF (1999) The GROMOS biomolecular simulation program package. *J Phys Chem A* 103(19):3596–3607
- Senftle TP, Hong S, Islam MM, Kylasa SB, Zheng Y, Shin YK, Junkermeier C et al (2016) The ReaxFF reactive force-field: development, applications and future directions. *NPJ Comp Mat* 2:15011
- Shanmuganathan R, Edison TNJI, Oscar FL, Ponnuchamy K, Shanmugam S, Pugazhendhi A (2019) Chitosan nanoparticles: an overview of drug delivery against cancer. *Int J Biol Macromol* 130:727–736
- Shelley JC, Shelley MY, Reeder RC, Bandyopadhyay S, Klein ML (2001) A coarse grain model for phospholipid simulations. *J Phys Chem B* 105(19):4464–4470

- Shi K, Wong N, Jessop TC, Wender PA, Dai H (2004) Nanotube molecular transporters: internalization of carbon nanotube–protein conjugates into mammalian cells. *J Am Chem Soc* 126(22):6850–6851
- Smith W, Forester TR, Todorov IT, Leslie M (2006) The DL poly 2 user manual. CCLRC, Daresbury Laboratory, Daresbury, Warrington WA4 4AD, England 2
- Srinivasu K, Ghosh SK (2012) Graphyne and graphdiyne: promising materials for nanoelectronics and energy storage applications. *J Phys Chem C* 116(9):5951–5956
- Stukowski A (2009) Visualization and analysis of atomistic simulation data with OVITO—the open visualization tool. *Mod Sim Mat Sci Eng* 18(1):015012
- Sundararajan PR, Kavassalis TA (1997) Molecular dynamics simulations of folding in cyclic alkanes. *Macromolecules* 30(17):5172–5174
- Tao W, Zhu X, Yu X, Zeng X, Xiao Q, Zhang X, Ji X et al (2017) Black phosphorus nanosheets as a robust delivery platform for cancer theranostics. *Adv. Mat.* 29(1):1603276
- Tieleman DP, MacCallum JL, Ash WL, Kandt C, Xu Z, Monticelli L (2006) Membrane protein simulations with a united-atom lipid and all-atom protein model: lipid–protein interactions, side chain transfer free energies and model proteins. *J Phys: Cond Matt* 18(28):S1221
- Van Der SD, Lindahl E, Hess B, Groenhof G, Mark AE, Berendsen HJC (2005) GROMACS: fast, flexible, and free. *J Comp Chem* 26(16):1701–1718
- Van Duin ACT, Dasgupta S, Lorant F, Goddard WA (2001) ReaxFF: a reactive force field for hydrocarbons. *J Phys Chem A* 105(41):9396–9409
- Venkata SYP, Saji KJ, Tiwari A (2016) Atomically thin MoS₂: a versatile nongraphene 2D material. *Adv Fun Mat* 26(13):2046–2069
- Viola F, Granados D, Ayuso-Sacido A, Rodríguez I (2016) Biomechanical cell regulation by high aspect ratio nanoimprinted pillars. *Adv Fun Mat* 26(31):5599–5609
- Vilhena JG, Rubio-Pareda P, Velloso P, Serena PA, Pérez R (2016) Albumin (BSA) adsorption over graphene in aqueous environment: influence of orientation, adsorption protocol, and solvent treatment. *Langmuir* 32(7):1742–1755
- Wang J, Liu G, Jan MR (2004) Ultrasensitive electrical biosensing of proteins and DNA: carbon-nanotube derived amplification of the recognition and transduction events. *J Am Chem Soc* 126(10):3010–3011
- Wang S, Li K, Chen Y, Chen H, Ma M et al (2015) Biocompatible pegylated MoS₂ nanosheets: Controllable bottom-up synthesis and highly efficient photothermal regression of tumor. *Biomaterials* 39:206–217
- Watanabe K, Taniguchi T, Kanda H (2004) Direct-band gap properties and evidence for ultraviolet lasing of hexagonal boron nitride single crystal. *Nat Mat* 3:404–409
- Yang H, Liu Y, Zhang H, Li Z (2006) Diffusion of single alkane molecule in carbon nanotube studied by molecular dynamics simulation. *Polymer* 47(21):7607–7610
- Yang W, Ratinac KR, Ringer SP, Thordarson P, Gooding JJ, Braet F (2010) Carbon nanomaterials in biosensors: should you use nanotubes or graphene? *Ang Chem Int Ed* 49(12):2114–2138
- Zhang L, Wang X (2015) Mechanisms of graphyne-enabled cholesterol extraction from protein clusters. *RSC Adv* 5(16):11776–11785
- Zheng M, Jagota A, Strano MS, Santos AP, Barone P, Chou SG, Diner BA, Dresselhaus MS, McLean RS, Onoa GB, Samsonidze GG, Semke ED, Usrey M, Walls DJ (2003) Structure-based carbon nanotube sorting by sequence-dependent DNA assembly. *Science* 302:1545–1548
- Zou J, Liang W, Zhang S (2010) Coarse-grained molecular dynamics modeling of DNA–carbon nanotube complexes. *Int J Num Meth Eng* 83(8–9):968–985
- Zuo G, Zhou X, Huang Q, Fang H, Zhou R (2011) Adsorption of villin headpiece onto graphene, carbon nanotube, and C60: effect of contacting surface curvatures on binding affinity. *J Phys Chem C* 115(47):23323–23328



Medical Diagnostics Based on Electrochemical Biosensor

8

Nalin H. Maniya and Divesh N. Srivastava

Abstract

This chapter focuses on the recent developments in the electrochemical biosensor. On the onset historical aspects of biosensors have been discussed followed by the current state of the art, which includes the fabrication, immobilization of the receptors and the linking chemistry, sensitivity, specificity, and target detection species. The importance of the electrode platform is outlined and classified into porous and nonporous. The sensor reported on various platforms has been reviewed.

Keywords

Electrochemical biosensor · Glassy carbon electrode · Screen-printed electrode · Plastic chip electrode · Nanoporous anodic alumina · Porous silicon · Mesoporous silica

8.1 Introduction

The biosensor market is growing rapidly and is expected to be valued at USD 31.5 billion by 2024 from the current value of USD 21.2 billion in 2019 (Biosensors Market Report 2019). According to the IUPAC, biosensors are defined as a self-contained integrated device, capable of providing specific quantitative or semiquantitative analytical information using a biological recognition element (bioreceptor), which is in contact with the transduction element (transducer) (McNaught and Wilkinson 1997). The biosensor is made up of two components: first, biological recognition element or bioreceptor that can be a complementary DNA, enzyme

N. H. Maniya · D. N. Srivastava (✉)

Analytical and Environmental Science Division & Central Instrument Facility, CSIR-Central Salt & Marine Chemicals Research Institute, Bhavnagar, India

e-mail: dnsrivastava@csmcri.res.in

© Springer Nature Singapore Pte Ltd. 2020

P. Chandra, L.M. Pandey (eds.), *Biointerface Engineering: Prospects in Medical Diagnostics and Drug Delivery*, https://doi.org/10.1007/978-981-15-4790-4_8

167

(or substrate), antigen (or antibody), or a receptor protein. Since the bioreceptors of a biosensor can bind to the target analyte very selectively, the biosensor offers very high selectivity compared to the chemical sensors. The second component of biosensor is a transducer that converts the analyte concentration into a measurable (optical, mass, electrical, or electrochemical) signal. They offer a number of distinct advantages such as high sensitivity, high specificity, reusability, label-free, short assay time, portability, and compact size in comparison to the traditional diagnostic methods (Thevenot et al. 2001). Biosensors have been developed for the range of applications from medical diagnostics, environmental monitoring, food safety, water quality to agriculture. The major application area of the biosensor is in the medical field for the diagnosis of different diseases, for example, cancer detection and blood glucose monitoring in case of diabetic patients, drug discovery, drug analysis, and whole blood analysis (Maniya 2018).

The interest in biosensors, in general, started with the introduction of the first generation glucose biosensor in 1962 (Clark and Lyons 1962). This initial electrochemical biosensor was based on the measurements of either depletion of the substrate (e.g., oxygen concentration) or generation of the product (e.g., hydrogen peroxide) in an enzyme catalyzed reaction. For example, glucose oxidase catalyzed oxidation of glucose into gluconate (Fig. 8.1). This was followed by the second-generation biosensors that were developed to overcome the drawbacks associated with the first generation biosensors. These biosensors used artificial mediators or nanomaterials to transport the signal to and from the enzyme. However many times the mediators are partially toxic. This improvement reduces the required potential window of the system, minimizing effects from interferents and helped in improving the selectivity (Ronkainen et al. 2010). The third-generation biosensors were then developed where the signal is transferred directly from the enzyme to the electrode without any intermediate stages or use of nanoparticles. These biosensors allow the continuous measurement of target species, for example, glucose in case of diabetes via subcutaneous biosensor. Electrochemical biosensors are popular due to low-cost fabrication of the microelectronic circuits and simple sensor setup with an easy interface and electronic read-out and processing. Further, the electrochemical biosensors offer several advantages such as miniaturization, low detection limits, small analyte volumes, and robustness (Das et al. 2016; Piro and Reisberg 2017).

Generally, biosensing can be performed in two detection protocols, viz., label-free and label-based detection. In label-free detection, the target species are not labeled or altered and are sensed in their natural forms. This detection method allows easy as well as convenient quantitative and kinetic measurement of molecular interaction in cost-effective manner. On the other hand, label-based detection involves the labeling of either target species or biorecognition molecules with suitable tags, such as dyes, enzymes (horseradish peroxidase, alkaline phosphatase), or nanoparticles (quantum dots) (Krismastuti et al. 2014; Medintz et al. 2005; Szili et al. 2011). The intensity of the signal is representative of the presence of the target species and also the interaction strength between target and biorecognition species. The label-based detection helps in increasing the sensitivity of the measurements; however, at the same time it suffers from the costly and laborious labeling processes. The labeling may also denature the biomolecule and interfere with the function of a

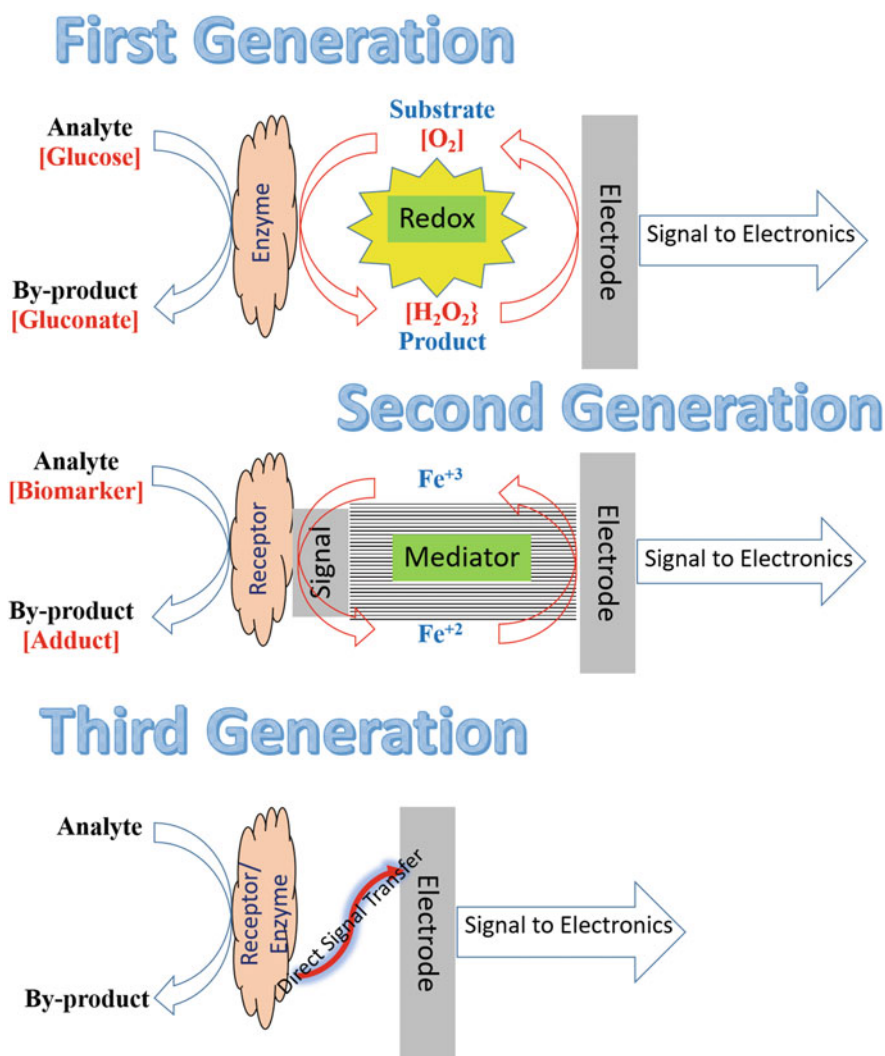


Fig. 8.1 Schematic diagram depicting sensing strategies in various generations of electrochemical sensors

biomolecule. Although label-free and label-based detection have their own positives and negatives, both are widely incorporated in the biosensors to get vital and complementary information regarding interactions among biomolecules.

The choice of electrode platform is also crucial for the performance of biosensors. The electrode not only provides the surface for the attachment of the receptor biomolecule but also in tailoring the electrochemical parameters like overpotential and electrode kinetics. The current progress in nanotechnology and advanced fabrication methods lead to the development of highly sensitive micro and nanostructured platforms for biosensor applications. Different porous and nonporous platforms have

been designed for various biosensing. Among them, porous platforms based on the nanoporous anodic alumina (NAA), porous silicon (PSi), mesoporous silica (MPS), and porous polymers whereas nonporous platforms such as glassy carbon electrode (GCE), screen-printed electrode (SPE), and plastic chip electrode (PCE) has been developed (Paul et al. 2019; Reta et al. 2018; Taleat et al. 2014; Zhao et al. 2016). Porous platforms offer distinct advantages such as the high surface area to volume ratio, size exclusion of interfering molecules, and theoretically high sensitivity due to high surface area compared to the nonporous platforms. On the other hand, nonporous platforms do not require tuning of pore size, porosity, etc. In the following sections, we furnish representative examples from the two classes of electrode platforms and biosensors reported on them in the literature.

8.2 Nonporous Material-Based Biosensor

8.2.1 Glassy Carbon Electrode (GCE)

Carbonaceous electrodes are important in biomedical applications as they are biocompatible and can be used as implantable electrodes (Kadefors et al. 1970). The implantable carbon electrodes have been used as stimulus electrode in cardiac pacemakers, cuff electrodes for peripheral nerve stimulation and retinal implants (Vomero et al. 2018). Among various carbonaceous materials, graphite is not apt for electrode fabrication due to its porous nature leading to inconsistent results. Glassy carbon is controlled pyrolyzed, highly pure, and compact form of carbon. GCE is electrically conductive, gas impermeable material of highly resistive to the chemical attack (Zittel and Miller 1965). GCE has been utilized for a number of biosensing applications based on electrochemical detection method. Some of the prominent work on GCE electrode are outlined below.

Xing and Ma (2016) prepared the amperometric sensor using hybrid nanocomposite of MoS₂ and reduced graphene oxide. The analysis of nanocomposite displayed porous and flower-like structure and a large specific surface. The electrochemical detection of ascorbic acid, dopamine, and uric acid was performed using the nanocomposite biosensor by cyclic voltammetry (CV) and differential pulse voltammetry (DPV). The recovery of these three species were more than 99% as detected from the spiked human serum samples.

The electrochemical determination of caffeic acid was performed on the nitrogen-doped carbon-modified GCE (Karikalalan et al. 2017). The carbon nanomaterials were prepared by the flame synthesis method. The fabricated biosensor displayed the superior electrocatalytic performance for the detection of the caffeic acid in a wide linear range of 0.01–350 μM with a limit of detection (LOD) of 0.0024 μM and the limit of quantification (LOQ) of 0.004 μM. Also, the good selectivity, stability, and reproducibility with detection of caffeic acid from red wine were also demonstrated. An electrochemical biosensor was developed for the detection of the Salmonella bacteria by immobilizing the nanocomposite of reduced graphene oxide (rGO) and carboxy-modified multi-walled carbon nanotubes (MWCNTs) on the GCE surface (Jia et al. 2016). The specific detection of Salmonella was obtained by covalently

binding amino-modified aptamer to the rGO-MWCNT composite. The binding of the Salmonella to the anti-Salmonella aptamer on the sensor surface blocked the electron transfer and caused the increase in impedance as measured by electrochemical impedance spectroscopy (EIS). The detection of Salmonella was obtained at a working voltage of 0.2 V in the range of $75\text{--}7.5 \times 10^5$ cfu/mL and detection limit of 25 cfu/mL.

The simultaneous detection of ascorbic acid, dopamine, and uric acid was performed on the GCE decorated with fullerene (C₆₀) and modified with platinum nanosheets by potentiostatic deposition method (Zhang et al. 2015). The DPV measurements of the electrode showed the three well-resolved voltammetric peaks for these biomolecules. The prepared biosensor showed detection from both real plasma and urine samples with good storage stability and reproducibility. The detection of ascorbic acid, dopamine, and uric acid was in the range of 10–1800, 0.5–211.5, and 9.5–1187 μM with LOD of 0.43, 0.07, and 0.63 μM , respectively. These values of detection range and LOD were almost comparable to the values obtained by Xing and Ma (2016). A similar biosensor for the simultaneous detection of paracetamol, tramadol, and caffeine was fabricated based on GCE and modified with poly(Nile blue) by electropolymerization of Nile blue monomer using CV (Chitravathi and Munichandraiah 2016). The coating of the poly(Nile blue) film helped in increasing the electroactive surface area and peak current and decreasing the overpotential of paracetamol, tramadol, and caffeine in comparison to the bare GCE. The biosensor displayed good selectivity and sensitivity for paracetamol, tramadol, and caffeine detections in a linear range of 2.0×10^{-7} – 1.62×10^{-5} M, 1.0×10^{-6} – 3.1×10^{-4} M, and 8.0×10^{-7} – 2.0×10^{-5} M, with LODs of 0.08, 0.5, and 0.1 μM , respectively. Further, the biosensor also demonstrated to detect these molecules in pharmaceutical dosage forms.

The detection of the tryptophan was carried out on the metal-organic framework MIL-101(Fe) and silver nanoparticles composite (AgNPs/MIL-101) modified GCE (Peng et al. 2016). The composite increased the oxidation current of tryptophan compared to the bare electrode. The CV and DPV were used to measure the electrochemical behaviors of tryptophan on the sensor surface. The oxidation peak currents were found to be proportional to the tryptophan concentrations in the ranges of 1–50 and 50–150 μM , respectively, with LOD of 0.14 μM . The detection of tryptophan from urine samples was also performed.

The simultaneous determination of hydroquinone and catechol was performed on the GCE by pre-electrolyzing GCE in ammonium carbamate aqueous solution (Wang et al. 2016). This modification improved the electrocatalytic properties of GCE for the electro-oxidation of hydroquinone and catechol due to the incorporation of the nitrogen to the electrode surface. The simultaneous detection of both hydroquinone and catechol was in the linear range of 5 to 260 μM and LOD of 0.2 μM . The biosensor also displayed detection from real river water samples with recoveries of more than 95%.

Recently, the determination of the uric acid was performed on the GCE modified with a nanocomposite consisting of Fe₃O₄ onto graphene sheets and SiO₂ layer (Movlaee et al. 2017). The electrochemical behavior of the uric acid on the electrode was studied by CV, DPV, and chronoamperometry. The uric acid detection

displayed the sharp oxidation peak current at 330 mV due to high electrocatalytic activity. The linear increase in peak current with an increase in acid concentration was seen in the range of 0.5–250 μM with the LOD of 0.07 μM . Further, the detection of uric acid from the urine samples was demonstrated with high reproducibility (RSD: 1.7–3.4%) and excellent recoveries. In order to perform modification of GCE and electro-oxidation of doxorubicin (DOX) at a low potential, graphene QD of low toxicity was prepared by pyrolyzing citric acid in alkaline solution (Hashemzadeh et al. 2016). The coating of the graphene QDs on the GCE resulted in a decrease in the overvoltage (-0.56 V) of the DOX oxidation reaction in comparison to the bare electrodes. This was due to the good electrocatalytic activity for the redox reaction of DOX and an increase in the rate of electron transfer of DOX due to the coating. The biosensor showed a determination of the DOX from the human plasma samples in a wide linear range of 0.018–3.6 μM and LOD of 0.016 μM with good stability.

8.2.2 Screen-Printed Electrode (SPE)

Although the GCEs are excellent at the laboratory level and for proof-of-concept experiments, for scale-up research and development they are not so practical. Therefore an ancient printing technique, the screen printing, has been adapted for easy and mass fabrication of electrodes. Now, screen printing on the electrode is one of the most promising methods for simple, rapid, and cost-effective production of biosensors (Windmiller and Wang 2013). The surface modification of SPEs can be easily performed with different linking chemistries to attach bioreceptors and to achieve a variety of improvements. The point-of-care applications with SPEs are possible due to its miniaturized size, low sample requirements, and compatibility with portable reading devices. Also, SPEs do not require tedious cleaning processes and avoid memory effects problems that are present in conventional solid electrodes (Taleat et al. 2014).

SPEs are prepared by layer-by-layer depositions of ink upon a solid substrate by using a mold, stencil, screen, or mesh. This screen-printing technology offers several important advantages, such as design flexibility, process automation, good reproducibility, and a wide choice of materials (Hernandez-Vargas et al. 2018). SPEs provide the opportunity to bring working, counter, and reference electrodes in a single structural unit. Printed on various substrates like plastic, paper, ceramic, or skin substrates, they can be conveniently modified using various inks. Silver and carbon inks are most frequently used in printing while gold, platinum, noble metals, and other inks are also used (Yan et al. 2012; Neves et al. 2012). A schematic diagram of screen printing of electrode is given in Fig. 8.2. The reference electrode track of the electrode is printed using silver ink while working electrodes are printed using graphite and other inks. The selectivity and sensitivity of the electrode are tuned by varying the composition of various inks used for printing. Carbon ink used for dispersion, printing, and adhesion tasks is prepared by graphite particles, polymeric binder, and other additives. It is most commonly used ink due to low-cost,

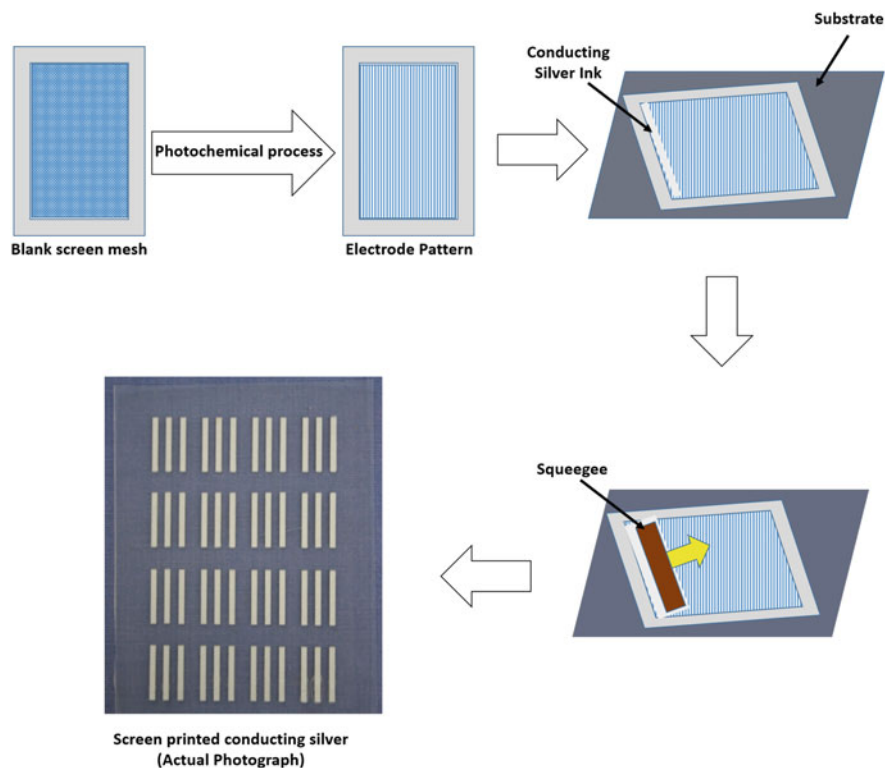


Fig. 8.2 Schematic diagram depicting various steps involved in fabrication of screen-printed electrodes

easy surface modifications, and chemical inertness. The performance of the biosensor and electron transfer reactivity of the electrode is strongly affected by the change in ink compositions such as type, size, or loading of graphite particles and printing and curing conditions. The screen-printed gold electrodes are now gaining increasing importance for the development of enzymatic, immuno, and geno-sensors due to the formation of the self-assembled monolayers (SAMs) through strong Au-S bonds on the electrode surface; however higher cost of gold restricts its application than carbon ink. In addition, the surface of SPEs can be easily modified with different bioreceptors, including DNA, enzymes, antibodies, synthetic recognition elements, and others (Renedo et al. 2007). Some significant work done on SPE has been discussed in the following paragraphs.

The detection of the 3-hydroxybutyrate was performed by using electrochemical biosensor based on the SPEs modified by reduced graphene oxide and thionine (Martínez-García et al. 2017). The biosensor was immobilized with an enzyme 3-hydroxybutyrate dehydrogenase. The amperometric detection due to the generation of NADH from the NAD^+ in the presence of 3-hydroxybutyrate was observed in the linear range of 0.01–0.4 mM and with LOD of 1 μM . The detection from the

spiked human serum samples was also demonstrated with two concentration levels of 0.033 and 0.29 mM with mean recoveries more than 98%. Recently, an immunosensor was developed using SPE for the detection of cancer biomarker human epidermal growth factor receptor-2 (HER2) antigen (Tallapragada et al. 2017). The anti-HER2 capture antibody was immobilized on the sensor surface without any prior surface treatment and then HER2 antigen was added. The detection was then performed in a sandwich format like ELISA by using biotinylated goat anti-human ErbB2 attached to the streptavidin conjugated horseradish peroxidase (HRP) as the detection antibody. The presence of HER2 antigen resulted in enzymatic degradation of the substrate 3,3',5,5'-tetramethylbenzidine (TMB). The linear increase in amperometric signal was observed with increase in antigen concentration with twofold linear range of 5–20 and 20–200 ng/mL, respectively. The values of 4 and 5 ng/mL were reported as the LOD and the LOQ for biosensor. The detection of antigen from real patient samples was also demonstrated.

The electrochemical biosensors have been developed by immobilizing the DNA probe specific to the certain genetic mutations, pathogens (for example, *E. coli* and Salmonella), or specific diseases (for example, herpes simplex virus, Epstein-Barr virus, and cytomegalovirus). DNA detection is done based on the DNA hybridization, which is measured by the electrochemical method. The SPE surface is generally fabricated using a gold-based ink to form well-ordered gold-thiol SAMs using DNA oligos. The different signal amplification strategies involving labeled-probes have been incorporated for DNA detection on the SPE biosensor. There are many studies where direct detection of DNA hybridization does not give the required sensitivity and LOD. Thus, amplification steps are therefore required to achieve very high sensitivity (nano to pico-gram per mL) and low LOD (pico to femto-gram per mL) (Taleat et al. 2014).

The detection of cancer biomarker prostate-specific antigen (PSA) was done on SPE printed by vegetable parchment (Yan et al. 2012). The graphene and HRP-labeled antibody (Ab2) functionalized with gold nanoparticles (GNPs) were used to increase conductivity, stability, surface area, and amplify the electrochemical signal on the SPE biosensor. By using this approach, LOD of 0.46 pg/mL and a wide linear range over six orders of magnitude was seen. Also, the PSA detection from human serum samples displayed acceptable concordance to the commercial turbidimetric immunoassay values.

SPE was also utilized for the multiplexed detection of carcinoembryonic antigen (CEA) and α -fetoprotein (AFP) in a sandwich-type immunoassay method (Lai et al. 2012). The capture antibodies were attached to the chitosan-modified SPEs. In sandwich immunoreactions, GNPs-modified antibodies were captured on the sensor surface, which further induced the silver deposition from a silver enhancer solution. Anodic stripping analysis was performed to detect deposited silver nanoparticles. The wide linear ranges of three orders of magnitude and LOD of 3.5 and 3.9 pg/mL for CEA and AFP, respectively, were obtained using this immunoassay. The detection results from clinical serum samples were in correlation with electrochemiluminescent test.

The multiplex detection of three breast cancer markers, cancer antigens 153 and 125 (CA 153, CA 125) and CEA was performed on a carbon electrode array containing three graphite working SPEs (Ge et al. 2012). Graphene was incorporated to increase the electron transfer efficiency. The capture antibody was immobilized on the GNPs-modified electrode surface. Then secondary antibody labeled with alkaline phosphatase (ALP) was captured on the sensor surface in a sandwich-type reaction and enzymatic hydrolysis of the 3-indoxyl phosphate to an indoxyl intermediate caused the reduction of the silver ions on the electrode surface. This silver deposition was measured by linear sweep voltammetry. The ALP label and silver deposition helped in amplifying the signal with a LOD of 1.5×10^{-3} U/mL for CA 153, 3.4×10^{-4} U/mL for CA 125, and 1.2×10^{-3} ng/mL for CEA.

The multiplex detection of four cancer biomarkers, viz., AFP, CEA, CA 125, and CA 153, were performed on the microfluidic paper-based biosensor by the integration of a signal amplification strategy (Wu et al. 2013). The graphene/chitosan was used to modify eight working electrodes, which had a common counter and reference electrodes and then the modified surface was immobilized with capture antibodies. The various concentrations of the antigen solutions were kept on each working electrode. To perform sandwich immunoreactions, nanobioprobe of monodispersed silica nanoparticles co-immobilized with HRP and antibody were added. The signal amplification was obtained by the application of graphene and silica nanoparticles. A solution containing O-phenylenediamine and hydrogen peroxide (H_2O_2) was added on the paper and the signal was detected by DPV by this paper-based electrochemical sensor. The detection of AFP, CEA, CA 125, and CA 153 was observed in the wide dynamic ranges of 0.001–100 ng/mL (LOD: 0.001 ng/mL), 0.005–100 ng/mL (LOD: 0.005 ng/mL), 0.001–100 ng/mL (LOD: 0.001 ng/mL), and 0.005–100 ng/mL (LOD: 0.005 ng/mL), respectively.

The SPE modified with carbon nanotube (CNT) and GNPs hybrid system was developed for the voltammetric detection of human anti-gliadin antibodies (AGA) IgA and IgG in serum samples specific to celiac disease (Neves et al. 2012). The surface modifications caused the amplification of the immunoreactions. The sensing was based on the gliadin-immobilized nanostructured surface and human autoantibodies. Then anti-human IgA or anti-human IgG antibodies labeled with ALP, and a mixture of 3-indoxyl phosphate with silver ions was incubated on the electrode. The silver deposition on the sensor surface was detected by anodic stripping voltammetry. The biosensor showed a LOD of 9.1 and 9.0 U/mL for AGA IgA and AGA IgG, respectively, with ability of detecting these antibodies in human serum samples.

The detection of the anti-transglutaminase (anti-tTG) IgA and anti-tTG IgG in human serum samples was performed on the array of 8-channel SPEs biosensor modified with a tTG by adsorption (Martín-Yerga and Costa-García 2015; Martín-Yerga et al. 2014). The study used anti-human antibodies labeled with Cd/ZnS quantum dots (QDs) for the immunoassay. The anodic stripping voltammetry was used to detect the Cd^{2+} release from the QDs after an acid attack. This approach allowed the sensitive detection of 2.2 and 2.7 U/mL of anti-tTG IgG and anti-tTG IgA, respectively, on the sensor surface.

The label SPE-based biosensor was developed for the detection of human C-reactive protein (CRP) (De Ávila et al. 2013). The detection was performed in a sandwich format on the surface of carboxylic-modified magnetic beads. The beads were captured on the disposable gold SPE by placing a magnet under the sensor surface. The HRP enzyme (used as a label) catalyzed degradation of the substrate was determined by measuring amperometric response at -0.1 V. This magneto-immunosensor showed a wide linear range of 0.07 – 1000 ng/mL with excellent LOD of 0.021 ng/mL and allowed the detection of CRP from dilute blood serum in the clinically relevant range.

The detection of biologically important mitochondrial metalloprotein cytochrome c (cyt c) containing a prosthetic group (heme) was obtained using SPE immunosensor in label-free manner (Pandiaraj et al. 2014). The polypyrrole (PPy) was electropolymerized on the SPE working electrode and the resulting platform was modified with either GNPs or CNTs incorporated via Nafion on the PPy matrix to enhance the direct electron transfer between the cyt c and the electrode surface. The electrode was then immobilized with a specific monoclonal antibody. The electrochemical immunosensing showed high sensitivity on both platforms; however GNP-based immunosensor (linear range = 2 nM– 150 μ M; LOD = 2 nM; sensitivity = 154 nA/nM) was better than the nanotube-modified platform. The detection of cyt c from cell lysates of cardiomyocytes also gave results in excellent correlation with standard ELISA.

The detection of acute myocardial infarction biomarker cardiac troponin T (cTnT) was performed on the SPEs prepared by adding amine-functionalized CNT into the printing ink during fabrication (Silva et al. 2013). The nonrandom and stable-orientated antibody was immobilized on the surface because of the presence of the amino groups. The CNTs also offered additional advantages of electrochemical properties, which helped in rapid and sensitive detection of cTnT by DPV. The current peak in DPV was decreased with increase in concentrations with a linear range of 0.0025 – 0.5 ng/mL and LOD of 0.0035 ng/mL. Also, the immunosensor showed results comparable to the electrochemiluminescent immunoassay from serum samples.

The SPEs were modified with a layer of citrate-capped GNPs in a one-step electrochemical technique and then immobilized with anti-cardiac troponin I antibody by electrostatic interaction for the label-free detection of the troponin I (Bhalla et al. 2012). The coating of gold layer acted as matrix for immobilization of antibody and as increased transduction properties. The binding of the highly charged nature of antigen caused the charging of SPE surface that was sensed by the capacitive component of the impedance. The biosensor showed LOD of 0.2 ng/mL, one order of magnitude better than ELISA.

The detection of the cancer biomarker CA125 was obtained on the label-free SPEs-based immunosensor (Ravalli et al. 2013). The GNPs were deposited on the electrode and SAM was formed on it by 11-mercaptoundecanoic acid. The anti-CA125 antibody was attached by 3-(3-dimethylaminopropyl)carbodiimide/N-Hydroxysuccinimide (EDC/NHS) linking chemistry. The surface modifications were characterized by CV and EIS. The sensor showed a linear response of electron

transfer resistance to the CA125 concentration in the range of 0–100 U/mL, LOD of 6.7 U/mL and also in serum spiked with CA125.

The SPE was modified with ZnO/Al₂O₃ nanocomposite for the sensitive and selective electrochemical detection of the ascorbic acid (Ganjali et al. 2017). The CV and DPV measurements were obtained for the determination of ascorbic acid on the electrode. The detection was seen in a linear range of 1.0–100 μ M with LOD of 0.6 μ M and from real samples. Acetylcholinesterase (AChE) biosensor was developed by step by step drop casting of dispersion of carbon black, chitosan, and AChE on the SPE (Talarico et al. 2016). This modification showed improved electrochemical response compared to the bare SPE and SPE modified only with chitosan. The enzymatic activity was measured by detecting the product thiocholine at +300 mV. The detection of pollutant paraoxon as a model compound was carried out on the biosensor as organophosphorus pesticides inhibit the AChE activity. The enzymatic inhibition for paraoxon was observed up to a concentration of 0.5 μ g/L and a low detection limit of 0.05 μ g/L. The detection from drinking water spiked with 0.5 μ g/L was also demonstrated with a good recovery value of $97 \pm 15\%$.

8.2.3 Plastic Chip Electrode (PCE)

The major technical bottleneck outstays in screen-printed electrodes is that its conducting layer is not the integral part of the electrode, and hence there is a possibility of its cracking or peeling. PCE is a recent development in electrode technology and is being exploited for various applications in different fields, including electrocatalysis, electrometallurgy, and anodic stripping voltammetry (Mondal et al. 2018; Perween et al. 2014; Perween and Srivastava 2017). Unlike SPE, PCE is a bulk conducting, self-standing composite electrode and hence stave off the major problem of peeling of conducting layer. PCE has also been demonstrated as a platform for ionic liquid-based solid-state reference electrode (Perween and Srivastava 2018). PCE is fabricated by the simple solution casting method at room temperature and without any additional requirement of sophisticated instruments that are generally required in the fabrication of other electrodes (Fig. 8.3). Being a self-standing, highly compact (Fig. 8.4a) composite, it can be cut in a chip of required dimension. A typical thickness of the chip is 450 microns. A random distribution of the conducting filler in the polymer matrix forms percolating channels for the passage of charge. Typically, graphite powder is used as conducting filler for the fabrication of PCE. The random distribution of the graphite into the polymer matrix makes the surface of the PCE rough (Fig. 8.4b), which relatively increases the surface area of the electrode compared to the flat electrodes. This increase in the surface area, therefore, helps in increasing the sensitivity of the biosensors. PCE is also advantageous for biosensing applications due to its low-cost, easy surface modifications, and excellent electrochemical properties.

The PCE-based electrochemical biosensor was designed for the highly sensitive and selective detection of the type (II) diabetes biomarker retinol binding protein 4 (RBP4) (Paul et al. 2019). The detection of RBP4 can be useful in the proper

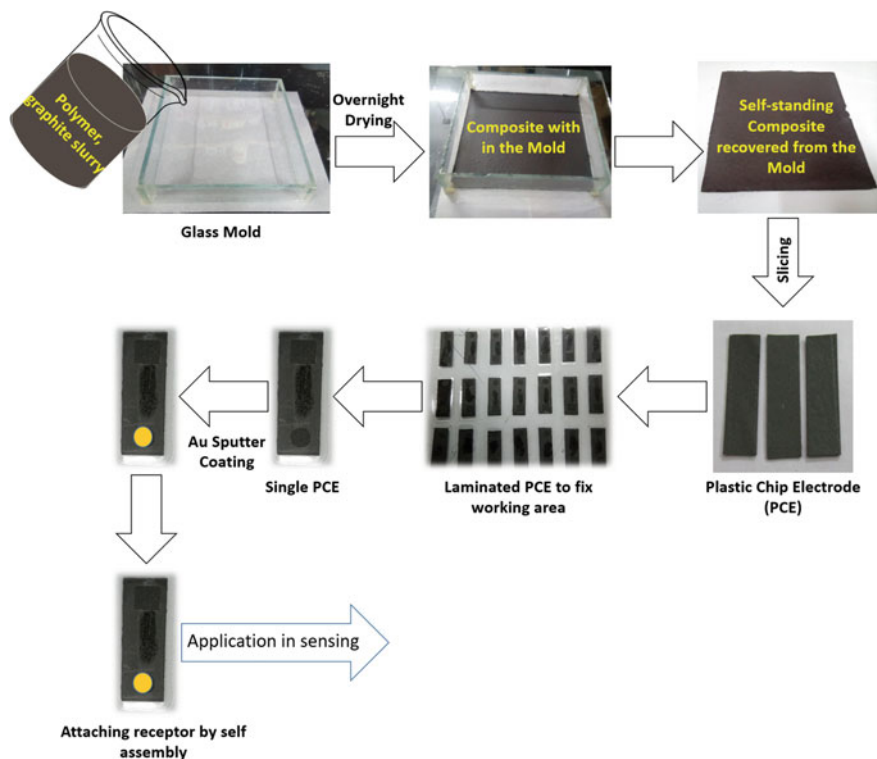


Fig. 8.3 Pictorial representation for making the plastic chip electrode

management of type (II) diabetes at early stage. The working area of PCE was sputter coated with a gold layer of 10 nm in order to immobilize the bioreceptor via SAMs of thiols. The surface was first modified with 4-aminothiophenol and then glutaraldehyde. The anti-RBP 4 antibody was attached to the electrode and EIS measurements were performed. The formation of Ag-Ab complex caused the increase in impedance in a wide concentration range of 100 fg/mL to 1 ng/mL and a detection limit of 100 fg/mL. The interference study using two proteins IgG and Vaspin was also conducted, which showed negligible interference on the PCE biosensor.

8.3 Porous Material-Based Biosensor

Porous platforms such as NAA, PSi, MPS, and porous polymers offer several advantages in comparison to the flat electrodes for biosensing applications (Reta et al. 2018). These platforms offer a very high surface area to volume ratio due to the porous structure and the easy surface modification ability. Due to the high surface area, a large number of bioreceptor molecules can be immobilized on the electrode,

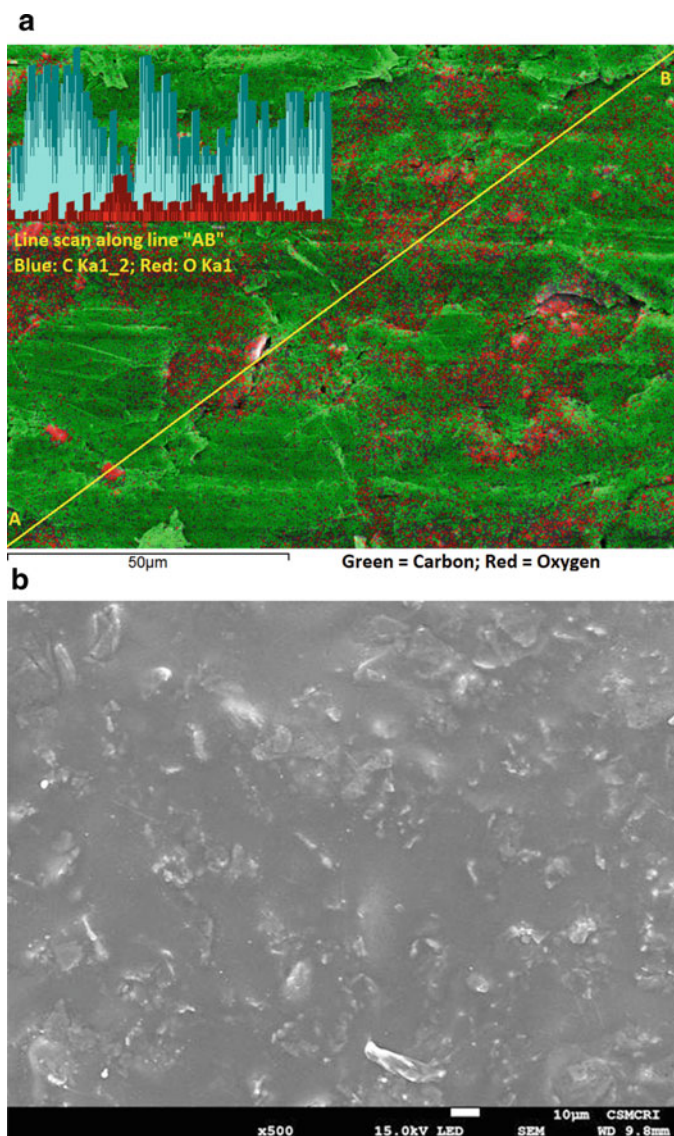


Fig. 8.4 (a) SEM elemental mapping of the cross-section of plastic chip electrode showing highly compact morphology (Inset: line profile along the line “AB”); (b) Surface SEM morphology showing rough surface area

which in turn increases the sensitivity of the biosensing device. The surface chemistry of the materials can be modified by grafting different molecules for the stability and attachment of the bioreceptor. Further, the pore size of the porous materials can be optimized for specific analyte sensing and also to filter out interfering molecules from the target sample. The specific binding of bioreceptor and biomolecule can be

sensed by various electrochemical techniques like potentiometry, amperometry, conductometry, or impedometry. With these advantageous properties, porous materials have shown great potential for electrochemical biosensing. Here, in this section, we will describe biosensing studies based on the nanoporous anodic alumina (NAA), porous silicon (PSi), mesoporous silica (MPS), and porous polymers (Table 8.1).

8.3.1 Nanoporous Anodic Alumina (NAA)

NAA has been exploited for a range of applications in drug delivery, biosensing, cell adhesion, cell growth, molecular separation, catalysis, solar cells, and energy storage. It is fabricated by anodization of high-purity aluminum in acidic solution by applying a specific voltage, which makes homogeneously distributed and self-ordered porous structure. The pore size, interpore distance, pore length, barrier layer thickness, and wall thickness of NAA can be optimized by varying anodization conditions including type of electrolyte, electrolyte composition, temperature, anodization voltage, current, and time. NAA of different geometric properties can be designed including pore diameter of 10–400 nm, interpore distance of 50–900 nm, porosity of 5–50%, pore density of 10^9 – 10^{11} pores/cm², and pore length of 10 nm to several hundreds of μm . The pretreatment of alumina is done by electropolishing, which makes a smooth surface to be used in the formation of long-range pore order (Rajeev et al. 2018).

The surface functionalization of the NAA is done to impart stability in acidic environment and to immobilize bioreceptor molecules specific to the target analyte for biosensing applications. Different modification strategies are explored for this purpose, including chemical and gas phase techniques. Among this, a self-assembling organosilane molecule with desired functional groups is most frequently used for biosensor development (Hasan et al. 2018; Pandey et al. 2013). The NAA is first treated with H_2O_2 to activate the hydroxyl groups, which allows the attachment of silane on the surface. The bioreceptor is then immobilized either directly to the self-assembled silane or through cross-linker such as glutaraldehyde. The second approach involves the functionalization of gold-coated NAA using alkane thiols, which form spontaneous SAMs. Another method for modification is a simple, inexpensive layer-by-layer assembly of polyelectrolyte multilayers on the surface (Krismastuti et al. 2015). Also, deposition of different metals such as gold, silver, platinum, nickel, palladium, cobalt, and titanium by thermal deposition and sputter coating are used to improve conductivity, as well as its optical, magnetic, and electrochemical properties.

NAA has several unique and interesting optical (reflectance, transmittance, chemiluminescence, and photoluminescence) and electrochemical (EIS, amperometry, voltammetry, and capacitance) properties for biosensor development. The material is stable under environmental conditions and chemically inert, which helps in detecting biomolecules in complex fluids without surface degradation and ensures long shelf life. Further, NAA can be fine-tuned to make specific pore size

Table 8.1 Selected literature reports, utilizing non-porous and porous materials based electrode platforms for electrochemical biosensing

Analyte	Bioreceptor	Transducer	Detection range	LOD	References
Ascorbic acid, dopamine, and uric acid	NA	GCE modified with MoS ₂ and reduced graphene oxide	12–5402, 5–545, and 25–2745 μ M	0.72, 0.05, and 0.46 nM	Xing and Ma (2016)
Caffeic acid	NA	Carbon modified GCE	0.01–350 μ M	0.0024 μ M	Karikalan et al. (2017)
Salmonella bacteria	Amino modified aptamer	rGO-MWCNTs modified GCE	$75\text{--}7.5 \times 10^5$ cfu/mL	25 cfu/mL	Jia et al. (2016)
Ascorbic acid, dopamine, and uric acid	NA	GCE with fullerene (C60) and platinum nanosheets	10–1800, 0.5–211.5, and 9.5–1187 μ M	0.43, 0.07, and 0.63 μ M	Zhang et al. (2015)
Paracetamol, tramadol, and caffeine	NA	GCE modified with poly(Nile blue)	2.0×10^{-7} – 1.62×10^{-5} M, 1.0×10^{-6} – 3.1×10^{-4} M, and 8.0×10^{-7} – 2.0×10^{-5} M	0.08, 0.5, and 0.1 μ M	Chitravathi and Munichandraiah (2016)
Tryptophan	NA	AgNPs/MIL-101 modified GCE	1–50 and 50–150 μ M	0.14 μ M	Peng et al. (2016)
Hydroquinone and catechol	NA	GCE modified with ammonium carbamate	5–260 μ M	0.2 μ M	Wang et al. (2016)
Uric acid	NA	GCE modified with Fe ₃ O ₄ onto graphene sheets and SiO ₂ layer	0.5–250 μ M	0.07 μ M	Movlaee et al. (2017)
Doxorubicin	NA	GCE coated with graphene QDs	0.018–3.6 μ M	0.016 μ M	Hashemzadeh et al. (2016)
3-Hydroxybutyrate	3-Hydroxybutyrate dehydrogenase	SPEs modified by rGO and thionine	0.01–0.4 mM	1 μ M	Martínez-García et al. (2017)
Human epidermal growth factor receptor-2	Anti-HER2 capture antibody	SPE	5–20 and 20–200 ng/mL	4 ng/mL	Tallapragada et al. (2017)

(continued)

Table 8.1 (continued)

Analyte	Bioreceptor	Transducer	Detection range	LOD	References
Prostate-specific antigen (PSA)	Capture antibody	Graphene and gold nanoparticles modified SPE	0.002–2 µg/mL	0.46 pg/mL	Yan et al. (2012)
CEA and AFP	Capture antibody	Chitosan modified SPE	5.0 pg/mL–5.0 ng/mL	3.5 and 3.9 pg/mL	Lai et al. (2012)
CA 153, CA 125, and CEA	Capture antibody	SPE modified by GNP _s	5.0×10^{-3} –50 U/mL, 1.0×10^{-3} –100 U/mL, and 4.0×10^{-3} –200 ng/mL	1.5×10^{-3} U/mL, 3.4×10^{-4} U/mL, and 1.2×10^{-3} ng/mL	Ge et al. (2012)
AFP, CEA, CA 125, and CA 153	Capture antibody	Graphene/chitosan modified SPE	0.001–100, 0.005–100, 0.001–100, and 0.005–100 ng/mL	0.001, 0.005, 0.001, and 0.005 ng/mL	Wu et al. (2013)
Human anti-gliadin antibodies IgA and IgG	Gliadin	SPE modified with CNT and GNP _s	NA	9.1 and 9.0 U/mL	Neves et al. (2012)
Anti-transglutaminase IgA and IgG	Transglutaminase	SPE	3–40 and 0–40 U/mL	2.7 and 2.2 U/mL	Martín-Yerga and Costa-García (2015) and Martín-Yerga et al. (2014)
Human C-reactive protein	Capture antibody	SPE	0.07–1000 ng/mL	0.021 ng/mL	De Ávila et al. (2013)
Cytochrome c	Monoclonal antibody	SPE modified with GNP _s or CNT _s	2 nM–150 µM (GNP _s)	2 nM	Pandiaraj et al. (2014)
Cardiac troponin T	Antibody	SPE _s prepared by adding amine-functionalized CNT	0.0025–0.5 ng/mL	0.0035 ng/mL	Silva et al. (2013)

Troponin I	Troponin I antibody	SPE modified with citrate-capped GNPs	0.2–12.5 ng/mL	0.2 ng/mL	Bhalla et al. (2012)
CA125	Anti-CA125 antibody	SPE modified with GNP	0–100 U/mL	6.7 U/mL	Ravalli et al. (2013)
Ascorbic acid	NA	SPE modified with ZnO/Al ₂ O ₃ nanocomposite	1.0–100 µM	0.6 µM	Ganjali et al. (2017)
Paraoxon	Acetylcholinesterase	SPE modified with carbon black and chitosan	0.1–0.5 µg/L	0.05 µg/L	Talarico et al. (2016)
Retinol binding protein 4 (RBP4)	Anti-RBP 4 antibody	Gold-coated PCE	100 fg/mL–1 ng/mL	100 fg/mL	Paul et al. (2019)
DNA	ssDNA	NAA	50 pM–3.8 nM	50 pM	Ye et al. (2014)
DNA	ssDNA	NAA	500–12.5 nM	12.5 nM	Wu et al. (2015)
Single nucleotide polymorphisms	DNA	NAA	2 µM	2 µM	Gao et al. (2015)
West Nile Virus	Antibody	NAA	53–4 pg/mL	4 pg/mL	Nguyen et al. (2009)
DENV-2	Anti-DENV-2 antibody	NAA	1–10 ³ pfu/mL	1 pfu/mL	Cheng et al. (2012)
Dengue-specific DNA sequence	DNA	NAA	1 × 10 ⁻¹² –1 × 10 ⁻⁶ M	2.7 × 10 ⁻¹² M	Deng and Toh (2013)
DENV-2 and DENV-3	2H2 antibody	NAA	1–900 pfu/mL	0.23 and 0.71 pfu/mL	Peh and Li (2013)
<i>E. coli</i> O157:H7	Antibody	NAA	10–10 ⁵ cfu/mL	10 cfu/mL	Joung et al. (2013)
<i>E. coli</i> O157:H7	Antibody	NAA	10 ⁰ –10 ⁴ cfu/mL	10 cfu/mL	Chan et al. (2013)
<i>E. coli</i> O157:H7 and <i>S. aureus</i>	Antibody	NAA	10 ² –10 ⁵ cfu/mL	10 ² cfu/mL	Tian et al. (2016)
CA15-3	Antibody	NAA	60–240 U/mL	52 U/mL	De la Escosura-Muniz and Merkoçi (2011)

(continued)

Table 8.1 (continued)

Analyte	Bioreceptor	Transducer	Detection range	LOD	References
MS2 bacteriophage	Antibody	PSi	1–10 ¹⁰ pfu/mL	6 pfu/mL	Reta et al. (2016)
Hyaluronidase	Hyaluronic acid methacrylate	PSi	0–5 mg/mL	NA	Tucking et al. (2018)
Glucose	NA	PSi with nickel nanoparticles on carbon paste electrode	2–5000 µmol/L	0.2 µmol/L	Ensafi et al. (2017)
CEA and AFP	Anti-CEA and anti-AFP antibody	MPS on ITO electrode	0.5–45 and 1–90 ng/mL	0.2 and 0.5 ng/mL	Lin et al. (2011)
AFP	Anti-AFP antibody	Graphene sheets and antibody-immobilized MPS on the GCE	0.1–100 ng/mL	0.06 ng/mL	Lin et al. (2013)
AFP	Anti-AFP antibody	MPS on GCE	1–90 ng/mL	0.2 ng/mL	Lin et al. (2012)
AFP	Anti-AFP antibody	MPS SBA-15	1–150 ng/mL	0.8 ng/mL	Lin et al. (2009)
Streptomycin	Aptamer	MPS film on the gold electrode	1 fg/mL–6.2 ng/mL	0.33 fg/mL	Roushani and Ghanbari (2019)
PSA	Aptamer	MPS film on the gold electrode	1–300 ng/mL	280 pg/mL	Argoubi et al. (2018)
IgG	Anti-IgG antibody	Polystyrene nanospheres on the ITO electrode	1–300 µg/mL	580 ng/mL	De La Escosura-Muñiz et al. (2015)
AFP	Anti-AFP antibody	Macroporous polyamine	0.01–1000 pg/mL	3.7 fg/mL	Liu et al. (2018)
Glucose	Glucose oxidase	Polystyrene-block-poly(4-vinyl pyridine) film	10–4500 µM	0.05 µM	Guo et al. (2018)

NA not available

that filter out large biomolecules, which reduces interference effect and biofouling. Also, the biocompatibility of this platform makes it attractive for biosensor development.

DNA detection was performed on NAA biosensor using the electrochemical method. The sensing was based on DNA hybridization of target sequences with immobilized complementary ssDNA in pores of the sensor (Vlassioux et al. 2005). The detection involved measurement techniques like CV, EIS, and direct current conductance. The DNA hybridization caused the partial blockage of the pores that resulted in limiting the diffusion of electroactive species toward the electrode. The pore size has a significant effect on sensing. Significant sensing was observed with 20 nm pores and it was completely vanished for 200 nm pores. A further, similar label-free electrochemical biosensor based on the NAA membrane having a 5'-aminated DNA probe was fabricated for the detection of 21mer DNA. The LOD of 3.1×10^{-13} M was reported with high selectivity demonstrated using sequences of single base mismatch and triple bases mismatch of a different strain of *Legionella* species (Rai et al. 2012).

NAA membrane-based impedance sensing was reported for rapid and sensitive DNA detection using additional amplification by GNP tags (Ye et al. 2014). The ssDNA was immobilized on the nanopores through linkers and the pore blockage caused by the DNA hybridization event was measured by EIS. The LOD of 50 pM was achieved after the amplification of detection signal by GNPs. A similar impedance biosensor for DNA detection was developed; however, the NAA membrane was fabricated at wafer-scale of well-controlled thickness, pore diameter, and overall pore density (Wu et al. 2015). The coating of silica nanoparticles (~ 20 nm) on the membrane was performed to increase the total surface area. Then ssDNA was immobilized to the (3-glycidioxypropyl) trimethoxysilane functionalized surface. The selectivity was demonstrated using non-complementary ssDNA and LOD of 12.5 nM was shown in phosphate-buffered saline solution.

The detection of single nucleotide polymorphisms (SNPs) is highly important for disease diagnosis and prevention. The NAA-based electrochemical biosensor was designed for the easy, label-free, and highly selective detection of SNPs. The nanochannels of the sensor were functionalized with a probe DNA/morpholino duplex and the diffusion flux of ferricyanide probe was monitored electrochemically. The sensing mechanism was based on the competitive binding of matched DNA and morpholino to the probe DNA, which causes a change of the surface charges. This approach helped in the detection of not only a single base or two base mismatched sequences but also the specific location of the mismatched base. Also, the detection of SNPs was demonstrated in the acute promyelocytic leukemia biomarker PML/RAR α fusion gene (Gao et al. 2015).

The NAA biosensor has been prepared for different virus detection, including West Nile Virus (WNV) and dengue. The detection of whole WNV particles was performed on the NAA membrane over a platinum disk electrode (Nguyen et al. 2009). The nanochannels of sensor were immobilized with an anti-WNV protein domain III (DIII) IgM antibody capture probe via physical adsorption. The detection signal was monitored based on the electrode's Faradaic current response toward

ferrocenemethanol during the formation of immunocomplex in the nanopores. The sensor was studied for detection of both WNV-DIII and the inactivated West Nile viral particle. The biosensor displayed sensitivities comparable to the polymerase chain reaction (PCR) techniques with low detection limit of 4 pg/mL and detection time of 30 min. The detection of WNV particles from whole blood was also demonstrated with relative standard deviation (RSD) of 6.9 %.

Several studies were performed for the detection of dengue virus on the NAA biosensor. The detection of dengue type 2 virus (DENV-2) was performed on the NAA-modified platinum electrode (Cheng et al. 2012). A sensing mechanism of monitoring of electrode's Faradaic current response toward redox probe was incorporated in this study as well. The immunocomplex formation between immobilized anti-DENV-2 monoclonal antibody and DENV-2 was characterized by DPV. The NAA biosensor showed detection in the range of 1–10³ pfu/mL and LOD of 1 pfu/mL with insignificant binding to the nonspecific viruses including Chikungunya virus, WNV, and dengue type 3 virus (DENV-3). In a different approach, detection of dengue-specific DNA sequence was performed by immobilizing the DNA probe sequence on the NAA (Deng and Toh 2013). The membrane was sputter-coated on both the sides by platinum electrode. The DNA hybridization in the nanochannels caused the partial blockage of ferrocyanide redox species to the platinum electrode, which was measured by EIS. A linear increase in pore resistance was observed with increase in target DNA concentration in the range of 1 × 10⁻¹² to 1 × 10⁻⁶ M. Also, the biosensor showed excellent selectivity being able to differentiate the complementary sequence from single base mismatched and non-complementary sequence with LOD of 2.7 × 10⁻¹² M. EIS method was also used in another study for the detection of dengue on NAA membrane of 60 μm thick and 13 mm in diameter. The membrane was coated with a submicron layer of platinum to use as both the working and the counter electrode. The pore resistance was changed according to the concentration of the DENV-2 and DENV-3. The detection time of 40 min and LOD of 0.23 and 0.71 pfu/mL was observed for DENV-2 and DENV-3, respectively (Peh and Li 2013).

The detection of bacteria *E. coli*, *S. aureus*, and *Legionella pneumophila* has been done on NAA biosensor. The impedimetric immunosensor was fabricated for the label-free detection of harmful food-borne pathogenic bacteria *E. coli* O157:H7 from whole milk (Joung et al. 2013). The hyaluronic acid was used to reduce the nonspecific binding of biomolecules and other cells on the sensor. The detection was observed in the range of 10–10⁵ cfu/mL with LOD of 10 cfu/mL based on the antibody-bacteria interactions. Further study on detection of bacteria from whole milk showed LOD of 83.7 cfu/mL. The nontarget bacteria such as *S. aureus*, *B. cereus*, and nonpathogenic *E. coli* DH5α were used to display high specificity of the sensor.

The ultrasensitive detection of *E. coli* O157:H7 was also investigated on the NAA membrane by using specific antibody-modified magnetic beads to enhance sensitivity. The membrane was immobilized with antibody via assembled polyethylene glycol (PEG)-silane linker and then the beads attached with bacterial cells were captured on the membrane. The binding of pure cells and magnetic bead-attached

cells to the antibody-immobilized membrane with or without the magnetic field was monitored by EIS. The magnetic bead-based cell concentration approach displayed ultrasensitive detection of 10 cfu/mL (Chan et al. 2013). The simultaneous detection of *E. coli* O157:H7 and *S. aureus* was reported based on the NAA membranes integrated with a microfluidic device. The non-biofouling PEG was used to make microfluidic chip. The biosensor showed a linear detection range of 10^2 – 10^5 cfu/mL with LOD around 10^2 cfu/mL and low cross-binding of nontarget bacteria (Tian et al. 2016). NAA biosensors with varied pore size and thickness were prepared depending on the size of the target species such as virus or bacteria.

The NAA biosensor was developed for the detection of cancer biomarker CA15-3 (De la Escosura-Muñiz and Merkoçi 2011). The nanochannel allowed the filtering of the interfering molecules and detection of proteins in buffer as well as in whole blood. For this, conductivity of antibodies attached membrane toward redox indicator was tuned by primary and secondary immunoreactions with proteins and GNPs. Further, silver deposition was used to enhance the nanopore blockage by GNPs, which decreased the diffusion of the signaling indicator through the nanochannel. The detection of CA15-3 up to 52 U/mL was obtained using this immunoassay.

8.3.2 Porous Silicon (PSi)

PSi has been widely accepted material with demonstrated potential in diverse biomedical applications such as biosensing, bioimaging, biomolecular screening, tissue engineering, and drug delivery (Maniya et al. 2015). This is due to the several unique physicochemical and optical properties of the PSi. The key properties of PSi for electrochemical biosensing applications are simple and easy fabrication, high surface area, various surface modifications opportunities, tunability of pore size, porosity and thickness, and biocompatibility. The PSi material can be fabricated by electrochemical etching of silicon wafer in hydrofluoric acid-based solution. The surface of PSi can be easily modified by well-established modification methods including the oxidation, hydrosilylation, silanization, and thermal carbonization (Maniya et al. 2016). The bioreceptor molecules such as antibody, aptamer, enzyme, peptide, DNA, or RNA can be attached to this modified surface. The excellent biocompatibility, biodegradability, and non-toxicity of PSi has been used for the real-time, in vivo biosensing and as implantable device applications. The electrochemical biosensing using PSi is less studied in comparison to the optical sensing. The mechanism for PSi electrochemical biosensing is the change in current and resistance that occurs due to the pore blockage when analyte binds to the receptor.

The label-free electrochemical detection of MS2 bacteriophage has been performed on PSi membrane-based biosensor (Reta et al. 2016). The sensing mechanism for biosensor was based on the nanochannel blockage that occurs when the bacteriophage binds to the immobilized capture antibodies which causes the decrease in oxidation current of the electroactive species. PSi membranes of different pore sizes (85, 57, and 40 nm) were fabricated by varying current density during etching process. The detached membrane was then transferred to the gold

slide and further modified with thermal hydrosilylation and EDC/NHS chemistry to immobilize anti-MS2 antibody. DPV-based measurements showed LOD of 6 pfu/mL in buffer and 17 pfu/mL in MS2 spiked in reservoir water samples for largest pore size PSi sensor.

The detection of bacterial enzyme hyaluronidase is also performed on hyaluronic acid-modified PSi electrochemical biosensor (Tucking et al. 2018). For this, hyaluronic acid methacrylate and PEG diacrylate polymers were coated on the thermally hydrocarbonized PSi surface. The presence of enzyme caused the degradation of hyaluronic acid methacrylate. The PSi biosensor showed concentration-dependent decrease in oxidation current as measured with DPV in both buffer and complex media such as bacterial supernatant and artificial wound fluid. A nonenzymatic glucose sensing using PSi electrochemical biosensor is also reported (Ensafi et al. 2017). PSi and nickel nanoparticle-based composite was prepared by in situ electroless assembly method. A sensor was fabricated based on carbon paste electrode having different amounts of PSi-Ni nanocomposite. The glucose detection in linear range of 2–5000 $\mu\text{mol/L}$ and a low LOD of 0.2 $\mu\text{mol/L}$ was observed with high stability, selectivity, and fast response time.

8.3.3 Mesoporous Silica (MPS)

MPS is another important porous material that has been studied for biosensor development due to its important characteristics. The MPS can be fabricated with very high surface area (up to 1500 m^2/g) and controllable channel diameter of 2–50 nm and shape. The fabrication of porous structure is done by using either nanoparticles or surfactant self-assembly as templates and then removal of these templates. The fabricated porous structure allows easy functionalization based on its hydroxyl-terminated surface.

A label-free MPS-based biosensor was fabricated for the simultaneous multiplexed detection of two tumor markers, including CEA and AFP (Lin et al. 2011). The MPS channels were co-immobilized with anti-CEA monoclonal antibody and ferrocenecarboxylic acid for label-free CEA detection. While anti-AFP monoclonal antibody and HRP were immobilized as a capture probe for AFP. The immunoassay reaction confined the antigens and substrates into the internal pore walls as the external surface of MPS were blocked. The nonconductive immunocomplex blocked the electron transfer, which was measured by the electrochemical method. This biosensor allowed the simultaneous detection of CEA and AFP with the detection limits of 0.2 and 0.5 ng/mL, respectively.

The fabrication of single-wall CNTs inside the channels of MPS was reported for the sensitive detection of AFP (Lin et al. 2013). The internal pore walls of MPS were attached with amino groups via its silanol groups, whereas external surface groups were blocked by trimethylchlorosilane (TMCS). These surface modifications allowed the covalent binding of the CNTs and anti-AFP antibodies inside the mesopores of MPS. The sensing electrode was fabricated using a layer-by-layer assembly of graphene sheets and antibody-immobilized MPS on the GCE. The

sensing based on the decrease in peak current due to the immunocomplex formation gave AFP detection in a linear range of 0.1 to 100 ng/mL with a LOD of 0.06 ng/mL. A similar strategy for AFP detection was used based on the MPS and GNPs (Lin et al. 2012). Aminopropyltriethoxysilane was used for the surface modification of the silanol groups on the internal pore walls while TMCS was used for the blocking of the silanol groups on the external surface of MPS. Then GCE was modified with MPS having anti-AFP antibody and GNPs confined inside the mesopores. This approach allowed the AFP detection in a range of 1 to 90 ng/mL with a detection limit of 0.2 ng/mL.

The MPS SBA-15 based immunoassay channeling sensor was designed for the sensitive detection of the AFP by immobilizing the ALP-labeled antibody as a biosensing element inside the mesopores. In order to increase the film adherence and prevent the leakage of antibody, ionic liquid-chitosan hybrid was used. The attachment of AFP to the anti-AFP antibody caused immunocomplex formation and the ALP-based catalysis of the substrate of 1-naphthyl phosphate. The peak current was decreased due to nanochannel blockage caused by nonconductive immunoconjugates. The detection of AFP in a range of 1–150 ng/mL and detection limit of 0.8 ng/mL was reported using this biosensor (Lin et al. 2009).

The electrochemical detection of streptomycin was performed on the MPS film coated on the gold electrode (Roushani and Ghanbari 2019). The coating of the silver nanoparticles on the MPS was used to increase the surface area, improve the electrical conductivity, and to bind a high degree of bioreceptor aptamer. The diffusion of hexacyanoferrate redox probe was hindered due to the binding of the streptomycin to the aptamer in the nanochannels of mesoporous film. The sensor showed a response in the 1 fg/mL to 6.2 ng/mL streptomycin concentration range and LOD of 0.33 fg/mL. The biosensing platform was also validated in milk and blood serum samples spiked with streptomycin.

Similar MPS thin film-based label-free aptasensor was designed for the detection of cancer marker PSA (Argoubi et al. 2018). The film was coated on the gold electrode and anti-PSA-specific DNA aptamer was covalently attached onto the outer surface of the silica nanopores. The detection of PSA in the range of 1–300 ng/mL and a detection limit of 280 pg/mL was demonstrated with high specificity, reproducibility, and storage stability. PSA detection from spiked artificial urine samples and in blood serum from a prostate cancer-free male patient was also validated. Also, depending on the surface chemistry and nanoconjugates used, the MPS can be recycled and reused by varying environment conditions such as high temperature and strong acid conditions (Hasan and Pandey 2016).

8.3.4 Porous Polymers

Porous polymers have been studied for the development of electrochemical biosensors. The electrochemical sensing was performed on nanochannel arrays of polystyrene nanospheres that were formed by the self-assembly method (De La Escosura-Muñiz et al. 2015). Porous polystyrene-based biosensor was designed

for the detection of IgG by immobilizing the anti-IgG antibody on the carboxyl-terminated nanospheres by EDC/NHS chemistry. The sensor development involved the fabrication of the polystyrene on the indium tin oxide (ITO) electrode and then screen printing onto a polyethylene terephthalate substrate. The well-ordered interparticle space or nanochannels were generated due to the assembly of nanospheres. The nanosphere sizes of 200 and 500 nm having a nanochannel diameter of 24 and 65 nm, respectively, were used in the study. The blocking of the diffusion of the redox probe in nanochannels was caused due to the immunocomplex formation by the binding of the IgG to the immobilized anti-IgG antibody, which resulted in decrease in DPV signal. A high specificity and LOD of 580 ng/mL were obtained using 200 nm nanospheres. Further, the IgG detection from human urine samples was also better compared to the previous reports using a nanochannel blockage approach based on NAA substrates.

The selective and sensitive detection of AFP was performed on the macroporous polyaniline doped with poly(sodium 4-styrene sulfonate) (Liu et al. 2018). The electrochemical biosensor showed high conductivity and large surface area and allowed the attachment of anti-AFP antibodies. The biosensor showed a reagentless AFP detection in a wide linear range of 0.01–1000 pg/mL and a detection limit of 3.7 fg/mL. The sensitivity of biosensor was two times higher in comparison to the planar polyaniline-modified electrode.

The biosensors based on the enzymes are studied tremendously. To develop enzymatic biosensors, the electrodes are required to immobilize the enzyme and fast electron transfer between the active sites of enzyme and electrode surface should occur. Specifically, porous electrodes can be highly beneficial due to their high surface area and fast electron transfer. Block copolymers allow the design of different hierarchically porous structures and tuning of the pore shapes and sizes by selectively etching the domains forming by a specific block(s). The prepared porous block copolymer showed both micropores and nanopores by macro- and meso-phase separation that was induced by spinodal decomposition. Then, the glucose oxidase enzyme was immobilized on the porous film. The detection of glucose in a range of 10–4500 μM was demonstrated with LOD of 0.05 μM and a response time of 2 s. Thus, it was reported that the block copolymer film could be used for immobilization of the enzyme and to develop novel high performance biosensor (Guo et al. 2018).

References

- Argoubi W, Sánchez A, Parrado C, Raouafi N, Villalonga R (2018) Label-free electrochemical aptasensing platform based on mesoporous silica thin film for the detection of prostate specific antigen. *Sens Actuators B Chem* 255:309–315
- Bhalla V, Carrara S, Sharma P, Nangia Y, Suri CR (2012) Gold nanoparticles mediated label-free capacitance detection of cardiac troponin I. *Sens Actuators B Chem* 161:761–768
- Biosensors Market Report. 2019. <https://www.marketsandmarkets.com/PressReleases/biosensors.asp>. Accessed 10 May 2019

- Chan KY, Ye WW, Zhang Y, Xiao LD, Leung PHM, Li Y, Yang M (2013) Ultrasensitive detection of *E. coli* O157: H7 with biofunctional magnetic bead concentration via nanoporous membrane based electrochemical immunosensor. *Biosens Bioelectron* 41:532–537
- Cheng MS, Ho JS, Tan CH, Wong JPS, Ng LC, Toh CS (2012) Development of an electrochemical membrane-based nanobiosensor for ultrasensitive detection of dengue virus. *Anal Chim Acta* 725:74–80
- Chitravathi S, Munichandraiah N (2016) Voltammetric determination of paracetamol, tramadol and caffeine using poly (Nile blue) modified glassy carbon electrode. *J Electroanal Chem* 764:93–103
- Clark LC Jr, Lyons C (1962) Electrode systems for continuous monitoring in cardiovascular surgery. *Ann NY Acad Sci* 102:29–45
- Das P, Das M, Chinnadayala SR, Singha IM, Goswami P (2016) Recent advances on developing 3rd generation enzyme electrode for biosensor applications. *Biosens Bioelectron* 79:386–397
- De Ávila BEF, Escamilla-Gómez V, Campuzano S, Pedrero M, Salvador JP, Marco MP, Pingarrón JM (2013) Ultrasensitive amperometric magnetoimmunosensor for human C-reactive protein quantification in serum. *Sens Actuators B Chem* 188:212–220
- De la Escosura-Muñiz A, Merkoçi A (2011) A nanochannel/nanoparticle-based filtering and sensing platform for direct detection of a cancer biomarker in blood. *Small* 7:675–682
- De La Escosura-Muñiz A, Espinoza-Castañeda M, Hasegawa M, Philippe L, Merkoçi A (2015) Nanoparticles-based nanochannels assembled on a plastic flexible substrate for label-free immunosensing. *Nano Res* 8:1180–1188
- Deng J, Toh CS (2013) Impedimetric DNA biosensor based on a nanoporous alumina membrane for the detection of the specific oligonucleotide sequence of dengue virus. *Sensors* 13:7774–7785
- Ensaifi AA, Ahmadi N, Rezaei B (2017) Nickel nanoparticles supported on porous silicon flour, application as a non-enzymatic electrochemical glucose sensor. *Sens Actuators B Chem* 239:807–815
- Ganjali MR, Nejad FG, Beitollahi H, Jahani S, Rezapour M, Larijani B (2017) Highly sensitive voltammetric sensor for determination of ascorbic acid using graphite screen printed electrode modified with ZnO/Al₂O₃ nanocomposite. *Int J Electrochem Sci* 12:3231–3240
- Gao HL, Wang M, Wu ZQ, Wang C, Wang K, Xia XH (2015) Morpholino-functionalized nanochannel array for label-free single nucleotide polymorphisms detection. *Anal Chem* 87:3936–3941
- Ge S, Yu F, Ge L, Yan M, Yu J, Chen D (2012) Disposable electrochemical immunosensor for simultaneous assay of a panel of breast cancer tumor markers. *Analyst* 137:4727–4733
- Guo T, Gao J, Qin X, Zhang X, Xue H (2018) A novel glucose biosensor based on hierarchically porous block copolymer film. *Polymers* 10:723
- Hasan A, Pandey LM (2016) Kinetic studies of attachment and re-orientation of octyltriethoxysilane for formation of self-assembled monolayer on a silica substrate. *Mat Sci Eng C* 68:423–429
- Hasan A, Saxena V, Pandey LM (2018) Surface functionalization of Ti6Al4V via self-assembled monolayers for improved protein adsorption and fibroblast adhesion. *Langmuir* 34:3494–3506
- Hashemzadeh N, Hasanzadeh M, Shadjou N, Eivazi-Ziaei J, Khoubnasabjafari M, Jouyban A (2016) Graphene quantum dot modified glassy carbon electrode for the determination of doxorubicin hydrochloride in human plasma. *J Pharm Anal* 6:235–241
- Hernandez-Vargas G, Sosa-Hernández J, Saldarriaga-Hernandez S, Villalba-Rodríguez A, Parra-Saldivar R, Iqbal H (2018) Electrochemical biosensors: A solution to pollution detection with reference to environmental contaminants. *Biosensors* 8:29
- Jia F, Duan N, Wu S, Dai R, Wang Z, Li X (2016) Impedimetric *Salmonella* aptasensor using a glassy carbon electrode modified with an electrodeposited composite consisting of reduced graphene oxide and carbon nanotubes. *Microchim Acta* 183:337–344

- Joung CK, Kim HN, Lim MC, Jeon TJ, Kim HY, Kim YR (2013) A nanoporous membrane-based impedimetric immunosensor for label-free detection of pathogenic bacteria in whole milk. *Biosens Bioelectron* 44:210–215
- Kadefors R, Reswick JB, Martin RL (1970) A percutaneous electrode for long-term monitoring of bio-electrical signals in humans. *Med & Biol Eng* 8:129–135
- Karikalan N, Karthik R, Chen SM, Chen HA (2017) A voltammetric determination of caffeic acid in red wines based on the nitrogen doped carbon modified glassy carbon electrode. *Sci Rep* 7:45924
- Krismastuti FSH, Pace S, Voelcker NH (2014) Porous silicon resonant microcavity biosensor for matrix metalloproteinase detection. *Adv Funct Mater* 24:3639–3650
- Krismastuti FSH, Bayat H, Voelcker NH, Schönherr H (2015) Real time monitoring of layer-by-layer polyelectrolyte deposition and bacterial enzyme detection in nanoporous anodized aluminum oxide. *Anal Chem* 87:3856–3863
- Lai G, Wang L, Wu J, Ju H, Yan F (2012) Electrochemical stripping analysis of nanogold label-induced silver deposition for ultrasensitive multiplexed detection of tumor markers. *Anal Chim Acta* 721:1–6
- Lin J, He C, Zhang S (2009) Immunoassay channels for α -fetoprotein based on encapsulation of biorecognition molecules into SBA-15 mesopores. *Anal Chim Acta* 643:90–94
- Lin J, Wei Z, Mao C (2011) A Label-free immunosensor based on modified mesoporous silica for simultaneous determination of tumor markers. *Biosens Bioelectron* 29:40–45
- Lin J, Wei Z, Chu P (2012) A label-free immunosensor by controlled fabrication of monoclonal antibodies and gold nanoparticles inside the mesopores. *Anal Biochem* 421:97–102
- Lin J, Wei Z, Zhang H, Shao M (2013) Sensitive Immunosenor for the label-free determination of tumor marker based on carbon nanotubes/mesoporous silica and graphene modified electrode. *Biosens Bioelectron* 41:342–347
- Liu S, Ma Y, Cui M, Luo X (2018) Enhanced electrochemical biosensing of alpha-fetoprotein based on three-dimensional macroporous conducting polymer polyaniline. *Sens Actuators B Chem* 255:2568–2574
- Maniya NH (2018) Recent advances in porous silicon based optical biosensors. *Rev Adv Mater Sci* 53:49–73
- Maniya NH, Patel SR, Murthy ZVP (2015) Development and in vitro evaluation of acyclovir delivery system using nanostructured porous silicon carriers. *Chem Eng Res Des* 104:551–557
- Maniya NH, Patel SR, Murthy ZVP (2016) Drug delivery with porous silicon films, microparticles, and nanoparticles. *Rev Adv Mater Sci* 44:257–272
- Martínez-García G, Pérez-Julián E, Agüí L, Cabré N, Joven J, Yáñez-Sedeño P, Pingarrón JM (2017) An Electrochemical enzyme biosensor for 3-hydroxybutyrate detection using screen-printed electrodes modified by reduced graphene oxide and thionine. *Biosensors* 7:50
- Martín-Yerga D, Costa-García A (2015) Towards a blocking-free electrochemical immunosensing strategy for anti-transglutaminase antibodies using screen printed electrodes. *Bioelectrochemistry* 105:88–94
- Martín-Yerga D, González-García MB, Costa-García A (2014) Electrochemical immunosensor for anti-tissue transglutaminase antibodies based on the situ detection of quantum dots. *Talanta* 130:598–602
- McNaught AD, Wilkinson A (1997) IUPAC. Compendium of chemical terminology, Gold Book. Blackwell Scientific Publications, Oxford
- Medintz IL, Uyeda HT, Goldman ER, Mattoussi H (2005) Quantum dot bioconjugates for imaging, labelling and sensing. *Nat Mater* 4:435–446
- Mondal A, Paul A, Srivastava DN, Panda AB (2018) NiO hollow microspheres as efficient bifunctional electrocatalysts for overall water-splitting. *Int J Hydrogen Energy* 43:21665–21674
- Movlaee K, Norouzi P, Beitollahi H, Rezapour M, Larijani B (2017) Highly selective differential pulse voltammetric determination of uric acid using modified glassy carbon electrode. *Int J Electrochem Sci* 12:3241–3251

- Neves MMPS, González-García MB, Santos-Silva A, Costa-García A (2012) Voltammetric immunosensor for the diagnosis of celiac disease on the quantification of anti-gliadin antibodies. *Sens Actuators B Chem* 163:253–259
- Nguyen BTT, Koh G, Lim HS, Chua AJS, Ng MML, Toh CS (2009) Membrane-based electrochemical nanobiosensor for the detection of virus. *Anal Chem* 81:7226–7234
- Pandey LM, Pattanayak SK, Delabouglise D (2013) Properties of adsorbed bovine serum albumin and fibrinogen on self-assembled monolayers. *J Phys Chem C* 117:6151–6160
- Pandiaraj M, Sethy NK, Bhargava K, Kameswararao V, Karunakaran C (2014) Designing label-free electrochemical immunosensors for cytochrome c using nanocomposites functionalized screen-printed electrodes. *Biosens Bioelectron* 54:115–121
- Paul A, Chiriaco MS, Primiceri E, Srivastava DN, Maruccio G (2019) Picomolar detection of retinol binding protein 4 for early management of type II diabetes. *Biosens Bioelectron* 128:122–128
- Peh AEK, Li SFY (2013) Dengue virus detection using impedance measured across nanoporous alumina membrane. *Biosens Bioelectron* 42:391–396
- Peng Z, Jiang Z, Huang X, Li Y (2016) A novel electrochemical sensor of tryptophan based on silver nanoparticles/metal–organic framework composite modified glassy carbon electrode. *RSC Adv* 6:13742–13748
- Perween M, Srivastava DN (2017) A cost-effective, unmodified platform for the detection of heavy metals via anodic stripping voltammetry at nanomolar level. *Chem Select* 2:4428–4432
- Perween M, Srivastava DN (2018) Designing ionic-liquid based practical reference electrode. *Ind J Chem Tech* 25:74–80
- Perween M, Parmar DB, Bhadu GR, Srivastava DN (2014) Polymer-graphite composite: a versatile use and throw plastic chip electrode. *Analyst* 139:5919–5926
- Piro B, Reisberg S (2017) Recent advances in electrochemical immunosensors. *Sensors* 17:794
- Rai V, Deng J, Toh CS (2012) Electrochemical nanoporous alumina membrane-based label-free DNA biosensor for the detection of *Legionella* sp. *Talanta* 98:112–117
- Rajeev G, Simon BP, Marsal LF, Voelcker NH (2018) Advances in nanoporous anodic alumina-based biosensors to detect biomarkers of clinical significance: a review. *Adv Healthcare Mater* 7:1700904
- Ravalli A, Pilon dos Santos G, Ferroni M, Faglia G, Yamanaka H, Marrazza G (2013) New label free CA125 detection based on gold nanostructured screen-printed electrode. *Sens Actuators B Chem* 179:194–200
- Renedo OD, Alonso-Lomillo MA, Martínez MA (2007) Recent developments in the field of screen-printed electrodes and their related applications. *Talanta* 73:202–219
- Reta N, Michelmore A, Saint C, Prieto-Simon B, Voelcker NH (2016) Porous silicon membrane-modified electrodes for label-free voltammetric detection of MS2 bacteriophage. *Biosens Bioelectron* 80:47–53
- Reta N, Saint CP, Michelmore A, Prieto-Simon B, Voelcker NH (2018) Nanostructured electrochemical biosensors for label-free detection of water- and food-borne pathogens. *ACS Appl Mater Interfaces* 10:6055–6072
- Ronkainen NJ, Halsall HB, Heineman WR (2010) Electrochemical biosensors. *Chem Soc Rev* 39:1747–1763
- Roushani M, Ghanbari K (2019) An electrochemical aptasensor for streptomycin based on covalent attachment of the aptamer onto a mesoporous silica thin film-coated gold electrode. *Microchim Acta* 186:115
- Silva BVM, Cavalcanti IT, Silva MMS, Dutra RF (2013) A carbon nanotube screen-printed electrode for label-free detection of the human cardiac troponin T. *Talanta* 117:431–437
- Szili EJ, Jane A, Low SP, Sweetman M, Macardle P, Kumar S, Smart RSC, Voelcker NH (2011) Interferometric porous silicon transducers using an enzymatically amplified optical signal. *Sens Actuators B Chem* 160:341–348

- Talarico D, Arduini F, Amine A, Cacciotti I, Moscone D, Palleschi G (2016) Screen-printed electrode modified with carbon black and chitosan: a novel platform for acetylcholinesterase biosensor development. *Anal Bioanal Chem* 408:7299–7309
- Taleat Z, Khoshroo A, Mazloum-Ardakani M (2014) Screen-printed electrodes for biosensing: a review (2008-2013). *Microchim Acta* 181:865–891
- Tallapragada SD, Layek K, Mukherjee R, Mistry KK, Ghosh M (2017) Development of screen-printed electrode based immunosensor for the detection of HER2 antigen in human serum samples. *Bioelectrochemistry* 118:25–30
- Thevenot DR, Toth K, Durst RA, Wilson GS (2001) Electrochemical biosensors: recommended definitions and classification. *Biosens Bioelectron* 16:121–131
- Tian F, Lyu J, Shi J, Tan F, Yang M (2016) A polymeric microfluidic device integrated with nanoporous alumina membranes for simultaneous detection of multiple foodborne pathogens. *Sens Actuators B Chem* 225:312–318
- Tucking KS, Vasani RB, Cavallaro AA, Voelcker NH, Schonherr H, Prieto-Simon B (2018) Hyaluronic acid-modified porous silicon films for the electrochemical sensing of bacterial hyaluronidase. *Macromol Rapid Commun* 39:1800178
- Vlassioug I, Takmakov P, Smirnov S (2005) Sensing DNA hybridization via ionic conductance through a nanoporous electrode. *Langmuir* 21:4776–4778
- Vomero M, Oliveira A, Ashouri D, Eickenscheidt M, Stieglitz T (2018) Graphitic carbon electrodes on flexible substrate for neural applications entirely fabricated using infrared nanosecond laser technology. *Sci Rep* 8:14749
- Wang X, Xi M, Guo M, Sheng F, Xiao G, Wu S, Uchiyama S, Matsuura H (2016) An electrochemically aminated glassy carbon electrode for simultaneous determination of hydroquinone and catechol. *Analyst* 141:1077–1082
- Windmiller JR, Wang J (2013) Wearable electrochemical sensors and biosensors: a review. *Electroanalysis* 25:29–46
- Wu Y, Xue P, Kang Y, Hui KM (2013) Paper based microfluidic electrochemical immunodevice integrated with nanobioprobes onto graphene film for ultrasensitive multiplexed detection of cancer biomarkers. *Anal Chem* 85:8661–8668
- Wu S, Ye WW, Yang M, Taghipoor M, Meissner R, Brugger J, Renaud P (2015) Impedance sensing of DNA immobilization and hybridization by microfabricated alumina nanopore membranes. *Sens Actuators B Chem* 216:105–112
- Xing L, Ma Z (2016) A glassy carbon electrode modified with a nanocomposite consisting of MoS₂ and reduced graphene oxide for electrochemical simultaneous determination of ascorbic acid, dopamine, and uric acid. *Microchim Acta* 183:257–263
- Yan M, Zang D, Ge S, Ge L, Yu J (2012) A disposable electrochemical immunosensor based on carbon screen-printed electrodes for the detection of prostate specific antigen. *Biosens Bioelectron* 38:355–361
- Ye WW, Shi JY, Chan CY, Zhang Y, Yang M (2014) A nanoporous membrane based impedance sensing platform for DNA sensing with gold nanoparticle amplification. *Sens Actuators B Chem* 193:877–882
- Zhang X, Ma LX, Zhang YC (2015) Electrodeposition of platinum nanosheets on C60 decorated glassy carbon electrode as a stable electrochemical biosensor for simultaneous detection of ascorbic acid, dopamine and uric acid. *Electrochim Acta* 177:118–127
- Zhao Y, Gaur G, Retterer ST, Laibinis PE, Weiss SM (2016) Flow-through porous silicon membranes for real-time label-free biosensing. *Anal Chem* 88:10940–10948
- Zittel HE, Miller FJ (1965) A glassy-carbon electrode for voltammetry. *Anal Chem* 37:200–203



Nanomaterial Functionalization Strategies in Bio-Interface Development for Modern Diagnostic Devices

9

Kuldeep Mahato, Ashutosh Kumar, Buddhadev Purohit, Supratim Mahapatra, Ananya Srivastava, and Pranjal Chandra

Abstract

Nano-biotechnology has paved a way towards the design and development of new diagnostic strategies and nano-medicine. The scope of recent nano-sensors for profound and selective sensing of numerous biomarkers is significant in different areas comprising health, environment, and food industries. To develop such systems often requires several functionalization steps for numerous nano-bio-conjugates, which are eventually applied for these biomedical applications. Moreover, to utilize the applications of nanomaterials present in the nano-bio-conjugates, there is a need to study the interactions happening at the nano-bio-interface. In view of such fresh growths in nanotechnology, the present book chapter has been framed underlining the part of nanomaterials in surface designing, biomolecular conjugations, and interactions happening at nan-bio-interface. In the chapter, the challenges towards working at the nano dimension and requirement of functionalization for biosensor development are addressed. Stress has been given on deciphering the classical strategies occurring at the nano-bio-interface, which

K. Mahato · A. Kumar · B. Purohit

Laboratory of Bio-Physio Sensors and Nano-bioengineering, Department of Biosciences and Bioengineering, Indian Institute of Technology Guwahati, Guwahati, Assam, India

S. Mahapatra

School of Biochemical Engineering, Indian Institute of Technology (BHU) Varanasi, Varanasi, Uttar Pradesh, India

A. Srivastava

Department of Pharmacology and Toxicology, NIPER Guwahati, Guwahati, Assam, India

P. Chandra (✉)

Laboratory of Bio-Physio Sensors and Nano-bioengineering, Department of Biosciences and Bioengineering, Indian Institute of Technology Guwahati, Guwahati, Assam, India

School of Biochemical Engineering, Indian Institute of Technology (BHU) Varanasi, Varanasi, Uttar Pradesh, India

e-mail: pranjal.bce@iitbhu.ac.in

are usually utilized for surface engineering and material functionalization. To put a better insight for the readers of interdisciplinary areas, an extended table has been incorporated, indicating the functionalization strategies and their uses.

Keywords

Nanomaterials · Nanoparticles · Surface functionalization · Nano-bio-interface · Nano-bio-conjugates

9.1 Introduction

Nano-biotechnology has been decisively recognized as a subdivision of nanotechnology, including all aspects of researches comprising applications of nanomaterials (NMs) in biological sciences (Mahato et al. 2018d). The description of what precisely constitutes a NM is not straightforwardly explained. The primarily established definition of the NMs was any material, consisting either organic or inorganic or both, having at least one dimension in <100 nm. Moreover, the materials are purposely fabricated at the nanoscale to obtain specific physical, chemical, mechanical, and optoelectronic properties (Vaddiraju et al. 2010). Classifications of materials, as described by international institutions, still define an upper size boundary of ~ 100 nm in at least one of the dimensions. Nevertheless, there are imperfect systematic pieces of evidence that firmly endorse this upper size limit for all kinds of NMs (Cao and Wang 2004; Labhasetwar and Leslie-Pelecky 2007; Mahato et al. 2018c; Savaliya et al. 2015). We described NMs as any material in the sub-micron dimension, produced from any means either biotic or abiotic that can be interfaced with biomolecules in an expedition of generating a new “value-added” unit. Moreover, the material must be deliberately shaped in the nano dimension to have distinct functional or structural entities arranged on its exterior or interior and exhibits distinctive characteristics or configuration that cannot be obtainable from the similar material in the bulk dimension.

The primary objective of nano-biotechnology emphasizes exploiting the intrinsic physical, mechanical, and catalytic properties of NMs to develop a novel assembly encompassing biomolecules with unique or novel properties (Chen et al. 2014; Fei et al. 2013; Gao et al. 2009). For instance, using NMs to facilitate drug delivery at the target destination, in vivo imaging, and biosensor development with the determination of clearing difficulties related with modern healthcare applications (Baker 2010; Baranwal et al. 2018a; Kumar et al. 2019e; Purohit et al. 2019c, 2020a). The following objective emphasizes applying the specific properties of biomolecules, which arise due to their biomolecular interactions, on designing the organized nano-devices of distinctive or new properties (Kim et al. 2009; Lin and Avouris 2008; Wang 2003). A striking illustration of this is applying nucleic acid assemblies to regulate the location and arrangement of nanoparticles (NPs) in the chase of making single molecular electronic devices at the sub-lithographic scale (Purohit et al.

2020b). We describe biomolecules including nucleic acids (i.e., DNA/RNA/PNA/LNA as genes, oligomers, aptamers, and ribozymes/DNAzymes), triglycerides, fatty acids, carbohydrates, proteins, peptides, etc., whether they are monomeric or polymeric (Simmel and Dittmer 2005). In a nano-bio-conjugate (NBC), the role of biomolecules can be of a functionally active entity that offers site for immobilization, catalysis, or therapeutic activity (Baranwal et al. 2016, 2018b) (e.g., antibodies or enzymes) or, otherwise, can be applied as a passive cover or support material (Subbiah et al. 2010; Veerapandian and Yun 2011; Willner and Willner 2010). To achieve the applications mentioned above, the development of several NBCs is needed, which can be utilized in the design and development of several healthcare technologies. The importance of applying NMs, and particularly NPs, as part of NBCs synthesis, ascends from the distinctive size-dependent physical, chemical, and optoelectronic characteristics, which they can provide to the resulting NBCs (Jariwala et al. 2013). The size-dependent features can comprise quantum-confined properties like photoluminescence of nano-crystals, surface plasmon resonances (SPR) of gold (Au) NPs, the electrical conductivity of carbon-based NMs, and the magnetic properties as well as catalytic properties of some metal nano-alloys and metal oxide NPs (Gao et al. 2009; Kumar et al. 2019c). Moreover, the NPs are also known to have high surface-to-volume (S/V) ratios and active interaction areas (Kumar et al. 2018, 2019a, c). This extraordinary S/V ratio not only delivers more spaces for interaction but also paves the way towards multi-functionalities onto the NMs. By the virtue of small size, the NMs offer ability of different reactive sites or chemical moieties onto the same particles, viz., dendrimer NPs, where several reaction and chemical sites can be presented for interfacial interactions (Purohit et al. 2019b; Wadhwa et al. 2019).

Intend of the book chapter stresses explaining various strategies involved for NBCs formation for improved biomedical applications. The bio-physico-chemical interactions of biomolecules applied during NBCs formation are also explained to make it appropriate for readers of interdisciplinary areas. Hopefully, this book chapter will inspire additional attention in the way of impressions related to NMs applications to sort out the difficulties in the design of NBCs and their applications in biomedical research. Attention has been paid to NMs introduction, bio-conjugation, and nano-bio-interface to deliver a new insight of interdisciplinary researches in the area of material engineering and applied biology. Emphasis has been given to justify the importance of nano-bio-conjugate interfacing not only for the development of nano-medicine but also for modern healthcare devices, including diagnostic devices such as the development of nano-bio-sensors. Herein, we emphasize on linkage chemistry applied for biomolecules interfacing onto the NMs, which eventually decide the achievement of nearly all the NBCs in their proposed applications. To provide a better understanding among readers of interdisciplinary researches, a table has been elucidated, indicating the strategies (targeted functional group, reactive group, product, and related mechanism) usually involved in NBCs formation. Irrespective of the precise value or research objective, interfacing biomolecules with NMs to make a novel functional unit is at the core of the interdisciplinary

research effort. Therefore, there is a need for understanding the challenges associated while working with NMs, which need to be measured during NBCs fabrication.

9.2 Challenges in Working with NMs

There are numerous challenges related to NBCs preparation that is significant enough to be considered for their optimum application. Primarily, NPs have extensive morphological variability not only in the form of shape and size but also in the form of constituent elements (Kumar et al. 2019b, 2020; Purohit et al. 2019a). Some NPs are uniform as they are made up of only one type of elements, such as Au NPs, Ag NPs, Pt NPs, and similar monometallic NPs, including Fe NPs, Pd NPs, etc. In other cases, NPs can be made up of mono or multi-metallic oxides, which not only affect the physical and chemical activities of NMs but also plays a crucial role in defining their shape and size (Mandal et al. 2018). The NMs are designed in such a way so that they can offer specific properties associated with their applications. Core-shell nanostructures are intentionally designed for their utilization (Ghosh Chaudhuri and Paria 2012; Levin et al. 2009; Wang et al. 2011). The core-shell nanostructures are designed in view of their intended applications, where the external shells guard and protect the internal structures that are occasionally essential for biological uses. Several NMs, including metallic, semiconductor, and carbon-based NMs, are hydrophobic that are required to be designed hydrophilic as well as compatible for biological interaction through surface modifications (Sapsford et al. 2011, 2013; Subbiah et al. 2010; Veerapandian and Yun 2011). This typically includes attachment or swapping of the hydrophobic structures with hydrophilic ligands or other layers that eventually make it capable of facilitating aqueous distribution. The process of developing hydrophilic ligands onto the hydrophobic surfaces is both complex as well as challenging that includes alteration of NMs at the level of changes of the small charged molecules to the formation of dendrimers, which are capable of complete encapsulation of the NPs (Sapsford et al. 2013). The covering ligands used for the fabrication of NBCs also deliver new chemical entities that can not only perform as active spots for consequent bio-conjugation but also act as a stabilizing agent of NMs. In the synthesis of NBCs, the agenda is to apply desirable biological molecules and conjugate them straight to the NPs surface with the help of surface-attached coating ligands, either directly or by applying small cross-linkers or other mediators (Agrawal et al. 2013; Chandra 2016; Chandra et al. 2012; Won et al. 2013; Yadav et al. 2013). Generally, bio-conjugation helps in precisely directing NPs in a sophisticated biological setting by bio-receptor elements (e.g., antibodies, aptamers) or permeates the NBCs to execute its biologically derived interactions like catalysis (e.g., enzymes, DNAszymes) (Chandra et al. 2013, 2015; Koh et al. 2011; Zhu et al. 2012a, b). Nano-bio-conjugate assembly can rapidly become multifaceted as many arrangements and iterations of the coating and ligand or biomolecules structure can occur (Thanh and Green 2010). In the unsophisticated design, the biomolecules interact straight to the core of NM. In the

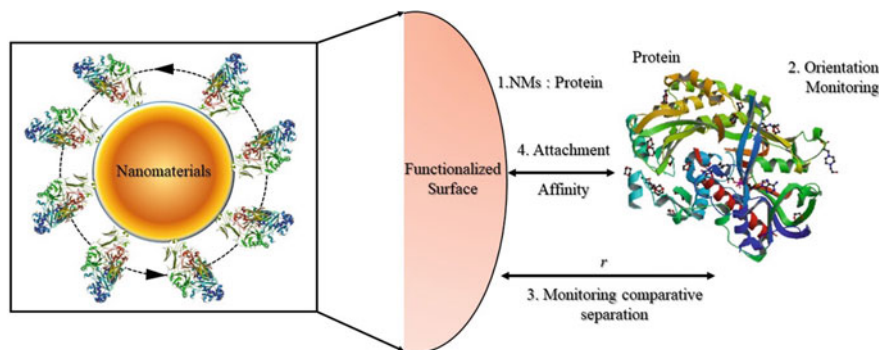


Fig. 9.1 Schematic depiction of the six “ideal” criteria that would aid in precise adherence of any biomolecules to the surface of NMs. The criteria comprise (1) controlling the ratio of biological molecules adhering onto the NMs; (2) monitoring the orientation onto the NMs; (3) controlling the comparative separation space from the NP; (4) monitoring the attachment affinity during NBCs formation; (5) conserving the best utility and activity of both NMs and bio-conjugates; and (6) reproducibility of NBCs with a range of biomolecules. Adapted from ref. Sapsford et al. (2013). Copyright 2013 ACS Publication Ltd

multifarious design, the NMs covers the biomolecules or, otherwise, biomolecules encapsulate the NM.

The ligand conjugation chemistry, as well as post conjugation ligand-NMs interactions, have significant inferences for the colloidal stability, particularly inside cellular surroundings. Moreover, it is worth to mention that ligand-NMs interactions will typically be exceedingly heterogeneous and cannot be uniform for the entire surface area (I. Medintz 2006a). Hence, it is evident to develop such NBCs, which can offer not only better bio-conjugation but also better interfacing.

Six comprehensive standards could define the “ideal” properties anticipated from nearly all NBCs fabrication chemistry, explained in Fig. 9.1 (I. Medintz 2006a; Sapsford et al. 2013). While considering a broad and non-descriptive bio-conjugation, one can adhere to biological molecules onto the NMs by controlling the following properties:

1. *Controlling the ratio of biological molecules adhering to the NMs.* Diverse applications of NBCs almost always need dissimilar ratios during fabrication; one ratio cannot be applied to several bio-conjugation strategies. The amount of biomolecules vastly regulates conjugation interactions and avidity. Equally, over-bio-conjugation can possibly damage conjugation interactions, though the surface of NMs and their curve can assist in mitigating this fairly (Medintz 2009).
2. *Monitoring the orientation onto the NMs.* The activity and binding capacity of aptamer, enzyme, protein, and antibody are reliant upon the exposure of their binding spots that can facilitate the interactions from surrounding. Nonspecific binding or electrostatic interactions during NBCs formation may result in heterogeneous adherence and eventually affect the activity of the final application.

3. *Controlling the comparative separation space from the NP.* Some applications demand controlled detachment at a specific distance, such as targeted drug delivery and sensing using Förster resonance energy transfer (I. L. Medintz 2006b, 2009).
4. *Monitoring the attachment affinity during NBCs formation.* Based on the application of NBCs, there is requirement for permanent or labile conjugation in between NMs and biomolecules, such as where drug delivery application is required the labile conjugation can provide a better performance, whereas in the case of immunoassays development the permanent attachment is needed for adherence of bio-receptors.
5. *Conserving the best utility and activity of both NMs and bio-conjugates.* During fabrication of NBCs, it is desirable that the function and activity of each constituting element should not be affected or altered. The loss of structural stability of NMs or loss of catalytic/capturing capacity of bio-receptors may ultimately affect the designed application of NBCs.
6. *Reproducibility of NBCs with a range of biomolecules.* Utmost application of a NBC fabrication strategy can only be achieved if the same strategy has the capacity to produce various types of NBCs using a different type of biomolecules.

The criteria, as mentioned above, are undisputable, though the challenge is in deciphering and designing the new fabrication strategy for NBCs.

In the research domain of nano-bio-conjugations, the word “nano-bio interface,” also known as “nanoscale interfaces to biology” and “corona of NMs,” has initiated to take on an explicit sense of their own (Hajipour et al. 2014; Nel et al. 2009). NMs, when presented to biotic settings such as blood, serum, and saliva, contribute in multipart bio-physico-chemical interactions with the natural molecules, and this is reflected in the least understood factor of NM activity in biotic settings (Gagner et al. 2012). The interchanges among NMs and the biotic molecules resulted in the subsequent properties they have on the NBCs, and its planned application has directed to the foundation of this research. For the NBCs formation, the adsorption of biomolecules to NMs is administrated by the hydrogen bonding interactions, London dispersion, pH of the environment, columbic forces, as well as by the lone-pair electrons available onto the ligands and NMs (Alkilany et al. 2013; Tang et al. 2015).

While designing and developing nano-medicine, this specific research domain has even more inferences (Baranwal and Chandra 2018; Noh et al. 2012). Moreover, the nano-dimensional architecture of NMs considerably affects the reaction kinetics on NM surfaces, so bio-conjugation chemistries must be improved for each type of NMs (Gagner et al. 2012; Sapsford et al. 2013; Willner and Willner 2010). Moreover, recent researches have shown the effects of NP dimension as well as involved surface chemistry adsorption of proteins that were justified by subsequent uptake of NBCs in macrophages (Behzadi et al. 2014). The subject can be intensified as each NM and NBCs can be anticipated to undergo very diverse exchanges based upon their own exclusive physical as well as chemical properties (Chandra 2015, 2016).

Moreover, it is worth to mention here, while the fabrication of NBCs, there could be a chance that the biological molecules may lose their activity because of confiscation, unfolding, denaturation, or blockage of active sites (Hajipour et al. 2014). Therefore, it is very much required to design and decipher new strategies that can be applied for designing and developing a novel NBC, which can withstand these limitations.

9.3 Bio-Conjugation Strategies for NBCs

NPs showing material properties like exterior color, SPR, conductivity, and affinity towards binding are significantly upgraded while functionalization with biological molecules (Cai et al. 2018; Hassan and Singh 2014; Xu et al. 2012). It is a crucial step, which not only decides the functional activity of NBCs but also offers the opportunity to design novel nano-sensors with improved sensing abilities (Akhtar et al. 2018; Chandra et al. 2011, 2014; Gagner et al. 2012; Tang et al. 2015). Designing a NM-based sensing system or development of any nano-bio-interface can be directed towards an analyte, which needs the coupling of bio-receptors to its active surface. The kind of bio-conjugation often demands specific linkers, which assist in addition to the NM surface. A mixture of aspects comprising shape, dimensions, morphologies, surface interaction, and the intrinsic elements of the NMs itself primarily decides selection of the conjugation strategy. Moreover, the surface ligands nature and their accessible, functional groups onto the NMs regulates the kind of biomolecules selected for NBCs formation. The choice of biomolecules is also decided by their size, chemical structures, as well as the ultimate function anticipated in the final use. In simple words, bio-conjugation can be covalent (comprising covalent bonding to the surface of NM or with the surface ligand) or noncovalent, comprising electrostatic interactions, other forms of adsorption, and encapsulation. To appropriately acclimatize and amend the outer surface of NMs, researchers have framed different methods to integrate the anticipated functional ability in the NBCs (Aubin-Tam and Hamad-Schifferli 2008). The common measures that are regularly applied for NMs functionalization are highlighted in Fig. 9.2. Figure 9.2 (i) shows the NPs functionalization method using electrostatic interactions to attach a peptide. In this method, electrostatic charges that are opposite to each other are exploited to facilitate electrostatic NP-peptide assemblage. Figure 9.2 (ii) shows the direct interaction technique that is extensively applied for AuNP functionalization. In this method, some specific protein peptides can attach to NMs surface due to high affinity towards NMs surface, such as the interactions of free thiols to the surface of AuNPs. Figure 9.2 (iii) shows the secondary interactions used for bio-functionalization; this method uses definite ligand–receptor interactions such as biotin–streptavidin coupling. Figure 9.2 (iv) shows covalent attachment technique; it uses the classical bio-functionalization chemistry like EDC-based coupling to carboxyl or NHS- and maleimide-mediated coupling to amines and thiols. Figure 9.2 (v) shows the encapsulation technique that is widely applied for peptides entrapment inside the final NBCs, which can be materialized during the

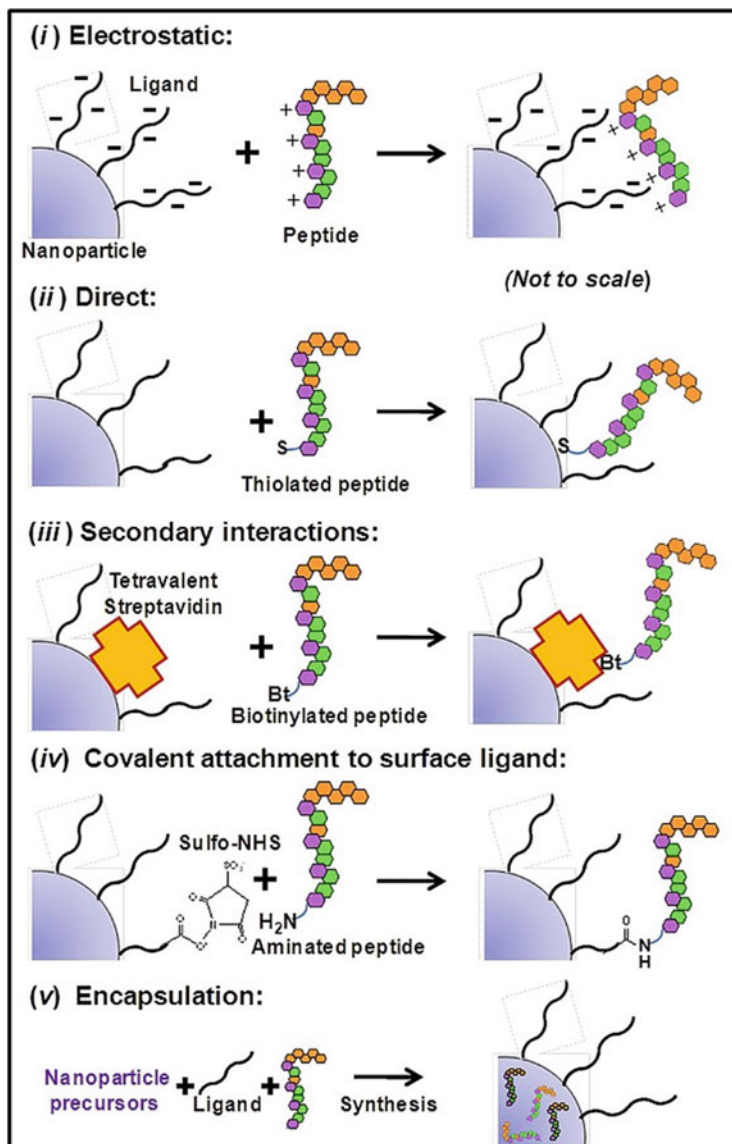


Fig. 9.2 Classical bio-functionalization approaches: (i) electrostatic binding; (ii) direct adherence; (iii) secondary interactions; (iv) covalent coupling; and (v) encapsulation. Reprinted with the permission from reference (Kumar et al. 2019c)

initial stage of synthesis of NBCs. Currently, NMs have been widely functionalized with several materials such as artificial polymers, bio-polymers, dendrimers, and small molecules by means of above-stated functionalization approaches. Attaining a specific functional group, for example, amine, carboxyl, thiol, and hydroxyl, is

greatly vital for attaching enzymes and antibodies onto the active surface of NMs, which is eventually determined by the functionalizing technique and reagents used for NBCs formations (Cai et al. 2018).

To provide amine group onto the NBCs, chemicals having free amine groups are applied like 3-Aminotriethoxy propyl silane (APTES), chitosan, serine, etc. (Conde et al. 2014; Hsiao et al. 2007; Markwalter et al. 2019; Subbiah et al. 2010; Thanh and Green 2010; Veerapandian and Yun 2011). Likewise, to provide carboxyl group onto the final NBCs, reagents having free carboxyl groups are used. The immobilization of bio-receptors, viz., antibodies/enzymes is a crucial step in biosensor development and it is very much significant to regulate the functionalizing agent during this attachment as its assembly may control the electron transfer through the sensor surface that eventually may alter the response generation in the biosensor. In the case of sensor development, the attachment of a bio-receptor onto a sensor matrix can be regulated by monitoring the overall movement of bio-recognition elements while keeping it in a comparatively distinct area utilizing bio-functionalization may result into enhanced stability and reusability of the sensor probe (Hassan and Singh 2014; Medintz 2009; Xu et al. 2012).

In other words, to exploit the properties of NMs in medicinal arenas, the external surface of the NMs needs to be altered suitably to deliver steadfastness, compatibilities, and functional activity. In the next section, we have briefly elucidated some key bio-functionalization strategies towards NBCs formation.

9.3.1 Covalent Coupling Strategies

The interactions applied for the coupling of bio-receptors to NM surface for analytical uses usually depend on a few critical bio-conjugation chemistries. Some very significant covalent coupling strategies are explained in upcoming sections, which are widely used to design NBCs for nano-biosensors and nano-medicines.

9.3.1.1 EDC/NHS Covalent Coupling

Most of the classic NMs synthesis strategies use compounds having carboxylates and primary amines, not only to provide surface stability but also to get uniform size distribution among NMs. Because of this, the wide presence of carboxylates and primary amines on NM surfaces provides an opportunity to interconnect the similar ligands present onto the bio-receptors. One of the most common covalent chemistry to generate functionalized NMs for diagnostics and biosensor development is the development of amide bonds. The standard chemical used for making amide bonds on NMs surfaces is 1-ethyl-3-(3-(dimethyl amino) propyl) carbodiimide (EDC), which is a zero-length cross-linking agent that generates an activated ester, which can successively interact to primary amines. Though, only EDC-activated esters react gently with primary amines, that often activate hydrolysis by-products, which constrain amide bonding. Accordingly, EDC is generally combined by NHS (N-hydroxysuccinimide) esters to increase the firmness of the initiated ester intermediary. The NHS-activated ester intermediary strongly reacts with nucleophiles of

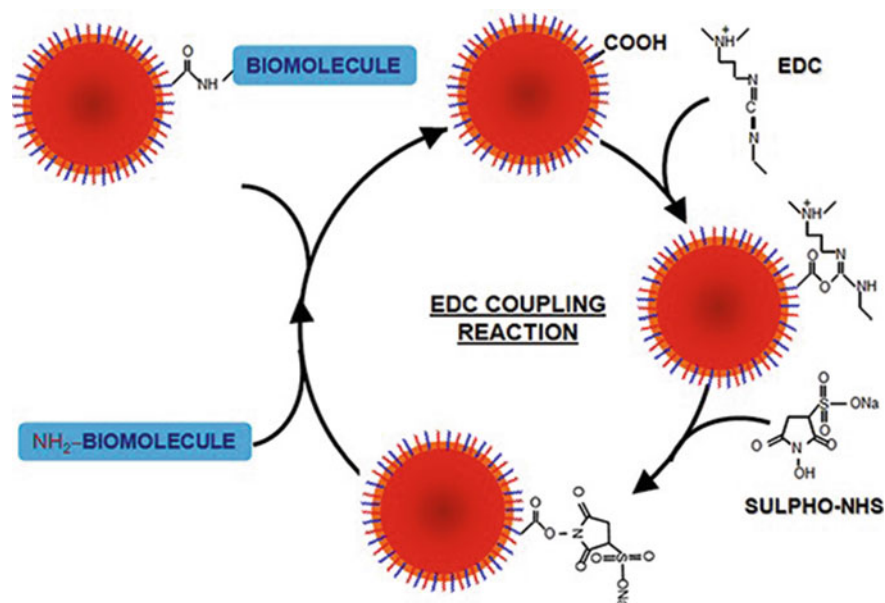


Fig. 9.3 EDC/NHS coupling method: In the presence of Sulfo-NHS, EDC can be utilized to convert carboxyl groups of NMs/biomolecules to amine-reactive Sulfo-NHS esters. Reprinted with permission from ref. Conde et al. (2014) with permission from ACS

primary amines to generate a stable amide bond. In simple words, the incorporation of NHS stabilizes the amine-reactive intermediary by altering this to an amine-reactive Sulfo-NHS ester, therefore enhancing the competence of EDC-mediated binding reactions. Water is gently used to remove the excess reagents and to interfere by-products. When EDC becomes soluble in water, the cross-linking can be achieved in normal physiological settings without adding additional organic solvents. EDC/NHS coupling is beneficial in creating both antibody-based as well as nucleic acid-based NBCs for biosensing probes. Since there is an inherent adequate presence of primary amines in antibodies, they are freely bonded to carboxylated NMs without any early pretreatment. Besides, the EDC bonding with imidazole allows bonding of ethylenediamine to the nucleic acids using 5' phosphate groups, creating 5'-amine-functionalized oligonucleotides, which can be attached to carboxylated surfaces of NMs (Conde et al. 2014) (Fig. 9.3).

Semiconductor NPs, magnetic NMs, and polymeric NMs have found uses in POC sensor development as well as are usually prepared with carboxylate groups or amine groups on the interface so that they can be applied for bio-conjugations via EDC/NHS coupling (Choudhary et al. 2016; Koh et al. 2011; Mahato et al. 2016, 2018d; Zhu et al. 2013). Generally, di-hydro-lipoic acid derivatives or various copolymers are utilized to stabilize the quantum dots, which install carboxylate groups on an interface. Furthermore, there are applications of magnetic NPs in biomedical diagnostics, which are also coated with carboxylated polymers to assist

additional functionalization using biomolecules/drugs having primary amine in their structure (Bhatnagar et al. 2018; Mahato et al. 2017, 2018a, b, 2019; Prasad et al. 2016). Alternatively, NPs or sensor surfaces can be layered with silica shells derivatives having carboxylate/amine functional groups. Nano-shells of silica are synthesized via the condensation of monomers of silica oxide, like tetraethyl-ortho-silicate (TEOS) or APTES, creating aminopropyl-silanols surfaces. A modified sensor, surfaces having aminopropyl-silanols, can consequently be coupled with bio-receptors via. EDC/NHS coupling. Along with providing functional groups for additional bio-conjugation, the encapsulation of NPs by silanols offers better bio-compatibility as well as guards the nuclear material from deprivation, making it an appropriate approach for the fabrication of diagnostic sensor systems.

9.3.1.2 Thiol Covalent Coupling

Another substantial coupling reaction to functionalize NMs and sensor surfaces is the bio-conjugation of thiols present either on bio-receptors or on the surface of NMs. Nucleic acids can be thiolated by using the same technique as explained in nucleic acids amine-functionalization technique (Markwalter et al. 2019; Sapsford et al. 2011, 2013). For thiol coupling, usually, cystamine is applied in place of ethylenediamine to add a disulfide bond, which can eventually be reduced with dithiothreitol (DTT) and give a 5'-thiolated oligonucleotide probe. Conversely, antibodies usually do not have free thiols and, hence, either have to be thiolated (by using Traut's chemical) or sliced at the inter-chain disulfides bond (via DTT or papain) to produce thiols for consequent bio-conjugation of NMs or sensor surfaces. The thiol coupling of biological molecules to noble metal NMs (stating about AuNPs or AgNPs) is usually done via coordinate dative bonds in which the sulfur lone pair electrons form strong bonding directly to the NMs surface itself (Fig. 9.4 (a)) (Markwalter et al. 2019). Otherwise, chemical reagents having thiol groups or NMs can be attached to each other by applying a hetero-bi-functional cross-linking agent derived from maleimide, usually sulfo-SMCC (succinimidyl-4-(N-maleimidomethyl) cyclohexane-1-carboxylate). A stable thiol-ether bond is formed in this reaction where the thiol group interacts with the maleimide functional group. Moreover, the NHS-ester module of sulfo-SMCC provides interaction sites for reaction with primary amines present in bio-receptors (Fig. 9.4 (b))(Markwalter et al. 2019).

9.3.1.3 Click Chemistry and Photochemical Cross-Linking

Several NM-based diagnostic sensors have been designed using photochemical cross-linking reactions and "click chemistry." Chemical compounds such as phenyl diazirines and phenyl azides produce reactive carbenes and nitrenes, respectively, upon the introduction of UV light and ultimately aids in novel bond formation in between carbon, nitrogen, and hydrogen. Such photochemical reactants can be incorporated into hetero-bi-functional cross-linkers, like sulfo-NHS-LC-diazirine, for bio-coupling of NMs and bio-receptors. "Click" chemistry denotes to bio-orthogonal chemical reactions having high production, minimal by-products, and require mild settings. The most shared "click" chemistry-based chemical

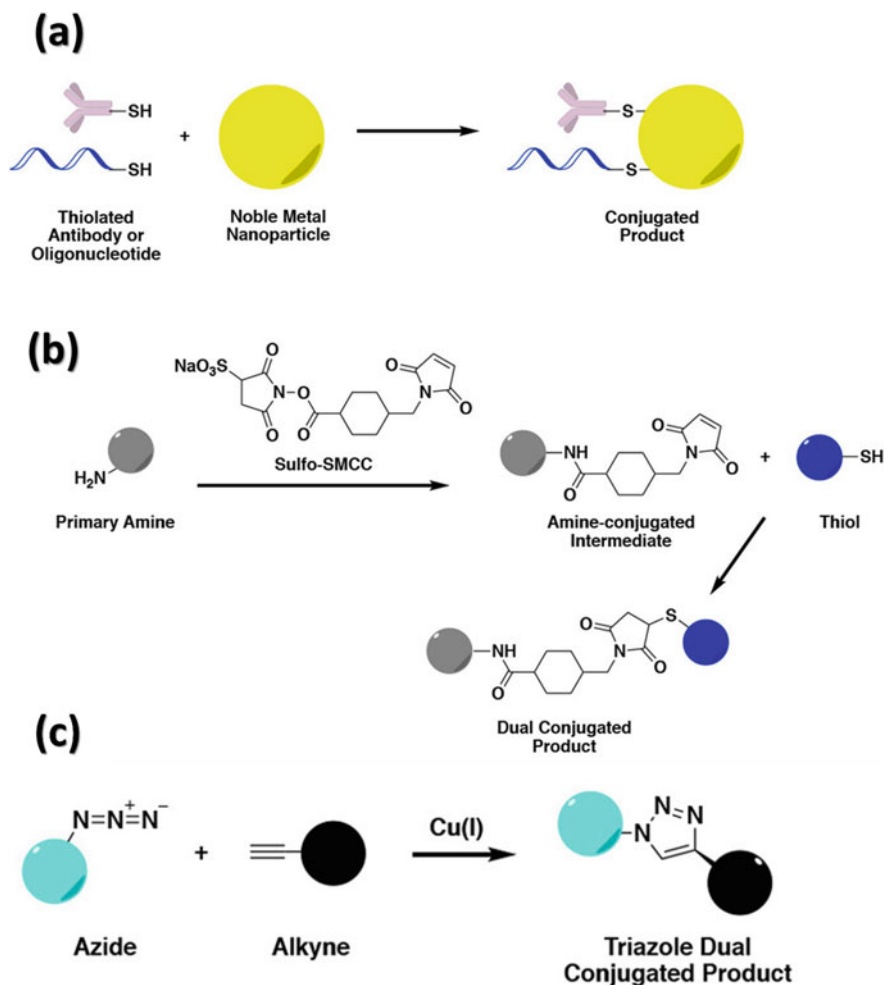


Fig. 9.4 (a) Thiol covalent coupling using antibody/oligonucleotide to a NP; (b) thiol conjugation of primary amine via hetero-bi-functional cross-linker using Sulfo-SMCC; and (c) “Click” chemistry attachment in between an azide and an alkyne in the existence of a copper catalyst. Reprinted with permission from ref. Markwalter et al. (2019) with permission from ACS

interaction is the attachment of an alkyne to an azide in the existence of a Cu(I), which is used for catalysis (Fig. 9.4 (c)) (Markwalter et al. 2019). There are many other chemical interactions related to “click” chemistry that attach NMs and bio-receptors.

9.3.1.4 Biotin–Streptavidin Coupling

Biotin–streptavidin coupling is the leading affinity-based conjugation strategy utilized for NMs functionalization, which is eventually applied for the development of modern diagnostic devices. A small protein molecule having molecular weight

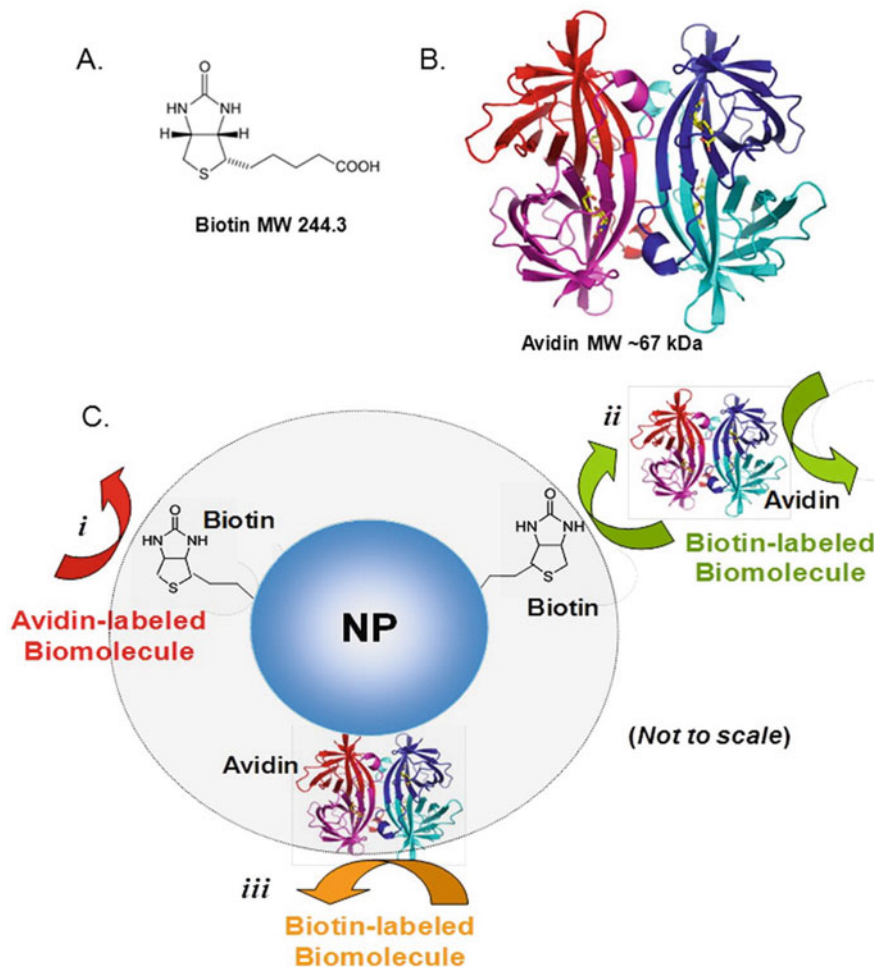


Fig. 9.5 Biotin–avidin coupling. (a) Biotin chemical structure; (b) tetrameric avidin ribbon model. Reprinted with permission from ref. Wilchek et al. (2006). (c) Schematic representation of the three frequently used biotin–avidin coupling for adherence biomolecules to NMs. (i) NP labeled with biotin bonded to biomolecule having avidin label; (ii) NP labeled with biotin bonded to biomolecule having avidin linker, by using an intermediate avidin linker; and (iii) NP labeled with avidin bonded to biotin-containing biomolecule. Reprinted with permission from ref. Sapsford et al. (2013)

nearly 1.3×10^{-15} KD, known as biotin, has an extraordinary affinity towards tetrameric bacterial protein streptavidin having molecular weight, nearly 60 KD (Markwalter et al. 2019; Sapsford et al. 2011, 2013). The established stoichiometry of biotin to streptavidin is 4:1 to make a highly stable bonding. The streptavidin–biotin complex formation strategies are a very common way of adhering biomolecules, like antibodies/DNA, etc. The coupling strategies are made apparent in Fig. 9.5, where two main approaches of bio-conjugation by means of biotin–streptavidin coupling has been ascribed (Thanh and Green 2010). The first, and

undoubtedly most practiced, method includes a streptavidin-functionalized NM being joined with a biotinylated biomolecule. It is essential to contemplate that the adherence of streptavidin to the NM in early alteration will possibly unclear one or more accessible biotin coupling places and, in combination with total heterogeneity rising from this strategy, the ultimate streptavidin-functionalized NM will undoubtedly show countless diverse alignments. Generally, streptavidin is coated to the surface of NMs by passive adsorption or by using a hetero-bi-functional cross-linker like sulfo-SMCC. The most common technique for biotinylating a bioreceptor is the attaching of sulfo-NHS biotin or NHS-(PEG) n-biotin to a primary amine. Though the streptavidin-biotin coupling is a comparatively stress-free job, a (PEG) n insertion can be incorporated to enhance the solubility of biotin (Conde et al. 2014; Sapsford et al. 2011).

Currently, there have been several numbers of strategies for NBCs formation, which has been emphasized in Table 9.1, where an apparent inventory of some common NBCs and their projected usefulness adequately imitates the extent of projected applications and the vitality underlying at the core of this research (Sapsford et al. 2013).

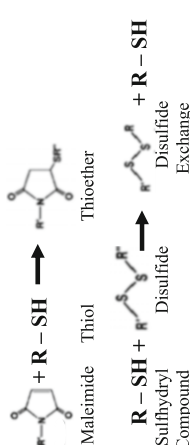
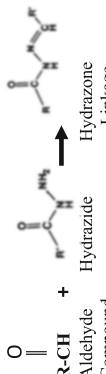
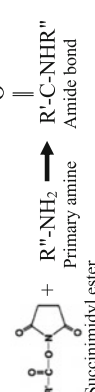
9.4 Conclusions

It can be concluded that diverse shapes and morphologies of the NMs and their composite alter the physical, chemical, and optical properties of the developed NBCs. To design a desired device for various applications and while working onto the interface at nano dimensions, there is a need of controlling the parameters, which governs the fabrication of NBCs like ratio of biomolecules, rate of conjugation, orientation of biomolecules and NMs at nano-bio-interface, attachment affinity, and reproducibility of the fabrication process. The well-planned functionalization approach not only provides desired NBCs, but also comprises profits of unsophisticated fabrication procedures and reasonable production cost. In this chapter, we attempted to deliver a brief image of existing techniques in the fabrication approaches of diverse NBCs. We conclude that NM of diverse shapes and sizes and their bio-conjugates functionalized with linker entities can provide an innovative aspect in research and expansion of recent biomedical policies that have auspicious prospects in analytical and therapeutic uses. It has the prospective to escalate the activity of new analytical devices and can transform biomedical engineering.

9.5 Future Prospects


To develop further revolutions in the region of biomedical researches, the collective energies from nanotechnologist and biotechnologist are highly anticipated. Though it is hard to establish novel strategies and regulate the properties of NMs at this dimension, it is essential to have desirable properties in the developed NBCs to

Table 9.1 List of common bio-functionalization strategies used for the fabrication of NBCs along with reaction mechanisms. Adapted from ref. Sapsford et al. (2013). Copyright 2013 ACS Publication Ltd

Target	Reactive group	Product	Reaction mechanism
Free thiol	Maleimide Haloacetyl/alkyl halide Arylating agents Aziridine Acryloyl derivatives Disulfide exchange-pyridyl disulfides, 5-thio-2-nitrobenzoic acid (TNB)	Thioether Thioether Thioether Thioether Thioether Mixed disulfides	 <p>Maleimide + R-SH → Thioether</p> <p>R-SH + R'-SH → Disulfide + R-SH Disulfide Exchange</p>
Aldehyde/ketone	Hydrazine Amines	Hydrazone Schiff's base (imine)	 <p>$\text{R}-\text{C}(=\text{O})-\text{H} + \text{Hydrazide Compound} \rightarrow \text{Hydrazone Linkage}$</p>
Free amine	N-hydroxysuccinimide ester (NHS) Acyl azides Isocyanates, Isothiocyanates Sulfonyl chlorides Aldehydes, Glifoxals, Epoxides, Oxiranes Carbonates Arylating agents Imidoesters Carbodiimides, anhydrides	Amide Amide Urea, thiourea Sulfonamide Imine, secondary amine Secondary amine Carbamate Arylamine Amidine Amine	 <p>Succinimidyl ester + R''-NH₂ (Primary amine) → R'-C(=O)-NHR'' (Amide bond)</p>

(continued)

Table 9.1 (continued)

Target	Reactive group	Product	Reaction mechanism
Carboxylate	Carbodiimides, Carbonyldiimidazole Dialkylanes, Diazoacetyl	Amides Ester	$\text{R}'\text{-C-OH} + \text{RN}=\text{C}=\text{NR} \longrightarrow \left[\text{R}'\text{-C-O-N} \begin{array}{c} \text{O} \\ \parallel \\ \text{N} \end{array} \text{R} \right] \text{Intermediate} + \text{R}''\text{-NH}_2 \text{ Primary amine}$ <p>Carboxylic Acid Carbodiimide O-Acylisourea Intermediate</p>
Hydroxyl	Epoxides, alkyl halogens Periodate Isocyanates, Carbonyldiimidazole, N,N'-disuccinimidyl carbonate, N, N'-hydroxysuccinimidyl chloroformate	Ether Aldehyde Carbamate or urethane	$\text{R-OH} + \text{N}=\text{C}=\text{O} \longrightarrow \text{R-O-C(=O)-NH}_2$ <p>Hydroxyl Compound Isocyanate Carbamate Linkage</p>
Reactive carbon (on a phenol, e.g., tyrosine)	Diazonium	Diazo bond	 <p>Diazonium Tyrosine Diazo bond</p>

increase the specific interactions at the interfaces. With the determinations devoted to the explorations, we have respectable inspirations to trust on NM and their bio-conjugates for the development of modern healthcare instruments. The biocompatibility study of numerous NBCs is tremendously significant in several *in vitro* and *ex vivo* studies, including cells, serum, blood, tissue slices, etc. that will establish the application of NBCs in *in vivo* settings.

Acknowledgments Dr. Pranjal Chandra thanks Prof. Pramod Kumar Jain, Director IIT(BHU) for providing necessary infrastructure for completion of this work. The work is supported by DST-Ramanujan grant SB/S2/RJN-042/2015 and IIT(BHU) start-up grant.

References

- Agrawal B, Chandra P, Goyal RN, Shim YB (2013) Detection of norfloxacin and monitoring its effect on caffeine catabolism in urine samples. *Biosens Bioelectron* 47:307–312
- Akhtar MH, Hussain KK, Gurudatt NG, Chandra P, Shim YB (2018) Ultrasensitive dual probe immunosensor for the monitoring of nicotine induced-brain derived neurotrophic factor released from cancer cells. *Biosens Bioelectron* 116:108–115
- Alkilany AM, Lohse SE, Murphy CJ (2013) The gold standard: gold nanoparticle libraries to understand the nano – bio interface. *Acc Chem Res* 46:650–661
- Aubin-Tam M-E, Hamad-Schifferli K (2008) Structure and function of nanoparticle – protein conjugates. *Biomed Mater* 3:34001
- Baker M (2010) Nanotechnology imaging probes: smaller and more stable. *Nat Methods* 7:957–962
- Baranwal A, Chandra P (2018) Clinical implications and electrochemical biosensing of monoamine neurotransmitters in body fluids, *in vitro*, *in vivo*, and *ex vivo* models. *Biosens Bioelectron* 121:137–152
- Baranwal A, Mahato K, Srivastava A, Maurya PK, Chandra P (2016) Phytofabricated metallic nanoparticles and their clinical applications. *RSC Adv* 6:105996–106010
- Baranwal A, Chiranjivi AK, Kumar A, Dubey VK, Chandra P (2018a) Design of commercially comparable nanotherapeutic agent against human disease-causing parasite. *Leishmania Sci Rep* 8:8814
- Baranwal A, Srivastava A, Kumar P, Bajpai VK, Maurya PK, Chandra P (2018b) Prospects of nanostructure materials and their composites as antimicrobial agents. *Front Microbiol* 9:422
- Behzadi S, Serpooshan V, Sakhtianchi R, Müller B, Landfester K, Crespy D, Mahmoudi M (2014) Protein corona change the drug release profile of nanocarriers: the “overlooked” factor at the nanobio interface. *Colloid Surface B* 123:143–149
- Bhatnagar I, Mahato K, Ealla KKR, Asthana A, Chandra P (2018) Chitosan stabilized gold nanoparticle mediated self-assembled gliP nanobiosensor for diagnosis of invasive *Aspergillus*. *Int J Biol Macromol* 110:449–456
- Cai P, Zhang X, Wang M, Wu Y-L, Chen X (2018) Combinatorial nano – bio interfaces. *ACS Nano* 12:5078–5084
- Cao G, Wang Y (2004) Nanostructures and nanomaterials: synthesis. Prop. Appl. World Scientific, London
- Chandra P (2015) Electrochemical nanobiosensors for cancer diagnosis. *J Anal Bioanal Tech* 6: e119
- Chandra P (2016) Nanobiosensors for personalized and onsite biomedical diagnosis. The Institution of Engineering and Technology, London
- Chandra P, Noh H-B, Won MS, Shim YB (2011) Detection of daunomycin using phosphatidylserine and aptamer co-immobilized on Au nanoparticles deposited conducting polymer. *Biosens Bioelectron* 26:4442–4449

- Chandra P, Koh WCA, Noh H-B, Shim YB (2012) In vitro monitoring of i-NOS concentrations with an immunosensor: the inhibitory effect of endocrine disruptors on i-NOS release. *Biosens Bioelectron* 32:278–282
- Chandra P, Noh H-B, Shim Y-B (2013) Cancer cell detection based on the interaction between an anticancer drug and cell membrane components. *Chem Commun* 49:1900–1902
- Chandra P, Suman P, Airon H, Mukherjee M, Kumar P (2014) Prospects and advancements in C-reactive protein detection. *World J Methodol* 4:1–5
- Chandra P, Noh HB, Pallela R, Shim YB (2015) Ultrasensitive detection of drug resistant cancer cells in biological matrixes using an amperometric nanobiosensor. *Biosens Bioelectron* 70:418–425
- Chen X, Ramström O, Yan M (2014) Glyconanomaterials: emerging applications in biomedical research. *Nano Res* 7:1381–1403
- Choudhary M, Yadav P, Singh A, Kaur S, Ramirez-Vick J, Chandra P, Arora K, Singh SP (2016) CD 59 targeted ultrasensitive electrochemical immunosensor for fast and noninvasive diagnosis of oral cancer. *Electroanalysis* 28:2565–2574
- Conde J, Dias JT, Grazi V, Moros M, Baptista PV, de la Fuente JM (2014) Revisiting 30 years of biofunctionalization and surface chemistry of inorganic nanoparticles for nanomedicine. *Front Chem* 2:1–27
- Fei L, Jing-Han Z, Yang-Long H, Song G (2013) Chemical synthesis of magnetic nanocrystals: recent progress. *Chinese Phys B* 22:107503
- Gagner JE, Shrivastava S, Qian X, Dordick JS, Siegel RW (2012) Engineering nanomaterials for biomedical applications requires understanding the nano-bio interface: a perspective. *J Phys Chem Lett* 3:3149–3158
- Gao J, Gu H, Xu B (2009) Multifunctional magnetic nanoparticles: design, synthesis, and biomedical applications. *Acc Chem Res* 42:1097–1107
- Ghosh Chaudhuri R, Paria S (2012) Core/shell nanoparticles: classes, properties, synthesis mechanisms, characterization, and applications. *Chem Rev* 112:2373–2433
- Hajipour MJ, Laurent S, Aghaie A, Rezaee F, Mahmoudi M (2014) Personalized protein coronas: a “key” factor at the nanobiointerface. *Biomater Sci* 2:1210–1221
- Hassan S, Singh AV (2014) Biophysicochemical perspective of nanoparticle compatibility: a critically ignored parameter in nanomedicine. *J Nanosci Nanotechnol* 14:402–414
- Hsiao VKS, Waldeisen JR, Zheng Y, Lloyd PF, Bunning TJ, Huang TJ (2007) Aminopropyltriethoxysilane (APTES)-functionalized nanoporous polymeric gratings: fabrication and application in biosensing. *J Mater Chem* 17:4896–4901
- Jariwala D, Sangwan VK, Lauhon LJ, Marks TJ, Hersam MC (2013) Carbon nanomaterials for electronics, optoelectronics, photovoltaics, and sensing. *Chem Soc Rev* 42:2824–2860
- Kim H, Maeng W-J et al (2009) Applications of atomic layer deposition to nanofabrication and emerging nanodevices. *Thin Solid Films* 517:2563–2580
- Koh WCA, Chandra P, Kim D-M, Shim Y-B (2011) Electropolymerized self-assembled layer on gold nanoparticles: detection of inducible nitric oxide synthase in neuronal cell culture. *Anal Chem* 83:6177–6183
- Kumar A, Sharma S, Pandey LM, Chandra P (2018) Nanoengineered material based biosensing electrodes for enzymatic biofuel cells applications. *Mater Sci Energy Technol* 1:38–48
- Kumar A, Purohit B, Mahato K, Chandra P. (2019a) CHAPTER 11. Advance engineered nanomaterials in point-of-care Immunosensing for biomedical diagnostics. *Immunosensors RSC* 238–266
- Kumar A, Purohit B, Mahato K, Mandal R, Srivastava A, Chandra P (2019b) Gold-iron bimetallic nanoparticles impregnated reduced graphene oxide based nanosensor for label-free detection of biomarker related to non-alcoholic fatty liver disease. *Electroanalysis* 31:2417–2428
- Kumar A, Purohit B, Maurya PK, Pandey LM, Chandra P (2019c) Engineered nanomaterial assisted signal-amplification strategies for enhancing analytical performance of electrochemical biosensors. *Electroanalysis* 31:1615–1629

- Kumar A, Roy S, Srivastava A, Naikwade MM, Purohit B, Mahato K, Naidu VGM, Chandra P (2019e) Chapter 10. Nanotherapeutics: a novel and powerful approach in modern healthcare system. In: Nanotechnology in modern animal biotechnology. Elsevier, pp 149–161
- Kumar A, Purohit B, Mahato K, Roy S, Srivastava A, Chandra P (2020) Design and development of ultrafast Sinaptic acid sensor based on electrochemically nanotuned gold nanoparticles and Solvothermally reduced graphene oxide. *Electroanalysis* 32(1):59–69
- Labhasetwar V, Leslie-Pelecky DL (2007) Biomedical applications of nanotechnology. John Wiley & Sons, Hoboken, NJ
- Levin CS, Hofmann C, Ali TA, Kelly AT, Morosan E, Nordlander P, Whitmire KH, Halas NJ (2009) Magnetic-plasmonic core-shell nanoparticles. *ACS Nano* 3:1379–1388
- Lin Y-M, Avouris P (2008) Strong suppression of electrical noise in bilayer graphene nanodevices. *Nano Lett* 8:2119–2125
- Mahato K, Prasad A, Maurya P, Chandra P (2016) Nanobiosensors: next generation point-of-care biomedical devices for personalized diagnosis. *J Anal Bioanal Tech* 7:e125
- Mahato K, Srivastava A, Chandra P (2017) Paper based diagnostics for personalized health care: emerging technologies and commercial aspects. *Biosens Bioelectron* 96:246–259
- Mahato K, Baranwal A, Srivastava A, Maurya PK, Chandra P (2018a) Smart materials for biosensing applications. In: Pawar PM, Ronge BP, Balasubramaniam R, Seshabhatter S (eds) *Techno-societal 2016*. Springer International Publishing, Cham, pp 421–431
- Mahato K, Kumar A, Maurya PK, Chandra P (2018b) Shifting paradigm of cancer diagnoses in clinically relevant samples based on miniaturized electrochemical nanobiosensors and microfluidic devices. *Biosens Bioelectron* 100:411–428
- Mahato K, Kumar S, Srivastava A, Maurya PK, Singh R, Chandra P (2018c) Chapter 14. Electrochemical Immunosensors: fundamentals and applications in clinical diagnostics. In: Vashist SK, Luong JHT (eds) *Handbook of immunoassay technologies*. Academic Press, pp 359–414
- Mahato K, Maurya PK, Chandra P (2018d) Fundamentals and commercial aspects of nanobiosensors in point-of-care clinical diagnostics. *3 Biotech* 8:149
- Mahato K, Nagpal S, Shah MA, Srivastava A, Maurya PK, Roy S, Jaiswal A, Singh R, Chandra P (2019) Gold nanoparticle surface engineering strategies and their applications in biomedicine and diagnostics. *3 Biotech* 9:57
- Mandal R, Baranwal A, Srivastava A, Chandra P (2018) Evolving trends in bio/chemical sensor fabrication incorporating bimetallic nanoparticles. *Biosens Bioelectron* 117:546–561
- Markwalter CF, Kantor AG, Moore CP, Richardson KA, Wright DW (2019) Inorganic complexes and metal-based nanomaterials for infectious disease diagnostics. *Chem Rev* 119:1456–1518
- Medintz I (2006a) Universal tools for biomolecular attachment to surfaces. *Nat Mater* 5:842
- Medintz IL (2006b) Recent progress in developing FRET-based intracellular sensors for the detection of small molecule nutrients and ligands. *Trends Biotechnol* 24:539–542
- Medintz IL (2009) Interfacing biology with nanomaterials. *Mater Today* 12:6–7
- Nel AE, Mädler L, Velegol D, Xia T, Hoek EMV, Somasundaran P, Klaessig F, Castranova V, Thompson M (2009) Understanding biophysicochemical interactions at the nano – bio interface. *Nat Mater* 8:543–557
- Noh HB, Lee KS, Chandra P, Won MS, Shim YB (2012) Application of a Cu-Co alloy dendrite on glucose and hydrogen peroxide sensors. *Electrochim Acta* 61:36–43
- Prasad A, Mahato K, Chandra P, Srivastava A, Joshi SN, Maurya PK (2016) Bioinspired composite materials: applications in diagnostics and therapeutics. *J Mol Eng Mater* 04:1640004
- Purohit B, Kumar A, Mahato K, Chandra P (2019a) Novel sensing assembly comprising engineered gold dendrites and MWCNT-AuNPs nanohybrid for acetaminophen detection in human urine. *Electroanalysis* 8. <https://doi.org/10.1002/elan.201900551>
- Purohit B, Kumar A, Mahato K, Roy S, Chandra P (2019b) Cancer cytosensing approaches in miniaturized settings based on advanced nanomaterials and biosensors. In: *Nanotechnology in modern animal biotechnology*, pp 133–147

- Purohit B, Mahato K, Kumar A, Chandra P (2019c) Sputtering enhanced peroxidase like activity of a dendritic nanochip for amperometric determination of hydrogen peroxide in blood samples. *Microchim Acta* 186:658
- Purohit B, Kumar A, Mahato K, Chandra P (2020a) Smartphone-assisted personalized diagnostic devices and wearable sensors. *Curr Opin Biomed Eng* 13:42–50
- Purohit B, Kumar A, Mahato K, Chandra P (2020b) Electrodeposition of metallic nanostructures for biosensing applications in health care. *J Sci Res* 64:68–73
- Sapsford KE, Tyner KM, Dair BJ, Deschamps JR, Medintz IL (2011) Analyzing nanomaterial bioconjugates: a review of current and emerging purification and characterization techniques. *Anal Chem* 83:4453–4488
- Sapsford KE, Algar WR, Berti L, Gemmill KB, Casey BJ, Oh E, Stewart MH, Medintz IL (2013) Functionalizing nanoparticles with biological molecules: developing chemistries that facilitate nanotechnology. *Chem Rev* 113:1904–2074
- Savaliya R, Shah D, Singh R, Kumar A, Shanker R, Dhawan A, Singh S (2015) Nanotechnology in disease diagnostic techniques. *Curr Drug Metab* 16:645–661
- Simmel FC, Dittmer WU (2005) DNA nanodevices. *Small* 1:284–299
- Subbiah R, Veerapandian M, Yun KS (2010) Nanoparticles: functionalization and multifunctional applications in biomedical sciences. *Curr Med Chem* 17:4559–4577
- Tang L, Wang Y, Li J (2015) The graphene/nucleic acid nanobiointerface. *Chem Soc Rev* 44:6954–6980
- Thanh NTK, Green LAW (2010) Functionalisation of nanoparticles for biomedical applications. *Nano Today* 5:213–230
- Vaddiraju S, Tomazos I, Burgess DJ, Jain FC, Papadimitrakopoulos F (2010) Emerging synergy between nanotechnology and implantable biosensors: a review. *Biosens Bioelectron* 25:1553–1565
- Veerapandian M, Yun K (2011) Functionalization of biomolecules on nanoparticles: specialized for antibacterial applications. *Appl Microbiol Biotechnol* 90:1655–1667
- Wadhwa R, Aggarwal T, Thapliyal N, Kumar A, Priya Y, Kumari V, Reddy BSC, Chandra P, Maurya PK (2019) Red blood cells as an efficient in vitro model for evaluating the efficacy of metallic nanoparticles. *3 Biotech* 9:279
- Wang ZL (2003) Nanobelts, nanowires, and nanodiskettes of semiconducting oxides – from materials to nanodevices. *Adv Mater* 15:432–436
- Wang F, Deng R, Wang J, Wang Q, Han Y, Zhu H, Chen X, Liu X (2011) Tuning upconversion through energy migration in core – shell nanoparticles. *Nat Mater* 10:968–973
- Wilchek M, Bayer EA, Livnah O (2006) Essentials of biorecognition: the (strept)avidin–biotin system as a model for protein–protein and protein–ligand interaction. *Immunol Lett* 103:27–32
- Willner I, Willner B (2010) Biomolecule-based nanomaterials and nanostructures. *Nano Lett* 10:3805–3815
- Won S-Y, Chandra P, Hee TS, Shim Y-B (2013) Simultaneous detection of antibacterial sulfonamides in a microfluidic device with amperometry. *Biosens Bioelectron* 39:204–209
- Xu M, Li J, Iwai H, Mei Q, Fujita D, Su H, Chen H, Hanagata N (2012) Formation of nano-bio-complex as nanomaterials dispersed in a biological solution for understanding nanobiological interactions. *Sci Rep* 2:406
- Yadav SK, Chandra P, Goyal RN, Shim Y-B (2013) A review on determination of steroids in biological samples exploiting nanobio-electroanalytical methods. *Anal Chim Acta* 762:14–24
- Zhu Y, Chandra P, Shim Y-B (2012a) Ultrasensitive and selective electrochemical diagnosis of breast cancer based on a hydrazine – Au nanoparticle – aptamer bioconjugate. *Anal Chem* 85:1058–1064
- Zhu Y, Chandra P, Song K-M, Ban C, Shim Y-B (2012b) Label-free detection of kanamycin based on the aptamer-functionalized conducting polymer/gold nanocomposite. *Biosens Bioelectron* 36:29–34
- Zhu Y, Chandra P, Shim YB (2013) Ultrasensitive and selective electrochemical diagnosis of breast cancer based on a hydrazine-Au nanoparticle-aptamer bioconjugate. *Anal Chem* 85:1058–1064



Bio-Nano-Interface Engineering Strategies of AuNPs Passivation for Next-Generation Biomedical Applications

10

Ashutosh Kumar, Buddhadev Purohit, Kuldeep Mahato, Supratim Mahapatra, Ananya Srivastava, and Pranjal Chandra

Abstract

Gold nanoparticles (AuNPs) have widely been used in various biomedical/clinical applications due to their enhanced physicochemical behavior and excellent optoelectronic properties. The AuNPs, due to its easy synthesis process, tunability, biocompatibility, and cost-effectiveness, found enormous attention in biomedical applications. However, the bare-surfaced AuNPs have long been debated, especially in the biomedical/clinical application. Thus, to make use of the synthesized AuNPs, it is passivated with various bio-based substances for the development of the bio-nano-interface or biocompatible interface to minimize the side effects of the bare metallic surface. This chapter inclines to discuss the contribution of such AuNPs having bio-nano-interface in state-of-the-art speculated various biomedical applications. Therefore, a short discussion on the AuNPs has been incorporated. In the next section, the need for its passivation is described. Herein, we have discussed various ways of AuNPs surface modification using several molecules with thiol, amine, amino acids, and biopolymers. In

A. Kumar · B. Purohit · K. Mahato

Laboratory of Bio-Physio Sensors and Nano-bioengineering, Department of Biosciences and Bioengineering, Indian Institute of Technology Guwahati, Guwahati, Assam, India

S. Mahapatra

School of Biochemical Engineering, Indian Institute of Technology (BHU) Varanasi, Varanasi, Uttar Pradesh, India

A. Srivastava

Department of Pharmacology and Toxicology, NIPER Guwahati, Guwahati, Assam, India

P. Chandra (✉)

Laboratory of Bio-Physio Sensors and Nano-bioengineering, Department of Biosciences and Bioengineering, Indian Institute of Technology Guwahati, Guwahati, Assam, India

School of Biochemical Engineering, Indian Institute of Technology (BHU) Varanasi, Varanasi, Uttar Pradesh, India

e-mail: pranjal.bce@iitbhu.ac.in

the last section, various biomedical applications that are being employed by using the passivated AuNPs having bio-nano-interface have been discussed, followed by the concluding remarks and future directions of this chapter.

Keywords

Gold nanoparticles · Bio-nano-interface · Surface passivation · Biomedical applications

10.1 Introduction

In contemporary scenarios, the clinical and biomedical technologies have found special attention towards their miniaturization (Chandra 2016; Chandra et al. 2017; Mahato et al. 2018b; Mahato et al. 2016b). This not only facilitates the smooth and intensive care to the patients but also offers to overcome various technical challenges associated with the clinical and biomedical practices for delivering the personalized onsite early-stage identification of the causative diseases (Purohit et al. 2020; Purohit et al. 2019). In order to achieve these goals, extraordinary capabilities of the nanomaterials have been exploited in recent past, where various noble metallic nanomaterials have been used (Kumar et al. 2019a; Kumar et al. 2019c; Kumar et al. 2019d; Mahato et al. 2019). Among these, gold-based nanoparticles have been widely used for the development of diagnostics and the therapeutics agents, due to their excellent optoelectronic properties, benign nature, and exceptional biocompatibility (Baranwal et al. 2018b; Jain et al. 2014; Reznikov et al. 2015; Zhao et al. 2016). The AuNPs synthesis process has been reported by the electrochemist Michael Faraday for the very first time in the early nineteenth century (Faraday 1857). Followed by this report, various attempts have been taken in synthesizing the AuNPs using the chemical, phytochemical, and physical-based synthetic processes (Chandra et al. 2013b). In chemical-based methods, the synthetic processes majorly involve the complete reduction of the positively charged oxidation states (+1 or +3), which have been attained by using various chemical, electrochemical, phytochemical medicated processes. In physical processes, attrition and pyrolysis have been used for obtaining AuNPs, which includes mechanical milling and vapor deposition processes (Mandal et al. 2018). Among all methods, the AuNPs synthesized from the chemical processes have been used for the clinical and biomedical applications due to the monodisperse nature of synthesized nanoparticles, which is mediated by the self-assembly (Baranwal et al. 2016; Boisselier and Astruc 2009; Daniel and Astruc 2004). To make the AuNPs suitable for biomedical and clinical applications, these nanoparticles are tuned by passivating with various moieties of chemical and biochemical origin, viz. amino acids, peptides, proteins, lipids, carbohydrates, fatty acids, and different other monomeric, polymeric, as well as biopolymeric substances (Kumar et al. 2019b; Mahato et al. 2019). Such tuning processes are essential not only to reduce the side effects of the metallic counterparts but also to achieve a higher degree of biological compatibility and tunability (Blanco et al. 2015; Sahoo

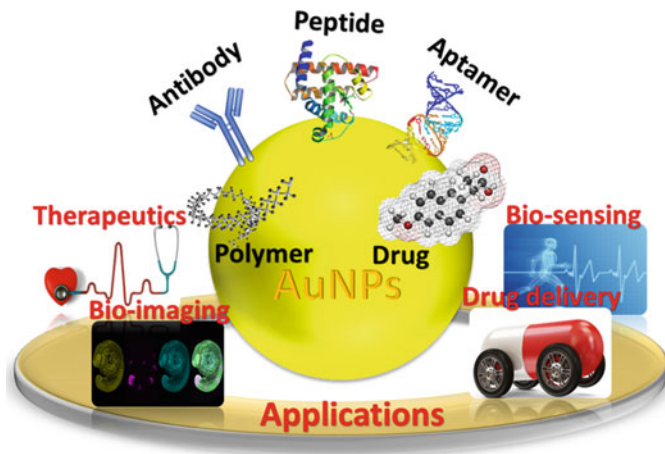


Fig. 10.1 Illustration showing the different components used for the AuNPs passivation to obtain bio-nano-interface and its widely used domains in biomedical disciplines

et al. 2017). Figure 10.1 summarizes various molecules that have been used for passivating AuNPs and the biomedical domains where the passivated AuNPs have been used.

10.2 Need of AuNPs Having Bio-Nano-Interface

The bare metallic parts are firstly passivated for employing the AuNPs in clinical or biomedical applications to obtain greater adaptability and efficacy in biological models. In various studies, it has been reported that the nanoparticles coated with molecules are more potently interacted with the biological models, viz. in vivo, in vivo, and ex vivo models, than bare nanoparticles (Chandra et al. 2013b; Park and Hamad-Schifferli 2010). Notably, in case of ex vivo and in vivo, non-engineered AuNPs are not preferred to be employed due to their toxic effects shown by the exposed bare metallic surface, which not only alters reaction properties of interacting molecules/metabolites but also alters the cellular/tissue functions by inducing the toxicity of various levels (Mahato et al. 2019; Villiers et al. 2010). In order to address these limitations, the bare AuNPs surface has been engineered to make a bio-nano-compatible interface. These AuNPs with bio-nano-interface have been reported to have excellent biocompatibility with negligible toxicity. So far various passivating molecules have been used to obtain AuNPs with bio-nano-interfaces, viz. thiols, amines, biocompatible polymers, and carboxy-terminated groups (Alex and Tiwari 2015; Chandra et al. 2012; Chandra et al. 2011; Koh et al. 2011; Zhu et al. 2012b, 2013; Zhu et al. 2012c). In addition, the outer bio-nano interfacial layer of the nanoparticle greatly influences a number of the chemical and physical properties like stability, solubility, and electronic states (Mandal et al. 2018a). Another problem associated with the loosely passivated layer of the biocompatible materials is that

these are prone to be mechanically destroyed or enzymatically degraded in a real-time application; thus, to ensure a high degree of adhesion, strong passivating components are used. For example, the Au-S covalent linking strategies have been exploited for anchoring the passivating molecules, viz. organo-thiols, disulfides, and cysteine rich macromolecules (Alex and Tiwari 2015). Similarly, various covalent linking strategies have been employed for achieving the nano-bio-interfaces at the AuNPs, including carbodiimide coupling, silane coupling, etc. (Craig et al. 2010).

10.3 The AuNPs: An Overview of Synthetic Procedures and Their Passivation for Obtaining Bio-Nano-Interface

The synthetic methods of AuNPs have been categorized under the “top-down” and “bottom-up” approaches, wherein the former technique the physical manipulations and in the later the chemical transformations are employed to obtain a range of surface engineered AuNPs (Fig. 10.2) (Mahato et al. 2019; Mandal et al. 2018). For applying them in biomedical and clinical applications, the chemically synthesized AuNPs were preferred due to their dispersal and the easy modification (Baranwal et al. 2016; Boisselier and Astruc 2009; Daniel and Astruc 2004). For these, the most common method for chemical-mediated synthesis of AuNPs is derived from the Turkevich model, where the gold salts are reduced using the passivating agent. The selection of these reducing agents/passivating agents are decided by the application depending on the perspective of AuNPs (Mahato et al. 2016a; Mandal et al. 2018; Prasad et al. 2016). For example, if the AuNPs have to use for in vivo applications, it should be passivated with a biocompatible layer consisting of biomaterials or proteins (Baranwal et al. 2018a).

In addition, if the application is oriented to the in vitro, there will have no particular requirement, and thus the non-proteinaceous/non-biomaterials agents could be used. Here, in this section, we describe various methods to obtain the AuNPs with nano-bio-interfaces, which eventually could be used for the in vivo, ex vivo applications.

10.3.1 Strategies for the Nano-Bio-Interface of AuNPs Using Thiol-Containing Moieties

Thiol-based bio-nano-interface modification of AuNPs: To obtain the bio-nano-interface to the AuNPs, these have been passivated using linker molecules in the recent past. Among all, the thiol groups have widely been used and are obtained by dissolving the chloroauric salts and the thiol-containing agents. In these strategies, the synthesis and the bio-nano-surface development are achieved by the simultaneous process, where the gold salt has been dissolved in the water and the passivating agent is dissolved in the organic medium and the synthesis is performed by the phase transfer process. For instance, in an example, AuCl_4^- ions are first obtained by dissolving gold salts in an aqueous medium and the phase transfer medium has been prepared by using the tetra-octyl ammonium bromide in toluene.

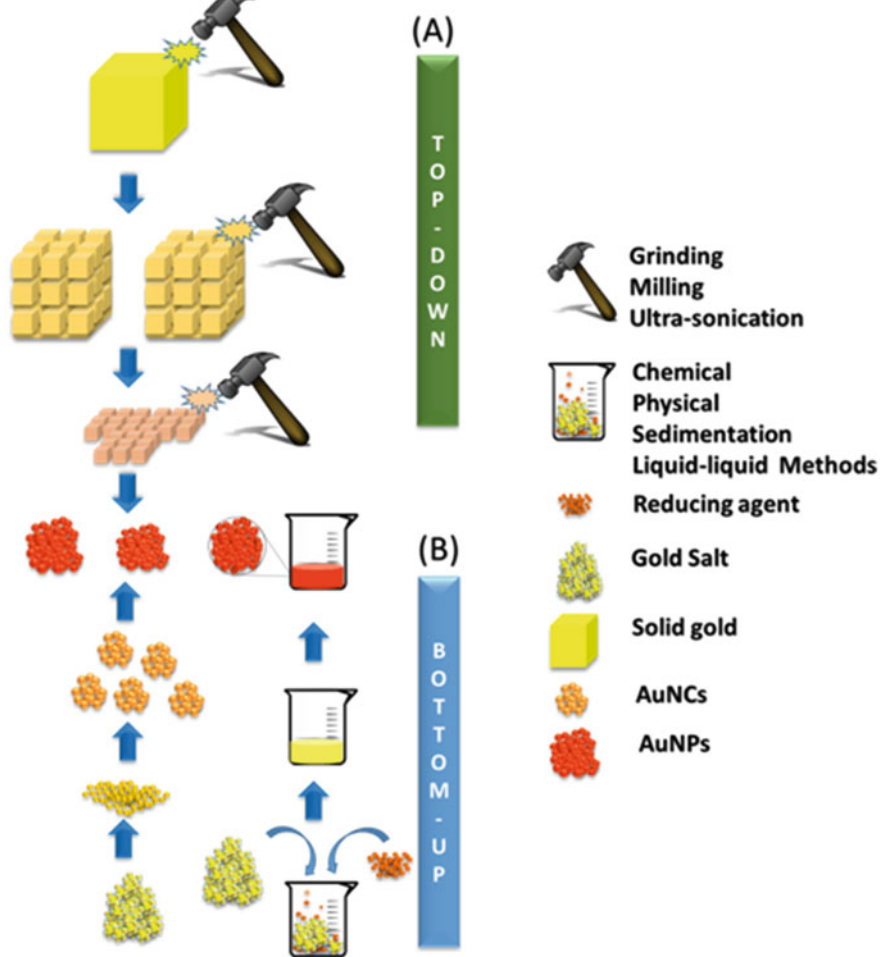


Fig. 10.2 Illustration showing the strategies for the AuNPs synthesis; (a) top-down approach, (b) bottom-up approach (Reprinted with the permission of Mahato et al. 2019, copyright Springer)

After that, the gold ions are extracted using the prepared toluene solution into the organic medium and reduced by sodium borohydride, and the passivation to obtain the nano-bio-interface is obtained by 1-dodecanethiol capping molecules (Chen and Kimura 1999; Hostetler et al. 1996; Templeton et al. 2000). In another example, the thiol-mediated bio-nano-interface onto the AuNPs has been obtained using the two-phase liquid-liquid system for simultaneous reduction of the gold salt in the presence of 4-mercaptoethanol (Brust et al. 1995). In addition to these, several attempts have been made to obtain thiol-mediated AuNPs with such nano-bio-interfaces, including thymine (Zhou et al. 2007), hexadecyl aniline (Ascencio et al. 2000), glutathione (Negishi et al. 2004), etc.

Secondary modification to the AuNPs following mixed-monolayer approach: Apart from the co-reduction processes with sulfur-containing thiol moieties, the AuNPs with bio-nano-interface have been developed by using the mixed monolayer approach where the AuNPs are passivated after their synthesis. The first attempts to this were made by Giersig and Mulvaney in 1993 using the alkanethiols moieties (Giersig and Mulvaney 1993). Due to their firm passivation, the particles were found extraordinarily stable and thus offered a better shelf life. Therefore, this strategy has been widely used for the synthesis of AuNPs having stable bio-nano-interface, were the most commonly adopted strategy is the thiol substitution of the passivating smaller thiol groups. Adopting this, several approaches have been reported. For example, Templeton et al. and Hostetler et al. have reported the substitution of anchored thiol ligands by the free thiol ligands (Hostetler et al. 1999; Templeton et al. 1998; Templeton et al. 2000). The other advantage of this strategy is using these the loading capacity to the AuNPs can be controlled. Apart from the classic model, the hybrid passivation has been incorporated in the recent past for obtaining application-oriented AuNPs with bio-nano-interface which includes thiol-terminated ligand and organic/inorganic dyes (Walter et al. 2002), biomolecules (Braun et al. 2009; Chen et al. 2005; Giljohann et al. 2010), drug molecules (Ghosh et al. 2008; Gibson et al. 2007), etc.

10.3.2 Strategies for the Bio-Nano-Interface of AuNPs Using Amine Moieties

Apart from the thiols, amine-based ligands are used for engineering the AuNPs surfaces to make the nanoparticles biocompatible. The synthesis of the AuNPs with the bio-nano-interface burst method has been widely employed following the thiol substitution with the thiol and amine groups at the surface. The significant advantages associated with these AuNPs are that these can be probed in several spectroscopic studies. So far, various attempts have been taken to synthesize the AuNPs. For instance, hydroxylamine has been for synthesizing such AuNPs (Graf and van Blaaderen 2002), which has been considered as a pioneering work for obtaining the AuNPs having amine-based bio-nano-interface. This groundbreaking work has paved the path for the synthesis of AuNPs with the bio-nano-interfaces using the organic amines. Here, the amine group serves as reducing as well as capping agents due to its effective redox potential. In addition to this, n-alkylamines have also been used for obtaining the bio-nano-interface at the AuNPs (Leff et al. 1996). Similar to this, several works have been reported for procuring such AuNPs in the past, including aminomethyl pyrene (Thomas and Kamat 2000), benzylamine (Thomas et al. 2002), 3-trimethoxysilylpropyl-diethylenetriamine (Zhu et al. 2005), oleylamine (Aslam et al. 2004), diamines (Selvakannan et al. 2004), porphyrins (Kotiahho et al. 2010), aromatic amines (Newman and Blanchard 2006), laurylamine (Kumar et al. 2003), tetraoctylammonium (Isaacs et al. 2005), and hyperbranched polyethylenimine (Duan and Nie 2007).

10.3.3 Strategies for the Nano-Bio-Interface of AuNPs Using Amino Acids

Since the amino acids are the biological building block of the proteins and having the amine groups available for passivating the AuNPs surface, it has also been used for obtaining the AuNPs with bio-nano-interface. Their unique functional group's abundance, viz. -SH and -NH₂, offers them to get layered over AuNPs surface, which eventually forms stable nanoparticles (Choudhary et al. 2016). Using amino acids, several approaches have been reported for obtaining the bio-nano-interface. For instance, lysine has been used for the synthesis of water-soluble AuNPs (Selvakannan et al. 2004), which shows the excellent water dispersibility when electrostatically stabilized. Another major advantage of these types of water-soluble AuNPs is that they can be lyophilized to make the powder form and can be kept for the longest time, and can be redispersed in the water when required. This makes it suitable for various applications in the intravenous and nanotherapeutics more easily. Similarly, tryptophan, aspartic acid (Shao et al. 2004), cysteine (Ma and Han 2008), and glutamic acid (Wangoo et al. 2008) have been employed for the passivation to obtain such AuNPs. The production of the water-dispersible nanoparticles has been readily employed in the fields of bioimaging, bio-labeling, and biosensing (Cumberland and Strouse 2002; Gittins and Caruso 2002).

10.3.4 Strategies for the Bio-Nano-Interface of AuNPs Using Biocompatible Polymers

Polymers are the macromolecules that offer excellent passivation to the metallic nanoparticle and thus provide them greater stability. The pioneering work was demonstrated by Helcher in 1718, using poly-saccharide as a passivating agent (Rac et al. 2014). The significant advantages of polymer-based passivation are these offers more extended stability, adjustable solubility, and high surface density (Chandra 2016; Chandra et al. 2012; Zhu et al. 2012a). Due to these advantages, the polymer-based passivation has been widely explored in the past using the biocompatible polymers, for example, poly (ethylene glycol), poly (vinyl alcohol), polyethyleneimine, poly (diallyl dimethyl ammonium chloride), poly- (vinyl methyl ether), and chitosan. The common strategies that have been used for obtaining the polymers assisted AuNPs having bio-nano-surfaces are broadly categorized under "grafting from" and "grafting to" based approaches.

Grafting-from technique: In this approach, the polymeric capping has been synthesized over the AuNPs surface. The growth of the chain is from the scaffold attached to the surface of it (Higuchi et al. 2007; Huo and Worden 2007; Kaholek et al. 2004; Shan and Tenhu 2007; Zhao et al. 2006). For this purpose, commonly, the alkyl thiol capping onto the AuNPs is employed as the precursor molecules, which have further been increased using polymerizations. This technique offers various advantages to controlling the thickness of the polymeric counterpart.

There have been several polymers used for obtaining such AuNPs in the recent past. For instance, Mandal et al. have reported a method for poly (methyl methacrylate) passivation onto the AuNPs surface by confined radical polymerization (Mandal et al. 2002). Similarly, poly(N-butyl acrylate) has been employed by using the atom transfer radical polymerization (Nuß et al. 2001). Apart from these, biopolymers have also been used to obtain the AuNPs having bio-nano-interface, including single-stranded oligonucleotide (Zhao et al. 2006), peptide (Higuchi et al. 2007), etc.

Grafting-to technique: In the “Grafting to” method, the AuNPs were synthesized in polymer aggregates, and the passivation has been employed after that. The prime advantage of this technique is the multiple availabilities of the functional groups, which offer the covalent passivation sites. In this strategy, the commonly used polymers are thioesters, thioether, thiol, and disulfides, which provide a chemical-bonded shell over the AuNPs surface (Aqil et al. 2008; Liu et al. 2007). Once the formation of AuNPs is completed, the chain propagation of the polymers is obtained by radical polymerization (Wang et al. 2007). The passivating cage has also been achieved by the cross-linking of the polymers for better stability. So far using this method various processes have been reported to obtain AuNPs having biocompatible nano-interface, viz. polyvinyl alcohol (Kwiatkowska et al. 2018), polyvinylpyrrolidone (Mohamed et al. 2017), polyethylene glycol (Ocal et al. 2018), polyvinyl pyridine (Zhang et al. 2018), polymethyl methacrylate (Zepon et al. 2015), Polyethylenimine (Lazarus and Singh 2016), polydiallyldimethyl ammonium chloride (Liu et al. 2016), and various biopolymers, viz. polysaccharides, proteins, peptides, etc. (Chowdhury et al. 2018).

10.4 Trending and Emerging Applications of Passivated AuNPs Having Bio-Nano-Interface

The bio-interface engineered AuNPs have been employed for various applications, which include personalized medicine, nanotherapeutics, nano-sensors, diagnostics, etc. (Chandra et al. 2010; Chandra et al. 2013b; Kumar et al. 2015). So far, the AuNPs containing bio-nano-interface have been exploited for numerous applications in various biomedical and clinical domains; this includes biosensing (Chandra et al. 2013a; Koh et al. 2011; Mahato et al. 2018a; Noh et al. 2012), drug delivery (Baranwal et al. 2018b), bioimaging (Wu et al. 2015), therapeutic (Rengan et al. 2015), etc.

10.4.1 Biosensing

AuNPs unique characteristics have extensively been employed for developing a number of a biosensor in various formats, including the optical and electrochemical forms (Chandra 2015; Kumar et al. 2015; Won et al. 2013; Zhu et al. 2012a). The exceptional optoelectronic properties of AuNPs, viz. surface plasmon, Raman

scattering, and fluorescence quenching, allow them to fabricate a wide range of biosensing strategies. A number of methods have been employed in the recent past for developing biosensors using AuNPs, where the fluctuation of surface plasmon resonance and optical properties have been measured to determine the bio-analytes in the range of clinical samples. For instance, a method developed by Taton et al. monitors the shifts in surface plasmon resonance bands of AuNPs have been measured on the fluctuation of the nucleic acid concentration (Taton et al. 2000). Similarly, the surface plasmon resonance technique has also been used for developing oral cancer diagnosis in in vivo and in vitro epithelial cancer cells (El-Sayed et al. 2005). Furthermore, when the AuNPs are aggregated, there is a substantial shift that occurs in the plasmon band causing the change in color appearances on exposure to the light; this eventually helps in the development of optical biosensors (Stockman 2011; Tanaka et al. 2006). Most of the naked eye biomedical/clinical diagnostics have been developed employing this property of the AuNPs. In these methods, the assessment of the target bio-analyte has been assessed by their direct/indirect action of triggering the aggregation or re-dispersion of AuNPs. For instance, the well-known kit for pregnancy test, the nano-bio-passivated AuNPs have been employed for the color appearance, which is mediated by the antibody, antigen coupling of the portentous biomarker (human chorionic-gonadotropin) (Tanaka et al. 2006). Similar to the colorimetric biosensor, fluorescence-based methods have also been used for diagnosing various analytes of clinical/biomedical importance. Among different fluorescence-based techniques, fluorescence resonance energy transfer-based methods have been used, where acceptor chromophore receives the energy from the donating chromophore pair. For instance, Zhang et al. have reported an AuNPs assisted fluorescence technique for the determination of the β -cyclodextrin (Zhang et al. 2008). In this format, the accuracy is a primary concern, which has been enhanced by introducing multicolored oligonucleotide-coupled dye to the AuNPs fluorophore-based nanoprobe (Ray et al. 2007). In electrochemical-based biosensor AuNPs have been employed for its conducting nature and available extensively large surface area for the conduction of the electrons (Mahato et al. 2016b). In a report from Zhu et al., a bifunctional probe-based biosensor has been demonstrated for the detection of the HER2 protein using the hydrazine-AuNPs-aptamer complex (Zhu et al. 2012b). In another report by Spampinato et al., a biosensor has been developed using the AuNPs assisted electrochemical for the determination of blood glucose levels in the clinical samples (Spampinato et al. 2016). Similarly, various other biosensors have been developed using the AuNPs by adding the improvised analytical performances of the biosensors for targeting the range of biomarkers/biomolecules, viz. drugs, neurotransmitters, heavy metal ions, bacterial/cancer cells, and different metabolites (Chandra 2016; Chandra et al. 2011; Zhu et al. 2012c).

10.4.2 Bioimaging

The excellent radiative properties of the AuNPs have led them to be used in clinical and biomedical imaging, where these facilitate the visualization contrast in the dark field microscopy. For instance, AuNPs having bio-nano-interface anchored with protein receptor (epidermal growth factor receptor) have been reported for the bioimaging of the cancer growth in vitro medium (El-Sayed et al. 2005). Moreover, the different geometries of the AuNPs were used for bioimaging, where the rods and cubes have been employed in the past by exploiting their photo-luminescence properties. In a report from Dreaden et al., such AuNPs have been employed for enhancing the contrast by femtosecond near-infrared region laser excitation (Dreaden et al. 2012), which have been reported to facilitate the better image by reducing the background noises and increasing the spatial resolution. Also, the optical signature of the AuNPs offers better in in vitro and in vivo imaging methods for detecting the cancerous mass and other specialized cells. For example, Durr et al. have reported a molecular imaging method using rod-shaped anti-EGFR antibodies anchored AuNPs, which has shown excellent spatial contrast in cancer bioimaging (Durr et al. 2007). Chandra et al. have also taken similar attempts for label-free bioimaging of cancer cells, where the interaction of the anticancer drug with the cell surface have been targeted to visualize the cancerous cells in vitro settings (Chandra et al. 2013a).

10.4.3 Therapeutics

The passivated AuNPs having biocompatible nano-interface also offers therapeutic compatibility due to their intrinsic photothermal properties; this has been exploited in the personalized diagnostics. Among all, photothermal therapy has been used widely for treating a number for the cancerous case. In photothermal therapy, the thermo-ablative properties of AuNPs are exploited to generate heat, which has been used for killing the targeted cancer cells using the near infrared or radio-frequency radiations (Huang et al. 2009; Jain et al. 2008). For instance, polyethylene glycol-coated rod-shaped AuNPs were employed for tumor inhibition in an animal model using near-infrared-based photothermal therapy (Dreaden et al. 2012). Similarly, the oligomeric aptamer-based AuNPs have been used for the therapeutics for cancer and viral-borne diseases (Wang et al. 2016). In a similar work, a nanocomposite comprising the aptamer-AuNP-graphene oxide-based photothermal activity has been used for killing the overexpressed MUC1 cancer cells MCF-7 with negligible damage of the healthy cells (Wang et al. 2016). The incorporation of the aptamer for passivation of the AuNPs offers amplified therapeutic efficiency by improving the specificity, stability, and uptake efficiency of biomolecules to obtain biocompatible selective nano-interface.

10.4.4 Drug Delivery

The AuNPs having bio-nano-interface have also been used in drug delivery applications in personalized medicine practices. Since these require the internalization of the drug load AuNPs in the targeted cells/tissues, it has to be coated with the biocompatible nano-interface for escaping the toxic effects mostly caused by the bare metallic part. The drug molecules are anchored by using the covalent modification or the non-covalent modification (Khandelia et al. 2014) depending on the species. For example, the prodrugs have been loaded using the covalent attachment, while the active drugs are generally attached to the non-covalent means for achieving the better release (Morgan et al. 2006). The payload can be controlled and tuned by internal and external stimuli such as pH (Polizzi et al. 2007), light (Han et al. 2006), and specific molecules (Hong et al. 2006). So far, various other molecules have also been attempted to deliver using the AuNPs having biocompatible passivation, including peptides, proteins, antibodies, and small molecules, viz. folic acid, paclitaxel, etc. For instance, Khandala et al. have reported polymer-coated AuNPs-protein conjugate that has been used for delivering the drug in the human cell line, and thereby achieved the target apoptosis (Khandelia et al. 2014).

10.5 Conclusions and Future Prospects

AuNPs are being the right candidate for the next generation of biomedical and clinical usage; however, the biocompatibility has been a debatable concern, especially in the bare surface. Thus, to minimize the side effects it has to be passivated with the biocompatible materials to achieve bio-nano-interface. The passivation of AuNPs is a crucial step for employing them in *in vivo/ex vivo* applications. This chapter describes various strategies adopted to obtain such passivated AuNPs having the bio-nano-interface coating. This chapter also describes various attempts taken using the AuNPs in the biomedical field, including biosensing, therapeutic, drug delivery, etc. Despite their tremendous application of the passivated AuNPs for next-generation biomedical applications, there are various concerns with AuNPs passivation including the appropriate thickness of the passivating layer, the anchoring component composition in the pro-drug anchoring. Hence, future work should be directed towards a better understanding of AuNPs behavior in biological systems.

Acknowledgments Dr. Pranjal Chandra thanks Prof. Pramod Kumar Jain, Director IIT(BHU) for providing necessary infrastructure for completion of this work. The work is supported by DST-Ramanujan grant SB/S2/RJN-042/2015.

Conflict of Interest The authors have no conflict of interest in this work to declare.

References

- Alex S, Tiwari A (2015) Functionalized gold nanoparticles: synthesis, properties, and applications – a review. *J Nanosci Nanotechnol* 15(3):1869–1894
- Aqil A, Qiu H, Greisch J-F, Jérôme R, De Pauw E, Jérôme C (2008) Coating of gold nanoparticles by thermosensitive poly (N-isopropylacrylamide) end-capped by biotin. *Polymer* 49 (5):1145–1153
- Ascencio JA, Pérez M, José-Yacamán M (2000) A truncated icosahedral structure observed in gold nanoparticles. *Surf Sci* 447(1):73–80
- Aslam M, Fu L, Su M, Vijayamohan K, Dravid VP (2004) Novel one-step synthesis of amine-stabilized aqueous colloidal gold nanoparticles. *J Mater Chem* 14(12):1795–1797
- Baranwal A, Mahato K, Srivastava A, Maurya PK, Chandra P (2016) Phytofabricated metallic nanoparticles and their clinical applications. *RSC Adv* 6(107):105996–106010
- Baranwal A, Kumar A, Priyadarshini A, Oggu GS, Bhatnagar I, Srivastava A, Chandra P (2018a) Chitosan: an undisputed bio-fabrication material for tissue engineering and bio-sensing applications. *Int J Biol Macromol* 110:110–123
- Baranwal A, Srivastava A, Kumar P, Bajpai VK, Maurya PK, Chandra P (2018b) Prospects of nanostructured materials and their composites as antimicrobial agents. *Front Microbiol* 9:422
- Blanco E, Shen H, Ferrari M (2015) Principles of nanoparticle design for overcoming biological barriers to drug delivery. *Nat Biotechnol* 33:941
- Boisselier E, Astruc D (2009) Gold nanoparticles in nanomedicine: preparations, imaging, diagnostics, therapies and toxicity. *Chem Soc Rev* 38(6):1759–1782
- Braun GB, Pallaoro A, Wu G, Missirlis D, Zasadzinski JA, Tirrell M, Reich NO (2009) Laser-activated gene silencing via gold nanoshell– siRNA conjugates. *ACS Nano* 3(7):2007–2015
- Brust M, Fink J, Bethell D, Schiffrin D, Kiely C (1995) Synthesis and reactions of functionalised gold nanoparticles. *Journal of the chemical society. Chem Commun* 16(16):1655–1656
- Chandra P (2015) Electrochemical nanobiosensors for cancer diagnosis. *J Anal Bioanal Tech* 6(1): e119
- Chandra P (2016) Nanobiosensors for personalized and onsite biomedical diagnosis. The Institute of Engineering and Technology, London
- Chandra P, Das D, Abdelwahab AA (2010) Gold nanoparticles in molecular diagnostics and therapeutics. *Dig J Nanomater Bios* 5(2):363–367
- Chandra P, Zaidi SA, Noh H-B, Shim Y-B (2011) Separation and simultaneous detection of anticancer drugs in a microfluidic device with an amperometric biosensor. *Biosens Bioelectron* 28(1):326–332
- Chandra P, Koh WCA, Noh H-B, Shim Y-B (2012) In vitro monitoring of i-NOS concentrations with an immunosensor: the inhibitory effect of endocrine disruptors on i-NOS release. *Biosens Bioelectron* 32(1):278–282
- Chandra P, Noh H-B, Shim Y-B (2013a) Cancer cell detection based on the interaction between an anticancer drug and cell membrane components. *Chem Commun* 49(19):1900–1902
- Chandra P, Singh J, Singh A, Srivastava A, Goyal RN, Shim YB (2013b) Gold nanoparticles and nanocomposites in clinical diagnostics using electrochemical methods. *J Nanopart* 2013:12
- Chandra P, Tan YN, Singh SP (2017) Next generation point-of-care biomedical sensors technologies for cancer diagnosis. Springer
- Chen S, Kimura K (1999) Synthesis and characterization of carboxylate-modified gold nanoparticle powders dispersible in water. *Langmuir* 15(4):1075–1082
- Chen J, Saeki F, Wiley BJ, Cang H, Cobb MJ, Li Z-Y, Au L, Zhang H, Kimmey MB, Li X (2005) Gold nanocages: bioconjugation and their potential use as optical imaging contrast agents. *Nano Lett* 5(3):473–477
- Choudhary M, Yadav P, Singh A, Kaur S, Ramirez-Vick J, Chandra P, Arora K, Singh SP (2016) CD 59 targeted ultrasensitive electrochemical immunosensor for fast and noninvasive diagnosis of oral cancer. *Electroanalysis* 28(10):2565–2574

- Chowdhury P, Roy B, Mukherjee N, Mukherjee S, Joardar N, Mondal MK, Roy D, Babu SPS (2018) Chitosan biopolymer functionalized gold nanoparticles with controlled cytotoxicity and improved antifilarial efficacy. *Adv Compos Hybrid Mater* 1(3):577–590
- Craig GA, Allen PJ, Mason MD (2010) Synthesis, characterization, and functionalization of gold nanoparticles for cancer imaging. In: *Cancer nanotechnology: methods and protocols*, pp 177–193
- Cumberland S, Strouse G (2002) Analysis of the nature of oxyanion adsorption on gold nanomaterial surfaces. *Langmuir* 18(1):269–276
- Daniel MC, Astruc D (2004) Gold nanoparticles: assembly, supramolecular chemistry, quantum-size-related properties, and applications toward biology, catalysis, and nanotechnology. *Chem Rev* 104(1):293–346
- Dreaden EC, Alkilany AM, Huang X, Murphy CJ, El-Sayed MA (2012) The golden age: gold nanoparticles for biomedicine. *Chem Soc Rev* 41(7):2740–2779
- Duan H, Nie S (2007) Etching colloidal gold nanocrystals with hyperbranched and multivalent polymers: a new route to fluorescent and water-soluble atomic clusters. *J Am Chem Soc* 129(9):2412–2413
- Durr NJ, Larson T, Smith DK, Korgel BA, Sokolov K, Ben-Yakar A (2007) Two-photon luminescence imaging of cancer cells using molecularly targeted gold nanorods. *Nano Lett* 7(4):941–945
- El-Sayed IH, Huang X, El-Sayed MA (2005) Surface plasmon resonance scattering and absorption of anti-EGFR antibody conjugated gold nanoparticles in cancer diagnostics: applications in oral cancer. *Nano Lett* 5(5):829–834
- Faraday M (1857) The Bakerian lecture: experimental relations of gold (and other metals) to light. *Philos Trans R Soc Lond* 147:145–181
- Ghosh P, Han G, De M, Kim CK, Rotello VM (2008) Gold nanoparticles in delivery applications. *Adv Drug Deliv Rev* 60(11):1307–1315
- Gibson JD, Khanal BP, Zubarev ER (2007) Paclitaxel-functionalized gold nanoparticles. *J Am Chem Soc* 129(37):11653–11661
- Giersig M, Mulvaney P (1993) Preparation of ordered colloid monolayers by electrophoretic deposition. *Langmuir* 9(12):3408–3413
- Giljohann DA, Seferos DS, Daniel WL, Massich MD, Patel PC, Mirkin CA (2010) Gold nanoparticles for biology and medicine. *Angew Chem Int Ed* 49(19):3280–3294
- Gittins DI, Caruso F (2002) Biological and physical applications of water-based metal nanoparticles synthesised in organic solution. *ChemPhysChem* 3(1):110–113
- Graf C, van Blaaderen A (2002) Metallodielectric colloidal core-shell particles for photonic applications. *Langmuir* 18(2):524–534
- Han G, You CC, Kim BJ, Turingan RS, Forbes NS, Martin CT, Rotello VM (2006) Light-regulated release of DNA and its delivery to nuclei by means of photolabile gold nanoparticles. *Angew Chem* 118(19):3237–3241
- Higuchi M, Ushiba K, Kawaguchi M (2007) Structural control of peptide-coated gold nanoparticle assemblies by the conformational transition of surface peptides. *J Colloid Interface Sci* 308(2):356–363
- Hong R, Han G, Fernández JM, Kim BJ, Forbes NS, Rotello VM (2006) Glutathione-mediated delivery and release using monolayer protected nanoparticle carriers. *J Am Chem Soc* 128(4):1078–1079
- Hostetler MJ, Green SJ, Stokes JJ, Murray RW (1996) Monolayers in three dimensions: synthesis and electrochemistry of ω -functionalized alkanethiolate-stabilized gold cluster compounds. *J Am Chem Soc* 118(17):4212–4213
- Hostetler MJ, Templeton AC, Murray RW (1999) Dynamics of place-exchange reactions on monolayer-protected gold cluster molecules. *Langmuir* 15(11):3782–3789
- Huang X, Neretina S, El-Sayed MA (2009) Gold nanorods: from synthesis and properties to biological and biomedical applications. *Adv Mater* 21(48):4880–4910

- Huo Q, Worden JG (2007) Monofunctional gold nanoparticles: synthesis and applications. *J Nanopart Res* 9(6):1013–1025
- Isaacs SR, Cutler EC, Park J-S, Lee TR, Shon Y-S (2005) Synthesis of tetraoctylammonium-protected gold nanoparticles with improved stability. *Langmuir* 21(13):5689–5692
- Jain PK, Huang X, El-Sayed IH, El-Sayed MA (2008) Noble metals on the nanoscale: optical and photothermal properties and some applications in imaging, sensing, biology, and medicine. *Acc Chem Res* 41(12):1578–1586
- Jain S, Hirst DG, O'Sullivan JM (2014) Gold nanoparticles as novel agents for cancer therapy. *Br J Radiol* 85(1010):101–113
- Kaholek M, Lee W-K, Ahn S-J, Ma H, Caster KC, LaMattina B, Zauscher S (2004) Stimulus-responsive poly (N-isopropylacrylamide) brushes and nanopatterns prepared by surface-initiated polymerization. *Chem Mater* 16(19):3688–3696
- Khandelia R, Jaiswal A, Ghosh SS, Chattopadhyay A (2014) Polymer coated gold nanoparticle–protein agglomerates as nanocarriers for hydrophobic drug delivery. *J Mater Chem B* 2(38):6472–6477
- Koh WCA, Chandra P, Kim D-M, Shim Y-B (2011) Electropolymerized self-assembled layer on gold nanoparticles: detection of inducible nitric oxide synthase in neuronal cell culture. *Anal Chem* 83(16):6177–6183
- Kotiaho A, Lahtinen R, Efimov A, Lehtivuori H, Tkachenko NV, Kanerva T, Lemmetyinen H (2010) Synthesis and time-resolved fluorescence study of porphyrin-functionalized gold nanoparticles. *J Photochem Photobiol A Chem* 212(2):129–134
- Kumar A, Mandal S, Selvakannan P, Pasricha R, Mandale A, Sastry M (2003) Investigation into the interaction between surface-bound alkylamines and gold nanoparticles. *Langmuir* 19(15):6277–6282
- Kumar A, Hens A, Arun RK, Chatterjee M, Mahato K, Layek K, Chanda N (2015) A paper based microfluidic device for easy detection of uric acid using positively charged gold nanoparticles. *Analyst* 140(6):1817–1821
- Kumar A, Purohit B, Mahato K, Chandra P (2019a) Chapter 11. Advance engineered nanomaterials in point-of-care immunosensing for biomedical diagnostics. In: *Immunosensors*. The Royal Society of Chemistry, pp 238–266
- Kumar A, Purohit B, Mahato K, Mandal R, Srivastava A, Chandra P (2019b) Gold-iron bimetallic nanoparticles impregnated reduced graphene oxide based nanosensor for label-free detection of biomarker related to non-alcoholic fatty liver disease. *Electroanalysis* 31(12):2417–2428
- Kumar A, Purohit B, Maurya PK, Pandey LM, Chandra P (2019c) Engineered nanomaterial assisted signal-amplification strategies for enhancing analytical performance of electrochemical biosensors. *Electroanalysis* 31(9):1615–1629
- Kumar A, Roy S, Srivastava A, Naikwade MM, Purohit B, Mahato K, Naidu VGM, Chandra P (2019d) Chapter 10. Nanotherapeutics: a novel and powerful approach in modern healthcare system. In: *Maurya PK, Singh S (eds) Nanotechnology in modern animal biotechnology*. Elsevier, pp 149–161
- Kwiatkowska A, Granicka LH, Grzeczkwicz A, Stachowiak R, Bączal P, Sobczak K, Darowski M, Kozarski M, Bielecki J (2018) Gold nanoparticle-modified poly (vinyl chloride) surface with improved antimicrobial properties for medical devices. *J Biomed Nanotechnol* 14(5):922–932
- Lazarus GG, Singh M (2016) In vitro cytotoxic activity and transfection efficiency of polyethyleneimine functionalized gold nanoparticles. *Colloids Surf B: Biointerfaces* 145:906–911
- Leff DV, Brandt L, Heath JR (1996) Synthesis and characterization of hydrophobic, organically-soluble gold nanocrystals functionalized with primary amines. *Langmuir* 12(20):4723–4730
- Liu Y, Shipton MK, Ryan J, Kaufman ED, Franzen S, Feldheim DL (2007) Synthesis, stability, and cellular internalization of gold nanoparticles containing mixed peptide-poly (ethylene glycol) monolayers. *Anal Chem* 79(6):2221–2229
- Liu X-P, Tong J, Yuan Z, Yang Y, Mao C-J, Niu H-L, Jin B-K, Zhang S-Y (2016) Highly sensitive electrochemical dopamine sensor from poly (diallyldimethylammonium chloride)-

- functionalized Graphene nanoribbon/gold nanoparticle nanocomposite. *J Nanosci Nanotechnol* 16(2):1645–1649
- Ma Z, Han H (2008) One-step synthesis of cystine-coated gold nanoparticles in aqueous solution. *Colloids Surf A Physicochem Eng Asp* 317(1):229–233
- Mahato K, Baranwal A, Srivastava A, Maurya PK, Chandra P (2016a) Smart materials for biosensing applications. In: *Techno-societal 2016, International Conference on Advanced Technologies for Societal Applications*, Springer, pp 421–431
- Mahato K, Prasad A, Maurya P, Chandra P (2016b) Nanobiosensors: next generation point-of-care biomedical devices for personalized diagnosis. *J Anal Bioanal Tech* 7:e125
- Mahato K, Kumar S, Srivastava A, Maurya PK, Singh R, Chandra P (2018a) Electrochemical immunosensors: fundamentals and applications in clinical diagnostics. In: *Handbook of immunoassay technologies*. Elsevier, pp 359–414
- Mahato, K., Maurya, P.K., Chandra, P., 2018b. Fundamentals and commercial aspects of nanobiosensors in point-of-care clinical diagnostics. *3 Biotech* 8(3), 149
- Mahato K, Nagpal S, Shah MA, Srivastava A, Maurya PK, Roy S, Jaiswal A, Singh R, Chandra P (2019) Gold nanoparticle surface engineering strategies and their applications in biomedicine and diagnostics. *3 Biotech* 9(2):57
- Mandal TK, Fleming MS, Walt DR (2002) Preparation of polymer coated gold nanoparticles by surface-confined living radical polymerization at ambient temperature. *Nano Lett* 2(1):3–7
- Mandal R, Baranwal A, Srivastava A, Chandra P (2018) Evolving trends in bio/chemical sensor fabrication incorporating bimetallic nanoparticles. *Biosens Bioelectron* 117:546–561
- Mohamed T, Matou-Nasri S, Farooq A, Whitehead D, Azzawi M (2017) Polyvinylpyrrolidone-coated gold nanoparticles inhibit endothelial cell viability, proliferation, and ERK1/2 phosphorylation and reduce the magnitude of endothelial-independent dilator responses in isolated aortic vessels. *Int J Nanomedicine* 12:8813
- Morgan MT, Nakanishi Y, Kroll DJ, Griset AP, Carnahan MA, Wathier M, Oberlies NH, Manikumar G, Wani MC, Grinstaff MW (2006) Dendrimer-encapsulated camptothecins: increased solubility, cellular uptake, and cellular retention affords enhanced anticancer activity in vitro. *Cancer Res* 66(24):11913–11921
- Negishi Y, Takasugi Y, Sato S, Yao H, Kimura K, Tsukuda T (2004) Magic-numbered Au n clusters protected by glutathione monolayers (n= 18, 21, 25, 28, 32, 39): isolation and spectroscopic characterization. *J Am Chem Soc* 126(21):6518–6519
- Newman J, Blanchard G (2006) Formation of gold nanoparticles using amine reducing agents. *Langmuir* 22(13):5882–5887
- Noh H-B, Chandra P, Moon JO, Shim Y-B (2012) In vivo detection of glutathione disulfide and oxidative stress monitoring using a biosensor. *Biomaterials* 33(9):2600–2607
- Nuß S, Böttcher H, Wurm H, Hallensleben ML (2001) Gold nanoparticles with covalently attached polymer chains. *Angew Chem Int Ed* 40(21):4016–4018
- Ocal SK, Patarroyo J, Kiremitler NB, Pekdemir S, Puentes VF, Onses MS (2018) Plasmonic assemblies of gold nanorods on nanoscale patterns of poly (ethylene glycol): application in surface-enhanced Raman spectroscopy. *J Colloid Interface Sci* 532:449–455
- Park S, Hamad-Schifferli K (2010) Nanoscale interfaces to biology. *Curr Opin Chem Biol* 14 (5):616–622
- Polizzi MA, Stasko NA, Schoenfisch MH (2007) Water-soluble nitric oxide-releasing gold nanoparticles. *Langmuir* 23(9):4938–4943
- Prasad A, Mahato K, Chandra P, Srivastava A, Joshi SN, Maurya PK (2016) Bioinspired composite materials: applications in diagnostics and therapeutics. *J Mol Eng Mater* 04(01):1640004
- Purohit B, Kumar A, Mahato K, Roy S, Chandra P (2019) Chapter 9. Cancer cytosensing approaches in miniaturized settings based on advanced nanomaterials and biosensors. In: Maurya PK, Singh S (eds) *Nanotechnology in modern animal biotechnology*. Elsevier, pp 133–147
- Purohit B, Kumar A, Mahato K, Chandra P (2020) Smartphone-assisted personalized diagnostic devices and wearable sensors. *Curr Opin Biomed Eng* 13:42–50

- Rac O, Suchorska-Woźniak P, Fiedot M, Teterycz H (2014) Influence of stabilising agents and pH on the size of SnO₂ nanoparticles. *Beilstein J Nanotechnol* 5(1):2192–2201
- Ray PC, Darbha GK, Ray A, Hardy W, Walker J (2007) A gold-nanoparticle-based fluorescence resonance energy transfer probe for multiplexed hybridization detection: accurate identification of bio-agents DNA. *Nanotechnology* 18(37). <https://doi.org/10.1088/0957-4484/18/37/375504>
- Rengan AK, Bukhari AB, Pradhan A, Malhotra R, Banerjee R, Srivastava R, De A (2015) In vivo analysis of biodegradable liposome gold nanoparticles as efficient agents for photothermal therapy of cancer. *Nano Lett* 15(2):842–848
- Reznikov AG, Salivonyk OA, Sotkis AG, Shuba YM (2015) Assessment of gold nanoparticle effect on prostate cancer LNCaP cells. *Exp Oncol* 37(2):100–104
- Sahoo SK, Misra R, Parveen S (2017) Nanoparticles: a boon to drug delivery, therapeutics, diagnostics and imaging. In: *Nanomedicine in cancer*. Pan Stanford, pp 73–124
- Selvakannan P, Mandal S, Phadtare S, Gole A, Pasricha R, Adyanthaya S, Sastry M (2004) Water-dispersible tryptophan-protected gold nanoparticles prepared by the spontaneous reduction of aqueous chloroaurate ions by the amino acid. *J Colloid Interface Sci* 269(1):97–102
- Shan J, Tenhu H (2007) Recent advances in polymer protected gold nanoparticles: synthesis, properties and applications. *Chem Commun* 2007(44):4580–4598
- Shao Y, Jin Y, Dong S (2004) Synthesis of gold nanoplates by aspartate reduction of gold chloride. *Chem Commun* (9):1104–1105
- Spampinato V, Parracino MA, La Spina R, Rossi F, Ceccone G (2016) Surface analysis of gold nanoparticles functionalized with thiol-modified glucose SAMs for biosens or applications. *Front Chem* 4:8e19
- Stockman MI (2011) Nanoplasmonics: past, present, and glimpse into future. *Opt Express* 19(22):22029–22106
- Tanaka R, Yuhi T, Nagatani N, Endo T, Kerman K, Takamura Y, Tamiya E (2006) A novel enhancement assay for immunochromatographic test strips using gold nanoparticles. *Anal Bioanal Chem* 385(8):1414–1420
- Taton TA, Mirkin CA, Letsinger RL (2000) Scanometric DNA array detection with nanoparticle probes. *Science* 289(5485):1757–1760
- Templeton AC, Hostetler MJ, Kraft CT, Murray RW (1998) Reactivity of monolayer-protected gold cluster molecules: steric effects. *J Am Chem Soc* 120(8):1906–1911
- Templeton AC, Wuelffing WP, Murray RW (2000) Monolayer-protected cluster molecules. *Acc Chem Res* 33(1):27–36
- Thomas KG, Kamat PV (2000) Making gold nanoparticles glow: enhanced emission from a surface-bound fluoroprobe. *J Am Chem Soc* 122(11):2655–2656
- Thomas KG, Zajicek J, Kamat PV (2002) Surface binding properties of tetraoctylammonium bromide-capped gold nanoparticles. *Langmuir* 18(9):3722–3727
- Villiers CL, Freitas H, Couderc R, Villiers M-B, Marche PN (2010) Analysis of the toxicity of gold nanoparticles on the immune system: effect on dendritic cell functions. *J Nanopart Res* 12(1):55–60
- Walter E, Murray B, Favier F, Kaltenpoth G, Grunze M, Penner R (2002) Noble and coinage metal nanowires by electrochemical step edge decoration. *J Phys Chem B* 106(44):11407–11411
- Wang Z, Tan B, Hussain I, Schaeffer N, Wyatt MF, Brust M, Cooper AI (2007) Design of polymeric stabilizers for size-controlled synthesis of monodisperse gold nanoparticles in water. *Langmuir* 23(2):885–895
- Wang CC, Wu SM, Li HW, Chang HT (2016) Biomedical applications of DNA-conjugated gold nanoparticles. *Chembiochem* 17(12):1052–1062
- Wangoo N, Bhasin K, Mehta S, Suri CR (2008) Synthesis and capping of water-dispersed gold nanoparticles by an amino acid: bioconjugation and binding studies. *J Colloid Interface Sci* 323(2):247–254
- Won S-Y, Chandra P, Hee TS, Shim Y-B (2013) Simultaneous detection of antibacterial sulfonamides in a microfluidic device with amperometry. *Biosens Bioelectron* 39(1):204–209

- Wu Q, Chen L, Huang L, Wang J, Liu J, Hu C, Han H (2015) Quantum dots decorated gold nanorod as fluorescent-plasmonic dual-modal contrasts agent for cancer imaging. *Biosens Bioelectron* 74:16–23
- Zepon KM, Otsuka I, Bouilhac C, Muniz EC, Soldi V, Borsali R (2015) Glyco-nanoparticles made from self-assembly of Maltoheptaose-block-poly (methyl methacrylate): micelle, reverse micelle, and encapsulation. *Biomacromolecules* 16(7):2012–2024
- Zhang N, Liu Y, Tong L, Xu K, Zhuo L, Tang B (2008) A novel assembly of Au NPs– β -CDs–FL for the fluorescent probing of cholesterol and its application in blood serum. *Analyst* 133(9):1176–1181
- Zhang Z, Sèbe G, Wang X, Tam KC (2018) Gold nanoparticles stabilized by poly (4-vinylpyridine) grafted cellulose nanocrystals as efficient and recyclable catalysts. *Carbohydr Polym* 182:61–68
- Zhao W, Gao Y, Kandadai SA, Brook MA, Li Y (2006) DNA polymerization on gold nanoparticles through rolling circle amplification: towards novel scaffolds for three-dimensional periodic nanoassemblies. *Angew Chem Int Ed* 45(15):2409–2413
- Zhao Y, Huang Y, Zhu H, Zhu Q, Xia Y (2016) Three-in-one: sensing, self-assembly, and Cascade catalysis of Cyclodextrin modified gold nanoparticles. *J Am Chem Soc* 138(51):16645–16654
- Zhou J, Beattie DA, Sedev R, Ralston J (2007) Synthesis and surface structure of thymine-functionalized, self-assembled monolayer-protected gold nanoparticles. *Langmuir* 23(18):9170–9177
- Zhu H, Pan Z, Hagaman EW, Liang C, Overbury SH, Dai S (2005) Facile one-pot synthesis of gold nanoparticles stabilized with bifunctional amino/siloxy ligands. *J Colloid Interface Sci* 287(1):360–365
- Zhu Y, Chandra P, Ban C, Shim Y-B (2012a) Electrochemical evaluation of binding affinity for Aptamer selection using the microarray chip. *Electroanalysis* 24(5):1057–1064
- Zhu Y, Chandra P, Shim Y-B (2012b) Ultrasensitive and selective electrochemical diagnosis of breast cancer based on a hydrazine–Au nanoparticle–aptamer bioconjugate. *Anal Chem* 85(2):1058–1064
- Zhu Y, Chandra P, Song K-M, Ban C, Shim Y-B (2012c) Label-free detection of kanamycin based on the aptamer-functionalized conducting polymer/gold nanocomposite. *Biosens Bioelectron* 36(1):29–34
- Zhu Y, Chandra P, Shim Y-B (2013) Ultrasensitive and selective electrochemical diagnosis of breast cancer based on a hydrazine–Au nanoparticle–Aptamer bioconjugate. *Anal Chem* 85(2):1058–1064



Electro-optical Analysis as Sensing System for Detection and Diagnostics of Bacterial Cells

11

O. I. Guliy and V. D. Bunin

Abstract

Identification of the physiological state of bacterial cells and stages of cell metabolism online is the most important area of research in laboratory practice, in the validation, optimization, and scale-up of biotechnological processes. Unfortunately, currently there are no methods, which would allow solving these problems by direct measurements. However, a number of these problems can be successfully solved by indirect methods of the measuring of the cell structures parameters.

The chapter outlines the essentials of electrophysical analysis in a concise and intelligible way, as well as demonstrates the fields of electro-optical (EO) analysis application for solving multiple challenges in applied microbiology based on experimental data. EO technique for studying suspended cells offers a fairly simple means for measurement of electric and morphometric properties of certain cell structures. The technique is rather fast as the analysis takes about 10 min; besides the measurement process can be fully automated. EO analysis technique does not involve fixation of specific reagents in the measuring cell, and can be applied for evaluation of both live and lyophilized bacteria transferred into a suspended state.

A unique detailed data on the development and/or certain exposure process is potentially available for each microorganism species. The method can also offer useful information regarding biophysical aspects of bacteria under exposure to specific agents. The described EO analysis method is quite promising for development of sensor systems and their use in the field of microbiology, healthcare, veterinary medicine, as well as in biotechnological processes.

O. I. Guliy (✉)

Institute of Biochemistry and Physiology of Plants and Microorganisms, Russian Academy of Sciences, Saratov, Russia

V. D. Bunin

EloSystem GbR, Berlin, Germany

© Springer Nature Singapore Pte Ltd. 2020

P. Chandra, L.M. Pandey (eds.), *Biointerface Engineering: Prospects in Medical Diagnostics and Drug Delivery*, https://doi.org/10.1007/978-981-15-4790-4_11

233

KeywordsElectro-optical analysis · Detection · Microbial cells · Sensing system

11.1 Introduction

Modern scientific age is notable for rapidly progressing biotech and medical research, including development and refinement of novel analysis methods of microbial cells and cellular structures to improve production processes as well as bacterial control and diagnostics.

Full information on the condition of prokaryotic cells can be obtained by defining the entire range of their physiological, biochemical, and physical parameters. These parameters are closely interrelated and can change in the course of cell vital activities and during its interaction with the environment. Along with that the changes in one group of parameters will be manifested to a greater or lesser extent through alteration of parameters in a different group.

From microbiological and biotechnological standpoint of practical interest are intravital biochemical and physiological cell characteristics. Yet instrumental analytical methods can mostly achieve time-lagged measurement of physical characteristics of a cell medium but rarely can measure the characteristics of cells themselves. The level of precision in describing physiological condition of cells based on indirect parameters is low and insufficient for the majority of modern tasks. Therefore, special attention is being given to direct methods of defining physiological condition of cells that would support real-time monitoring and validation of biotechnological processes.

Electrophysical analytical methods offer novel approach to evaluation of intravital physiological cell parameters and their heterogeneity. They are based on cell probing with oscillating electrical field and ensure measurement of electrical parameters in cellular structures related to electric polarizability changes. The initial parameters of cellular structures are their specific conductivity and dielectric permittivity.

The methods used for measuring electric polarizability are based on the effects of exposing cells suspended in aqueous medium to electric field force. Physical manifestations of this exposure can include the effects of cell electro-orientation or electrorotation. Electro-orientation is manifested in cell transition to oriented state (Bunin and Voloshin 1996), whereas electrorotation consists in their continuous spinning (Gimsa et al. 1991, 1995).

This chapter will focus on the principles of electro-optical (EO) analysis method. An integral parameter in EO method of analyzing cell suspensions is electric polarizability of a layered object under various electric field frequencies, evaluated via registering the changes in optical properties of the studied suspension. In addition, there is a possibility to separately define the parameters of different cellular structures through electric field frequency variation. For detailed description of this measurement procedure the reader can refer to several articles (Bunin and Voloshin

1996; Ignatov et al. 2008; Guliy et al. 2017), and a brief summary is provided further below.

Application of EO method for analysis of electrical parameters in cellular structures offers multiple undeniable advantages. The influence of maintenance medium on the precision of measuring polarization parameters is negligible and predictable. The impact of measurement process on the cells is quite mild, which supports retention of their viability. Besides, this is an operational method, and the measurement process can be fully automated. It can be applied both for real-time process analysis and for steady-state cell studies. This field of analysis allows studying specific and nonspecific cell interactions with various markers, and offers cell detection and identification solutions.

Looking at the place of electro-optics in the taxonomy of physical analysis methods it is noteworthy that this method supplements and expands functionality of optical cell structure analysis method, which is based on the differences in refraction index of cell structures. As follows from the theory of polarization of substances, the value of substance refraction index within the optical range corresponds to dielectric permittivity asymptotics of cell structure material. Yet EO analysis additionally allows assessing specific conductivity of cell structure material as well as using functional dependence of changes in these parameters on electric field frequency.

The aim of this work is to outline the essentials of electrophysical analysis in a concise and intelligible way, as well as to demonstrate the fields of electro-optical analysis application for solving multiple challenges in applied microbiology based on experimental data.

11.2 Cell Behavior in Electric Field

The majority of analytical techniques are based on using electric characteristics of cellular structures and cells as a whole. It is commonly known that two parameters describe the electrical properties of a substance, namely specific conductivity σ and dielectric permittivity ε (Bottcher 1982).

The integral parameter that incorporates them is complex dielectric permittivity:

$$\sigma = \sigma/j\omega + \varepsilon \quad (11.1)$$

where ω —is electric field frequency.

The relationship between these parameters and cell metabolism will be reviewed further below, and here we will focus on the fundamentals of evaluating these parameters in cells.

A microbial cell features a complex structure and comprises several structures possessing different electrical properties. Therefore, an analytical measuring technique for electrical parameters of cellular structures should be capable of analyzing them separately, either directly or indirectly. In the simplest case the technique can be limited to a cell model with two cellular structures—membrane and cytoplasm,

and their complex electrophysical parameters $\hat{\epsilon}_{\text{mem}}$ and $\hat{\epsilon}_{\text{cyt}}$, respectively. Since the cells are in a suspended state, third complex parameter of a suspension medium $\hat{\epsilon}_{\text{out}}$ is always added. Inclusion of additional layers in the model, e.g., cell wall, will not substantially enhance capabilities of the method and therefore is not covered here.

If a microbial cell is exposed to alternative electrical field, electric charges are formed at the boundaries between cellular structures. In the above case these will be cytoplasm and membrane interface, as well as membrane and maintenance medium contact area. This phenomenon is known as Maxwell-Wagner polarization effect (Miroshnikov et al. 1986). Distribution and the absolute value of the induced charges are defined by the relation between electrophysical parameters of adjacent cellular structures and their relative thickness. Interaction between the induced charges and the field leads to transition of cells into a more energetically stable state, which is manifested in their orientation change. In the limiting case of high electric field intensity the exposed cells can line up along electric field vector or across it depending on the ratio of electrophysical parameters of contiguous structures.

Electrophysical cell parameters cannot be determined in case of complete cell orientation. Of major interest are weak cell orientation cases, when the degree of cell orientation is proportional to the cumulative value of charges induced at cell structure interfaces and can change.

In this case it only remains to relate the degree of cell orientation with the changes in one of the registered optical suspension parameters: light scattering, optical density, or birefringence. Historically the preference has been given to measurement of optical density OD increase in a non-polarized monochromatic light.

Combined application of field-induced cell polarization leading to cell orientation change with optical registering of these changes is called electro-optic effect. The combination of these phenomena is shown in Fig. 11.1A, and for a more detailed theory the reader can refer to Dukhin (1977), Stoylov (1991), and Bunin (2002).

Noteworthy, one steady-state parameter ΔOD is registered on each electric field frequency ω , and there are four electrophysical parameters of a cell with cytoplasm and membrane, namely: σ_{mem} , ϵ_{mem} , σ_{cyt} , and ϵ_{cyt} . Two electrophysical parameters of suspension medium— σ_{out} and ϵ_{out} —are added to the above. What can help simplify this situation? Dielectric permittivity of the medium ϵ_{out} is a constant. The changes in dielectric permittivity of cytoplasm (ϵ_{cyt}) and membrane (ϵ_{mem}) are minor.

Specific conductivity of the medium σ_{out} should anyway be reduced to negligible values. This should be done on the grounds of several assumptions. The differences q_1-q_2 and q_3-q_4 are increased, which forces the cell to change its orientation and balance the electric force and the thermal effect of the medium. This is accompanied by the increase in electro-optical signal amplitude. With the decrease in q_1 and q_4 the influence of ambient electrical conductivity on the measured electro-optical signal is avoided. Double electric layer around the cell becomes stretched and will not shield the electric field.

To isolate the two remaining specific conductivity parameters σ_{cyt} and σ_{mem} from electro-optical signal with almost constant dielectric permittivity parameters, parametric change of electric field frequency is applied in the course of

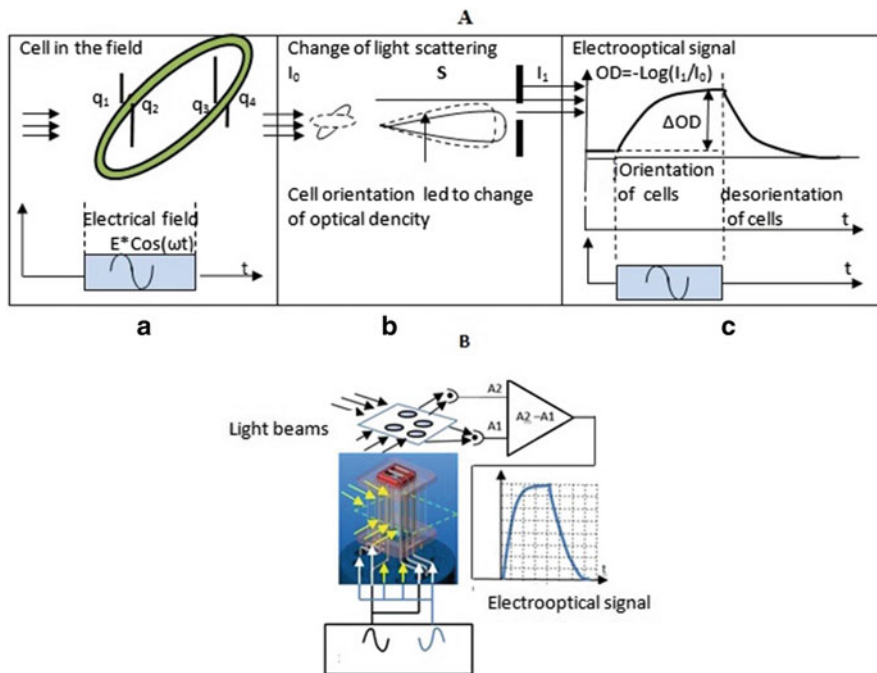


Fig. 11.1 (A) Single-layer cell model in electric field $E \times \cos(\omega t)$: (a) induced charges q_1 – q_4 , (b) light scattering change following cell orientation, (c) optical density change following cell orientation. (B) Microbial suspension optical density change in the course of EO experiment

measurement. As a result, ΔOD data array is obtained on various electric field frequencies. This data array is called frequency dispersion or electro-optical signal spectrum.

Thus, logarithmic frequency dependence of the difference between optical density of δOD suspension measured with non-polarized light beam propagation along and across the orientating field direction was expressed in the form of orientation spectra. This difference is limited by optical density value in a chaotic cell orientation state (Bunin 2002).

Electro-optical signal can be characterized by two parameters—steady-state value of electro-optical signal after completion of orientation processes ΔOD , and the relaxation curve pattern. The design of microbial suspension optical density measurement in the course of EO experiment is shown in Fig. 11.1B. Steady-state value of electro-optical signal is used for calculation of electric cell properties, and relaxation curve shape—for calculation of cell size distribution or in a simplistic case—to determine the average cell size in a suspension (De la Torre and Blumfield 1981).

When using electric field frequencies within the range of 400–600 kHz, the steady-state value of ΔOD signal becomes proportional to cytoplasm-specific conductivity within the accuracy of the constant $\sigma_{cyl} = \sim \Delta OD(\omega)$. Membrane

conductivity evaluation σ_{mem} is performed using steady-state signals on the three points of the spectrum $\Delta\text{OD}(\omega)$ within the frequency range of 0.8–2.2 mHz. To study surface interactions steady-state signals $\Delta\text{OD}(\omega)$ of full spectrum are used within the frequency range of 1 kHz to 5 mHz.

In the ideal case of homogenous cell size the relaxation curve shape can be described by one exponential function. For cell suspension with morphometric heterogeneity of the cells this will be a sum of exponential functions. Each exponent represents one cell fraction with certain size, and the weight factor defines contribution of this fraction in total signal. It was revealed in multiple experiments that the pattern of cell size distribution remains almost the same for the majority of processes. Yet the distribution scale can vary considerably. Cell size distribution and, correspondingly, the relaxation curve representing this process is elongated with general size increase in each fraction or is compressed in case of its decrease. To describe the timescale changes of the relaxation curve only one morphometric parameter is used—the average size—which will be used further on in the examples of how can electro-optic results be used. For a cell fraction homogeneous in size, the relaxation curve is described as an exponential curve. The exponent is defined by a product of cell size analytical function multiplied by kinematic viscosity of the medium. Cell size function in the theory of orientation-disorientation of particles is called a particle rotational diffusion coefficient (Shchyogolev et al. 1994).

An important factor is the optical density of the studied cell sample. To avoid any influence of optical density on electro-optical signal value, the measurements should be taken within the low range of this parameter, when no multiple scattering of light takes place in the suspension. Normalization of electro-optical signal by optical density value allows eliminating the influence of this parameter on the end result only within a relatively narrow range of its variation.

11.3 Relationship Between Electrophysical Parameters, Cell Metabolism, and Surface Interactions

As mentioned above, electro-optical analysis allows determining cytoplasm-specific conductivity σ_{cyt} . It is worth providing more insight on how this parameter is related to cell vital activities. Cell metabolism processes are defined by ion flows present in any biochemical transformations to a greater or lesser extent. Contribution of each ion type to the integral parameter of cytoplasm-specific conductivity is proportional to their concentration K_i and mobility μ_i (Williams and Williams 1972):

$$\delta_{\text{cyt}} = \sum \mu_i \times K_i \quad (11.2)$$

where K_i is the concentration of i -type ions in a cell structure
 μ_i — i -type ion mobility

At the stage of σ_{cyt} value calculation, the method excludes ions with low concentration and/or low mobility. After such filtration of ion pool by mobility and concentration values, the pool only contains a portion of H^+ ions, which

participate in redox reactions, K^+ ions as protein protectors, as well as ions of weak organic acids—by-products of cell metabolism.

Ion concentration in cytoplasm is influenced by the dissociation rate of the compounds the ions have been a part of. For example, dissociation constants for the majority of organic frequencies are within the pH range of 4.5–5.0. At each stage of cell development intracellular pH and dissociation constant determine the number of bound ions possessing neutral charge and capable of approaching the inner wall of electrically charged membrane. Only non-charged molecules can get through the membrane and reach the environment via active transport.

Another key factor determining specific conductivity values is cell and solution temperature. It influences specific conductivity of cytoplasm σ_{cyt} as well as the absolute viscosity value, which in its turn affects the timescale of relaxation curve, and consequently the average cell size value.

11.4 Cell Preparation for Electro-optical Measurement

If performed correctly, electro-optical method of measuring specific conductivity and average cell size ensures a relative measurement error not more than 2.0%. Not many nondestructive cell analysis methods can offer such high precision and data reproducibility. However to reach such precision several requirements must be met:

1. Accurate measurement of initial optical density of the suspension. Calibrated suspension dilution and application of multiple scattering compensation algorithms, if required.
2. Multifold decrease in suspension conductivity. Specific conductivity of a maintenance medium should not exceed 5–10 $\mu\text{Sm/cm}$. Therefore, filtering the initial suspension, sediment washing, and resuspension in deionized water are essential sample preparation stages. In case of wide cell concentration range in the studied sample, for example, during cultivation process monitoring, suspension dilution always precedes its filtration. This protects the filter from overload. Deviation of suspension-specific conductivity from certain constant, e.g., 10 $\mu\text{Sm/cm}$, should be accounted for and compensated with a corrective function.
3. The prepared sample temperature should remain the same throughout the whole measurement cycle. This can be achieved by setting and adjusting deionized water temperature as the main heat carrier.
4. Optical density of the prepared sample should remain the same for all samples within the measurement cycle.

A distinctive feature of electro-optical method is the possibility to automatically test the results. If there is a suspicion that cell size increase takes place due to osmotic pressure between cytoplasm and ambient medium, this uncertainty can be solved by performing a series of measurements on one sample. Cell size retention within the average cell size measurement error during the period of sample preparation and throughout the measurement procedure is the most cogent argument of hypoosmosis

absence. In extreme cases of exceptionally labile cells there is always an option to use a compensating additive, such as inositol sugar, which is not utilized by microorganisms.

Auto-testing of one cell sample in serial measurements allows evaluating membrane integrity for resting cells. If cell membranes are damaged, specific conductivity of cytoplasm σ_{cyl} will start decreasing after a period of time. In case of cells in active growth phase, repeated measurements taken on a single sample allow controlling active transport efficiency as well as the efficiency of toxic metabolites elimination from these cells.

11.5 Sample Preparation and Electro-optical Method Procedures

After sample preparation, the microbial cell sample should have optical density within 0.05–0.15 OD units in a 10 mm cuvette at the wavelength of 660–680 nm throughout the whole measurement cycle. This is the zone of single light scattering by the cells with no attenuation. The lower OD threshold is determined by a sufficient magnitude of electro-optical signal. The upper threshold ensures working with the starter culture with typical OD values of 0.2–0.4. The method supports working with ultra-low concentrations, such as cell identification even with 500 cells/ml. This involves a more complex measurement procedure, data accumulation, and filtering. All this will increase analysis time. When using initial samples with optical density within the range of 0.1–25.0 OD units, the measurement system's own capabilities are sufficient with max suspension pre-filtration dilution coefficient of 10. When upper OD threshold is exceeded, additional calibrated dilution of initial sample is required with the dilution factor $G = 1-10$.

Specific conductivity of a sample σ_{med} should not exceed 10 $\mu\text{S/cm}$. To obtain such a low value initial sample desalting should be performed. To reduce filtering time, the procedures of cell sedimentation on the filter, their washing, and resuspension in a low-conducting medium are required. Only this method supports solution desalting within a short period of time.

Therefore, sample preparation should include the following procedures:

- Measurement of initial suspension optical density.
- Sample dilution to obtain an amount of cells in the sample that would be safe for the filter.
- Three-stage process of cell transfer into a low conductivity medium, which includes their precipitation, washing, and resuspension.
- Setting calibrated optical density value in the sample for electro-optical analysis.

Electro-optical measurement procedure includes:

- Generating electric field of certain frequency (ω), strength (E), and duration (T) in the measuring cell.

- Measuring the optical signal with the cells oriented and disoriented.
- Performing measurements with variation of one electric field parameter to obtain spectral (ω change), field (E change), or orientation dependencies. Nevertheless, each of these dependencies with a chosen classification represents a single measurement. Field and orientation dependencies are used for selecting appropriate measurement conditions and are usually performed only once when starting the works with a new cell culture. If such measurements with fixed E and T values are taken repeatedly, a time dependence of electrophysical/morphometric parameters or electrophysical/morphometric process profile will be obtained.

11.6 Single Measurements of Electrophysical Cell Parameters

Isolated measurements of electrophysical cell parameters are typical for cells in a stationary phase. Just like certain body temperature level is characteristic for humans, specific conductivity σ_{cyt} is a consistent indicator of a cell's condition. This parameter has different values depending on the type of intracellular metabolism. For rapidly growing cells with small generation time of 10 min to several hours, it can reach 1000 $\mu\text{S}/\text{cm}$ or more. For cells with generation time of several days, it can be several tens of $\mu\text{S}/\text{cm}$. Yet for each cell type after conventional development this parameter demonstrates amazing reproducibility in a stationary phase. Spectral characteristics of various bacterial cell types and spores in a stationary growth phase are shown in Fig. 11.2.

As mentioned above, to determine specific conductivity σ_{cyt} , only the electric field frequency range marked with two rectangles in Fig. 11.2 is used. The difference in spectral shapes for different strains is conditioned by their morphometric parameters—size and offset (=lateral axis/ transversal axis), and the absolute value—by intracellular metabolism intensity.

For routine measurements, both the absolute value of specific conductivity σ_{cyt} and its relative value can be used. In the first case, to convert the measured electro-optical ΔOD signal into the absolute value of specific conductivity σ_{cyt} parametric dependence of electro-optical signal on specific electrical conductivity of the medium is used. Yet in practice relative measurements are usually enough since the conversion factor is a constant and does not change throughout the measurement process for any cell strain.

11.6.1 Determination of Cell Survivability

Determination of cell viability is the most typical example of single electro-optical measurements. The following parameters are used for such assessment: electric field frequency ω within 400–600 kHz, field intensity E below 50 V/cm, and field exposure duration assuring cell orientation above 95%. With a single-staged construction of dependence between relative cell viability and σ_{cyt} level, electro-optical method offers a replacement for labor-intensive manual cell viability evaluation

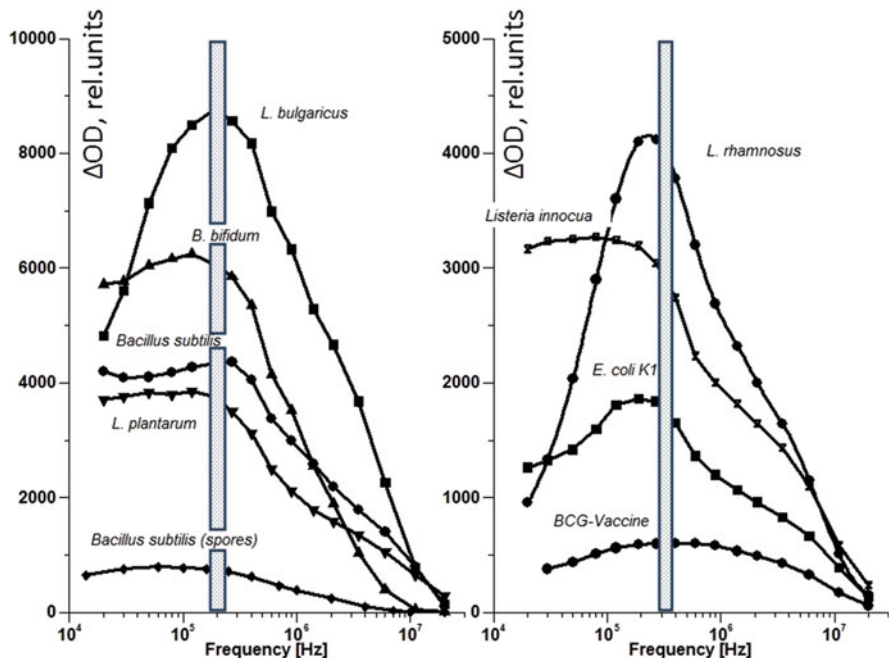


Fig. 11.2 Electro-optical spectrum examples for various cell types in stationary growth phase

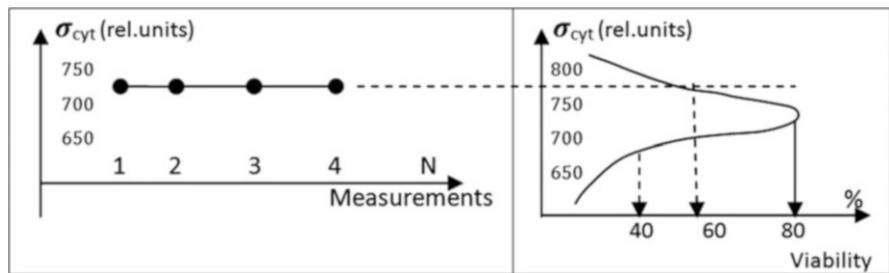


Fig. 11.3 Relationship between relative survivability (%) and specific conductivity of cytoplasm σ_{cyt} , N-number of measurements taken

technique. Furthermore, it does not matter which reference viability assessment technique was used for calibration measurements. Relative measurement error in this case does not exceed 2–3%. If data reliability is questioned, this parameter can be checked using a direct method. Statistic reliability of the result is determined by the number of cells “N” in a measuring cell and is equal to “N” value of about 10^5 .

Figure 11.3 shows the technique of converting specific electric conductivity value σ_{cyt} into relative cell viability (%).

The reason behind viability decrease for σ_{cyt} values above optimal level is the excessive concentration of toxic metabolites. The cause of viability decrease if σ_{cyt} value is below optimal level could be low cellular energy status.

When determining the absolute value of the concentration of viable cells, independent evaluation of total absolute cell concentration C is required. To measure this parameter, Lambert–Beer law is applied, linking concentration C with optical density OD of a suspension at single light scattering by particles.

$$C = 1/A \times G \times \text{OD} \quad (11.3)$$

where A —average particle scattering cross-section value

G —coefficient of sample dilution prior to measurement

OD—sample optical density after dilution.

There is a known analytical relationship, which links a scattering cross-section with cell size. As mentioned above, cell size is determined using a relaxation curve of cell disorientation after exposure to electric field. Addition of relative viable cell concentration to the calculated cross-section value allows obtaining an absolute value of viable cell concentration with a relative error below 5%. The measurements can be taken both on liquid samples acquired from biotechnological processes and on dry lyophilized samples upon suspending them.

11.6.2 The Effect of Antibiotics on Cells

The given assay type is based on low-frequency electro-optical measurements at 50–60 kHz and is performed on cells in a stationary state. The action of antibiotic on bacteria is closely linked to changes in their biochemistry metabolic pathways, as well as in their morphology (cell lengthening, swelling, bending, chain or ball formation, lysis) (Brian 1984; Antibiotic Resistance Protocols 2010).

Some antibiotic classes were used: ampicillin, kanamycin, and cloramphenicol (Guliy et al. 2016). *E. coli* was used in the study as a model, and the general study design consisted in comparison of cell suspension electro-optical analysis results obtained for two *E. coli* strains. One of the strains was sensitive to the antibiotic and the other was resistant to it.

As an example, Fig 11.4 demonstrates the spectral measurement results and the profile of the electro-optical signal during interaction of microbial cells with ampicillin. The biological activity of beta-lactam is mainly linked to its ability to interact with the microbial cell surface, thereby changing the barrier properties of the cytoplasmic membrane. Ampicillin also was active against several gram-negative organisms, including coliforms; therefore *E. coli* cells were used in the study. Before electro-optical measurement, *E. coli* suspensions were incubated with ampicillin. From the results in Fig. 11.4, it is obvious that the change in the electro-optical signal occurred within 5 min after treatment of the cells with ampicillin. To examine the surface electrophysical properties of the cells under ampicillin exposure, experiments were also conducted with the antibiotic-resistant strain *E. coli* K-12

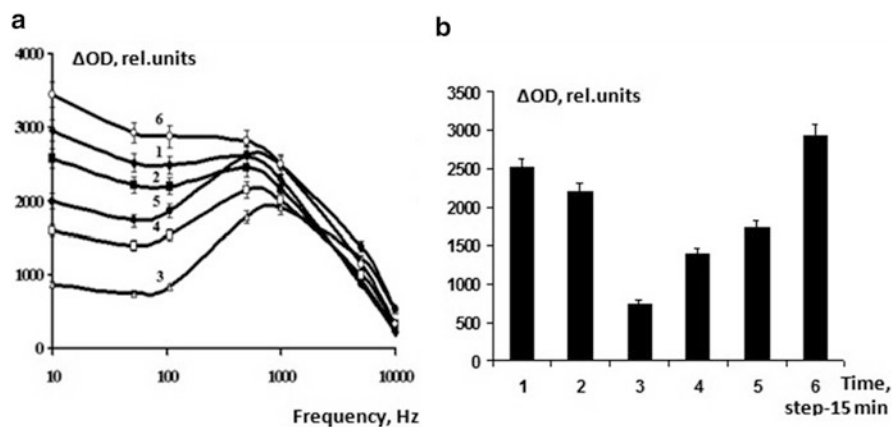


Fig. 11.4 The series of the spectra measurements (a) and profile of interaction process on the frequency $\omega = 52$ kHz (b) for *E. coli* K-12 cells after incubation with ampicillin ($50 \mu\text{g ml}^{-1}$) at time (min): (1)—without antibiotic (control); (2)—5; (3)—15; (4)—30; (5)—45; (6)—60 min

(pUC-18), which harbors plasmid pUC-18, carrying ampicillin resistance. The experimental conditions were similar to those involving the ampicillin-sensitive *E. coli* K-12. After incubation of the cells (pUC-18) with ampicillin, no significant changes in the operating system of the cell suspension were observed, which shows the strain's resistance to ampicillin. This means that the sensitive and resistant *E. coli* K-12 strains demonstrate different EO effect dependences on the ampicillin amount added to the cell suspension.

Antibiotics influence the physiology of bacterial cells on many levels. Instead of simply compensating for the direct cellular defects caused by drugs, bacteria respond to antibiotic treatment with alterations in morphology, molecular composition, metabolism, etc. (Mitosch and Bollenbach 2014). The interplay of these processes results in a complex reaction with cell surface damage accompanied by ion and charge redistribution recorded by the EO sensor.

Therefore, incubation of the antibiotic-sensitive strain with an antibiotic (e.g., ampicillin, chloramphenicol, kanamycin) leads to a significant change in the electro-optical signal value, yet no such changes were recorded in the suspension of the antibiotic-resistant strain. Consequently, the sensitive and resistant *E. coli* strains demonstrate different surface electrophysical properties, so the EO signal changes induced by these antibiotics can be used as a test to examine resistance to this antibiotic in bacteria (Gulyi et al. 2005, 2016).

Routine biological methods for the determination of antibacterial resistance of microbial cells based on cultivation of microorganisms with subsequent microbiological and biochemical analysis are labor-intensive and time consuming and use relatively expensive equipment. Alternatively, electro-optical analysis can offer rapid assessment of microbial cell antibiotic resistance.

11.6.3 Analysis of Phage-Cell Interaction Process

Phage-based therapy holds much promise for healthcare development. The use of specific phages for the detection and elimination of infectious bacteria is an ideal solution to the treatment of relevant diseases. The absence of chemotherapy side effects and the low cost of formulations are among the undisputed advantages of phage-based therapy. The weakness of this method consists in the need for rapid discovery of an optimal solution when screening a large number of bacteriophage-microbial cell combinations. The electro-optical method of screening, based on studying the kinetics of change in the bulk and surface electrophysical cell properties, offers a simple, rapid, and efficient solution to this problem.

Infection of bacteria by a bacteriophage starts with the recognition of the host through binding to an outer membrane receptor. Bacteriophage inject their genetic material into bacteria, replicate by the hundreds per cell, and then burst out before moving on to the next host cell. In the case of a tailed phage, this binding triggers conformational changes that are transmitted along the tail to the capsid, allowing its opening and the release of the viral genome, which causes a change in the electrophysical parameters of the cell structures. Bacteriophage specificity has been shown at both species and strain levels. Specific bacteriophages are very good indicators for determining the species and type of bacteria. Therefore, bacteria could be detected on the basis of the measurement of their electro-optical spectra in the absence and presence of phages.

The phage-cell interaction is fairly complex and depends on the structure of the phage itself (Stengele et al. 1990; Jakes et al. 1988) on the presence of F-pili in bacteria (Russel et al. 1988). In our work, *Escherichia coli* XL-1 and the bacteriophage M13K07 served as a model system. The bacteriophage M13 is an *E. coli*-specific filamentous phage family *Inoviridae*. It is a long and thin virus that infects *E. coli* without cell lysis (Overman et al. 1996; Endemann and Model 1995). The infection of *E. coli* male cells by the bacteriophages M13, fd, or f1 begins with the interaction of the minor phage capsid protein g3p (gene 3 protein) with bacterial F-pili and subsequently with the integral membrane protein TolA (Endemann and Model 1995; Click and Webster 1997). For controlling phage transfection to the *E. coli*, the bacteria in an LB nutrient medium containing kanamycin were used, because phage M13K07 is resistant to this antibiotic (Hoogenboom et al. 1991). The cells grew well with kanamycin, indicative of phage transfection.

Research has shown that the combination of the EO-approach with a phage as a recognition element has excellent potential for the mediator-less detection of the formation of a phage-bacteria complex. The interaction of *E. coli* with phage M13K07 induces a strong and specific electro-optical signal as a result of substantial changes of the EO properties of the *E. coli* XL-1 suspension infected by M13K07. The electro-optical data for the whole interaction is given in Fig. 11.5. The signal was specific even in the presence of a foreign microflora (*E. coli* K-12 and *Azospirillum brasilense* Sp7) (Bunin et al. 2004a).

Isolating the changes in σ_{cyt} only is challenging with such a low frequency. The electro-optical signal reflects the mixture of this parameter and surface electric

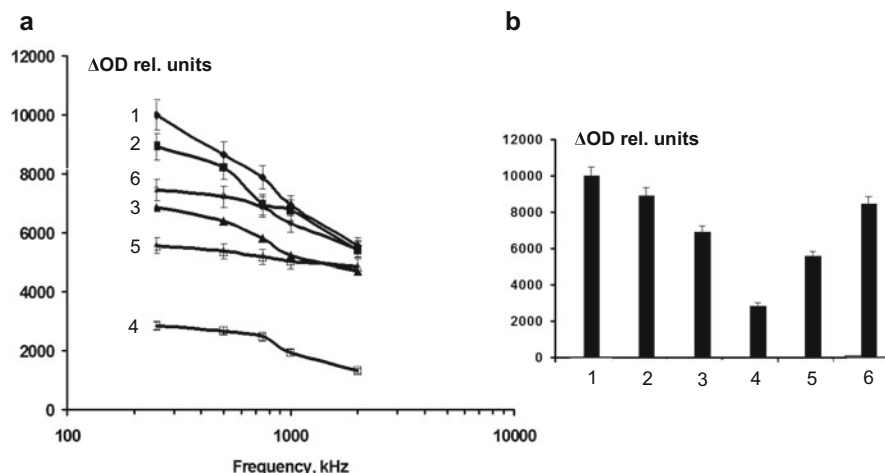


Fig. 11.5 The series of the spectra measurements (a) and profile of interaction process on the frequency $\omega = 52$ kHz (b) for *E. coli* XL-1 cells after incubation with bacteriophages at time (min): (1)—without phages (control); (2)—1; (3)—10; (4)—30; (5)—60; (6)—90 min

parameters such as the specific electric conductivity of the surface and its dielectric permittivity.

Combining of the electro-optical approach with phage use has the following advantages: (1) bacteria from biological samples need not be purified, (2) the phage infection is specific, (3) exogenous substrates and mediators are not required for detection, and (4) it is suitable for any phage-bacterium system when bacteria-specific bacteriophages are available.

Combination of the EO approach with phage technology comprises a generic technology that enables rapid and specific detection of viable bacteria and might serve as a basis for the development of portable biosensor systems for the detection of pathogens in medical research, food processing, and environmental analysis.

11.6.4 Studying of Surface Cellular Interactions by the Electro-optical Method

Combination of an EO technique with immunochemistry was proposed to investigate the binding of antibodies to microorganisms. Studies demonstrate high potential of using the electro-orientation technique for monitoring the *Listeria monocytogenes*-antibody (Bunin et al. 2004b) and *Azospirillum brasilense*-antibody reactions (Gulyi et al. 2007). Live vaccine strains of *Listeria monocytogenes*, *Azospirillum brasilense* Sp245, and monoclonal antibodies against *L. monocytogenes* and polyclonal antibodies against *A. brasilense* Sp245 were used as model systems.

During the formation of biospecific complexes of *L. monocytogenes*-monoclonal antibodies, a change in the electro-optical signal was observed. This process required

20–25 min, which is enough for full process description. Typically, the interaction led to a decrease in the electro-optical signal within the frequency range 10–100 kHz. The frequency $\omega = 50\text{--}60$ kHz was found to be more efficient for performing the measurements.

For testing of the cross interaction, various combinations of cells and markers were investigated. It was found that only the specific interaction changed the electro-optical signal. The presence of nonspecific markers mixed with one bacterial species is not reflected by the electro-optical signal. Conversely, electro-optical analysis selects only a complex-specific marker plus bacteria in the mixture of different kinds of nonselected bacteria.

This interaction feature can be used to detect small numbers of specific bacteria. The selected marker is fixed on the surfaces of magnetic particles and interacts with specific bacteria. Magnetic particles are separated from the suspension and the selected bacteria are separated from the magnetic particle fraction by using some physical action. This allows one to make an inexpensive and highly sensitive rapid detection instrument.

Thus, determination of the presence of certain bacteria in a mixed sample is achievable through the application of antibodies specific to certain bacterial species and comparison of the spectra of the bacterium in the presence and absence of antibodies.

For rapid bacterial detection, certain genetic engineering technologies for cloning recognized fragments, so-called “hypervariable immunoglobulin domains,” can also be used. They offer selectivity comparable to that of hybrid technologies but at a lower price. One of them is the antibody phage display technique, based on the formation of a combinatorial library of antibodies, in which the variable regions of light and heavy chains are coupled and represented at the surface of filaments.

Studying the possibility of using the electro-optical method for the detection of cells of *A. brasilense* model strain Sp245 with mini-antibodies, the affinity selection (biopanning) of them was usually repeated several times in order to select clones possessing higher sensitivity and productive activity. Evaluation of the sensitivity of the obtained phage antibodies by dot analysis showed that it had increased after the third round of selection, and the titer of the obtained mini-antibodies to whole cells of *A. brasilense* Sp245 was 1:8000, as determined in the enzyme immunoassay. At the same time, the results of selection of phage-displayed mini-antibodies showed that the mini-antibodies to lipopolysaccharide were more sensitive than anti-flagellin mini-antibodies.

The magnitude of the electro-optical parameters during interaction of an *A. brasilense* Sp245 suspension with anti-lipopolysaccharide phage-displayed mini-antibodies is of particular interest owing to the role of O-specific antigen (lipopolysaccharide) in the intraspecies classification of *Azospirillum*. The results of electro-optical analysis with different concentrations of such mini-antibodies confirmed the high level of interaction between anti-lipopolysaccharide mini-antibodies and *A. brasilense* Sp245 cells (Dykman et al. 2012).

Using electro-optical analysis and electron microscopy, we observed a biospecific interaction of cell surface antigenic determinants with phage antibodies raised against the lipopolysaccharide of *H. seropedicae* Z78 (Guliy et al. 2019).

Therefore, in view of the fact that the results of the dot-assay and the electro-optical method agree nicely with the data obtained by electron microscopy, it can be stated that the suggested method offers efficient assessment of the extent of epitope exposure on the bacterial cell surface and it can thus be used for the development of a rapid test for the interspecies differentiation of bacteria with the help of antibodies or phage-mini-antibodies.

11.7 Continuous Monitoring of Periodic Cultivation Processes

Monitoring of cultivation processes using the above classification refers to process profile measurement. For periodic cultivation process it encompasses the time period from inoculation of initial culture into a fermenter to stationary process phase. A sufficient time interval between electro-optical measurements is less than half of culture generation time. No changes take place in a suspension within shorter time intervals. A typical profile of periodic cultivation process of *E. coli* K-12 cells is shown in Fig. 11.6.

Such profiles are typical for cell metabolism accompanied by synthesis of weak organic acids. In aerobic cultivation, acetic acid plays this role. The reason behind

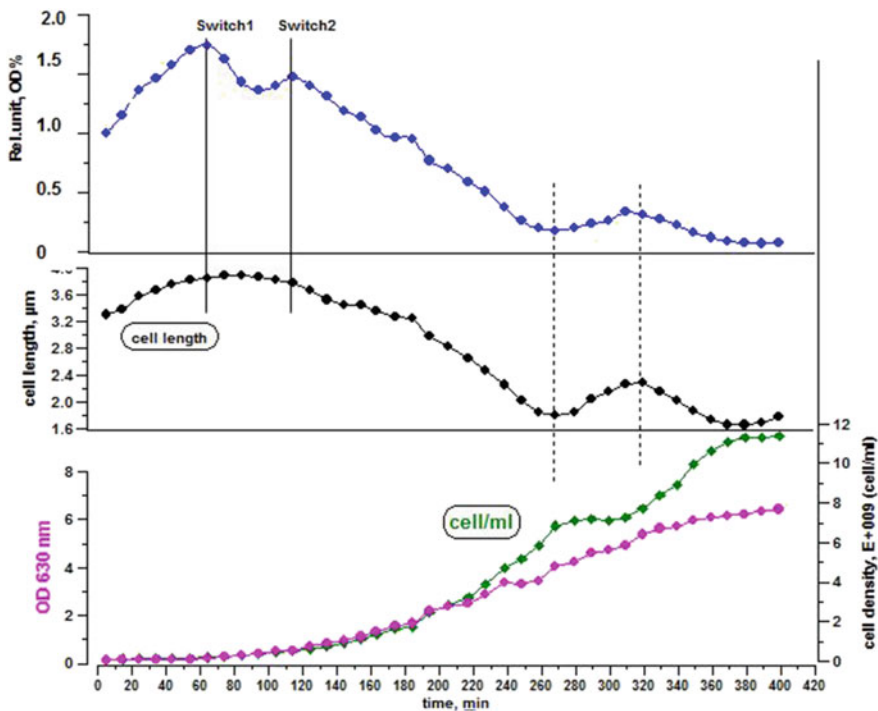


Fig. 11.6 The profiles of cytoplasm-specific conductivity, average cell size, and cultural liquid optical density during periodic cultivation of aerobic *E. coli* K-12 cells

formation of these profile types is excessive energy substrate contents in the cultural liquid. Unfortunately, the intracellular mechanism of energy substrate glycolysis inhibition with an intermediate product excess turned out to be inefficient in these cells (Warnecke and Gill 2005; Kumary et al. 2000; Roe et al. 1998; Emmerling 2002).

Due to the difference in pyruvate generation intensity in the course of glycolysis and its utilization by Krebs cycle, pyruvate is accumulated in the cells. Its excess is a negative factor and the cell tries to find alternative ways to decrease its concentration. Several ways of such utilization have been identified and are known as aplerotic ways. The end product of biochemical transformations is formation of acetate ions and reduction of high-energy compounds. Sadly, this negative process of toxic metabolite synthesis brings more problems for the cell, than the positive process of increasing its energy potential. Figure 11.7 shows that the flowchart interlinking glycolysis process, Krebs cycle, and typical aplerotic ways of pyruvate utilization.

A cell has several options to decrease concentration of toxic acetate ions. Due to the negative charge on the inner membrane surface, acetate ions have almost no chance to use the way of passive diffusion over concentration gradient. The option of active transport of acetic acid molecules emerges only after considerable intracellular pH decrease and the increase in the number of non-dissociated molecules in cytoplasm. Yet there is one more way to decrease concentration of these ions. It consists in accumulation of additional water in the cell, which can pass through the membrane freely. Cell size is increasing, and specific concentration of toxic substance in cytoplasm decreases. This process is clearly visible in the average cell size dynamics profile.

Upon reaching a somewhat low pH value (in Fig. 11.6. profile this took place 80 min after the process start), active transport of acetic acid molecules into ambient medium begins and its concentration in cytoplasm starts decreasing. Meanwhile, energy substrate concentration in cultural liquid usually drops to a low level. Pyruvate accumulation stops at the junction point between glycolysis and Krebs cycle. With some time delay the cell starts excreting water and shrinking.

In the specific cytoplasm conductivity σ_{cyt} diagram along with the bell-shaped signal a weak auto-wave process of the cell's biochemical activity can be seen. This process is driven by the elements of the same biochemical activity of cells as the one leading to the main bell-shaped signal formation.

The discussed profiles of σ_{cyt} alteration and average cell size change include a lot of detail, supporting identification of various properties and stages of cell metabolism:

Absolute value of cytoplasm electric conductivity at the beginning and at the end of the process as well as max value of the parameter during exponential growth phase (EP).

Presence of inflection points with local maxima, called metabolic switch.

The rate of cytoplasm conductivity change during EP and before the end of the process.

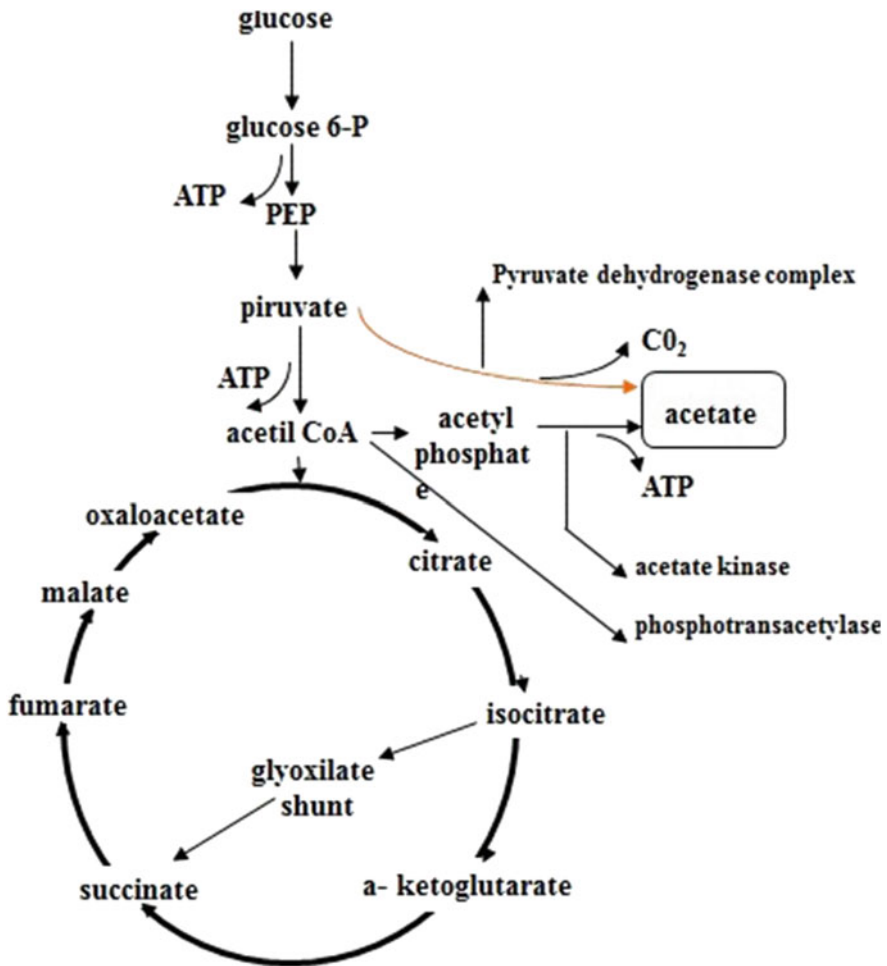


Fig. 11.7 Flowchart interlinking glycolysis process, Krebs cycle, and aprotic ways of pyruvate utilization

Absolute value of average size at the beginning and at the end of the process as well as max average size value during exponential growth phase (EP).

The rate of average size change during EP and before the end of the process.

Maximum or minimum of alteration profile for the parameter related to specific conductivity of the membrane.

There are multiple data sets available prepared based on these criteria. Some of them are particularly noteworthy. The initial specific cytoplasm conductivity value and average cell size in the inoculum determine their readiness for the next cultivation cycle. The value of these parameters is directly linked with the values observed in the previous cultivation cycle of these cells. There are several profile patterns for

these parameters at the final stage of the previous cultivation cycle, including specific conductivity σ_{cyt} decrease and the increase in average size. This is the most critical and negative case of cell metabolism condition, which rules out the possibility to use the cells as inoculum. Concentration of various non-dissociated toxic substances remained high, and the cells use their last chance to decrease it via water accumulation.

11.7.1 Identification of Metabolic Switch Points

Of special interest are the studies of metabolic switch points. At least two simple metabolic switches linked with activation of active transport mechanisms can be distinguished in Fig. 11.7. For other bacterial cultures the number of these simple metabolic switch points can be considerably higher. At the same time, other metabolic switch types can also be encountered in cultivation processes. During the process of periodic cultivation metabolic activity of *Clostridium acetobutylicum* cells has a metabolic switch indicative of their transition from butanol synthesis to acetone and ethanol synthesis (Jenne et al. 2008). It is accompanied by a rapid drop in σ_{cyt} followed by a slight increase and subsequent decrease during the sporulation process. It is quite challenging to determine the onset of sporulation process with conventional methods, and this process is irreversible after formation of the first spores. Analysis of changes in σ_{cyt} parameter allows to identify the cell development stage preceding sporulation and prevent it by removing the suspension and adding a new portion of nutrient medium.

In the process of recombinant strain cultivation two more metabolic keys occur—induction of target product biosynthesis, and the point when target product utilization as an energy source is initiated. Figure 11.8 shows a part of σ_{cyt} alteration profile during the process of cultivation of recombinant insulin-producing *E. coli* strain.

The peak concentration of intracellular insulin corresponds to the local minimum of specific electric conductivity of the cytoplasm. From cellular metabolism standpoint this moment can be described as the time when the main cycle of recombinant product biosynthesis is over and preparations for its utilization commence.

The process of target product biosynthesis in recombinant cells is extremely complicated, since it includes a battery of biochemical transformations. Electro-optical monitoring ensures identification of several key points of this process and supports shaping an optimal biosynthesis management strategy.

If the values of the given parameters are identical both in the ongoing process and in the reference one, complete validation of the ongoing process can be stated. Such strategy is used for scaling the cultivation processes at all stages.

There are multiple means for correcting the ongoing process and adjusting it to suit the reference one. This includes fractional supply of energy substrate, alteration of nutrient medium composition, and/or changing physical parameters of the cultivation process: mass exchange, mixing, temperature, and cultural liquid pH shift characteristics. In any case the response to different actions can be easily measured and the process management strategy can be adjusted on the go.

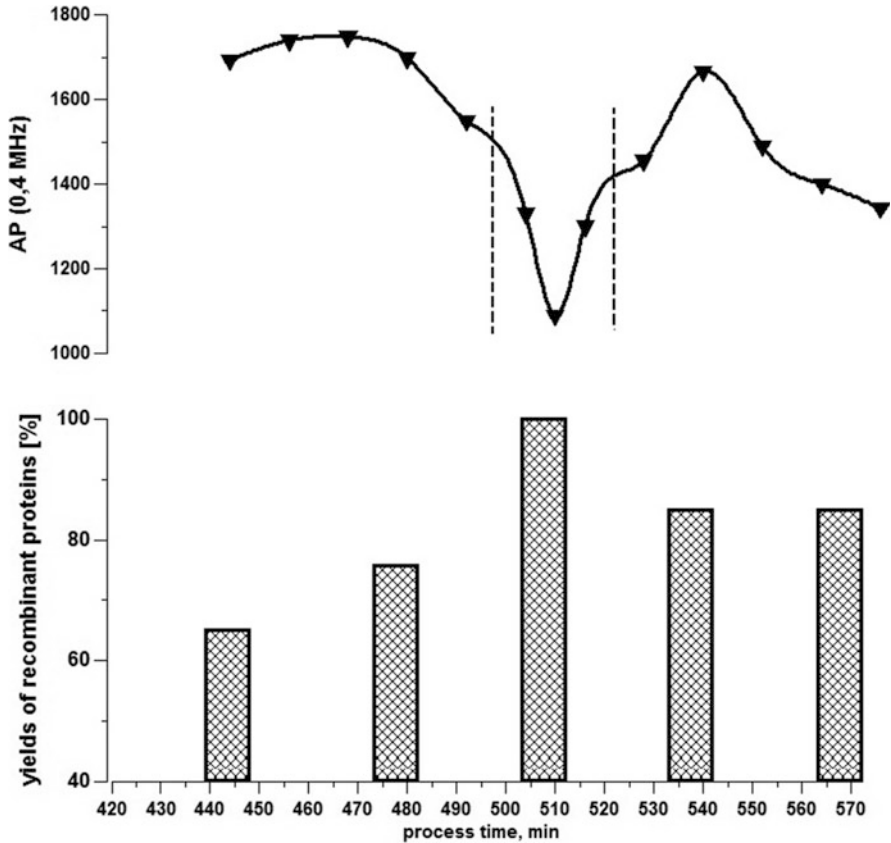


Fig. 11.8 The profile of cytoplasm-specific conductivity σ_{cyt} alteration and insulin concentration change

11.8 Conclusion

The examples given above capture only a fraction of tasks for electro-optical monitoring of cell metabolism processes and identification of various processes involving bacterial cells. Electro-optical technique for studying suspended cells offers a fairly simple means for measurement of electric and morphometric properties of certain cell structures. With adequate equipment sample preparation and evaluation process would require minimal effort by the personnel. The technique is rather fast as the analysis takes about 10 min; besides the measurement process can be fully automated. EO analysis technique does not involve fixation of specific reagents in the measuring cell, and can be applied for evaluation of both live and lyophilized bacteria transferred into a suspended state. Moreover, the effect of

measurement procedure on bacterial cells is negligible and the procedure itself requires no additional markers or chemical components.

The results obtained using electro-optical analysis can be easily interpreted by personnel with various skill levels. A unique detailed data on the development and/or certain exposure process is potentially available for each microorganism species. The method can also offer useful information regarding biophysical aspects of bacteria under exposure to specific agents.

Therefore, the described EO analysis method is quite promising for development of sensor systems and their use in the field of microbiology, healthcare, veterinary medicine, as well as in biotechnological processes (Chandra 2016; Guliy et al. 2016, 2017, 2019; Ignatov et al. 2008).

References

- Antibiotic Resistance Protocols (2010) Second edition, Gillespie SH, McHugh TD (ed), Methods in molecular biology, vol. 642. Springer Science+Business Media, LLC.
- Botcher GPF (1982) Theory of electrical polarizability, vol 1. Academic Press, New York
- Brian LE (1984) Bacterial resistance and sensitivity to chemotherapeutic agents. Meditsina Publishers, Moscow
- Bunin VD (2002) Electrooptical analysys of a suspension of cells and its structure. In: Encyclopedia of surface and colloid science. M. Dekker Publisher, New York, NY, pp 2032–2043
- Bunin VD, Voloshin AG (1996) Determination of cell structures, electrophysical parameters, and cell population heterogeneity. J Colloid Interface Sci 180:122–126
- Bunin VD, Ignatov OV, Guliy OI, Zaitseva IS, Dykman LA, O'Neil D, Ivnitski D (2004a) Electro-optical analysis of the *Escherichia coli*–phage interaction. Anal Biochem 328:181–186
- Bunin VD, Ignatov OV, Guliy OI, Voloshin AG, Dykman LA, O'Neil D, Ivnitski D (2004b) Studies of listeria monocytogenes-antibody binding using electro-orientation. Biosens Bioelectron 19(2):1759–1761
- Chandra P (2016) Nanobiosensors for personalized and onsite biomedical diagnosis. The Institute of Engineering and Technology, London
- Click EM, Webster RE (1997) Filamentous phage infection: required interactions with the TolA protein. J Bacteriol 179:6464–6471
- De la Torre G, Blumfield VA (1981) Hydrodynamic properties of complex, rigid biological macromolecules; theory and application. Q Rev Biophys 14(1):31–139
- Dukhin SS (1977) Electrooptic of colloid. Naukova Dumka, Kiev
- Dykman LA, Staroverov SA, Guliy OI, Ignatov OV, Fomin AS, Vidyasheva IV, Karavaeva OA, Bunin VD, Burygin GL (2012) Preparation of miniantibodies to Azospirillum brasilense Sp245 surface antigens and their use for bacterial detection. J Immunoass Immunochem 33:115–127
- Emmerling M (2002) Metabolic flux responses to pyruvate kinase knockout in *Escherichia coli*. J Bacteriology 184:152–164
- Endemann H, Model P (1995) Location of filamentous phage minor coat proteins in phage and in infected cells. J MolBiol 250:496–506
- Gimsa J, Glasser R, Fuhr G (1991) Theory and application of the rotation of biological cells in rotating electric fields (electrorotation). In: Schutt W, Klinkmann H, Lamprecht I, Wilson T (eds) Physical characterization of biological cells. Basic research and clinical relevance. Verlag Gesundheit GmbH, Berlin, pp 295–322
- Gimsa J, Pruger B, Eppmann P, Donath E (1995) Electrorotation of particles measured by dynamic light scattering-a new dielectric spectroscopy technique. Colloid Surface A 98:243–249

- Guliy OI, Ignatov OV, Markina LN, Bunin VD, Ignatov VV (2005) Action of ampicillin and kanamycin on the electrophysical characteristics of *Escherichia coli* cells. Intern J Environ Anal Chem 85(12–13):981–992
- Guliy OI, Matora LY, Burygin GL, Dykman LA, Ostudin NA, Bunin VD, Ignatov VV, Ignatov OV (2007) Electrophysical characteristics of *Azospirillum brasilense* Sp245 during interaction with antibodies to various cell-surface epitopes. Anal Biochem 370:201–205
- Guliy OI, Bunin VD, Volkov AA, Korzhenevich VI, Ignatov OV (2016) Electrooptical analysis of microbial cells suspensions for estimation of antibiotic resistance. Cell Biochem Biophys 74 (4):537–543
- Guliy OI, Bunin VD, Korzhenevich VI, Ignatov OV (2017) Electro-optical assays for immunoindication of microbial cells. Curr Immunol Rev 13(2):153–162
- Guliy OI, Velichko NS, Fedonenko YP, Bunin VD (2019) Use of an electro-optical sensor and phage-displayed miniantibodies for immunodetection of *Herbaspirillum*. Talanta 202:362–368
- Hoogenboom R, Griffiths AD, Johnson KS, Chiswell DJ, Hundson P, Winter G (1991) Multi-subunit proteins on the surface of filamentous phage: methodologies for displaying antibody (FAB) heavy and light chains. Nucleic Acids Res 19:4133–4137
- Ignatov OV, Guliy OI, Bunin VD (2008) Electro-optical analysis as a tool for determination of microbial cells with the help of specific bacteriophages. In: Lechuga LM, Milanovich FP, Skladal P, Ignatov O, Austin T (eds) Commercial and pre-commercial cell detection technologies for defence against bioterror—technology, market and society. Springer, The Netherlands, pp 45–53
- Jakes KS, Davis NG, Zinder ND (1988) A hybrid toxin from bacteriophage f1 attachment protein and colicin E3 has altered cell receptor specificity. J Bacteriol 170:4231–4238
- Junne S, Klein E, Angersbach A, Goetz P (2008) Electrooptical measurements for monitoring metabolite fluxes in acetone-butanol-ethanol fermentation. Biotechnol Bioeng 99(4):862–869
- Kumary S, Beatty CM, Browning DF, Busby SJW, Simel EJ, Hovel-Miner G, Wolfe AJ (2000) Regulation of acetyl coenzyme a synthetase in *Escherichia Coli*. J Bacteriol 182(15):4173–4179
- Miroshnikov FI, Fomchenkov VM, Ivanov AJ (1986) Electrophysical analysis and cell separation. Nauka, Moscow. (in Russian)
- Mitosch K, Bollenbach T (2014) Bacterial responses to antibiotics and their combinations. Environ Microbiol Rep 6(6):545–557
- Overman SA, Tsuboi M, Thomas GJ (1996) Subunit orientation in the filamentous virus Ff (fd, f1, M13). J Mol Biol 259:331–336
- Roe AJ, McLaggan D, Davidson I, O’Byrne C, Booth IR (1998) Perturbation of anion balance during inhibition of growth of *Escherichia Coli* by weak acids. J Bacteriol 180(4):767–772
- Russel M, Whirlow H, Sun TP, Webster RE (1988) Low-frequency infection of F-bacteria by transducing particles of filamentous bacteriophages. J Bacteriol 170(11):5312–5316
- Shchyogolev SY, Khlebtsov NG, Bunin VD, Sirota AI, Bogatyrev VA (1994) Inverse problems of spectroturbidimetry of biological disperse systems with random and ordered particle orientation. Proc SPIE 2082:167–176
- Stengele I, Bross P, Garcés X, Giray J, Rasched I (1990) Dissection of functional domains in phage fd adsorption pro-teín. Discrimination between attachment and penetration sites. J Mol Biol 212 (1):143–149
- Stoylov SP (1991) Colloids electro-optics, theory, techniques, applications. Academic Press, London
- Warnecke T, Gill RT (2005) Organic acid toxicity, tolerance, and production in *Escherichia Coli* biorefining application. Microb Cell Factories 4:25–30
- Williams V, Williams H (1972) Basic physical chemistry for the life science. Freeman WH and Company, San Francisco